

SOUTHERN RIO GRANDE RIFT KINEMATICS AND GEOCHRONOLOGY, BIG BEND FOLD GEOMETRY, AND THE
USE OF REAL DATA IN GEOSCIENCE EDUCATION: CONTRIBUTIONS TO THE UNDERSTANDING
OF BIG BEND GEOLOGY AND TO PUBLIC GEOSCIENTIFIC LITERACY

JESSICA MOORE KELSCH
Doctoral Program in Geosciences

APPROVED:

Jason Ricketts, Ph.D., Chair

Diane Doser, Ph.D.

Richard Langford, Ph.D.

Lin Ma, Ph.D.

Joseph Satterfield, Ph.D.

Stephen Crites, Ph.D.
Dean of the Graduate School

DEDICATION

This dissertation is dedicated to anyone who enjoys solving the multi-dimensional puzzles of structural geology and plate tectonics to understand Earth history; to all people who are curious about how any part of the Earth system works and how human society relates to it; to Earth Science educators who are finding better ways to share this fundamental science and its relevance; and to my mother, Michelle Elise.

SOUTHERN RIO GRANDE RIFT KINEMATICS AND GEOCHRONOLOGY, BIG BEND FOLD GEOMETRY, AND THE
USE OF REAL DATA IN GEOSCIENCE EDUCATION: CONTRIBUTIONS TO THE UNDERSTANDING
OF BIG BEND GEOLOGY AND TO PUBLIC GEOSCIENTIFIC LITERACY

by

JESSICA MOORE KELSCH, M.S.

DISSERTATION

Presented to the Faculty of the Graduate School of
The University of Texas at El Paso
In Partial Fulfillment
of the Requirements
for the Degree of

DOCTOR OF PHILOSOPHY

Department of Earth, Environmental and Resource Sciences

THE UNIVERSITY OF TEXAS AT EL PASO

December 2023

ACKNOWLEDGMENTS

I wish to thank and esteem my dissertation chair Dr. Jason Ricketts for his invaluable mentorship and support, which has consistently included the right balance of guidance, freedom, and redirection, and without which I could not have progressed in good time in this venture or had so much fun learning. The same goes for Dr. Diane Doser regarding her guidance around all of my projects but Chapter Four in particular, and for her sharing her experience and knowledge in geoscience education with me. Thanks also to Dr. Joe Satterfield for maps, field trips, and constructive conversations that contributed to the progress of this research. I also thank my unofficial mentor and friend Dr. Pat Dickerson for her insightful responses to my frequent questions and her unwavering interest in my research.

My experience as a UTEP graduate student in the Earth, Environmental, and Resource Sciences department was fun and enriching and was enhanced profoundly by three aspects beyond the excellent mentorship from members of my dissertation committee: Ongoing awareness of my status and subsequent assistance from Annette Veilleux; exceptional teaching assistantships with Jason Ricketts and Rip Langford; and courses from several exceptional professors, in particular Kate Giles and Diane Doser.

I am grateful for financial assistance for my research from the West Texas Geological Society, the American Association of Petroleum Geologists, and the Sul Ross State University Faculty Research Enhancement program. I also extend gratitude to the Sul Ross State University provost, Dr. Bernie Canteñs, and to the SRSU Natural Sciences Department faculty for providing me with time, when critical, to spend on my dissertation.

Utmost gratitude goes to Jeff Kelsch for making do during my work on this project.

ABSTRACT

The Big Bend region of Trans-Pecos Texas preserves a rich record of Rio Grande rifting and Laramide-age contraction that provide intrigue to national and state park visitors and field trips for undergraduate geology students. Despite its well-exposed geologic record, the Big Bend region remains an underutilized natural laboratory for studying these two tectonic events. This dissertation combines structural studies of Rio Grande rift and Laramide structures with public outreach and geoscience education studies focused on the Big Bend region.

In Chapter 2, existing extensional-kinematic studies from parts of this region are compiled with new fault kinematic and U-Pb geochronologic data from normal and strike-slip fault surfaces across the Sunken Block and Black Gap grabens of the southern Rio Grande rift. These data delineate an early and long-lived NE-SW orientation of principal stretch (S_1) lasting from at least 30.1 ± 3.1 Ma to at least 13.7 ± 0.9 Ma. Clockwise rotation of S_1 to NW-SE followed the early orientation after 13.7 ± 0.9 Ma, agreeing with a widely cited regional clockwise shift in tension and extension at ~ 10 Ma reported in the northern Rio Grande rift and the Basin and Range province. The locations documenting this progressive rotation of S_1 in the southern Rio Grande rift also suggest that later faulting narrows and is constrained to the Sunken Block graben.

Chapter 3 focuses on a footwall syncline under a Laramide thrust fault that is exposed in cross-section in a cliff wall at the end of the Dog Canyon trail in Big Bend National Park. This structure provides an opportunity to test fold models and is also societally relevant because it is a popular hiking trail for park visitors. Structural analysis reveals evidence of three deformation events preserved in minor structures within the folded rock. First and second in this geologic history were orthogonal flexure and horizontal contraction related to fault-propagation folding in front of and under the west-southwest-verging Santiago thrust fault. The third deformational event was horizontal extension interpreted to be

associated with late Cenozoic Rio Grande rifting. This geologic history and an explanation of the structural analysis behind it are presented as a panel to be installed by the National Park Service as an interpretive wayside exhibit in front of the cliff on the Dog Canyon trail.

Chapter 4 presents a geoscience education study, involving undergraduate students of all majors in core-science geology classes at two universities near the Big Bend region. For this study, students interacted with either locally or globally sourced geoscientific data within in-class quantitative exercises and were surveyed to query the outcomes of their engagement, knowledge-retention, critical-thinking skill, and perceptions of the relevance of the exercise topics to human society. The group exposed to local data returned higher scores and rankings than those exposed to global data after four of the five exercises, indicating a lead in each of those outcomes but most clearly in critical-thinking skill and in their perception of the relevance of the geoscientific topic.

TABLE OF CONTENTS

ABSTRACT.....	v
TABLE OF CONTENTS.....	vii
LIST OF TABLES.....	xi
LIST OF FIGURES.....	xii
CHAPTER 1: INTRODUCTION.....	1
CHAPTER 2: KINEMATIC AND GEOCHRONOLOGIC EVIDENCE DOCUMENTING ROTATION OF CRUSTAL EXTENSION AND NARROWING OF RIFT FAULTING IN THE SUNKEN BLOCK GRABEN OF THE SOUTHERN RIO GRANDE RIFT, TRANS-PECOS TEXAS	3
2.1 Abstract.....	4
2.2 Introduction	5
2.3 Background & Previous Work	7
2.3.1 Geology of the southern rift	7
2.3.1.1 Basins of the southern Rio Grande rift.....	9
2.3.1.2 Border Corridor Transform Zone	13
2.3.2 Previous analyses of extensional strain in the Big Bend region.....	16
2.3.3 Previous analyses of calcite slickenlines for fault movement dating	22
2.4 Methods.....	24
2.4.1 Field analyses: measurement of fault-surface striae and determination of sense of motion ..	24
2.4.2 Computational analyses: Determination of principal strain axes for each measurement and for kinematically compatible populations of measurements.....	27
2.4.3 Geochronologic and geochemical analysis of co-seismic calcite slickenlines.....	30
2.4.4 Trace-element analysis of co-seismic calcite slickenlines.....	31
2.5 Results.....	32
2.5.1 Kinematic analysis: stretch axes determined from striated fault surfaces.....	32
2.5.1.1 Castolon graben	35
2.5.1.2 Northern Sunken Block	35
2.5.1.3 Old Ore Road.....	36
2.5.1.4 South Sierra del Carmen	37
2.5.1.5 Dagger Flat	39
2.5.1.6 North Black Gap graben	40
2.5.2 Geochronologic analysis	41
2.5.3 Trace-element data.....	45

2.6 Discussion.....	47
2.6.1 Extension-direction history of the southern rift from kinematic and geochronologic data.....	47
2.6.2 Evidence for structural narrowing of the southern Rio Grande rift in Trans-Pecos Texas and questions about its relationship to the BCTZ and the rest of the Rio Grande rift.....	53
2.6.3 The use of U/Pb geochronology.....	56
2.7 Conclusion.....	59
CHAPTER 3: INTRA-FOLD STRAIN ANALYSIS OF DOG CANYON SYNCLINE	60
3.1 Abstract.....	61
3.2 Introduction	62
3.3 Background	63
3.3.1 NPS outreach/ public education	63
3.3.2 Tectonic setting.....	64
3.3.3 Local geology.....	66
3.3.4 Theoretical strain partitioning in folded rock	69
3.4 Methods.....	71
3.4.1 Image capture	71
3.4.2 Geologic cross-section	71
3.4.3 Mapping of intrafold structures.....	71
3.4.4 Interpretation of local strain ellipses	73
3.4.5 Direct measurements of lineated surfaces at canyon floor.....	74
3.4.6 Creation of on-trail interpretive exhibit.....	74
3.5 Results.....	75
3.5.1 Fracture map.....	75
3.5.2 Cross-section.....	83
3.5.3 Three-dimensional mapping of fracture patterns and kinematic indicators.....	87
3.6 Discussion.....	89
3.6.1 Interpretation of deformation at Dog Canyon.....	89
3.6.1.1 The fold is a syncline in the footwall of a fault-propagation fold.....	89
3.6.1.2 Fractures in the cliff wall record multiple strain events.....	90
3.6.2 Panel to submit to NPS for interpretive wayside exhibit at end of Dog Canyon trail.....	94
3.7 Conclusions	97
CHAPTER 4: A CASE STUDY COMPARING UNDERGRADUATE STUDENTS’ ENGAGEMENT, KNOWLEDGE RETENTION, AND PERCEPTIONS OF RELEVANCE OF GEOSCIENCE AFTER IN-CLASS EXERCISES USING DATA THAT IS EITHER LOCALLY OR GLOBALLY SOURCED	98

4.1 Abstract.....	99
4.2 Introduction	100
4.3 Background and Previous Work.....	102
4.4 Methods.....	107
4.4.1 Creation and delivery of demographic-data survey	107
4.4.2 Creation and delivery of exercises.....	107
4.4.2 Design & delivery of student assessment for evaluation of effects of exercises	112
4.4.3 Evaluation of student survey data	113
4.4.4 Data analysis	114
4.5 Results.....	116
4.5.1 Pre-exercise survey results comparing local-data group to global-data group.....	116
4.5.1.1 Demographic data.....	116
4.5.1.2 Pre-exercise content results.....	118
4.5.2 Post-exercise survey data	119
4.5.2.1 Post-exercise survey questions across all exercises	119
4.5.3 Scored and self-ranked answers by exercise, comparing local-data to global-data group	121
4.5.3.1. Geologic structures exercise	121
4.5.3.2 Earthquakes exercise.....	122
4.5.3.3 Volcanoes exercise	123
4.5.3.4 Climate	124
4.5.3.5 Flooding exercise.....	125
4.5.3.6 Students' rankings on their engagement and perception of relevance.....	127
4.5.4 Final survey results.....	130
4.6 Discussion.....	134
4.7 Conclusions	142
REFERENCES.....	143
APPENDICES	153
Appendix 1. Collected fault-surface kinematic data.....	154
Appendix 2. Geochronologic and geochemical data	165
Appendix 3. In-class exercises.....	170
Appendix 4. Survey questions.....	231
Appendix 5. Post-climate-exercise ranking data.....	251
Appendix 6: Word clouds.....	252

VITA.....256

LIST OF TABLES

Table 2.1. Calcite slickenline samples collected for U/Pb geochronologic analysis, source of sample, kinematic population to which the striated slickenline sample belongs, analyses run, and resultant U/Pb age if obtained.	43
Table 2.2. Calcite slickenline samples collected for U/Pb geochronologic analysis, not analyzed.....	44
Table 3.1. Rock units exposed in the vicinity of Dog Canyon.	69
Table 3.2. Kinematic data collected from ground-level outcrops.	88
Table 3.3. Relevant "Big Ideas" and supporting concepts from the Earth Science Literacy Initiative's Earth Science Standards for US public education.	95
Table 4.1. Descriptions of in-class exercises distinguishing type and source of data, type of analysis required, and how much of exercise is unique to GG and LG students.	111
Table 4.2. Types and examples of questions on post-exercise surveys.....	112
Table 4.3. Rubric for scoring answers to content questions and higher Bloom's level critical-thinking questions	114
Table 4.4. Summary of percentages of correct scores between local and global groups by question type.	120
Table 4.5. Table showing differences in total percent of correct scored answers on five post-exercise surveys between student groups exposed to local or global data sets in the in-class exercises.	127
Table 4.6. Percentage of high ranked impressions following the earthquakes and floods exercises.	129
Figure 4.14. Final survey relevance-ranking results from students at SRSU.	131
Table 4.7. Tabulations of relevance-ranking data from final-survey questions administered to SRSU students.	131
Table 4.8. Percent change among both data groups at SRSU from the beginning to end of the semester in their perceptions of the relevance of geoscience.	132
Table 4.9. Delineation of data sources and methods of manipulation of data in the five exercises, from information presented in Table 4.1.	136
Table 4.10. Critical-thinking questions asked following the structures, earthquakes, volcanoes, and climate exercises.	139
Table 4.11. Order in which the five in-class exercises were presented and worked at SRSU and ASU....	140

LIST OF FIGURES

Figure 2.1. Outline of basins of the Rio Grande rift and other tectonic elements in New Mexico, west Texas, and northern Chihuahua.....	6
Figure 2.2. Map of the Big Bend area of Trans-Pecos Texas showing grabens and geographic and geologic features mentioned in text.....	9
Figure 2.3. Geologic map of Big Bend region indicating location of published extensional-strain determinations referred to in the text.	19
Figure 2.4. REY trends from Nuriel et al., 2012 of their different categories of fault-related calcite occurrence.	23
Figure 2.5. Map of Big Bend region of west Texas displaying locations of kinematic measurements.	25
Figure 2.6 Sketch depicting the Aki-Richards sign convention for consistent labeling of thrust or normal sense of motion from fault-surface rake measurements.	25
Figure 2.7. Model describing formation of slip-fiber lineations in spaces between faults where new precipitate is striated into slickenlines. Photo shows slip-fiber lineations on normal-fault surface in Dagger Flat.	26
Figure 2.8. Left: Figure from Fossen (2016) after Petit (1987) showing chatter marks possible on top-to-the-right fault surfaces that would indicate sense of motion. Photo on right from Paint Gap Hills is an example of Petit’s sketch (c) with polished striations on the stoss sides of very low-relief ridges and neither lineations nor fault mineralization on the lee sides. Fault surface shows that the missing block moved down to the right (oblique sinistral motion.) Field in photo is approximately 0.5m across.	27
Figure 2.9. Plot in FaultKin8 of all kinematic data for the northern Sunken Block’s measured faults showing the orientation of individual fault surfaces (black great circles,) slip direction (black dots) and sense (black arrows,) and each fault’s calculated P (blue dot) and T (red dot) axis.....	30
Figure 2.10. Selected outcrop photos of lineations on fault surfaces, all in Cretaceous limestone formations.....	33
Figure 2.11. Selected outcrop photos of lineations on fault surfaces.	34
Figure 2.12. Three kinematically compatible populations of fault-kinematic measurements from Castolon graben.	35
Figure 2.13. Three kinematically compatible populations of fault-kinematic measurements from the northern Sunken Block graben..	36
Figure 2.14. Two kinematically compatible populations of fault-kinematic measurements from the Old Ore Road area inside the eastern margin of the Sunken Block.	37
Figure 2.15. Three kinematically compatible populations of fault-kinematic measurements from the southern Sierra del Carmen	38
Figure 2.16. Fault-brecciated shear zone outcropping at base of Boquillas fault.	39
Figure 2.17. Two kinematically compatible populations of fault-kinematic measurements from the Dagger Flat area.	40
Figure 2.18. Two kinematically compatible populations of fault-kinematic measurements from the northern Black Gap graben.....	41
Figure 2.19. Mapped locations of all field sites of kinematic measurements (white square) and samples collected at some of those sites (grey circle,) quantity of samples in each kinematic population in parentheses, double-ended arrow indicating stretch axis of kinematic population).....	42

Figure 2.20. Chondrite-normalized REE concentrations for samples indicated in Table 2.1.....	46
Figure 2.21. Stereographic plots of kinematic populations of fault measurements (this study) and published S1 axes arranged by location (southwest to northeast) from RLFZ in the southern BCTZ to Black Gap graben, with north = up on each stereonet.....	48
Figure 2.22. Figures from Zoback et al., 1981 presenting a Miocene (~20-10Ma) field of least principal stress (σ_3 , equivalent to maximum stretch direction referred to in this study) on the left, and the modern field of the same (σ_3) on the right.....	50
Figure 2.23. Portion of World Stress Map (WSM) produced for western Texas and eastern New Mexico, with all Trans-Pecos-area earthquake data, and M>5.0 data for the Midland and Delaware basins, superimposed.	52
Figure 2.24. Map showing the most confident <10Ma stretch directions from fault kinematic data, and earthquakes in the Trans-Pecos. Kinematic data are from this study, Imrecke et al., 2015 (at Chalk Draw fault), Zimmerman, 2005 (at Old Ore Road), and Conley et al., 2023 (in Indio Mountains).	54
Figure 3.1. Interpretive wayside exhibit presented on a 42 in. by 24 in. kiosk at the Goat Mountain parking area on Ross Maxwell Drive in BBNP.	64
Figure 3.2. Map of Laramide fold axes, monocline hinges, and reverse faults in the Big Bend area.....	65
Figure 3.3. Geologic map of the Dog Canyon area.	67
Figure 3.4. Photo looking north-northeast over Dog Canyon from the western (upright) limb of the footwall syncline within the Kdr (Del Rio Clay) as a group of Sul Ross State University Structural Geology students observe folding.	68
Figure 3.5a-e. Orthogonal flexure model, wherein rock in one mechanical layer is extended parallel to the layer boundary in a fold's outer hinge, and shortened parallel to the boundary in the inner hinge...70	70
Figure 3.6. Southward-up geologic map of the Dog Canyon area showing cross section line (blue).....	72
Figure 3.7. Mechanical-strain models used to map fractures and interpret strain axes.....	73
Figure 3.8. Traces of structures possible at fault terminations.	73
Figure 3.9. Orthomosaic of southern wall used as a base map in Dog Canyon.....	76
Figure 3.10: Vertical geologic map, remotely interpreted from orthomosaic, with traces of bedding, fractures, and fault surfaces mapped.	77
Figure 3.11. Section of cliff wall with conjugate shear fractures (green.)	79
Figure 3.12. Mode I fractures (yellow) perpendicular to bedding surface (blue) indicating outer-arc stretching.	80
Figure 3.13. Mode I fractures (yellow) "inside" three separate pull-apart structures bounded by bedding (blue) and fault (red) surfaces. Also in this location are fault terminations mapped as splays (upper left) and wing cracks (lower right,) although the latter may be instead mapped as Mode I fractures indicating sense on that fault.	81
Figure 3.14. Faults (red) and bedding surfaces (blue) in places are difficult to distinguish.	82
Figure 3.15. Bedding surface (blue) interpreted to be offset by fault (red) in upper left quadrant of image.....	82
Figure 3.16. Small fault (red) offsetting bedding surface (blue) in a reverse sense.	83
Figure 3.17. Apparent-view geologic cross-section through south wall of Dog Canyon (looking southeast and south).	84
Figure 3.18. Pi-diagram calculation of the fold axis.....	85
Figure 3.19. Two pull-apart structures on Dog Canyon's south wall at the canyon floor with annotated senses of motion (arrows) and locations of measured slickenlines (red squares).	87

Figure 3.20. Slip surfaces with slickenlines measured at ground level in Santa Elena limestone in Dog Canyon.	88
Figure 3.21. Structural cross section restored to before normal faulting shows the fault-propagation fold of the Santiago thrust.	90
Figure 3.22. Oriented strain ellipses interpreted from fracture orientations.	92
Figure 3.23. Proposed geologic history of the Dog Canyon area from earliest to most recent.	93
Figure 3.24 Plan for interpretive wayside exhibit at end of Dog Canyon trail.	96
Figure 4.1. Example of unordered data.	104
Figure 4.2. Student groups by academic major.	117
Figure 4.3. Student groups by population of their hometowns.	117
Figure 4.4. Student groups by their previous experience with science.	118
Figure 4.5. Percent of scores attained by students in the local (LG) and global (GG) data groups by type of questions, across all exercises.	119
Figure 4.6. (a) Percentages of each score (0, 1, 2, and 3) for all knowledge-retention questions across all exercises.	120
Figure 4.7. Percentages of scores of student responses to questions on the post-structure-exercise survey.	122
Figure 4.8. Percentages of scores of student responses to questions on the survey following the earthquake exercise.	123
Figure 4.9. Percentages of scores of student responses to questions on the survey following the volcanoes exercise.	124
Figure 4.10. Percentages of scores of student responses to questions on the survey following the climate exercise.	125
Figure 4.11 Percentages of scores of student responses to questions on the survey following the floods exercise.	126
Figure 4.12. Ranked scores from questions following the earthquake exercise.	128
Figure 4.13. Ranked scores from questions following the floods exercise.	129
Figure 4.14. Final survey relevance-ranking results from students at SRSU.	131
Figure 4.15. Comparisons between ranking results on end-semester and beginning-semester surveys among SRSU students.	132
Figure 4.16. Comparison of student scores within data groups but between exercises.	138

CHAPTER 1: INTRODUCTION

The Big Bend region of west Texas exposes well preserved evidence of the two most recent major tectonic events from western North America's geologic history: 1) Late Mesozoic- early Cenozoic contraction synchronous with the Laramide orogeny and with Mexican folding and thrusting, and 2) Late Cenozoic Rio Grande rifting. This area has 4,500 square kilometers of public land between Big Bend National Park (BBNP) and Big Bend Ranch State Park, and abundant annual visitorship from tourists and from undergraduate geology classes from Texas and Louisiana universities. Some of the undergraduate field trips target well exposed and condensed extensional and contractional geologic structures for geologic mapping exercises. Because of the striking exposures, both parks particularly emphasize geologic history as part of their public educational outreach to visitors. This dissertation has taken advantage of such accessible exposures in and around BBNP and contributes to the understanding of Rio Grande rift and Laramide contractional tectonics in the Big Bend area. This dissertation also aims to contribute to general geoscientific literacy among people in non-STEM fields, imperative for this country's prosperity as human society continues to push against tightening ecological limitations, assessing how undergraduate students' interaction with geoscientific data affects their perception of geology's relevance.

In Chapter two of this dissertation, new and published extensional-fault kinematic data from around the Big Bend area are compiled with new U/Pb ages of syn-rift fault rocks to propose a geologic history of both the southern rift and the regional strain field. These results are compared with existing models from the more thoroughly investigated segment of the Rio Grande rift in New Mexico and from the Basin and Range province. This study therefore represents an important contribution to our

understanding of the evolution of the Rio Grande rift in an understudied segment of this important structural feature.

Chapter three presents a structural analysis of a Laramide-age footwall syncline exposed in a canyon cut through a Rio Grande rift horst block within the easternmost part of BBNP and which is reached by a popular hiking trail. The fold offers an exceptional opportunity to investigate models of fold formation in contractional environments by mapping minor structures along its arc. Because the outcrop is not accessible above the floor of the ~60 meter cliff face, drone imagery was collected and merged into a basemap on which to map and interpret the minor structures. The results of this study are reported here and are further presented in a single-panel visual display to be exhibited on an educational wayside exhibit installed by the National Park Service at the trail end.

The investigation presented in Chapter four is also concerned with increasing public geoscientific literacy but this time in querying undergraduate students of all majors in core geoscience classes at two universities near the Big Bend. In this case study, enrolled students participated in five quantitative in-class exercises working with real geoscientific data of either a local or a global source. These two separate student groups, exposed to either local or global data, were then surveyed on their engagement, content retention, critical thinking skill, and perception of the relevance of the exercise topic. Results of this study demonstrate that even non-geoscience majors show more critical thinking ability and are more impressed by the relevance of geoscience to human society when they work with real geoscientific data that are local in origin, as opposed to data that are globally sourced.

CHAPTER 2: KINEMATIC AND GEOCHRONOLOGIC EVIDENCE DOCUMENTING
ROTATION OF CRUSTAL EXTENSION AND NARROWING OF RIFT FAULTING IN THE
SUNKEN BLOCK GRABEN OF THE SOUTHERN RIO GRANDE RIFT, TRANS-PECOS
TEXAS

2.1 Abstract

New fault-lineation data from twenty normal and strike-slip faults across the Sunken Block and Black Gap grabens in the southern Rio Grande rift of Trans-Pecos Texas delineate separate directions of principal stretch (S1) through the southern rift's extensional history. Three U/Pb ages of oriented calcite slickenlines in the Sierra del Carmen and Black Gap graben constrain a NE-SW orientation of S1 to at most 30.1 ± 3.1 Ma and at least 13.7 ± 0.9 Ma. The latter agrees with a suspected ~ 10 Ma clockwise rotation of S1 from NE-SW to NW-SE that lacks local age control but correlates to a widely cited regional clockwise shift in tension and extension reported in the northern Rio Grande rift and the Basin and Range province. Age constraints defining the progressive rotation of S1 in the southern Rio Grande rift also suggest that later faulting narrows into the Sunken Block graben, with at least the original faults outside of the eastern edge of the Sunken Block abandoned some time before onset of NW-SE stretch. Questions remain about the involvement of the Border Corridor Transform Zone to the west and northwest of the Sunken Block. Also, NNE-SSW extension may be the most recent S1 orientation in the Sunken Block and may be affected by the Southern Great Plains region as it correlates with stretch directions inferred from downhole stress data in the Delaware and Midland basins.

2.2 Introduction

The Rio Grande rift is a focus of continental extension in the western North American plate that trends from southern Colorado to northern Chihuahua (Figure 2.1). The rift has been active for 30-35 million years, following regional Laramide deformation and widespread magmatism across western North America. Multiple studies have focused on kinematic analysis of normal faults of the northern and central segments of the rift (from northern to southern New Mexico; e.g. Liu et al., 2019; Minor et al., 2013; Caine et al., 2017; Rodriguez-Gonzales, 2019), but similar studies are largely lacking in the southern rift (from Van Horn south-southeastward to the Big Bend region of Trans-Pecos Texas and Chihuahua.) The extensional province in southwest Texas has been referred to as either the easternmost province of the Basin and Range (e.g. Henry, 1988; Maler, 1990) the southern extent of the Rio Grande rift (e.g. Dickerson & Muehlberger, 1994; Dickerson, 2013) or both, wherein either the rift in the Trans-Pecos is a subprovince of the Basin and Range province (e.g. Page et al., 2008) or the Basin and Range is equated to “rifting across the western North American crust” (Henry, 1998). Ricketts and others (2021) concluded from multiple data sets that areas east of Deming, New Mexico are part of the southern Rio Grande rift. In this paper I will refer to this region as the southern section of the Rio Grande rift, the Trans-Pecos section of the Rio Grande rift, and as the southern rift.

This paper presents a compilation of new and published kinematic data from extensional faults of the southern section of the Rio Grande rift in west Texas southwest of the Pecos River (Trans-Pecos Texas). These data document an evolving strain field in the southern Rio Grande rift and provide a critical new dataset for testing models of extensional strain that have been proposed for the Rio Grande rift. This project uses kinematic and geochronologic data to answer two main questions: (1) What is the strain history of the southern Rio Grande rift in Trans-Pecos Texas since ca. 35 Ma, and (2) How does strain in the southern segment of the rift compare to other parts of the Rio Grande rift?

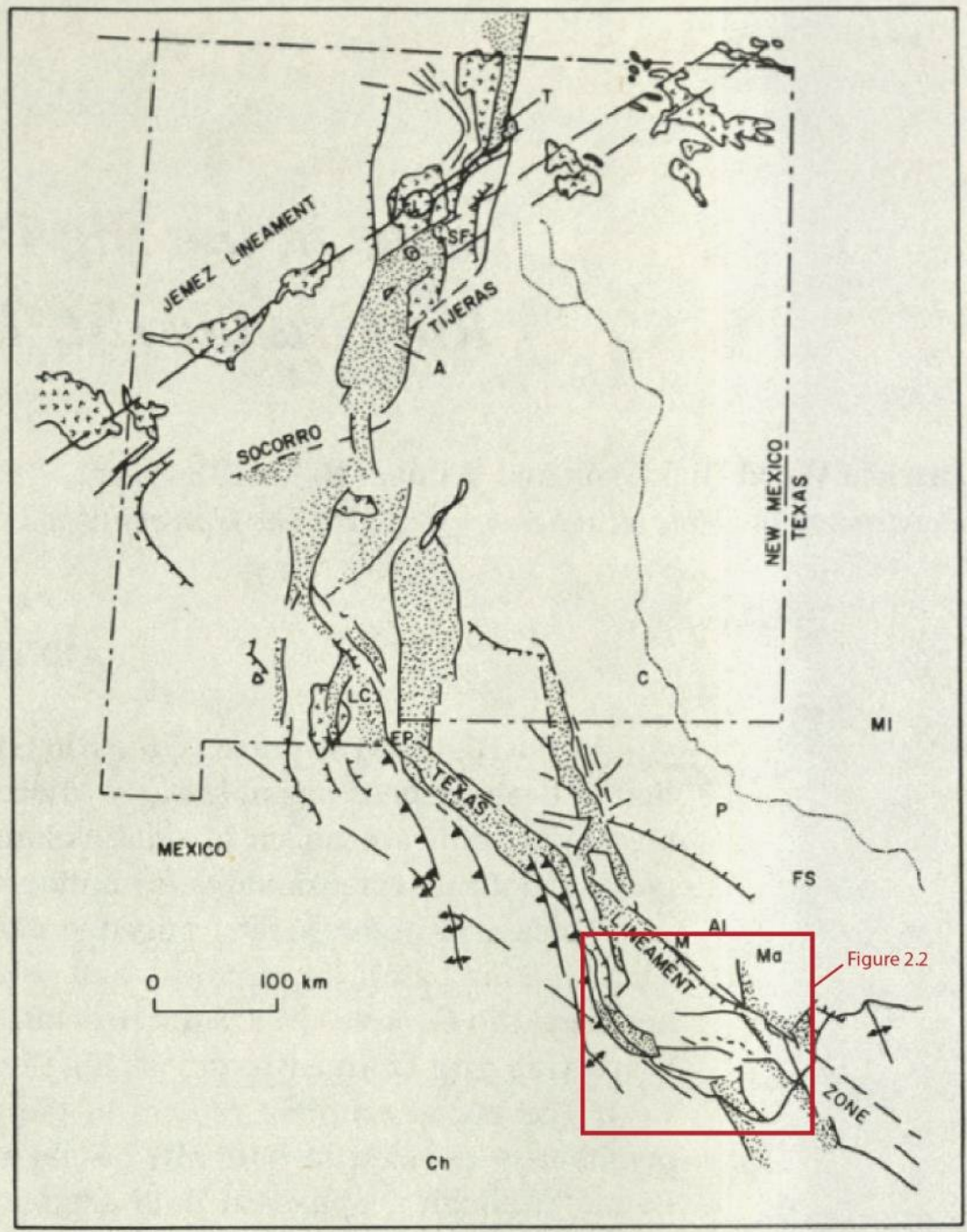


Figure 2.1. Outline of basins of the Rio Grande rift and other tectonic elements in New Mexico, west Texas, and northern Chihuahua. Figure is from Dickerson and Muehlberger, 1994. Dotted line is Pecos River defining eastern boundary of Trans-Pecos Texas. Dashed line in Texas and Chihuahua outlines the Texas Lineament of Muehlberger, 1980. A, Albuquerque; Al, Alpine; C, Carlsbad; Ch, Chihuahua; EP, El Paso; FS, Fort Stockton; J, Jemez Mountains; LC, Las Cruces; M, Marfa; Ma, Marathon; MI, Midland, P, Pecos; SF, Santa Fe; T, Taos.

2.3 Background & Previous Work

2.3.1 Geology of the southern rift

The Rio Grande rift in the Big Bend portion of Trans-Pecos Texas is defined by north-northwest-striking, steeply dipping normal faults that accommodate no more than 10% extension (Henry and Price, 1986; Henry, 1988), and by west-east-striking dextral-normal faults that transferred that extension eastward from the trend of the Rio Grande rift in New Mexico (Dickerson and Muehlberger, 1994). This system of fault initiated during the late Oligocene. Extensional features are superimposed on older contractional structures and basins that formed approximately 75-50 million years ago coincident with the Laramide Orogeny (e.g., Lehman, 1991; Moustafa, 1988). These contractional structures have since been dissected and are now exposed within Cretaceous marine rocks that lie along rift flank uplifts. Because of a regional southward dip, evidence of the late Paleozoic Ouachita Orogeny is also observable in the middle and late Paleozoic sedimentary rocks exposed in the Marathon fold-thrust belt north of Big Bend, and a small window through an early Oligocene laccolled area.

Rocks exposed at the surface in the Big Bend area predominantly include Albian through Santonian limestones, Campanian through Eocene clastic rocks, and 48-17 Ma intrusive and extrusive igneous rocks of the Trans-Pecos magmatic province. Of the latter, all rocks younger than 25 Ma are syn-extensional, and they have a primitive composition indicating infiltration of the lithosphere by asthenospheric material (James and Henry, 1991; Dickerson and Muehlberger, 1994; Dickerson, 1995; Henry et al., 1991; White et al., 2006.)

This is also an area of elevated heat flow, with both active hot springs (Dickerson & Muehlberger, 1994; Henry, 1977) and warm-spring travertine deposits as young as mid-late Pleistocene (Dickerson, 2013). Several hot springs and hot wells are mapped in central and northern Presidio graben and ~15 km west of the southwest corner of Presidio graben at Peguis canyon in Mexico (Figure 2.2;

Henry, 1977). A well just south of Chalk Draw fault yields hot water (Dickerson and Muehlberger, 1994). Hot springs also flow in Tornillo graben at Hot Springs and Boquillas canyons of the Rio Grande in the southeast Sunken Block, and 2 km west of Manuel Benavides on Rio San Carlos (Henry, 1977; Figure 2.2). Henry (1977) compiled reports to reveal an increase in thermal gradient from central into Trans-Pecos Texas toward the Rio Grande from 15-18°C/km to 18-29°C/km.

The Sunken Block of Udden (1907) occupies most of the Big Bend area from the NE-dipping Terlingua fault at Santa Elena Canyon northeast to the western edge of the Sierra del Carmen. There is no thick and widespread late Cenozoic unit filling the Sunken Block, but smaller grabens locally have approximately 1 km of basin fill (Dickerson and Muehlberger, 1994). The Sierra del Carmen east of the Sunken Block, with the Black Gap graben on its east, is not a simple horst block but consists of elevated blocks of bookshelf-style normal faulting and several large conjugate normal faults (Turner et al., 2011).

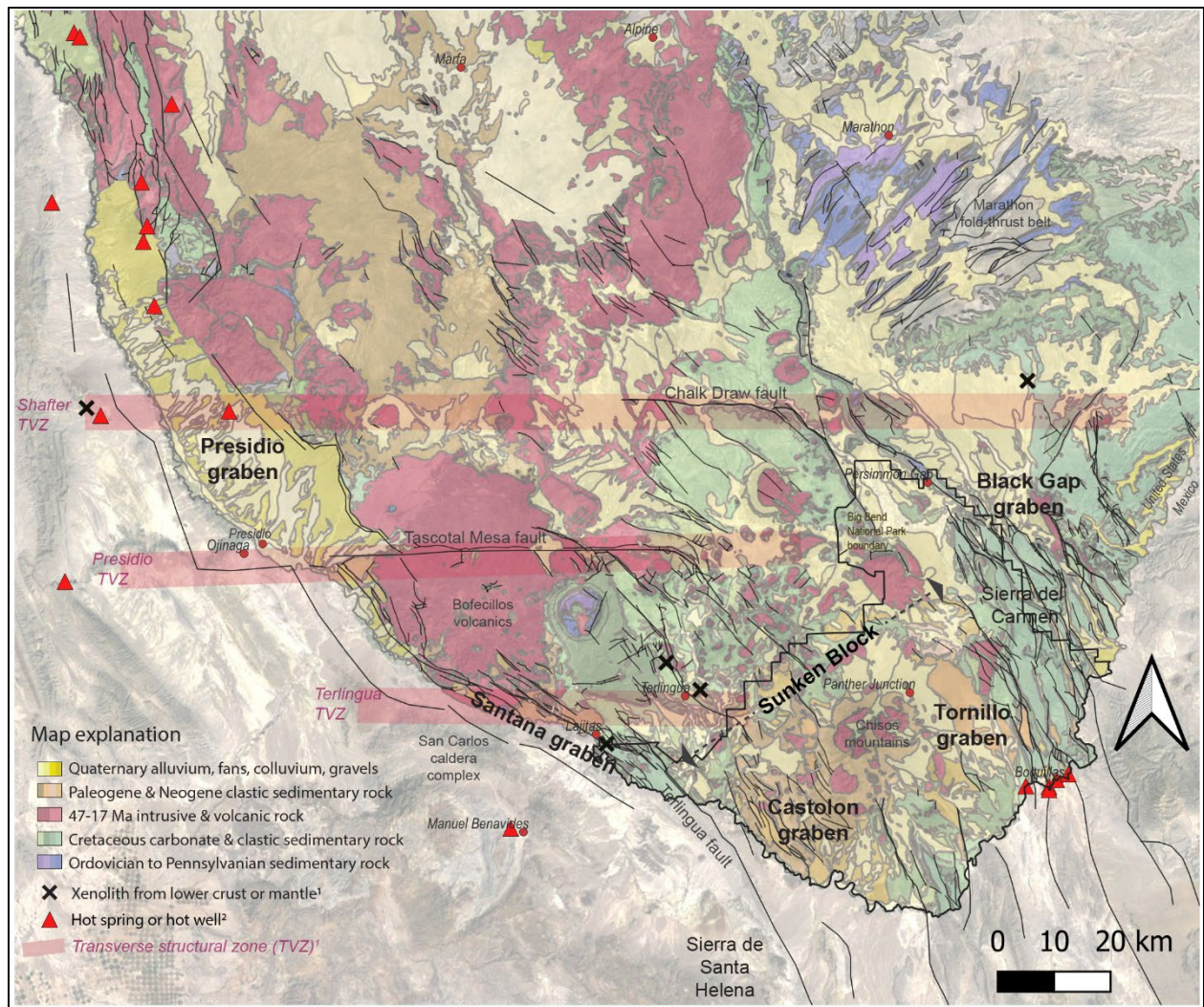


Figure 2.2. Map of the Big Bend area of Trans-Pecos Texas showing grabens and geographic and geologic features mentioned in text.1: Dickerson and Muehlberger, 1994. 2: Henry, 1977. Geology from Texas Bureau of Economic Geology.

2.3.1.1 Basins of the southern Rio Grande rift

Major grabens of the Big Bend segment of the southern rift include, from west to east, Presidio, Santana, Sunken Block, and Black Gap grabens (Figure 2.2). The Sunken Block contains two smaller half-grabens, the Castolon and Tornillo grabens, which dip away from the mini-horst of the pre-rift Chisos mountains magmatic complex (Dickerson and Muehlberger 1994; Page et al., 2008; Figure 2.2).

The western limit of the Sunken Block is the Terlingua fault zone, also the western limit of the Castolon graben. The NW- and NNW-striking, down-to-northeast Terlingua fault has approximately 855 m of stratigraphic offset at Santa Elena Canyon on the Rio Grande, increasing to at least 1,350m approximately 15 km south of the canyon where the fault is the eastern escarpment of the Sierra de Santa Helena or Sierra Ponce (Dickerson and Muehlberger, 1994). The eastern boundary of the Sunken Block is the west side of the Sierra del Carmen (also referred to as Sierra del Caballo Muerto or Dead Horse Mountains). The eastern boundary is not a single fault but a series of northwest and north-northwest-trending faults that left-step to the southeast in Big Bend. The eastern margin of the Sunken Block in Mexico is reported to have 1,800 m of relief (Charleston, 1981).

The northern edge of the Sunken Block is defined by the steep, down-to-the-north Chalk Draw fault. Northwest-striking faults of the northern Sunken Block are the ends of the east-west-striking transfer zones (Chalk Draw and Tascotal Mesa) that transfer extension east of the Presidio graben (Dickerson and Muehlberger, 1994). The Tascotal Mesa fault zone has accumulated 735 m of normal displacement on NW-striking pull-apart faults and ~1 km of dextral offset along the main fault, which has also recorded some vertical-axis rotation within volcanic rocks along both sides starting in the Oligocene and later than 17 Ma (Dickerson, 2013; Helesic, 2020). Normal faults in the northeastern Sunken Block cut Quaternary alluvium and talus, and the youngest Quaternary detritus is deposited over these normal faults (Satterfield and Dyess, 2007).

Dickerson and Muehlberger (1994) compare the Sunken Block to the San Luis basin of the northern Rio Grande rift. Albeit expressing less structural relief, they describe the Sunken Block as a wide block with two grabens and a central horst. However, the Chisos “uplift” in the center of the Sunken Block is dominantly magmatic and not structural, and the two subbasins are half grabens or asymmetric grabens. When the Trans-Pecos extensional province is considered a rift, the Sunken Block is

either included as part of the Rio Grande rift (e.g. Dickerson, 1995; Dickerson and Muehlberger, 1994) or it is excluded (Olsen et al., 1987, who cite the southern terminus of the Rio Grande rift as the Presidio graben). It is also either included as part of the Texas Lineament (e.g. Moustafa, 1988; Maler, 1990), also referred to as the Border Corridor Transform Zone (BCTZ), or is considered the northern basin of the southern Rio Grande rift past the southeastern terminus of the BCTZ, and may extend the rift southward into Mexico at least 150 km (e.g. Dickerson, 1995; Dickerson, 2013).

The Castolon basin complex inside the Sunken Block is ~20 km x 50 km or longer as it continues south-southeast into Mexico. Burro Mesa fault is the largest of the small-throw, west-dipping faults comprising its eastern edge, and its western edge is the Terlingua fault, also the western edge of this part of the Sunken Block. A 28 Ma rhyolite intruding a fault in the Castolon graben indicates that the earliest normal faulting in Castolon graben is older than 28 Ma. This is the oldest evidence for rift-related faulting in the southern rift (Dickerson and Muehlberger, 1994). Castolon graben clastic sediment fill is approximately 1,000 m thick, and an angular unconformity between the lower and upper Miocene units of that basin fill reveals “structural activity” preceding deposition of the upper Miocene sediments (Dickerson and Muehlberger, 1994). Castolon is the only basin of the southern rift preserving an early structural history with sedimentation. It is also the only basin eroded deeply enough to reveal that it is not notably asymmetric, although this does not reflect all southern rift basins because gravity data show asymmetry in the Presidio graben (Dickerson and Muehlberger, 1994; from La Freniere, 1977).

The 8 km x 20 km Tornillo graben is inside the northeastern Sunken Block. Its eastern edge is shared with that of the Sunken Block as several normal faults that bound the horst block of Sierra del Carmen (Figure 2.2). The down-to-the-north Chalk Draw fault is somewhat on trend but has the opposite polarity of the fault zone at the east edge of the Tornillo basin (Dickerson and Muehlberger,

1994), possibly in part because the intervening, fractured Oligocene Rosillos laccolith diffuses and terminates the Chalk Draw fault at its southeast (Imrecke et al., 2015).

The Tornillo graben is young, with its oldest graben fill dated at 11 to 9 Ma from fossilized late Miocene vertebrates (Stevens and Stevens, 1985). Hot springs occur along the southeastern margin of this graben (Figure 2.2). A fault along Tornillo Creek that partly forms the eastern margin of the Tornillo graben offsets Quaternary calcrete layers (Stevens and Stevens, 1985). The Dugout Wells fault at its western margin also offset Quaternary basin fill (Dickerson and Muehlberger, 1994).

The 22 x 50 km Black Gap graben is bounded on its west by the northwest-trending Sierra del Carmen, which exposes Laramide folds and faults in Cretaceous limestones. Its eastern boundary trends north-south and juxtaposes relatively undeformed Cretaceous limestone against graben fill. Its eastern boundary shows one kilometer of structural relief; a 22 Ma basalt is offset 140 m. A 23 Ma basalt also on the eastern border includes mantle xenoliths (Figure 2.2; Dickerson and Muehlberger, 1994 after Dahl and Lambert, 1986). Young basalt is more voluminous in this basin than any other of the southern Rio Grande rift. The only other young basalt is in the Bofecillos lavas, between the Presidio and Santana grabens.

The Santana graben, also referred to as part of the Redford-Lajitas fault zone (RLFZ), is an overall-east-striking group of horsts and grabens that trend west-northwest, show oblique slip, and whose faults have up to 625 m of vertical displacement (Henry, 1998; Dickerson, 1980; Dickerson and Muehlberger, 1994). It lies within the Santana/ San Carlos caldera complex southeast of Presidio and Ojinaga. The 26.3 Ma Santana Tuff overlays the earliest of these faults, indicating that extension began before 26.3 Ma. These faults are also referred to as "Late Cenozoic" (Muehlberger, 1980), though there is no information about Quaternary movement.

The Presidio graben's western edge has an estimated 900 m of displacement (Haenggi, 1966; Henry, 1977). Hot springs and travertine deposits occur along and near this fault (Henry, 1977; Figure

2.2). Onset of basin development is well constrained at early Miocene by vertebrate fossils and 23-22 Ma K-Ar ages of interbedded lavas slightly unconformable on Eocene-Oligocene volcanic & volcanoclastic rock (Stevens and Stevens, 1985; Dickerson and Muehlberger, 1994). There is Quaternary movement on the west end of the Tascotal Mesa fault where it intersects the southern Presidio graben (Dickerson and Muehlberger, 1994).

2.3.1.2 Border Corridor Transform Zone

A major component of the extensional province in southwest Texas was first named by Muehlberger (1980) as the Texas Lineament Zone, an 80 km-wide northwest-southeast-trending region that extends over 400 km from El Paso southeast to Persimmon Gap and south into north Coahuila along the Sierra del Carmen, and a southwestern edge adjacent to the Chihuahua trough. The southern ends of the southern rift grabens of New Mexico either terminate (Salt basin) or turn (Hueco basin) at the northern edge of the Texas Lineament near El Paso (Figure 2.1; Muehlberger, 1980).

This lineament was renamed, re-outlined, and redefined by Dickerson (1995; 2013) as the Texas-Chihuahua Border Corridor Intracontinental Transform Zone (BCTZ) and cited to act as a transform between, and to link the southern edge of, the N-S-striking Mesilla graben of southern New Mexico and the northern edge of the NNW-SSE-striking Sunken Block of the Big Bend. The BCTZ contains grabens, basement cored uplifts, strike-slip faults and duplexes, and transfer zones of varying scales (Dickerson, 1995; 2013). The BCTZ includes the comparatively narrow northwest- to north-northwest-trending southern Hueco, southern Presidio, and Santana grabens (Dickerson, 2013), but excludes the north- to north-northwest-trending basins of the Sunken Block that presumably extend southward into Mexico as the southern arm of the Rio Grande rift. The BCTZ probably originated at 1.4 Ga (Muehlberger, 1980; Dickerson, 1995), participated in several tectonic events since then, and most recently was repurposed as a rift transform zone.

Transform zones are broad, oblique-slip transtensional steps connecting rift segments that can be hundreds of kilometers long and that are hypothesized to coincide with long-lived deep and wide lithospheric discontinuities (Dickerson, 1995). They contain grabens and transfer zones, also referred to as accommodation zones, which separate asymmetrically dipping rift basins (Rosendahl, 1987). Transfer fault zones form on reactivated supra-crustal ancient discontinuities, while transform fault zones are reworking deep lithospheric boundaries, perhaps deep, steeply dipping suture zones of ancient collisional orogens (Chorowicz, 1989). Both transform and transfer zones can parallel or reactivate ancient structures and strike at a high angle to the rift trend, act as steps between rift segments, and enact transtension (Dickerson, 1995). Both the Tascotal-Mesa fault and Chalk Draw fault are transfer zones within the BCTZ that served to transfer extension ~80km eastward by reactivating similar, east-striking basement structures during ENE extension (Henry, 1998; Dickerson, 2013).

2.3.1.2.1 Transverse structural zones

Grabens of the southern rift are shorter in length than those of the northern rift because “transverse structural zones”, part of the BCTZ, subdivide the region into small structural units. While most basin-bounding faults in the southern Rio Grande rift region including the southern BCTZ strike northwest to north-northwest, those varying-size basins either terminate, change their size or strike, or step laterally at these west-trending discontinuities (Dickerson, 1980; Dickerson & Muehlberger, 1994; Figure 2.2). Dickerson (1980) documents thirteen transverse structural zones between 29° and 31.5° North within the BCTZ. Hot springs, syn-rift basalt bodies, and lower crust or mantle xenoliths are found at a minimum of three of these transverse structural zones, suggesting mantle penetration of the lithosphere along them (Figure 2.2; Dickerson & Muehlberger, 1994). The transverse zones of the southern rift segment or link rift grabens, but ‘none has yet functioned as a transform’ (Dickerson and Muehlberger, 1994).

The Presidio transverse structural zone is at the southern margin of Presidio graben and contains the east-west trending Tascotal Mesa fault zone, which has had a pre- and syn-extensional history and may reactivate a Precambrian fabric (Figure 2.2; Dickerson 2013). Pre-rift volcanism along the Presidio transverse zone occurred from 44 to 27.4 Ma, plus syn-rift primitive basalt at 24-22 Ma and 17 Ma (Dickerson and Muehlberger, 1994; Dickerson, 2013). The Terlingua transverse zone is the southern end of the Terlingua uplift, an eastward-verging Laramide monocline. It links the Santana graben and Castolon graben and is less distinct than the Presidio transfer zone as it is not defined by an east-west dextral fault. It is partially defined by syn-rift 24-20 Ma basalts with lower crust/upper mantle xenoliths including lherzolites, amphibolites, spinel peridotites, and pyroxenites (Dickerson and Muehlberger, 1994; Figure 2.2).

2.3.1.2.2 Basement influence

Basement control on geometry and kinematics of the Trans-Pecos region have been investigated because of oblique patterns of geometry and kinematics in the extensional faults and because of the long and active tectonic history of the region (e.g., Moustafa, 1988; Maler, 1990; Page et al., 2008; Henry, 1998; Dickerson, 1995). The notable normal faults both from extension and contraction in the region trend north-northwest (Figure 2.2), and this trend also parallels at least one Proterozoic rift-related normal fault (Muehlberger, 1980; Whitmeyer and Karlstrom, 2007; Dickerson et al., in prep). Lineations in Bouger gravity and magnetic data correspond to the three transverse structural zones (Dickerson and Muehlberger, 1994, after Keller et al., 1981), of which at least two (Presidio, Terlingua) have been active since at least the Permian (Ammon, 1981; Henry, 1988).

Dickerson (2013) constructed physical models to infer fabrics in the basement below the volcanic and sedimentary cover and concluded that the BCTZ is superposed on a long-lived discontinuity and on an orogenic belt that was active at 1 Ga and 60 Ma as well as on Paleozoic and Mesozoic sedimentary basins. Henry (1998) noted that the geometry and kinematics of the RLFZ can be

reproduced on a model of a west-east-dextral basement discontinuity. He proposed that both the Tascotal Mesa fault and the RLFZ reactivated east-striking basement structures when they transferred extension eastward from the Presidio graben during ENE-WSW extension, and that the basement structure under the single Tascotal Mesa fault must shallow and narrow compared to a deeper and wider discontinuity under the wider RLFZ. Moustafa (1988) proposed a west-northwest-trending basement fabric paralleling the Texas Lineament in the southern Sierra del Carmen east of the Sunken Block because the pull-apart grabens bounded by NNW normal faults terminate against west-northwest en echelon faults, and Laramide monoclines are also terminated by the west-northwest fault zones.

New Mexico rift structures are also superposed on northwest-trending structures at least as old as Laramide (Caine et al., 2017; Rodriguez-Gonzales, 2019.) Rodriguez-Gonzales (2019) determined that east-west tension drove extension through all parts of the New Mexico segment of the rift as well as the northern section of the BCTZ, indicating that differing rift-basin geometries across multiple latitudes in New Mexico manifested from crustal anisotropies that preexisted the onset of that stress field and preempted purely Andersonian extensional failure. Caine and others (2017) hypothesized that west-east strain manifests as differently trending structures because of basement fabrics in the Espanola basin of northern New Mexico.

2.3.2 Previous analyses of extensional strain in the Big Bend region

Northeast-oriented horizontal tensile stress (σ_3) initiating crustal extension in Trans-Pecos Texas may have begun at 31 Ma after a shift from northeast compressive stress (σ_1) during the Laramide contractional event based on dominant dike orientations in the BCTZ south of Van Horn (Price and Henry, 1986). Subsequent total extension in the southern portion of the Rio Grande rift is estimated to be 4-8% over distances of 60-125 km (Dickerson & Muehlberger, 1994; Dickerson 1995). This is less than total extension in New Mexico, which ranges from 8-12% in the San Luis basin (Kluth et al., 1994) to 17-25% in the northern Albuquerque basin (Russell and Snelson, 1994; Roy et al., 1999) to as much as 30-

33% in the southern Albuquerque basin (Russell and Snelson, 1994). Thus, while total extension in the Rio Grande rift increases to the south in Colorado and New Mexico, it decreases again in Trans-Pecos Texas. Stretch in Trans-Pecos TX was first estimated at a direction perpendicular or more westerly to the trend of the TX lineament, or WSW - ENE, based on graben geometry and fault offset (Muehlberger, 1980). Northwest and NNW-trending fractures dated to 23-19 Ma support NE and ENE extension south of Van Horn (Dasch et al., 1969) and in the Bofecillos mountains (McDowell, 1979). In the southern Sierra del Carmen east of the Sunken Block, WNW- and NNW-striking faults occur in right-stepping en echelon zones to create “rhomb grabens” proposed to accommodate dextral motion during extension that defines NE-SW stretch (Moustafa, 1988). Dextral-normal oblique motion is also shown in the west-east-striking faults, which supports NE-SW stretch (Dickerson and Muehlberger, 1994; Henry, 1998; Henry et al., 1991). West-northwest splays from the fault in the Alazan basin accommodated normal motion, and in an extensional duplex of the west-east-striking, dextral-slip Tascotal Mesa fault zone, the northwest-striking, normal-slip Solitario fault offsets 21.6 ± 0.4 Ma basalt, revealing NE-SW extension after the eruption of that flow (Dickerson, 2013; Dickerson and Muehlberger, 1994). Several authors have also documented extension accompanied by right-lateral divergent wrenching on NNW-trending graben faults of the southern rift, however, which accommodates NW-SE stretch (e.g., Dickerson, 1980; Muehlberger, 1980; DeCamp, 1985; Moustafa, 1988).

Locations of published fault-kinematic data predicting stretch direction in the southern rift are presented here and as Figure 2.3. In six locations in the southern parts of the BCTZ between the southeastern Presidio graben and the western boundary of the Sunken Block at the Terlingua fault, Henry (1998) calculated NE-SW to W-E maximum horizontal stretch (S_1) orientations from $\sim 120^\circ$ slickenline measurements on fault surfaces. North of the Sunken Block at the east-west-striking Chalk Draw fault where the fault bends to the southeast, Imrecke and others (2015) analyzed a large population of Mode-I fractures, shear fractures, and fault surfaces near and within an early Oligocene

igneous intrusion concluding dominantly NE-SW-directed extension along this fault segment and at its termination in the laccolith, with a lesser and younger population reflecting northwest-oriented stretch.

Others report sparser fault-lineation orientations as part of broader studies, and among these are disparate directions of stretch in addition to the expected NE-SW orientation. Four measurements of horizontal, dextral-sense slickenlines on the west-east-striking Tascotal Mesa fault indicate a NE-SW stretch direction (Dickerson, 1995). Sixteen lineations on the Burro Mesa normal fault and its splays in the east margin of Castolon graben in Cretaceous clastic rocks show mostly ENE-WSW, and some NNE-SSW stretch axes (Parker, 2022). Three mapped slickenline measurements from normal faults on the east side of the Mariscal Mountain anticline in Cretaceous limestone suggest a NE-SW stretch axis (Dickerson et al., 2010). A normal fault juxtaposing two Cretaceous limestones in Dagger Flat near Dog Canyon preserves two populations of slickenline orientations yielding both NE-SW and W-E stretch (Neufeld and Kelsch, 2023; and this study), although lack of age control on the horizontal slickenlines leaves open the possibility that they may not be part of rifting. Numerous fracture-plane measurements in the Cretaceous rocks hosting the McKinney Hills laccolith may indicate both NE-SW and to a lesser extent NNW-SSE stretch related to extension in addition to laccolith emplacement (Zimmerman, 2005). Nine slickenline measurements from faults offsetting the 32 Ma McKinney Hills laccolith reveal WNW-ESE and N-S stretch (Martin, 2007).

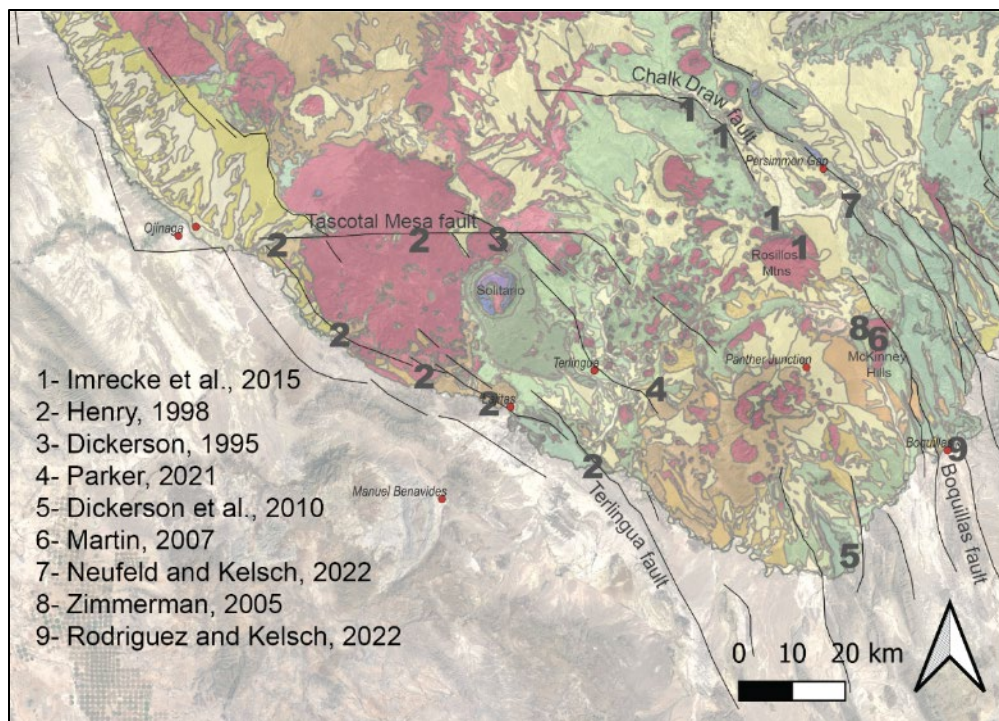


Figure 2.3. Geologic map of Big Bend region indicating location of published extensional-strain determinations referred to in the text.

Some kinematic and geometric evidence from the Big Bend region and BCTZ reveal more than one direction of horizontal crustal stretch at the same locales during the period of late Cenozoic extension. While many reports are of a singular NE-SW or ENE-WSW stretch (S1) orientation, at least a second orientation – either WNW-ESE, NW-SE, or N-S – is also revealed in fault kinematic data and by orientations of dikes of known emplacement age, and also perhaps N-S or NNE-SSW.

Along the southeastern bend of the Chalk Draw fault, abundant northwest-striking mode-I fractures reveal NE-SW stretch are crosscut in some places by fewer, younger northeast-striking mode-I fractures, documenting that a period of northeast-oriented stretch was overprinted by a later, minor phase of northwest-oriented stretch (Imrecke et al., 2015). Other evidence presented from the Big Bend region for two directions of stretch is the Tornillo graben’s north-trending geometry and 11 to 9 Ma oldest graben fill, indicating a later shift from NE-SW to NW-SE extension that correlates to a rotation in stretch direction widely recognized in the southwest (Dickerson and Muehlberger, 1994).

Deformed bedding planes in a 4m x 1m fault-brecciated shear zone adjacent and parallel to the NNW-striking Boquillas fault that offsets two Cretaceous limestone units reveal two perpendicular poles of rotation and directions of motion, one of which is comparable to two perpendicular slickenline orientations on the nearby Boquillas fault (Rodriguez and Kelsch, 2022; this study). The normal dip-slip of these calculated senses of motion matches the normal-sense slickenlines on the adjacent Boquillas fault and indicates NE-SW stretch. The dextral strike-slip of these calculated senses of motion does not match the sinistral slickenlines on the fault and may indicate NW-SE stretch, although since the strike-slip movement is dextral, this may reflect NE-SW Laramide shortening and not NW-SE rift extension. No cross-cutting relationships of shear zone planes assist with this puzzle.

On the west side of the Sunken Block at the NW- to NNW-striking Terlingua fault, DeCamp (1985) observes multiple rake directions on several parallel surfaces and interprets two separate extensional events, but without direct measurement of slickenlines because of inaccessibility: a post-33.7Ma dextral divergent wrenching event expressed by horizontal slickenlines on left-stepping, en echelon, NW-trending faults, yielding northwest stretch, and a late Miocene northeast stretch expressed by dip-slip movement along the Terlingua fault and parallel synthetic faults. DeCamp (1985) had proposed that the NE-SW extension event recorded on these faults was later, only because those lineations were more abundant.

North of the Big Bend region in the Permian Basin, downhole tools record variable current states of maximum horizontal stress in five homogenous regions (Snee and Zoback, 2018). Without inference of tectonic compression these maximum horizontal stress axes must be σ_2 (not σ_1), with σ_1 vertical, and so σ_3 is the linear orientation in the horizontal plane perpendicular to their denoted max horizontal stress and can also be interpreted as maximum stretch or S1. The horizontal S1 axes from this study vary from NE, NW, NNE to NNW across a 400 km region. In the Delaware Mountains and foothills between

the Salt and Permian basins, slickenlines on northeast-striking faults in the Bell Canyon formation reveal NW-SE extension (Hentz and Henry, 1989). These faults are younger than the north-northwest-striking faults, suggesting that ENE-WSW stretch was followed by NW-SE stretch there.

Northwest of the Big Bend region in the BCTZ, silver-copper-lead veins in Precambrian redbeds in the Sierra Diablo and Indio Mountains strike northeast and east-northeast and are presumed to have formed during “later Basin and Range” northwest extension at ~10 Ma (Price and Henry, 1985). Most slickenlines on normal faults in the Indio Mountains document northeast stretch, but a smaller population of slickenlines on the same faults reveal northwest stretch (Rodriguez-Gonzales, 2019; Conley, 2020; Conley et al., 2023). Northwest- and northeast-trending dikes of the Rim Rock dike swarm were analyzed by whole-rock K-Ar ages and determined to document rotation of tension between 24 and 20 Ma from NE-SW to W-E (Dasch et al., 1969). Those ages were confirmed with later mineral K-Ar geochronology but the tension axis was proposed to have remained oriented NE-SW (Henry and Price, 1986).

Several detailed structural analyses from the northern Rio Grande rift segments in New Mexico also document that the orientation of horizontal stretch rotated, with variable timing among the studies. A NE-SW horizontal extension axis is reported to have rotated clockwise to NW-SE at or shortly after 26 Ma near Abiquiu based on onset of sedimentation basinward of northwest-striking faults but perhaps at ~10 Ma on faults farther north (Liu et al., 2019). They also cite a “cryptic” latest stage of north-south extension in the Española basin of northern New Mexico. Caine and others (2019) present kinematic evidence for WNW-ESE stretch in the Española basin and report that it is an anomalous orientation within a regional W-E tension field, perhaps from basin influence. Minor and others (2013) determined that tension in the Santo Domingo basin also rotated from NE-SW to NNW-SSE in Pleistocene time, but that the later rotation was a local effect of bounding-basin influences. From

various locations in the rift in southernmost New Mexico, Carciumaru and Ortega (2017) document earliest brief NE-SW extension rotating to a W-E orientation. Rio Grande rift faults in southern New Mexico also host slickenlines of multiple kinematically distinct populations determining stretch directions of NE-SW, W-E, NW-SE, and N-S (Rodriguez-Gonzalez, 2019).

2.3.3 Previous analyses of calcite slickenlines for fault movement dating

Striated calcite precipitates on fault surfaces can kinematically describe deformation events, and because uranium may substitute for calcium in calcite matrices these precipitates may be analyzed with U-Pb geochronology, or if younger than 1Ma with U-Th geochronology (e.g., Nuriel et al., 2012, Reiners et al., 2018; Yang et al., 2021; Mottram et al., 2020; Eyal et al., 1992). Nuriel and others (2011; 2012) investigated four distinct crystal structures of fault-related calcite occurrences from the Dead Sea fault under cathodoluminescence, with trace-element geochemistry, and by U-Th geochronology to define distinct occurrences of calcite resulting from different geologic events in a fault zone. Where calcite crystals show one bright color in CL light they grew quickly and presumably in one event, whereas lower CL colors correlate to longer crystal precipitation between seismic events. Calcite slickenlines along the Dead Sea fault zone in Nuriel and others' work (2011, 2012) have relatively high chondrite-normalized REE concentrations (approximately between 1 and 10; Figure 2.4) and high (bright) CL colors. The U/Th age of this occurrence of calcite also aligns with known deformation events and so these slickenlines are interpreted to occur syntectonically, synchronous with fault movement. Euhedral calcite vein precipitates in their study which they refer to as 'cement' also have high REE concentrations between approximately 1 and 10 and high CL colors, U/Th ages aligning with deformation events, and therefore also are interpreted to occur syntectonically. Their defined occurrence of calcite coating (on top of calcite slickenlines) displays low chondrite-normalized REE values (approximately between 0.1 and 1; Figure 2.4) and a low CL, and U/Th ages that are between known deformation events, and therefore

their 'coating' category has interseismic origin. Nuriel and others (2012) also noted that all fault-related calcite occurrences display Ce-negative and Eu-negative anomalies, with those anomalies more significant in calcite of the syntectonic occurrences and least in the interseismic 'coating' category. Their data also show a slight Gd-positive anomaly in all samples.

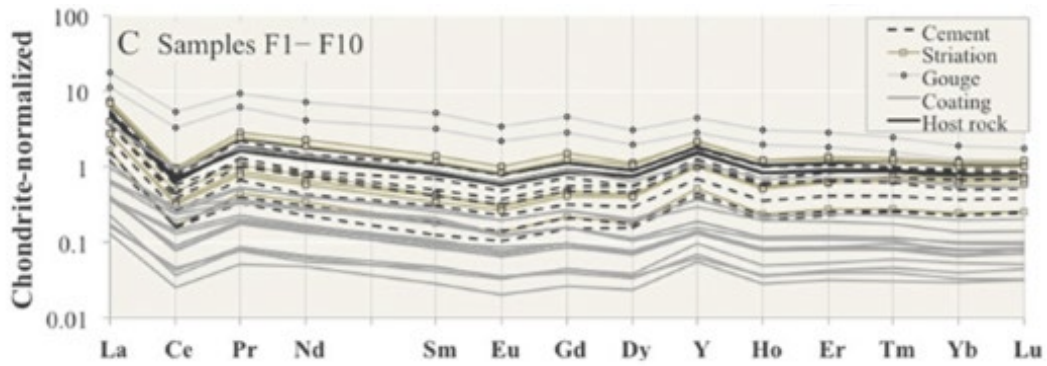


Figure 2.4. REY trends from Nuriel et al., 2012 of their different categories of fault-related calcite occurrence. "Cement" = euhrdal co-seismic veins adjacent to faulted surfaces. "Striation" = syntectonic calcite slickenlines. "Coating" = interseismic precipitates

2.4 Methods

2.4.1 Field analyses: measurement of fault-surface striae and determination of sense of motion

Slip along fault surfaces can be recorded in striations, including lineated mineralized material precipitated and deformed on a fault surface as it moves, or in ridge-and-groove lineations within the host rock scoured as two sides of a fault move relative to each other. Slickenlines reveal the direction of fault-block movement along a fault plane, and either slip-fiber lineations or chatter marks on the fault surface reveal the sense of shear along that direction.

Sites used in this study were selected in several ways: by identification of single kinematic measurements from published maps, by discussion in published work of multiple slickenlines whose measurements were averaged, by personal communication, or by walking mapped fault traces to spot polished slickensided surfaces. 308 measurements of slickenlines from 17 sites were collected to determine slip on these faults; these locations are presented in Figure 2.5. On each lineated fault surface, the planar orientation of fault surfaces and the rake of striations on the surfaces were measured, and sense of motion was determined. Rake was measured as the angle in the fault plane below horizontal and was recorded via the Aki-Richards convention wherein rake value recording reverse motion is a positive-numbered angle above the in-surface horizontal line and rake value recording normal motion is a negative-numbered angle below the in-surface horizontal line (Allmendinger, 2016; Figure 2.6).

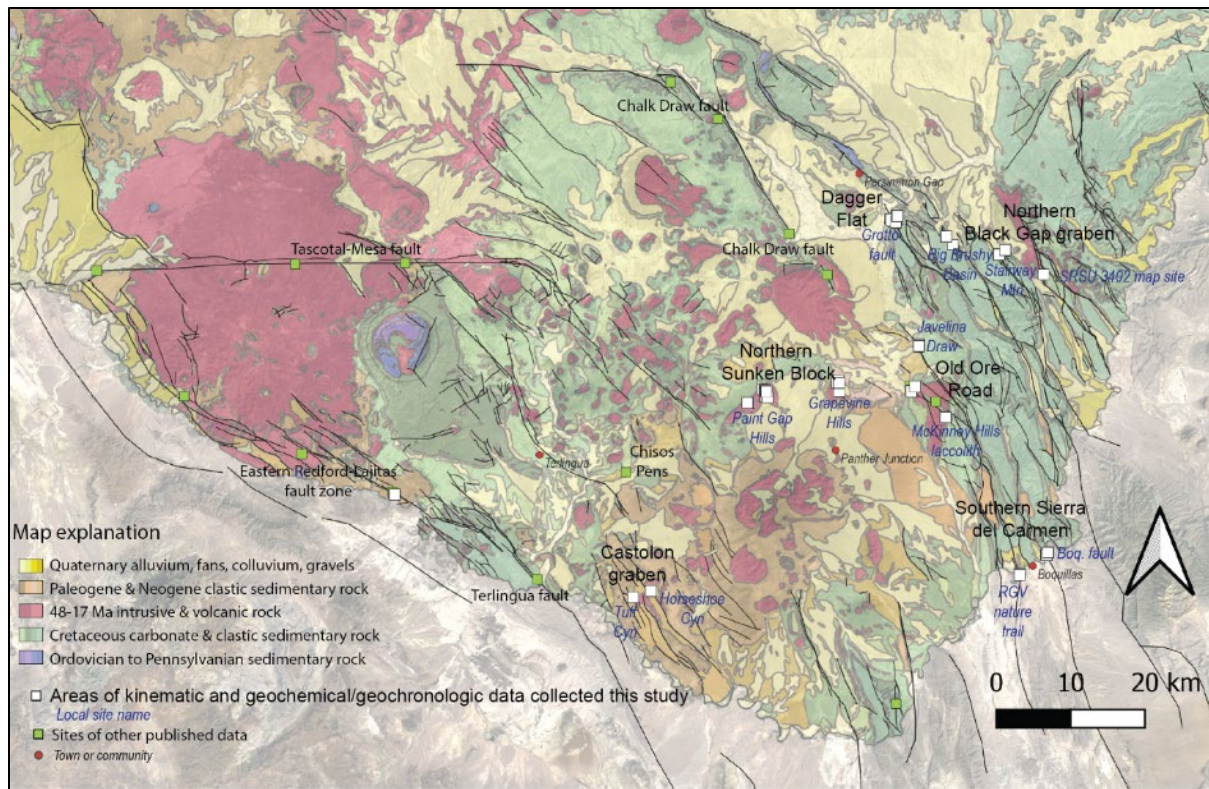


Figure 2.5. Map of Big Bend region of west Texas displaying locations of kinematic measurements. White squares: locations of kinematic and geochemical/geochronologic data collected this study, labeled by six geographic groupings. Green squares: other published data (refer to Figure 2.3 for sources.) The Sunken Block extends from the down-to-northeast Terlingua fault to the down-to-southwest fault cutting the intrusive rock at Old Ore Road.

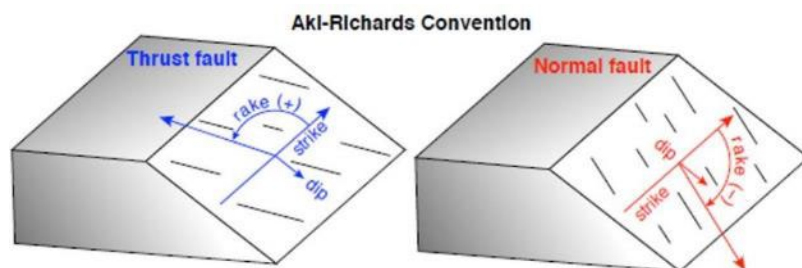


Figure 2.6 Sketch depicting the Aki-Richards sign convention for consistent labeling of thrust or normal sense of motion from fault-surface rake measurements. Figure from Allmendinger, 2016.

Beyond rake measurements which indicate *direction* of fault-block movement, *sense* of motion must also be determined to calculate strain tensors. Sense of motion in this study area is discernable from one of two features formed on rock during fault motion. Slip-fiber lineations are present when

enough material is available to crystallize syntectonically in gaps between fault blocks and to leave a steep “front edge” which maintains the small gap during continued faulting (Figure 2.7, left). In the rocks of this study area that material consists of the components of calcite derived from the ubiquitous Cretaceous limestones that are either exposed along the fault outcrops or are the nearby country rock hosting the faulted igneous rock. An example of calcite slickenlines whose edges also form slip-fiber lineations recording normal motion is presented as Figure 2.7, right.

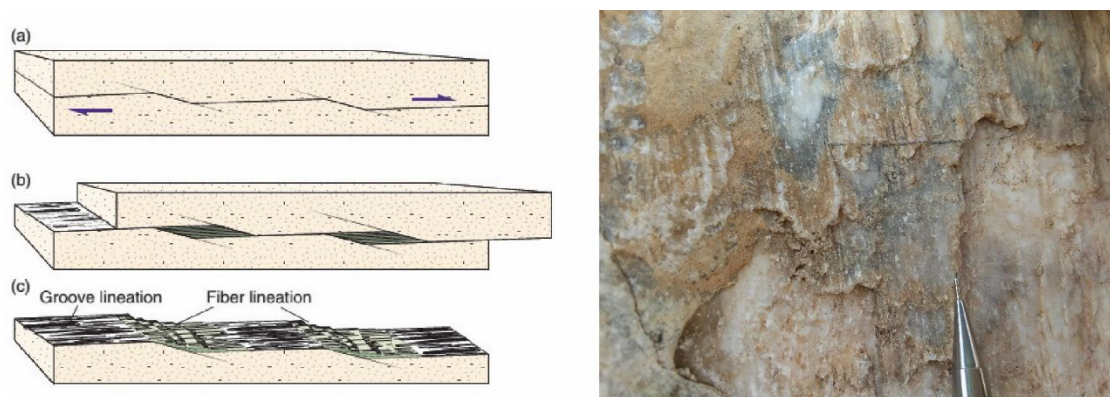


Figure 2.7. Model (left) describing formation of slip-fiber lineations in spaces between faults where new precipitate is striated into slickenlines. Photo (right) shows slip-fiber lineations on normal-fault surface in Dagger Flat. Image on left from Fossen, 2016.

The second of this study’s slip-sense indicators on fault surfaces occurs most commonly in the Oligocene intrusive igneous rocks. These are chatter marks of Petit’s (1987) P-criteria wherein well-polished striations are present on only the stoss sides of an undulating fault surface and no striations are present on the lee sides (Figure 2.8 c). In this case there is not enough crystallization to form slip-fiber lineations. The undulating surfaces are at very low angle to the fault plane and thus the polished stoss and unpolished lee sides may be determined as much by touch as by sight. Also, the T fractures presented in the theoretical figure (Figure 2.8 c) are not apparent in these outcrops though they may continue into the rock unseen (Figure 2.8, right).

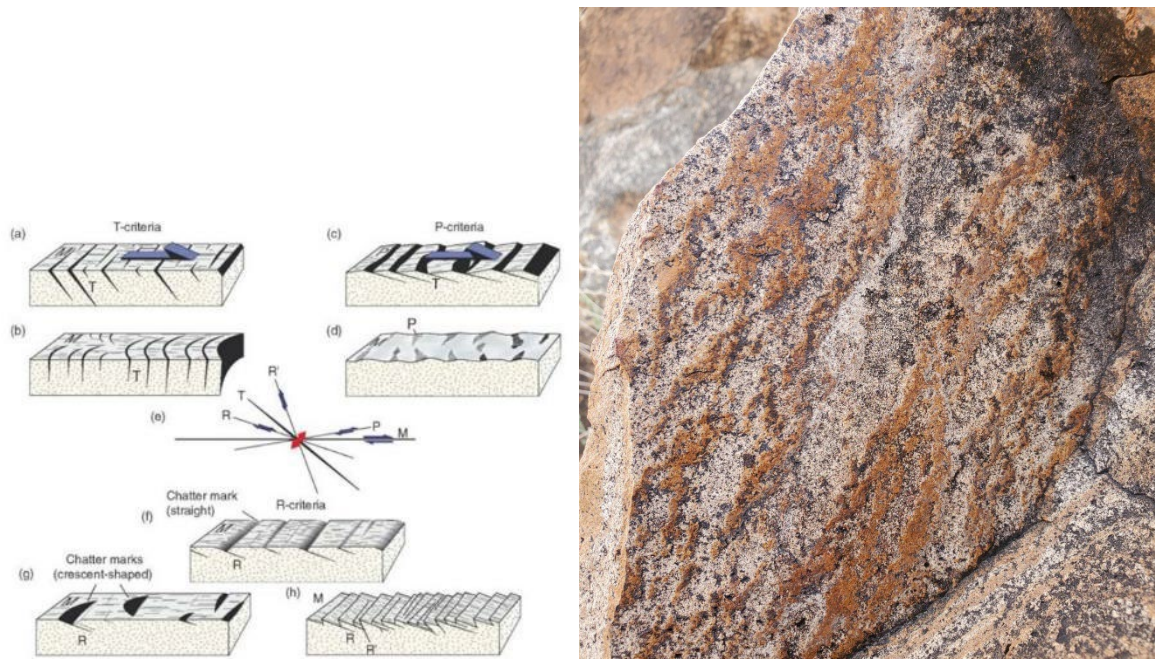


Figure 2.8. Left: Figure from Fossen (2016) after Petit (1987) showing chatter marks possible on top-to-the-right fault surfaces that would indicate sense of motion. Photo on right from Paint Gap Hills is an example of Petit's sketch (c) with polished striations on the stoss sides of very low-relief ridges and neither lineations nor fault mineralization on the lee sides. Fault surface shows that the missing block moved down to the right (oblique sinistral motion.) Field in photo is approximately 0.5m across.

A ranking system was applied to each sense of motion determination grading its confidence from A (highest confidence) and B (high confidence) to C (probable) and D (lowest confidence). Only C and above were included in strain-axis calculations. In some cases sense-of-motion was inferred by geologic relationships and not the outcrop features described above. The same confidence rating applied in these cases. In some cases, sense-of-motion was indeterminate. These were not recorded, or were recorded and discarded.

2.4.2 Computational analyses: Determination of principal strain axes for each measurement and for kinematically compatible populations of measurements

Many studies have used kinematic indicators to calculate orientations of principal stress following the method of Angelier (1984). It is as revealing, and more direct, to calculate strain tensors instead (e.g., Fossen, 2016). Within the framework of Detailed Structural Analysis, kinematic analysis may yield paleostress orientations (e.g. Davis et al., 2011) but determination of paleostrain-axis

geometries in the crust from collected kinematic data is more direct, does not require assumptions about potentially complex rheology, and is ample for the reconstruction of horizontal directions of tectonic plate movements. This study reconstructs paleostress orientations from multiple fault localities. Where previous studies have used kinematic data to report paleostress directions (e.g., Zoback and Zoback, 1980), I correlate their orientation of modern or ancient least principal stress (σ_3) with that of maximum stretch or extension (S_1). I assume a coaxial relationship to strain such that σ_1 parallels S_3 and σ_3 parallels S_1 , even though Edelman (1989) posits that a finite strain ellipse calculated from outcrop measurements may be oblique to the stress field that produced it, and therefore we cannot learn the orientation of paleostress. Despite this, Davis (1996) describes the goal of detailed structural analysis to lead from geometric and kinematic data directly to determination of stress data. Also, Angelier (1984; 1989) defines a method of deducing orientation of the stress tensor responsible for faulting rock via documentation of kinematic indicators on faults. Many studies reporting paleostress probably interpret the same orthogonality to deduce stress from strain, however, so it is likely legitimate to correlate orientations of stress and strain as orthogonal counterparts when citing published stress determinations.

Principal strain axes T (extension, or S_1) and P (shortening, or S_3) were calculated within the FaultKin8 program (Marrett and Allmendinger, 1990; Allmendinger et al., 2012) from fault kinematic data collected in the field. Required inputs to FaultKin for each calculation of minimum and maximum stretch axis are strike, dip, rake, and sense of motion. For each of these measurements FaultKin computes the plunge and trend of its three orthogonal strain axes (S_1 or T, S_3 or P, and also the intermediate S_2) using the linked Bingham method (Allmendinger, 2016). Each individual fault-surface measurement with its kinematic information makes a pair of P and T axes but in this study of an extensional tectonic system just the trend of the S_1 or T axis is of interest and is reported. Kinematic

data, which include field measurements and the T-axis trend computed by FaultKin, are presented as Appendix 1.

To determine the orientations of stretch axes that are most representative in each of the six different grouped regions, kinematically compatible populations of fault measurements with the most individual line-plane data in a group were determined. To find these populations, all data for one region were plotted in FaultKin including each fault's P and T axes. FaultKin computes an average set of strain axes from any plotted population as well as the 3D fault-plane solution of conjugate quadrants of extension and contraction that conform to those three axes (Figure 2.9). From this display inside FaultKin any individual fault-lineation measurements' strain tensors that do not align with the calculated strain quadrants can be manually unchecked to be removed from the plot, which refreshes the calculated average on screen to only consider fault measurements that are shown. Continued manual deselecting of individual faults' measurements allows for definitions of populations or sets of faults that do align with a given orientation of strain axes. Depending on which individual fault measurements were toggled off first each resultant set of average strain axes may differ slightly. For this reason each location was iterated several times to ensure that the T-trends of each population were similar each time.

Because FaultKin defines 3D quadrants with the S1, S2, and S3 axes, kinematic compatibility requires those fields of extension and contraction to be maintained by both the trend and the plunge of each component kinematic axis, and two separate resultant populations may have similar or identical S1 trends. They are still presented as separate populations and noted where that is the case.

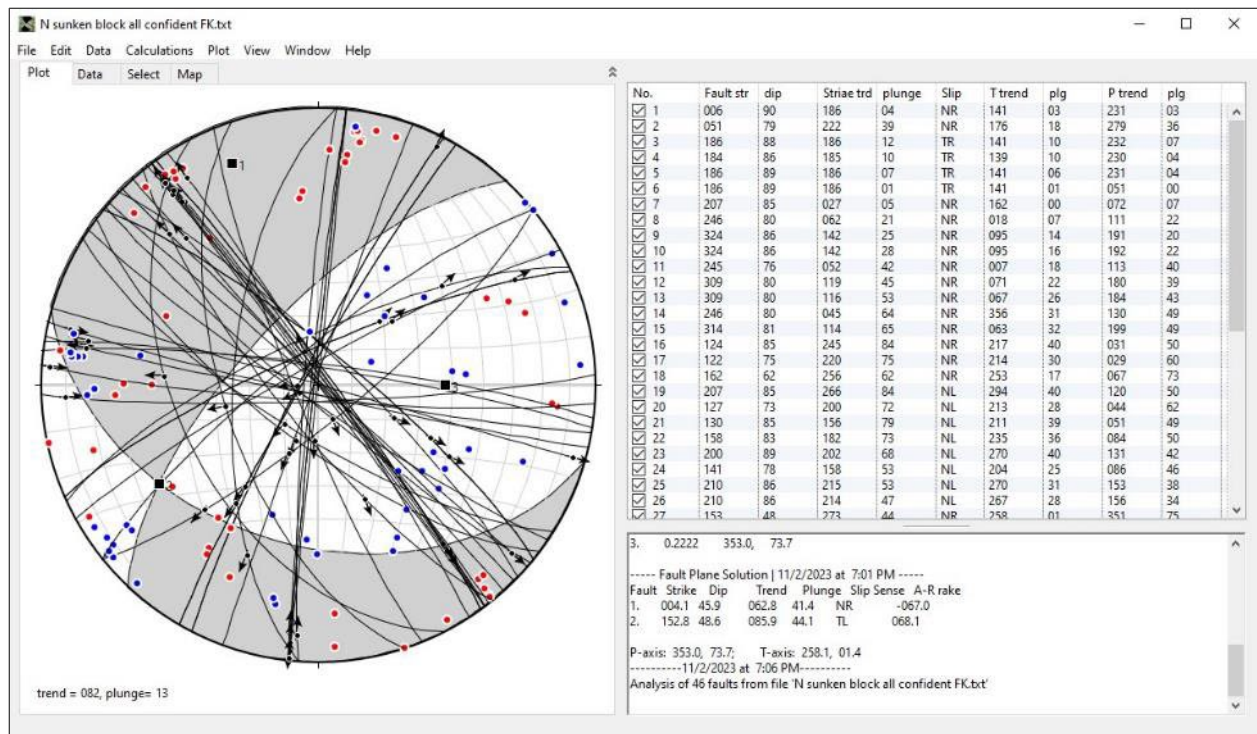


Figure 2.9. Plot in FaultKin8 of all kinematic data for the northern Sunken Block's measured faults showing the orientation of individual fault surfaces (black great circles,) slip direction (black dots) and sense (black arrows,) and each fault's calculated P (blue dot) and T (red dot) axis. Also shown are quadrants of stretch (grey) and contraction (white) corresponding to the average S1 ("1") and S3 ("3") axes that are averages of the individual measurements. The upper right panel lists each fault-orientation measurement and allows one at a time to be plotted such that the stereonet is recalculated.

After kinematic grouping for each of the six grouped locations, trends of the stretch orientations for all populations at each location were arranged along a SW to NE cross-section of the study area to look for patterns.

2.4.3 Geochronologic and geochemical analysis of co-seismic calcite slickenlines.

Where precipitated calcite slickenlines were present and extractable from a fault surface, samples of the calcite were collected for absolute-age determination via U/Pb geochronology after in-situ orientation data were collected. Primary sampling targets were from the syn-tectonic 'striations' category of Nuriel and others (2012); 30 of these were collected. Secondly, two samples of euhedral calcite adjacent to the collected striated surface were analyzed to determine whether they were from

the coeval, syntectonic 'cement' category. Samples were visually assessed for ample volume and absence of weathering and then three subsamples were collected from each selected sample by drilling to obtain ~500mg of powder which was homogenized using an agate mortar. Samples were analyzed for U/Pb ages at the CEEIR laboratory at UTEP following techniques described in Yamaoka and others (2016).

2.4.4 Trace-element analysis of co-seismic calcite slickenlines

Because two of the first batch of four samples returned with very high errors, subsequent samples were first analyzed to ensure adequate U concentration for the U/Pb analysis. Because this analysis also yields trace element data, these data were graphed for each subsample to assess correlations between the categories of calcite defined by Nuriel and others (2012).

2.5 Results

2.5.1 Kinematic analysis: stretch axes determined from striated fault surfaces

To build upon the wealth of data collected and assessed by others in various parts of the Big Bend area, I collected kinematic data on mapped extensional faults in the six regions presented in Figure 2.5. Orientations of striated fault planes measured in the field are plotted on lower-hemisphere equal-area stereonet. Photos of select data- and sample-collection sites are presented in Figures 2.10 and 2.11. Data are presented by location from west to east as Figures 2.12 through 2.20. At each of the six grouped locations more than one kinematically compatible population was determined, indicating multiple extension directions and suggesting the possibility of evolving strain fields through time. For each location a P (shortening) and T (extension) axis are calculated from each kinematically compatible population of fault measurements, and the trend of the T axis is presented.



Figure 2.10. Selected outcrop photos of lineations on fault surfaces, all in Cretaceous limestone formations. Pencil, ruler, or compass as scale in all photos except (a) which is ~2m tall in the center. (a) and (b): Boquillas fault in south Sierra del Carmen. (c): Splay of Boquillas fault. (d) – (f): Grotto fault in Dagger Flat. (g) and (h): fault surface in limestone north of Stairway Mountain in Black Gap graben.



Figure 2.11. Selected outcrop photos of lineations on fault surfaces. Pencil, ruler, or pencil marks as scale in all photos except (f). (a) and (b): Tuff Canyon in Castolon graben. (c): Grapevine Hills in northern Sunken Block. (d) and (e): Paint Gap Hills in northern Sunken Block. (f)-(h): McKinney Hills near Old Ore Road. (a) through (g) show fault surfaces in Oligocene igneous rock; (h) shows calcite slickenlines in limestone.

2.5.1.1 Castolon graben

Twenty fault plane and slickenline orientations were collected in Oligocene volcanic rocks in Horseshoe canyon and Tuff canyon (Figures 2.5, 2.11a and b). Population 1 (n=13) includes mostly oblique slip normal faults and yields a T-axis trend of 292° (Fig. 2.12). Population 2 (n=5) faults are normal faults with a calculated T-axis trend of 201°. A third population of faults (n=2) are strike-slip faults that are not compatible with population 1 or 2 and give a calculated T-axis trend of 341°. Interpretations of population 3 are tenuous due to the low number of faults in this group. No cross-cutting relationships were observed.

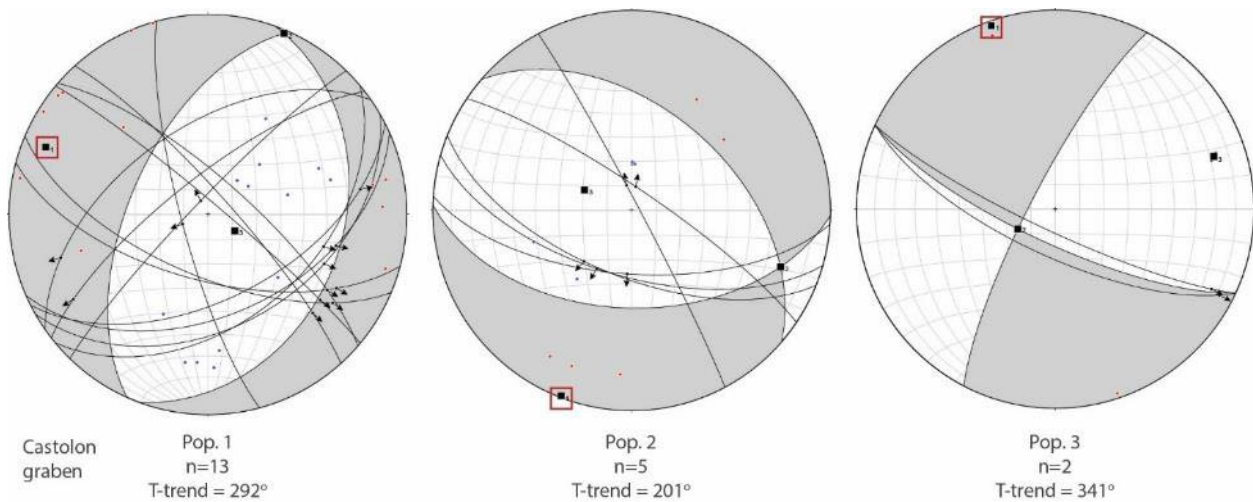


Figure 2.12. Three kinematically compatible populations of fault-kinematic measurements from Castolon graben. Maximum stretch axis is calculated as T-trend, and is labeled with a '1' and boxed in red on the stereonet.

2.5.1.2 Northern Sunken Block

Within the Oligocene intrusions of Paint Gap Hills and Grapevine Hills in the northern Sunken Block, 46 fault plane and slickenline orientations were measured along mapped faults that have no previously published kinematic data (Figure 2.5). These faults cut Oligocene intrusive rocks at the measurement and sampling sites, and Cretaceous sedimentary rocks farther along strike. All measurements were collected in faulted Oligocene igneous rock. Most slickenlines are present on the polished stoss sides of chattermarks (Figure 2.11 c-e), and in one site there is calcite precipitate on the lee sides (Figure 2.11 d and e). These calcite masses were sampled but did not provide enough material

to analyze geochronologically. Kinematically compatible populations of resultant strain-tensor quadrants for the northern Sunken Block measurements are presented as Figure 2.13. Population 1 (n=14) yields a calculated T-axis trend of 148°. These faults are steeply dipping strike-slip faults. Population 2 (n=20) gives a calculated T-axis trend of 187° from oblique-slip faults with variable orientations and dips. Population 3 faults (n=12) are not compatible with populations 1 or 2, and give a calculated T-axis trend of 267°. No cross-cutting relationships between any fault lineations were observed.

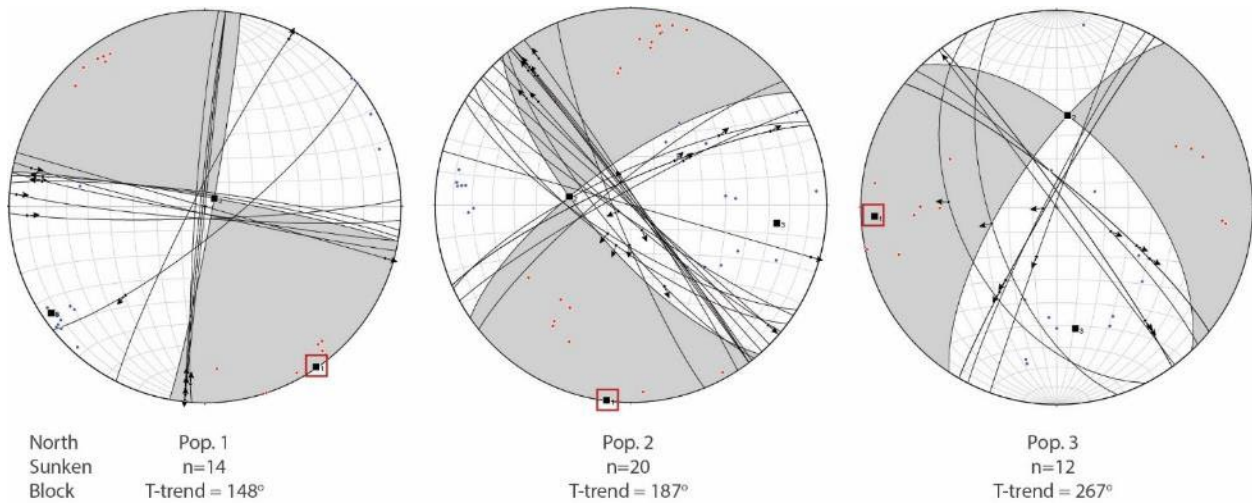


Figure 2.13. Three kinematically compatible populations of fault-kinematic measurements from the northern Sunken Block graben. Maximum stretch axis is calculated as T-trend, and is labeled with a '1' and boxed in red on the stereonet.

2.5.1.3 Old Ore Road

Within the Oligocene McKinney Hills laccolith and Cretaceous limestones at the laccolith's edge, 36 fault plane and slickenline orientations were measured from mapped faults along Old Ore Road (Figures 2.5, 2.11 f-h). Measurements on faults in the igneous rock were taken from either grooved wall rock (e.g. Figure 2.11 f) or weathered mineralized surfaces (Figure 2.11 g), while measurements on faults in the limestone were of calcite slickenlines and slip-fiber lineations (2.11 h). Calculated strain-axis measurements comprise two separate kinematically compatible populations (Figure 2.14). Population 1 (n=24) measurements are from a set of NW-striking, normal to oblique-slip faults and give a calculated

T-axis trend of 070° . Population 2 ($n=12$) includes faults with wide variation in orientation and gives a T-axis trend of 186° .

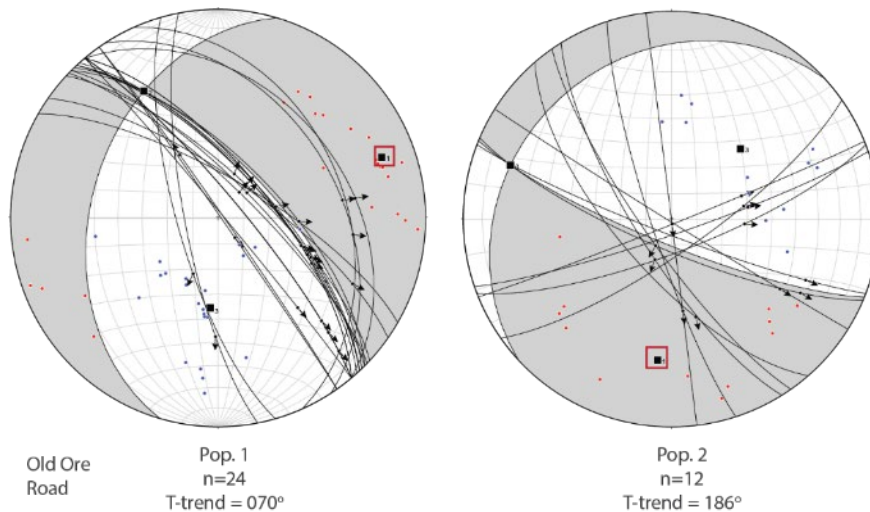


Figure 2.14. Two kinematically compatible populations of fault-kinematic measurements from the Old Ore Road area inside the eastern margin of the Sunken Block. Maximum stretch axis is calculated as T-trend, and is labeled with a '1' and boxed in red on the stereonet.

2.5.1.4 South Sierra del Carmen

This collection of 45 fault plane and slickenline measurements come from the Boquillas fault and a splay along and near Boquillas Canyon trail, and a fault in Rio Grande Village along and near the campground nature trail (Figures 2.5, 2.10 a–c). All faults offset Cretaceous limestones and are mapped consistently in the literature as normal faults. Kinematically compatible populations of resultant strain-tensor quadrants for the southern Sierra del Carmen measurements are presented as Figure 2.15. Population 1 ($n=19$) gives an average T-axis trend of 246° . Population 2 ($n=16$) contains steeply-dipping strike-slip faults that give a calculated T-axis trend of 009° . The T-axis trend for population 3 ($n=10$) is 096° . The visible dip-slip (population 1) and sinistral strike-slip (population 2) slickenlines are shown together in Figures 2.10 b and c on the main Boquillas fault.

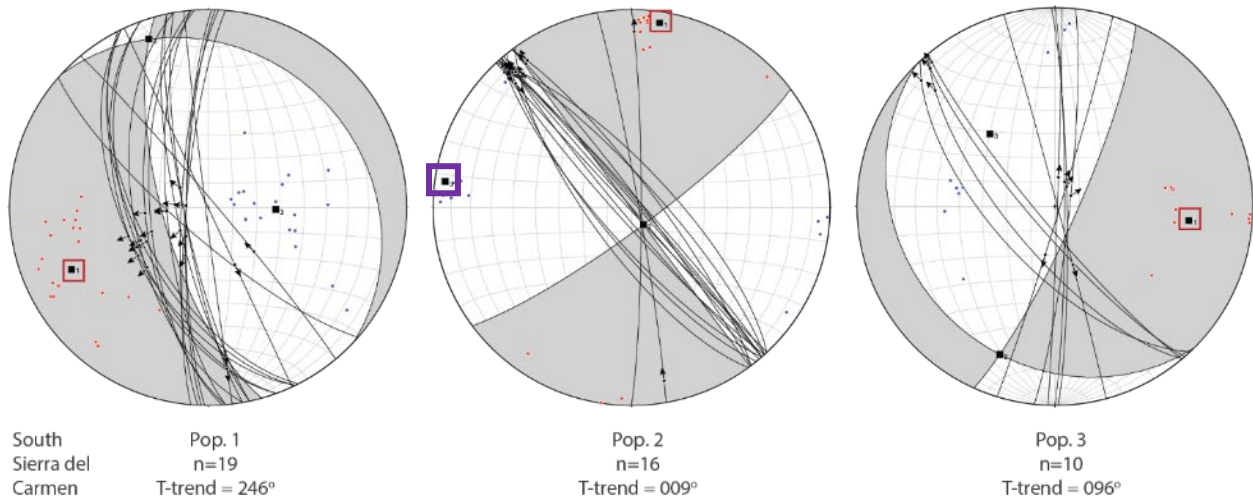


Figure 2.15. Three kinematically compatible populations of fault-kinematic measurements from the southern Sierra del Carmen. Maximum stretch axis is calculated as T-trend, and is labeled with a '1' and boxed in red on the stereonet. Population 2's S3 (contraction) axis is boxed in purple.

Normal dip-slip motion on the steep Boquillas and adjacent faults is clearly extensional, but because the youngest rock faulted in the southern Sierra del Carmen is Cretaceous, attribution of timing of the shallow-rake fault movements is not clear. In addition to the normal dip-slip and sinistral strike-slip motion recorded in slip-fiber lineations on the fault surfaces (Figure 2.10 a-c), an additional kinematic indicator is present in the form of a well-preserved S-C fabric in a brecciated shear zone adjacent to the Boquillas fault surface (Figure 2.16), recording dextral motion along the fault at this location. Stereographic analysis of the dextral S-C fabric reveals motion via a NW-SE extension axis (Rodriguez and Kelsch, 2022). Maler's (1990) analysis of a small pull-apart graben along the Boquillas fault 4 km north of these measurements attributes the fault's sinistral sense to Laramide contraction, and recognizes dextral motion as most likely active during extension. Shallow-rake slip-fiber lineations recording sinistral motion on the Boquillas fault (Figure 2.10 a; Figure 2.15 Pop. 2) may therefore be recording WNW-ESE contraction during regional Laramide shortening and not NNE-SSW tension during rifting. Dextral motion determined by the fault-brecciated shear zone adjacent to the Boquillas fault is

thus more likely to be recording NW-SE extension and not NE-SW shortening. It is possible that this fault has a more prolonged and complex geologic history that may be difficult to unravel.



Figure 2.16. Fault-brecciated shear zone outcropping at base of Boquillas fault. Photo looking approximately west-southwest. Well-preserved S-C fabric at this location shows west-block-to-the north-northwest or dextral motion along this fault. Note the large sigma clasts with asymmetric tails being pointed to.

2.5.1.5 Dagger Flat

Three unnamed faults east of Nine Point Draw primitive campground provided 75 fault plane and slickenline measurements entirely in Cretaceous limestones (Figures 2.5, 2.10 d–f). Like in the southern Sierra del Carmen, these faults only cut Cretaceous limestone and are mapped as normal faults although there are generally two striation orientations on the same NW-striking surface on one of the faults (e.g. Figure 2.10 f). Kinematically compatible populations of resultant strain-tensor quadrants for the Dagger Flat measurements are presented as Figure 2.17. Population 1 (n=62) has a calculated T-axis trend of 251°. The remaining 13 measurements form population 2 with an average T-axis trend of 083°.

Although these two populations give similar T-axis trends, they form different 3D kinematic populations because their P-axes differ.

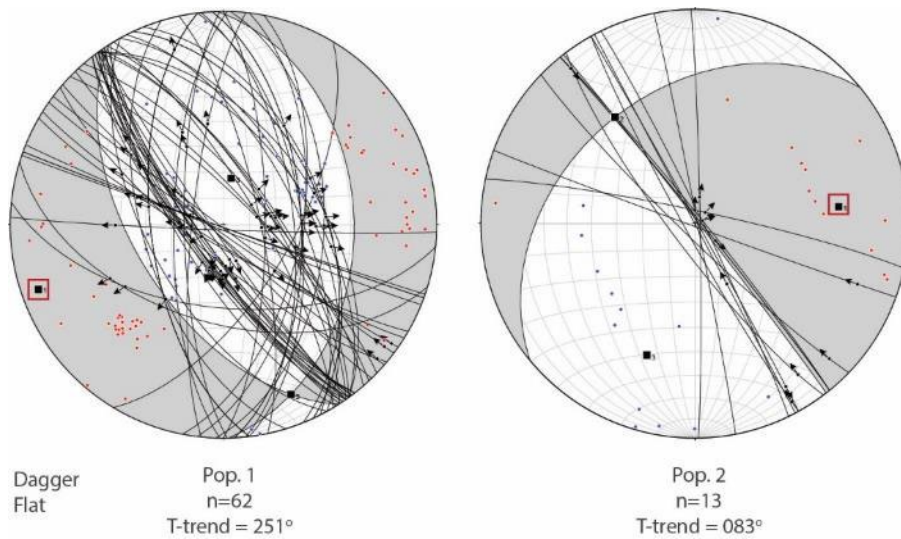


Figure 2.17. Two kinematically compatible populations of fault-kinematic measurements from the Dagger Flat area. Maximum stretch axis is calculated as T-trend, and is labeled with a '1' and boxed in red on the stereonet.

Because the measured faults in Dagger Flat only cut Cretaceous limestone units, the same ambiguity of attribution of strike-slip motion applies here as it does in the southern Sierra del Carmen. Dip-slip motion on steeply dipping faults is easily attributable to extension (Population 1; Figure 2.17 left), but W-E stretch determination from dextral-oblique slip (Population 2) may actually be N-S contraction. Further, sense indication is most confident for the dip-slip population of slickenlines while the dextral sense determination has probable confidence. No surface was found with clear cross-cutting relationships between the two populations of striation orientation, as even where they are proximal they are on separate planes within the fault zone.

2.5.1.6 North Black Gap graben

Unnamed faults cutting both early Miocene volcanic rock and Cretaceous limestone in Big Brushy basin, north Stairway Mountain, and east of highway 2627 south of Black Gap WMA headquarters provided 36 measurements (Figure 2.5). Measurements are in both lithologies but where they are taken in limestone, volcanic rock is offset on the same fault within tens of meters, indicating

these faults are post-early Miocene. Sense indications in both limestone and volcanic rock come from calcite slip-fiber lineations, although in the volcanic rock the calcite is of low volume. Kinematically compatible populations of the strain-tensor quadrants for the northern Sunken Block measurements are presented as Figure 2.18. Population 1 (n=30) gives an average T-axis trend of 239°. Population 2 with (n=6) also reflects NE-SW stretch with a T-axis trend of 062°, but as in the measurements from Dagger Flat, in a Linked Bingham analysis they are kinematically incompatible because of varying P-axis orientations.

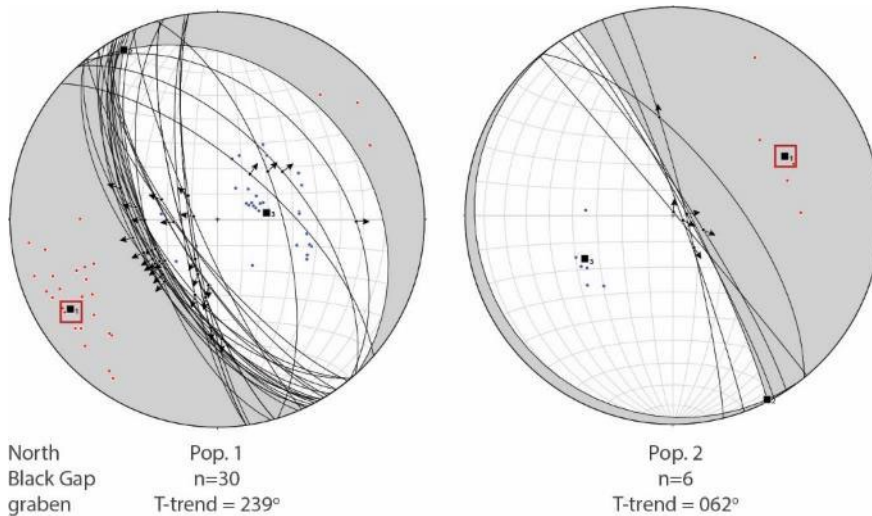


Figure 2.18. Two kinematically compatible populations of fault-kinematic measurements from the northern Black Gap graben. Maximum stretch axis is calculated as T-trend, and is labeled with a '1' and boxed in red on the stereonet.

2.5.2 Geochronologic analysis

Twenty-nine samples of calcite were collected from nine field sites at seven locations for geochemistry and U-Pb geochronologic age determination through the CEEIR lab at UTEP (Figure 2.19; Table 2.1). These samples include 26 oriented calcite slickenlines and three euhedral crystals from brittle fault zones. Sixteen of these samples have been analyzed for major and trace element data and/or U-Pb geochronology. Seven samples were analyzed for only geochemistry, 7 were analyzed for geochronology, and 5 were analyzed for both (Table 2.1).

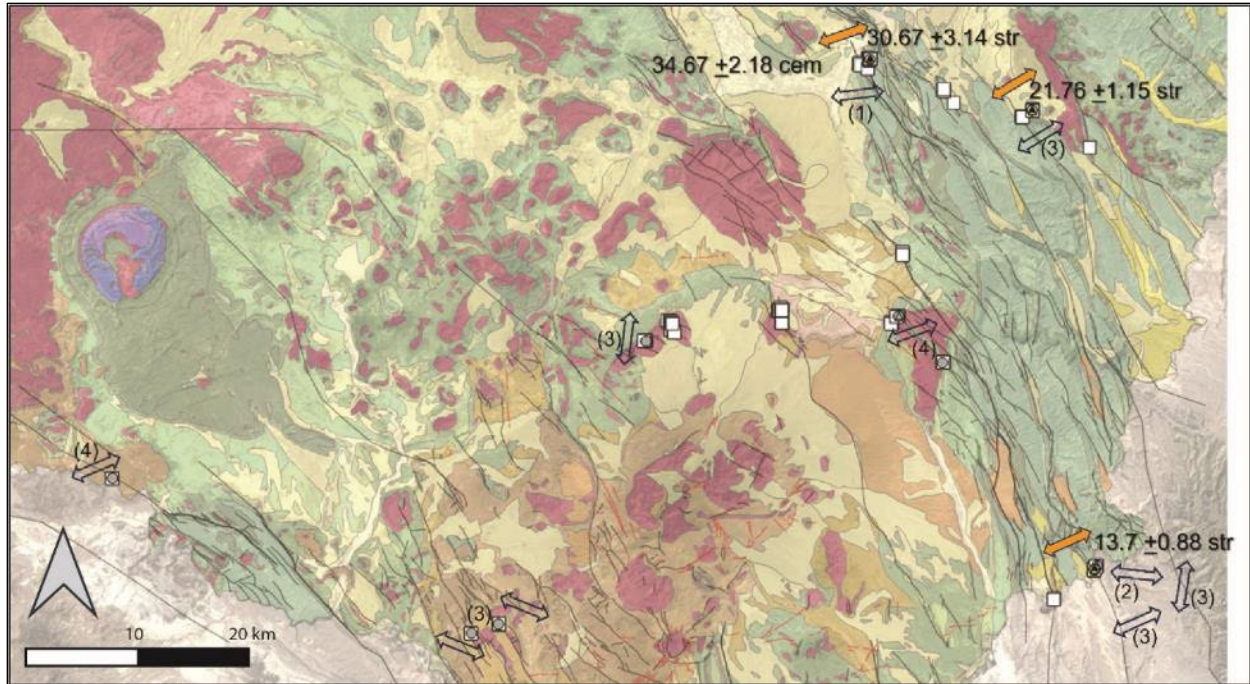


Figure 2.19. Mapped locations of all field sites of kinematic measurements (white square) and samples collected at some of those sites (grey circle,) quantity of samples in each kinematic population in parentheses, double-ended arrow indicating stretch axis of kinematic population) Analyzed samples are shown in unfilled triangle within the circle, and samples with U/Pb geochronologic results are shown with filled triangle. U/Pb ages in Ma. Three ages are from striated calcite slickenlines (str) and one is from an associated euhedral crystal vein ("cem") immediately adjacent to the striated sample.

Table 2.1. Calcite slickenline samples collected for U/Pb geochronologic analysis, source of sample, kinematic population to which the striated slickenline sample belongs, analyses run, and resultant U/Pb age if obtained. The three samples with no kinematic population are euhedral crystals from veins associated with the striated sample.

Sample no.	Site	Place	Longitude (-)	Latitude (+)	Rock faulted (all LS except Kp)	Kinematic population (NE, NW,...)	Batch no.	Trace element	Enough U y/n? (≥ 0.2 ppm)	U/Pb attempt	U/Pb age (Ma)
GR04	grotto fault	Dagger Flat	103.12061	29.6091	Kbu/Kbo	ENE (251°)	1			Y	30.67 +- 3.14
GR04ax	grotto fault	Dagger Flat	103.12061	29.6091	Kbu/Kbo	n/a	1			Y	euhedral xl age 34.6 +- 2.18
GR02	grotto fault	Dagger Flat	103.12061	29.6091	Kbu/Kbo	E (083°)	1			Y	
GR02ax	grotto fault	Dagger Flat	103.12061	29.6091	Kbu/Kbo	n/a	1			Y	
sm01a	N Stairway Mtn	N Black Gap	102.97197	29.568243	Kbu/Kse	NE (239°)	2	Y	Y	Y	21.76 +- 1.15
bq6	bqf main	S SdCarmen	102.91534	29.202176	Kbu/Kbo	NE (246°)	2	Y	Y	Y	13.7 +- 0.88
sm03	N Stairway Mtn	N Black Gap	102.97197	29.568243	Kbu/Kse	NE (239°)	2	Y	Y	Y	
sm04	N Stairway Mtn	N Black Gap	102.97197	29.568243	Kbu/Kse	NE (239°)	2	Y	Y	Y	
bqtr.07	bqf main	S SdCarmen	102.91534	29.202176	Kbu/Kbo	E (096°)	2	Y	Y	Y	
oor.f5	McK hills	Old Ore Rd	103.09451	29.404211	Kp (siliciclastic)	NE (070°)	2	Y	N		
bqtr.05	bqf splay	S SdCarmen	102.91266	29.204911	Kbu	NE (246°)	2	Y	N		
bqtr.03	bqf splay	S SdCarmen	102.91266	29.204911	Kbu	E (096°)	2	Y	N		
bqtr.03x	bqf splay	S SdCarmen	102.91266	29.204911	Kbu	n/a	2	Y	N		
bqf.27	bqf main	S SdCarmen	102.91498	29.201665	Kbu/Kbo	NE (246°)	2	Y	N		
bqf.33	bqf main	S SdCarmen	102.91498	29.201665	Kbu/Kbo	N (009°)	2	Y	N		
bqf.39	bqf main	S SdCarmen	102.91498	29.201665	Kbu/Kbo	N (009°)	2	Y	N		

Table 2.2. Calcite slickenline samples collected for U/Pb geochronologic analysis that were not analyzed. Reasons not analyzed: (a) not enough material; (b) material too weathered; (c) sample remains to be analyzed. 1: Samples taken from site of Henry (1998) and not part of this study's kinematic groupings.

Sample no.	Site	Place	Longitude (-)	Latitude (+)	Rock faulted	Strike/dip/rake	Kinematic population (NE, NW,...)	Reason not analyzed
sm05	N Stairway Mtn	N Black Gap	-102.97197	29.568243	K limestone	165/62/-97	NE (239°)	a
oor.02	McK hills	Old Ore Rd	-103.09455	29.404232	Olig. Igneous	325/88/-61	NE (070°)	a
oor.03	McK hills	Old Ore Rd	-103.09455	29.404232	Olig. Igneous	315/67/-113	NE (070°)	a
oor.?	McK hills	Old Ore Rd	-103.05428	29.367387	Olig. Igneous	318/71/-124	NE (070°)	a?
bqtr.04	bqf splay	S SdCarmen	-102.91266	29.204911	K limestone	170/59/-80	NE (246°)	b
bqf.29	bqf main	S SdCarmen	-102.91498	29.201665	K limestone	312/79/-106	N (009°)	a?
hc01a	horseshoe cyn	Castolon graben	-103.46107	29.158147	Olig. Igneous	235/54/-30	NW (292°)	b
hc02a	horseshoe cyn	Castolon graben	-103.46096	29.158084	Olig. Igneous	105/63/-30	NW (292°)	b
tc03a	tuff cyn	Castolon graben	-103.48592	29.150684	Olig. Igneous	165/79/-89	NW (292°)	a
pgh.01	Paint Gap Hills	N Sunken Block	-103.32599	29.384422	Olig. Igneous	323/89/-19	N (187°)	c
pgh.01	Paint Gap Hills	N Sunken Block	-103.32599	29.384422	Olig. Igneous	327/87/-13	N (187°)	c
pgh.01	Paint Gap Hills	N Sunken Block	-103.32599	29.384422	Olig. Igneous	323/87/-20	N (187°)	c
LJ1	Lajitas Stables	Redford-Laj FZ	-103.81495	29.274536	K limestone	109/87/-03	ENE ¹	c
LJ2	Lajitas Stables	Redford-Laj FZ	-103.81495	29.274536	K limestone	109/85/-176	ENE ¹	c
LJ3	Lajitas Stables	Redford-Laj FZ	-103.81495	29.274536	K limestone	109/81/-172	ENE ¹	c
LJ4	Lajitas Stables	Redford-Laj FZ	-103.81495	29.274536	K limestone	111/85/-178	ENE ¹	c

Three reportable U-Pb ages were determined from striated calcite slickenline samples GR04, SM01a, and BQ6, and all striated samples that were successfully dated are from outcrops that record northeast-southwest stretch axes. One reportable age was determined from an associated vein crystal immediately adjacent in outcrop to the GR04 striated sample (GR04x). All samples are from fault surfaces in limestone. Sample GR04 from the informally named Grotto fault southwest of Dog Canyon in the Dagger Flat group produced an age of 30.67 ± 3.14 Ma. This slickenline measurement is in the ENE-WSW stretch kinematic population in the Dagger Flat area. A euhedral crystal from a vein adjacent to the striated surface produced an age of 34.6 ± 2.18 Ma. Striated sample SM01a from an unnamed northwest-striking fault at the north end of Stairway Mountain in the Black Gap graben was measured at

21.76±1.15 Ma. This slickenline measurement is from the NE-SW stretch kinematic population in this area. The youngest U-Pb date is from striated sample BQ6 from the Boquillas fault in the southern Sierra del Carmen, which was measured at 13.7±0.88 Ma. This slickenline measurement belongs to the NE-SW stretch axis population.

Of the 12 samples that did not reveal ages, 7 had been assessed as too low in uranium to attempt a geochronologic determination. The remaining 5 did contain ample uranium for the analysis but nonetheless yielded high errors and no reportable ages (Table 2.2). All 12 samples except one are from surfaces of faults that cut limestone; the single non-limestone sample is from a fault cutting the siliciclastic Cretaceous Pen formation adjacent to an Oligocene intrusion.

2.5.3 Trace-element data

Twelve samples were assessed for ample uranium content as a precursor to U/Pb geochronologic analysis, and the same analysis yielded trace-element concentrations. Eleven of these samples are from striated calcite slickenlines and one is from a euhedral vein crystal adjacent to a striated sample (Table 1). Chondrite-normalized data are presented in Figure 2.20.

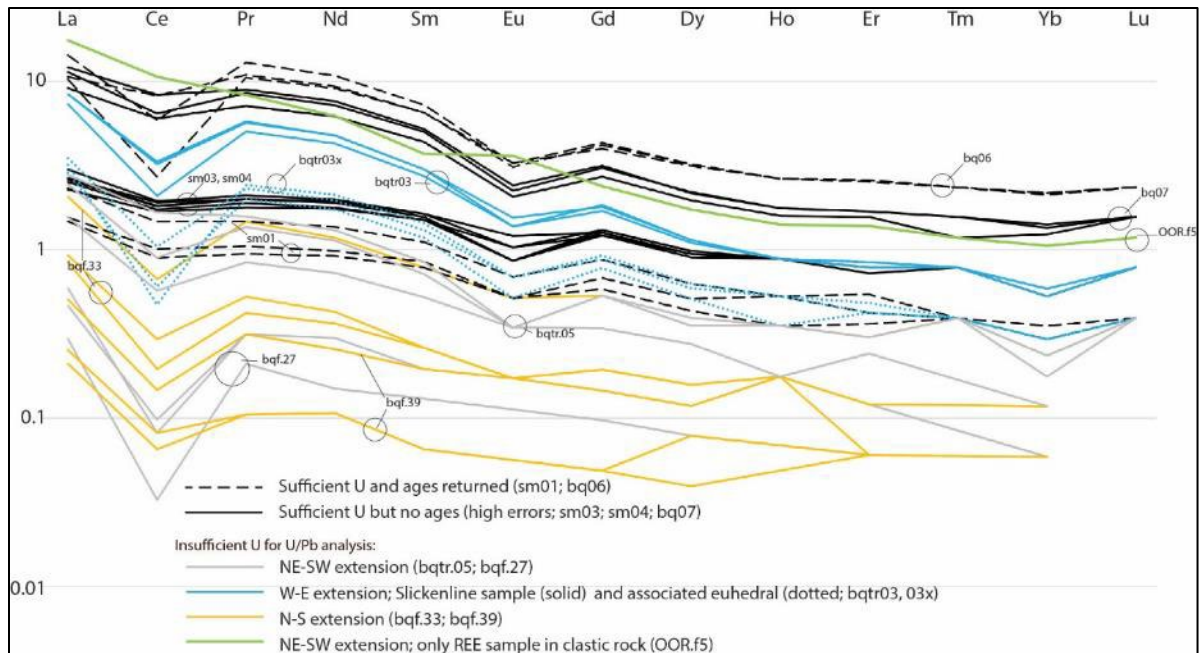


Figure 2.20. Chondrite-normalized REE concentrations for samples indicated in Table 2.1. All samples except OOR.f5 consist of three separate subsamples with their own concentrations displayed. Several samples have “0” concentrations of Eu, Ho, Tm, and Lu. Chondrite values are from Sun and McDonough, 1989.

Eleven of the twelve samples consist of three subsamples whose concentration measurements are displayed. Samples sm01 and OOR.f5 each show a lesser Ce-negative anomaly than all other samples. All samples along the Boquillas fault except bq07 show a significant Ce-negative anomaly. Samples with sufficient U to run U/Pb analysis also have higher normalized concentrations overall, but this is not exclusive because OOR.f5 and bqtr03 and 03x also have higher normalized concentrations.

2.6 Discussion

2.6.1 Extension-direction history of the southern rift from kinematic and geochronologic data

The three samples from calcite slickenlines with U/Pb ages each record NE-SW crustal stretching, which indicates that NE-SW stretch persisted in the Big Bend region from at least 30.7 ± 3.1 Ma to 13.7 ± 0.9 Ma. The onset age of northeast extension in Trans-Pecos Texas is well-documented at 32-30 Ma based on orientations of dated dikes and veins from the central Sunken Block to the Van Horn area (Price and Henry, 1984; 1985) although extensional faulting is not documented until at least 28 Ma based on emplacement of a dike along a normal fault in the Castolon graben (Dickerson and Muehlberger, 1994; Stevens and Stevens, 1985). Kinematic data from this study also suggest stretch directions of W-E, WNW-ESE, and NW-SE within the Sunken Block. Lineations in the Sunken Block are mostly either chattermarks, non-mineralized grooves in the igneous host rock, or striated calcite in amounts too small for bulk-dissolution U/Pb analysis (perhaps because of the distance of limestone country rock from these intrusions and flows), or in occurrences that are too oxidized for analysis. These non-northeast stretch directions may also occur in the Sierra del Carmen although absence of clear sense indicators on strike-slip fibers and absence of age control younger than the Albian limestones must leave open the possibility that those data record pre-rift contraction.

Kinematic measurements of rakes on fault surfaces in this study combine to yield multiple kinematically compatible populations of slickenlines (Figures 2.12 – 2.18) that suggest changing or rotating strain fields. When combined with new U-Pb ages from this study and existing geochronologic data with known extension directions, these fault-kinematic data are compatible with a model where extension direction in the southern segment of the Rio Grande rift rotated through time (Fig. 2.21).

Studies have suggested that extension in the central segment of the rift of central and northern New Mexico rotated clockwise (Liu et al., 2019; Minor et al., 2013). If the southern segment of the rift in

Trans-Pecos Texas also deformed by a clockwise-rotating strain field, then the early and long-lived NE-SW stretch recorded with these data would have transitioned to W-E stretch, which would have subsequently been supplanted by WNW-ESE to NW-SE stretch.

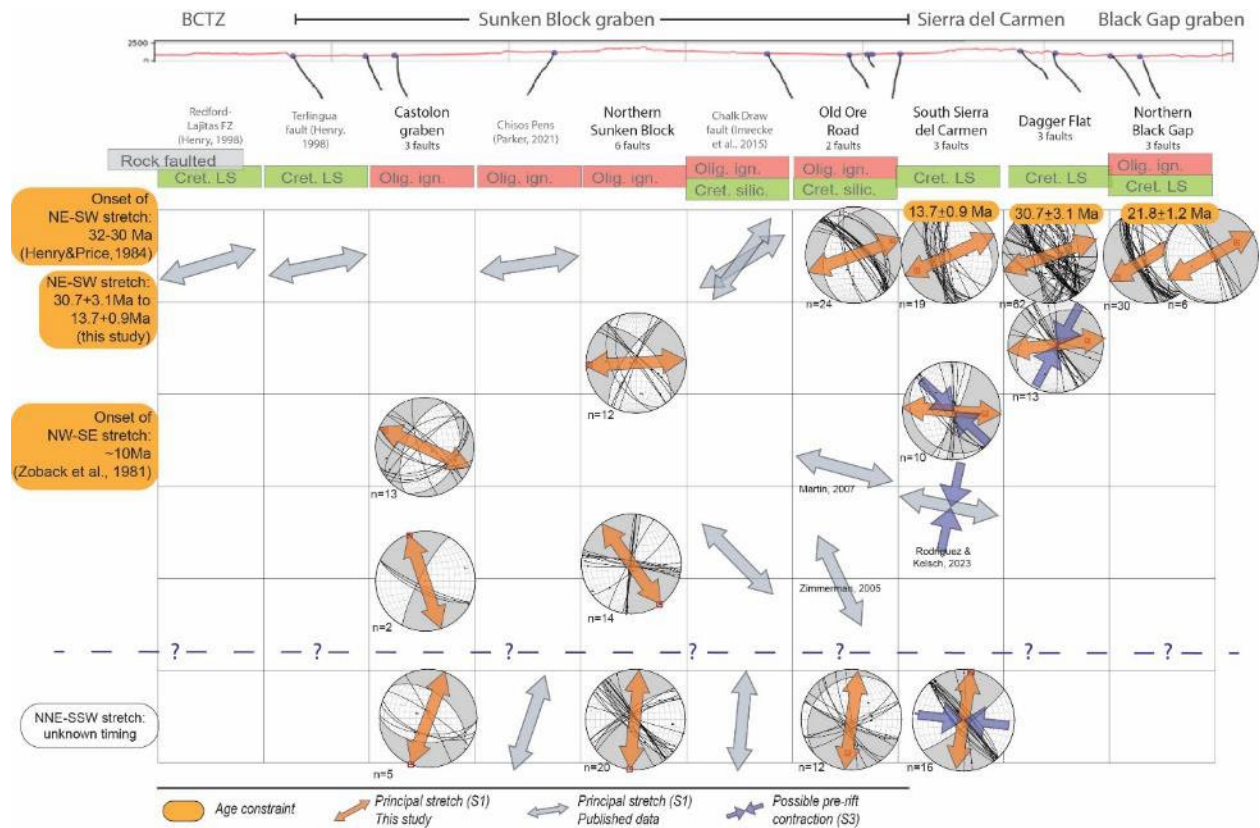


Figure 2.21. Stereographic plots of kinematic populations of fault measurements (this study) and published S1 axes arranged by location (southwest to northeast) from the RLFZ in the southern BCTZ to Black Gap graben, with north = up on each stereonet. Locations are listed across the top. All locations from this study represent between 2 and 6 fault surfaces each. Published data are referenced either on the S1 arrows or by location at the top of the figure. The rock offset in each location is indicated under the place name to indicate the oldest possible age of faulting (as that of the youngest rock faulted); rock ages from Page et al., 2008. Geochronologic results from this study are highlighted in orange at the location and kinematic population to which that sample belongs. Age constraints for particular stretch directions are highlighted in orange on the left of the figure. Kinematic populations are presented in proposed chronological order from top (earliest) to bottom (latest). A progression is presented through time from 32-30 Ma (top) to recent (bottom) showing proposed clockwise rotation of horizontal crustal stretch direction from early northeast stretch to later northwest stretch, and perhaps most recently at N-S or NNE-SSW stretch. Purple double arrows in data from the southern Sierra del Carmen and Dagger Flat present an alternative possibility of contraction via strike-and-oblique-slip motion on faults that cut Cretaceous rock only and therefore may have preceded Oligocene and later extension. Note this data arrangement's localization of later faulting into the Sunken Block. SW-NE cross section at top of figure is sketched after Turner et al. (2011) and Moustafa (1988) on a profile produced from a 10-m DEM in QGIS.

The most widely-cited constraint on the termination of NE-directed stretch in the Rio Grande rift and the Basin and Range province is ~10 Ma, when the regional stress field shifted clockwise from NE-SW to mostly NW-SE, WNW-ESE, and localized N-S tension in the northern and southern Basin and Range and the Rio Grande rift, based on dated dike orientations and fault-kinematic data from several sites in Nevada, Arizona, and New Mexico (Zoback and Zoback, 1980; Zoback et al., 1981; Figure 2.22). Zoback and others (1981) proposed that the cause of this regional clockwise rotation in tension was an increase in the coupling of the Pacific and North American plates at their transform margin which at last superimposed the San Andreas system's dextral shear onto the previous ENE-WSW tension field. Either the San Andreas fault reached a critical length allowing that increased coupling, the rate of relative motion across the plate boundary increased, or a pole of rotation shifted that increased friction at the boundary (Zoback et al., 1981). Bird (2002) revisited the model of a critical length of the San Andreas being reached to increase coupling of the plates, calculating 20 to 50 degrees of clockwise rotation in maximum horizontal compression (mhc), or σ_1 , between 22Ma and present in western US and Mexico between latitudes of 28°N and 41°N. This resulted from the transform plate boundary at the western edge of the North American plate not only lengthening, but its northern tip translating northward and thereby adding a component of dextral shear to horizontal extension at latitudes south of that northern tip. This is based on a data set of 369 "paleostress direction indicators" which include dikes, veins, and fault-slip vectors.

The model of regional 10-Ma clockwise rotation of stretch from ~NE-SW to ~NW-SE is cited for a shift in extension direction in the western Española basin of the northern Rio Grande rift (Liu et al., 2019), in the Indio Mountains of west Texas in the BCTZ (Price and Henry, 1985), in the western Delaware basin (Hentz and Henry, 1989), along the Chalk Draw fault of the northern Sunken Block (Imreke et al., 2015), and elsewhere in Big Bend where a shift in stretch direction is speculated (e.g. Martin, 2007).

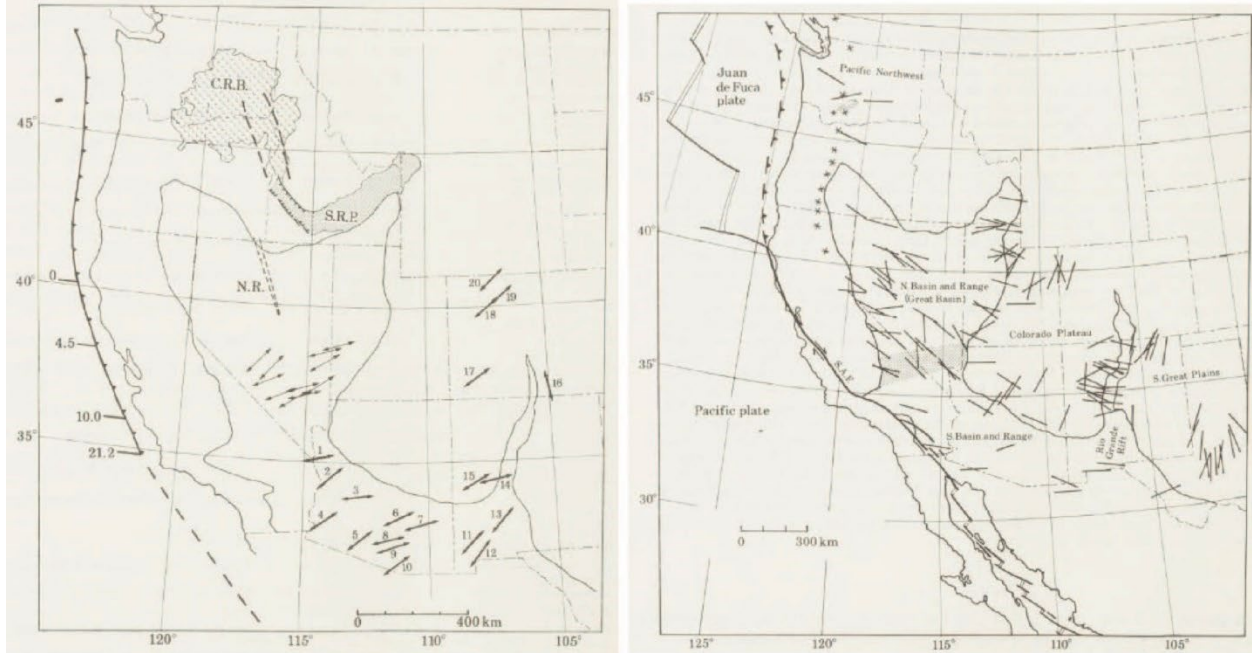


Figure 2.22. Figures from Zoback et al., 1981 presenting a Miocene (~20-10Ma) field of least principal stress (σ_3 , equivalent to maximum stretch direction referred to in this study) on the left, and the modern field of the same (σ_3) on the right.

Other work has suggested that in the absence of absolute age control, the change in stretch direction in the Trans-Pecos region could be as early as 17 Ma, just after the youngest igneous activity, presuming that the ubiquitous northwest-striking faults would not allow magma ascent under a new northwest extension regime (Dickerson and Muehlberger, 1994; Henry, 1983; 1991). In this study a 13.7 ± 0.9 Ma U-Pb age comes from a fault slickenline that records northeast stretch. This datapoint therefore does not support a 17 Ma change in direction, but does agree with the ~10 Ma change often cited from Zoback and others.

The age of NNE-SSW stretch recorded in kinematic data from the northern Sunken Block, Old Ore Road, south Sierra del Carmen (this study), and the Chalk Draw fault (Imrecke et al., 2019) is uncertain (Figure 2.21, bottom row). Following a model of clockwise rotation of the stretch axis, either it is very early, preceding NE-SW stretch, or it is the most recent stretch direction. While there are records of N-S stretch in the northern Basin and Range (Figure 2.22 right; Zoback et al., 1981), the present-day stress field of western Texas and surrounding regions reveals approximate NNE-SSW horizontal tension

(approximated as NNE-SSW extension) in parts of the Delaware basin and Central Basin Platform north of the study area, although there are many disparate modern directions in a small area (Figure 2.23; Snee and Zoback, 2018). Zoback and Zoback (1980) and Zoback and others (1981) map a consistent ~N-S tension field in the Southern Great Plains, including the Delaware and Permian basins, with an abrupt edge of that field approximating the northeast boundary of the Trans-Pecos region (Figure 2.22, right). That mapped ~N-S tension is either the passive partner of active, albeit small, W-E compression from Mid-Atlantic Ridge push (Zoback and Zoback, 1980), or is part of the Gulf Coastal Plain's continental-margin growth faulting (Zoback et al., 1981). Regardless, it is difficult to imagine a tectonic scenario with overlapping stress fields that would not simply combine. Here we leave open the possibility that the NNE-SSW stretch in the Big Bend region is the most recent and is related to the modern Southern Great Plains stress field (Zoback and Zoback, 1980; Zoback and others, 1981).

Displacements are partitioned in oblique rift basins either by a regional stress field being changed through time, or by a consistent regional stress field having local variations due to preexisting weak zones (e.g. Morley, 2010; Liu et al., 2019). Explicitly, normal-slip and strike-slip faults parallel each other *either* because of a change of a regional stress field through time *or* from a single regional stress field that partitions displacement into normal- and strike-slip components (Oldow and Craig, 1992). This study's kinematic and geochronologic data lead to the proposal that the regional stress field did rotate clockwise through time (Figure 2.21), but earthquake and other modern stress data in the region reveal that strain can also be partitioned spatially (Figure 2.23), and may leave more questions about local basement influence on strain manifested from a background stress field.

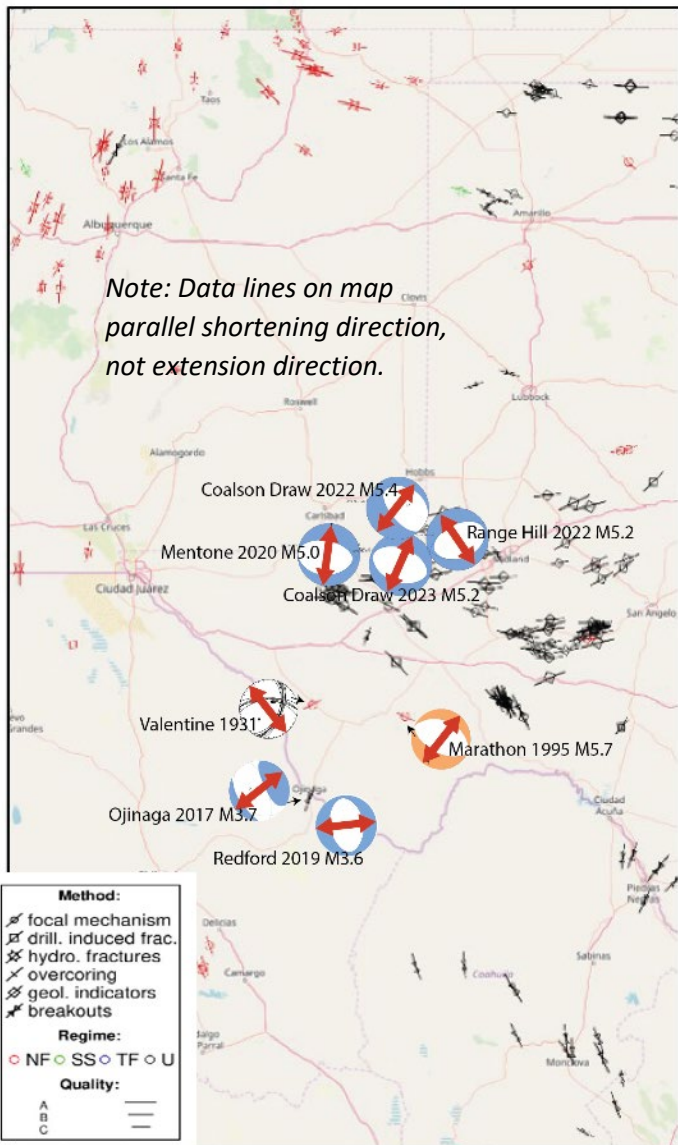


Figure 2.23. Portion of World Stress Map (WSM) produced for western Texas and eastern New Mexico, with all Trans-Pecos-area earthquake data, and $M > 5.0$ data for the Midland and Delaware basins, superimposed. Red arrows highlight tension axes of earthquake focal mechanisms. WSM displays orientations of maximum horizontal compression (σ_{1H}), i.e. principal tension in the horizontal direction and therefore extension direction (stretch, or S_1) is perpendicular to these lines. Regime codes refer to normal, strike-slip, and thrust faults. Superimposed fault-plane solutions do not obscure WSM data. Ojinaga WNW stretch on WSM is borehole breakout. There was also an earthquake in 2017. Marathon and Van Horn stretch data on the WSM are the same earthquakes noted with fault-plane solutions. Map legend explains WSM symbology. Colored fault-plane solutions are from USGS.gov. Black and white fault-plane solution is from Doser, 1987.

2.6.2 Evidence for structural narrowing of the southern Rio Grande rift in Trans-Pecos Texas and questions about its relationship to the BCTZ and the rest of the Rio Grande rift

Proposed progression of extension direction in the southern Rio Grande rift also supports an inward localization of faulting into the Sunken Block through time. Northeast extension is recorded in all parts of the study area but additional stretch directions are recorded only inside the Sunken Block graben (Figures 2.22; 2.24). NE-SW extension persisted from ~30.7 to 13.7 Ma based on new U-Pb calcite geochronology and may have lasted until ~10 Ma (e.g., Zoback et al., 1981). Clockwise rotation of the strain field suggests that W-E and NW-SE stretch documented in the Sunken Block is younger than NE-SW stretch, supporting a model where faulting was concentrated within the Sunken Block. The wider rift margins were abandoned after the shift in extension direction. These wider regions include Black Gap graben, perhaps Sierra del Carmen on the east, the Redford-Lajitas fault zone of the BCTZ, and the remainder of the southern Bofecillos block north of the RLFZ (Henry, 1998) on the west (Figure 2.21). Similar structural narrowing has been documented elsewhere in the Rio Grande rift. Ricketts and others (2015) documented a progression of faulting in the southern Albuquerque basin where master normal faults at the rift margins became inactive while younger normal faults emerged basinward. Minor and others (2013) concluded that active rifting narrowed toward the axis of the Santo Domingo basin in the late Miocene. Ascribing the NNE-SSW stretch as the latest event may also be supported by narrowing of the rift, because that direction of stretch appears to be constrained to the Sunken Block.

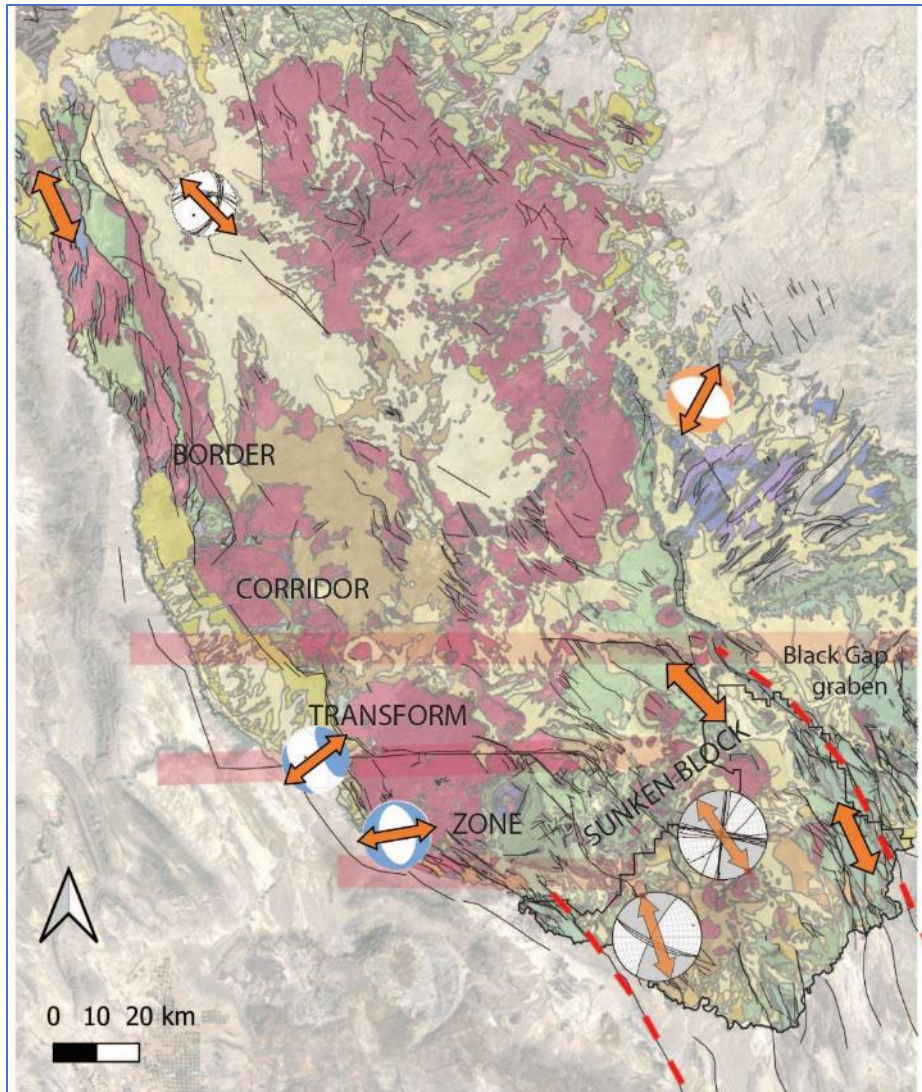


Figure 2.24. Map showing the most confident <math><10\text{Ma}</math> stretch directions from fault kinematic data, and earthquakes in the Trans-Pecos. Kinematic data are from this study, Imrecke et al., 2015 (at Chalk Draw fault), Zimmerman, 2005 (at Old Ore Road), and Conley et al., 2023 (in Indio Mountains). This map does not include the NNE-SSW stretch directions recorded within the Sunken Block, as their age is uncertain, although they may be latest.

Quaternary faulting has occurred within and on the margins of the Sunken Block: the east and west bounding faults of Tornillo graben (Satterfield and Dyess, 2007; Dickerson and Muehlberger, 1994) and along the west edge of the Sunken Block at the Terlingua fault (e.g. Satterfield and Ashmore, 2009). Quaternary faulting has also occurred outside of the Sunken Block along the west-east transfer faults in the BCTZ: along the central Tascotal Mesa fault (Dickerson, 2013) and at its west end where it bounds the Presidio graben (Dickerson and Muehlberger, 1994), and at the west end of the Chalk Draw fault in

the Plata subbasin (Dickerson, pers. comm., 2023). None of these faults provide kinematic information. Earthquake data are also available outside the Sunken Block in the Big Bend part of Trans-Pecos (Figures 2.23; 2.24). The earthquakes closest to, but outside, the Sunken Block produced NE-SW to NNE-SSW extension, while the 1931 Valentine earthquake farther northwest but also in the BCTZ showed NW-SE extension. Fault data from the Indio Mountains (Conley et al., 2023) include a kinematic population of NNW-SSE-stretch which may be the most recent activity (Figure 2.23). These disparate directions, plus lack of earthquake or geochronologic fault data inside the Sunken Block, raise the question of how these and other faults of the BCTZ relate to rift narrowing and outer-fault abandonment. Also, since earthquake data at Ojinaga, Redford, and Marathon reveal northeast stretch but earthquake data near Valentine reveal northwest stretch, then *if* the most recent stretch in the Sunken Block is northwest, is the Sunken Block kinematically connected to the farther parts of the BCTZ but not those immediately adjacent? Alternatively, if the most recent stretch in the Sunken Block is north-northeast, is the Sunken Block's stretch coupling with that of the Delaware and Midland basins? Geochronologic data from NW-stretch slickenlines in the Sunken Block are needed to help solve this problem.

Another question raised is how the BCTZ may link the Sunken Block graben to the grabens of the southern New Mexico portion of the Rio Grande rift (Dickerson and Muehlberger, 1994; Dickerson, 2013). The bend in the Rio Grande rift at the BCTZ (Figure 2.1) and the transfer structures within it likely follow preexisting zones of lithospheric weakness. The northwest-trending zone of the BCTZ and the Sierra del Carmen have been active at least since the Laramide; the northwest-trending Chihuahua trough overlapping part of the BCTZ was active during the Jurassic; the BCTZ parallels at least one Proterozoic rift-related normal fault; and the west-east Tascotal Mesa and Chalk Draw faults parallel and reactivate basement trends (Dickerson, 2013).

The Rio Grande rift from northern Colorado to southern New Mexico experienced synchronous opening from 25-10 Ma (Landman and Flowers, 2013; Ricketts et al., 2016) followed by continued

extension at slower rates that continued through the Quaternary (e.g., McCalpin et al., 2005; Olig et al., 2011; Berglund et al., 2012; Ricketts et al., 2014; Armour et al., 2018; Murray et al., 2019). A shift in extension direction via clockwise rotation from west to northwest is documented in northern New Mexico (Minor et al., 2013; Liu et al., 2018); multiple kinematically incompatible but undated populations, including northwest and west-northwest, were also documented in southern New Mexico (Rodriguez-Gonzalez, 2019).

The southern BCTZ and the Sunken Block have extended synchronously with the rift basins in New Mexico and Colorado and have also experienced a clockwise rotation in extension direction from northeast to northwest, but total extension is less in the southern rift and early extension in the southern rift was northeast and not east. Nonetheless it is warranted to state that all these parts of the rift are kinematically connected. It may be that structures within the BCTZ transfer but attenuate extension from the New Mexico segment of the Rio Grande rift; that the sub-lithosphere activity of decoupling of the Farallon slab under New Mexico is localized there; or that there is overlap of the Southern Great Plains' strain regime into the southern rift; or some combination of these.

2.6.3 The use of U/Pb geochronology

Analyzed samples from the study area contained variable and mostly low uranium concentrations, rendering most samples either unable to be measured for U/Pb geochronology or producing high errors. Marine limestones like the deformed Cretaceous units in the study area are originally high in U, but after dissolution in the meteoric realm this U is diluted before reprecipitation unless it is concentrated by organic processes during diagenesis, and these samples may therefore produce high errors (Reiners et al., 2018). Faults with continued access to ground water may have new material precipitated over long, interseismic periods of time on top of syntectonic calcite slickenlines, as in Nuriel and others' (2012) 'coating' category of fault-related calcite. Ground water may also react with

existing slickenlines in this situation of relatively high contact time to recrystallize and dilute the syntectonic, higher-U calcite.

Six of the eight samples from the Boquillas fault and its splay had too low a U-concentration to conduct the U/Pb geochronologic analysis, possibly indicating persistent contact with ground water and U dilution. This is one of the two longest-trace faults mapped within the southern Sierra del Carmen (e.g. Moustafa, 1988; Maler, 1990; Turner et al., 2011) and may therefore have persistent depth to ground water. Alternatively because it is part of a system of small-throw parallel faults it offsets two stratigraphically adjacent formations and could be considered too small itself to have the depth to persistent uranium-diluting ground water. One of the samples from the main fault recording NE-SW stretch did produce a U/Pb age.

Two samples from the Grotto fault are from slickenlines and two are from adjacent euhedral crystals. One pair produced U/Pb ages and the other did not; this batch was not analyzed for U before U/Pb analysis but it is presumed that U was low enough to yield high errors. This fault juxtaposes two adjacent stratigraphic units and is not mapped with a long trace.

All three slickenline samples from a normal fault on the north side of Stairway Mountain contain enough U to analyze, and one of the three yielded a usable U/Pg age. This fault is unnamed, it offsets Cretaceous Santa Elena limestone against itself, and it is mapped as part of a system of parallel NNW- to NW-striking normal faults of the Black Gap graben. Given the low offset it may be these slickenlines did not have the persistent ground-water contact to cause either coating or diluted recrystallization.

From the four successfully analyzed samples, two were also analyzed for trace elements. These two samples have chondrite-normalized REE concentrations between 2 and 15 (bq6) and between 0.2 and 2.3 (sm01). These compare favorably to reported ranges for syntectonic calcite occurrences from Nuriel and others (2011; 2012), but so do many of the unsuccessfully analyzed samples. In addition to

trace-element analysis (rare earth plus yttrium), Nuriel and others (2012) investigated samples under cathodoluminescence and found that very bright CL, indicating crystallization that was completed during a single precipitation event, also is observed in calcite formed during fault movement. In their case samples with bright CL also contained the higher concentrations of chondrite-normalized REE's, whereas their low-REE samples describe their 'coating' category, which is interseismic. Some of this study's samples with sufficient U to run U/Pb analysis also have higher normalized REE concentrations overall but these do not define syntectonic crystal growth because three samples with insufficient U also have higher normalized concentrations.

Absence of a clear pattern in trace-element data indicates that REE analysis would not be an efficient first assessment tool in the Big Bend region, but the complexity in uncertainty of fitness for U/Pb geochronology may be solved in future kinematic and geochronologic analyses by viewing slickenline samples under CL in an SEM to determine their brightness and therefore their likelihood of being undiluted syntectonic crystals appropriate for U/Pb geochronology. Thus, the first criterion for sampling in future studies would still be kinematic relevance, while consideration of a fault surface's potential time spent in the saturated zone will still have import but may be efficiently assessed with CL imaging.

Furthermore, future studies may be able to use low-volume calcite samples with in-situ laser ablation ICP-MS, rather than the 1.5 g of sample needed to use the bulk dissolution techniques of this study. Laser-ablated samples can be smaller-volume (e.g., Roberts and Walker, 2016), potentially allowing analysis of the samples from faults cutting igneous rocks that contain less calcite in their kinematic indicators from the Sunken Block that record NW-SE stretch.

2.7 Conclusion

Geochronologic and kinematic data from fault-surface lineations support a clockwise rotation of extension direction from an early and long-lived NE-SW orientation to NW-SE after 13.7 ± 0.9 Ma in the Big Bend part of the southern Rio Grande rift. This may be related to an established clockwise rotation at ~ 10 Ma within the Basin-and-Range- and the New Mexico segment of the Rio Grande rift.

The spatial occurrence of S1 changing through time appears to show narrowing of the rift at the latitude of the Sunken Block (e.g., abandonment of the Black Gap graben), that may be coincident with the change in stretch direction. Narrowing through time is a characteristic of narrow (as opposed to wide) continental rifts.

Questions remain about the relationship of the BCTZ to the Sunken Block. Further kinematic and geochronologic analysis is warranted for faults of the BCTZ and the Sunken Block. The application of U/Pb geochronology to calcite slickenlines in faults of the southern rift is promising and should be continued. Because only small amounts of calcite are present especially on lineated surfaces in the Sunken Block's igneous rocks, laser ablation is preferred to bulk dissolution because of the smaller sample size required. Due to the potential for meteoric water to recrystallize formerly co-seismic calcite in a fault zone to material more diluted in uranium over time (and also to reset the crystallization age), CL should be used to select samples for geochronology once they return from the field.

CHAPTER 3: INTRA-FOLD STRAIN ANALYSIS OF DOG CANYON SYNCLINE

3.1 Abstract

Dog Canyon in Big Bend National Park, Texas exposes vertical beds of a portion of a reclined syncline on a ~200m x 60m cliff wall at the end of a moderate and popular hiking trail. Imagery of the wall was captured and converted to a single orthomosaic photo exposing complex joint patterns that were then mapped to interpret localized strain-axis orientations documenting a three-stage strain history between late Cretaceous or early Paleogene contraction and Neogene extension. The syncline is in the footwall of a fault-propagation fold. Strain analysis indicates that earliest strain occurred by orthogonal flexure during folding ahead of the west-southwest-verging Santiago thrust fault. Second, the lower, upright limb of the syncline was horizontally contracted as the thrust fault cut the upper limb of the fold. Last, the hinge and upper limb extended horizontally either upon relaxation of contraction or during Neogene extension. A cross-section and the geologic history are presented as a panel to be installed as an interpretive wayside exhibit in front of the cliff on the Dog Canyon trail.

3.2 Introduction

Striking intrafold mesostructures within near-vertical limestone beds are exposed at ground level and higher in a 55 to 65-meter-high cliff wall at the end of the popular, moderate-hike Dog Canyon trail in Big Bend National Park. In addition to hikers, this location is visited by undergraduate structural geology classes from several universities in Texas and Louisiana each spring break to practice geologic mapping skills. At this location a Laramide thrust fault and footwall syncline provide a well-exposed and challenging map area. The approximately 500-meter-length canyon exposes the near-vertical limb of this fold, so this exposure presents an effective cross-section through the upper limb and part of the hinge of this footwall syncline. Readily observed kinematic indicators at the level of the canyon floor, combined with overturned, near-vertical beds of the upper limb, afford an opportunity to present to the public some of the local geologic history and the tools and processes that geoscientists use to reveal it.

This project contains two components. First it is a strain study of rocks exposed in Dog Canyon. To do this, drone imagery was combined with structural observations at ground level to constrain intrafold deformation. The second part of this project aims to provide an overview of the local geologic history to visitors of Dog Canyon by producing an educational exhibit at the trail's end.

3.3 Background

3.3.1 NPS outreach/ public education

There is no shortage of archived and active geoscientific research in the US' National Park Service (NPS) lands, from both NPS- and non-NPS scientists. Although most of this research is presented strictly in geoscience literature and academic conferences, the NPS counts 'interpretation' of park resources for the public as a paramount task, to "connect people to their parks" (nps.gov, n.d.) and provide opportunities for all visitors to understand and make a connection with the resources and features within them. Among the strategies employed by NPS is lay-level description of geoscience tools and findings to help the public understand how geologists interpret the subsurface and decipher geological features and history (e.g. Stein et al., 2015). Another strategy is linkage of geologic resources to human interest, for example associating soil science with carbon sequestration, biodiversity, and ecosystem services (Southard and Eckert, 2016).

Big Bend National Park (BBNP) in south Brewster County, Texas was visited by 518,000 people in 2022. It comprises 3,243 square km and has approximately 70 interpretive wayside exhibits presenting scientific and historical information to park visitors (Figure 3.1). One of its three Park Purposes is to provide opportunities to "foster understanding and appreciation of the natural ... history" of the region (NPS, 2017). Park scientists are continually looking for more ways to provide these opportunities.



42 X 24 INCHES | 88% OF ACTUAL SIZE | 4/2004 (2011) | BIG BEND NATIONAL HISTORICAL PARK | Wayside Exhibit 57

Figure 3.1. Interpretive wayside exhibit presented on a 42 in. by 24 in. kiosk at the Goat Mountain parking area on Ross Maxwell Drive in BBNP.

3.3.2 Tectonic setting

Contractional deformation in Trans-Pecos Texas is documented as part of the Laramide Orogeny between the northeastern margin of the Chihuahua tectonic belt, the Sierra del Carmen, monoclines and folds of the southern Big Bend region and northern Chihuahua, and the Lower Canyons of the Rio Grande (Figure 3.2). Most of the contraction deformation recorded is via folds and thrust faults in the Chihuahua tectonic belt and the Sierra del Carmen, and broad gentle folds are present between them.

Laramide faulting along the northeastern margin of the Chihuahua tectonic belt and into Trans-Pecos Texas started after 75 Ma (Erdlac, 1990). Two directions of contraction in two episodes reportedly define Laramide deformation there and in the rest of the Trans-Pecos. These include northeast contraction in early Laramide, followed by east-northeast in late Laramide (Price and Henry, 1984; DeCamp, 1985). Sedimentary and stratigraphic data from the Laramide Tornillo basin reveal that Laramide tectonism occurred in two phases between 70 and 50 Ma (Lehman, 1991) and Surpless and others (2015) also model two separate, but undated, phases of contraction at the Stillwell anticline.

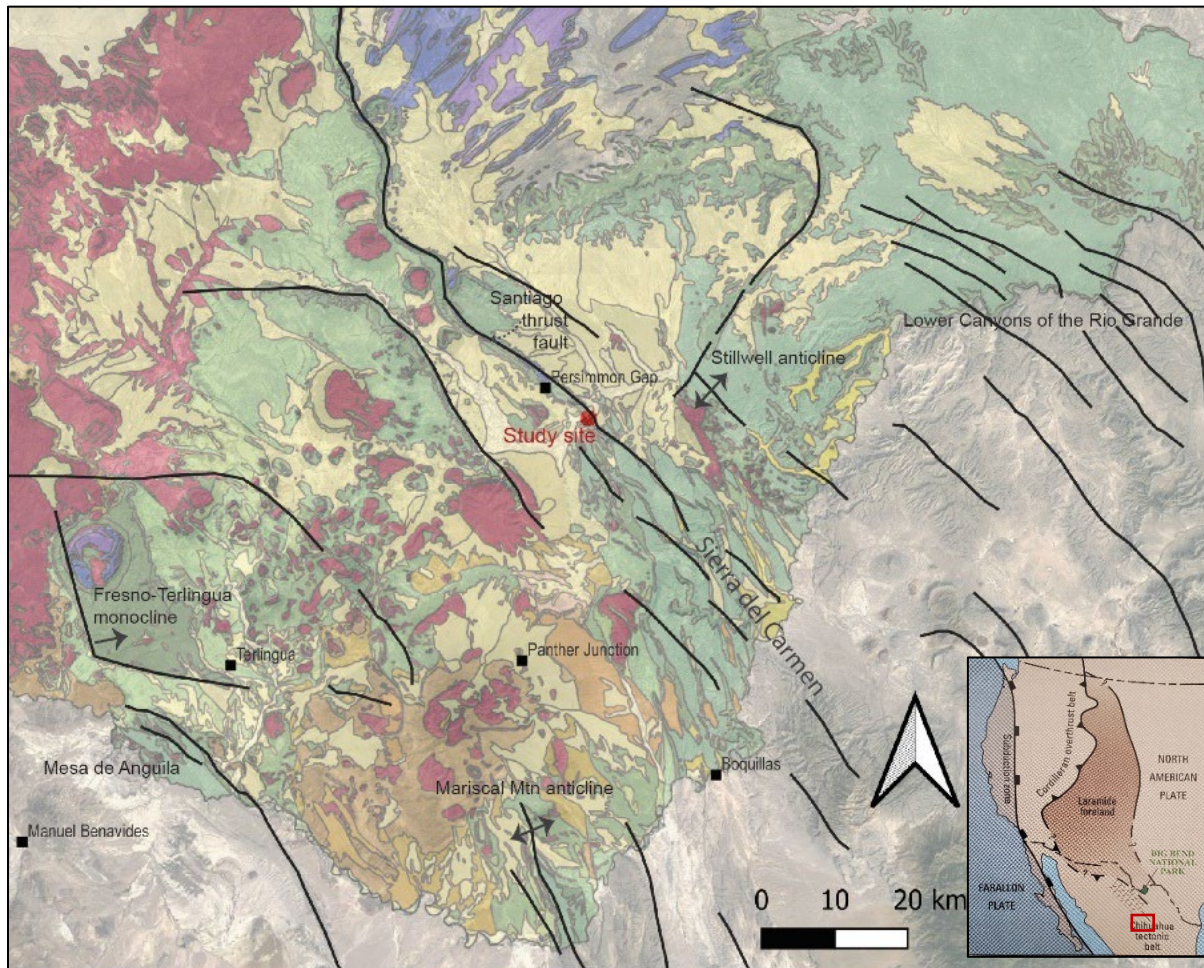


Figure 3.2. Map of Laramide fold axes, monocline hinges, and reverse faults in the Big Bend area. Structures are from Surpless et al. (2015). Inset map from Turner et al. (2011).

Several studies of Laramide contractional structures in the Big Bend region point to east-northeast contraction along west-east and northwest-trending structures, resulting in left-lateral transpressive oblique strain (Erdlac, 1990; Maler, 1990; Moustafa, 1988; Cobb and Poth, 1980; Muehlberger, 1980). The left-stepping Terlingua monocline (Fig. 3.2) formed northwest-striking sinistral strike-slip faults under N62E compressive stress defined by tectonic stylolites after 66 Ma (Erdlac, 1990). Laramide sinistral shear is also observed at Mesa de Anguila, where principal compressive stress direction of N45-55E is defined by calcite twinning fabrics, structural stylolites, and faults and joint systems (DeCamp, 1985). Surpless and others (2015) measured slickenlines and tectonic stylolites at the Stillwell anticline in the northeastern Sierra del Carmen and used forward modeling to demonstrate oblique strain from reverse reactivation of left-stepping en-echelon normal faults in Paleozoic rock, producing monoclines in overlying Cretaceous strata. Sinistral shear on Laramide structures is also observed farther west to Lajitas Mesa and Bofecillos Mountains (Henry, 1998; Muehlberger, 1980).

3.3.3 Local geology

The trace of the northeast-dipping Santiago thrust fault trends northwest to north-northwest along the Sierra del Carmen (Figure 3.2). The fault's eastward dip and westward vergence require that it branches from a deeper thrust farther east, possibly from the blind thrust fault that created the Stillwell anticline 12 km east of and parallel to the Santiago thrust in the Black Gap graben (Surpless et al., 2015). Along the Sierra del Carmen trend, the Santiago thrust and at least one associated branch place Paleozoic to older Cretaceous limestone above younger Cretaceous rock. The Santiago thrust is in places cut or reactivated by east-dipping normal faults that drop the eastern parts of these relatively complex structures into the Black Gap graben.

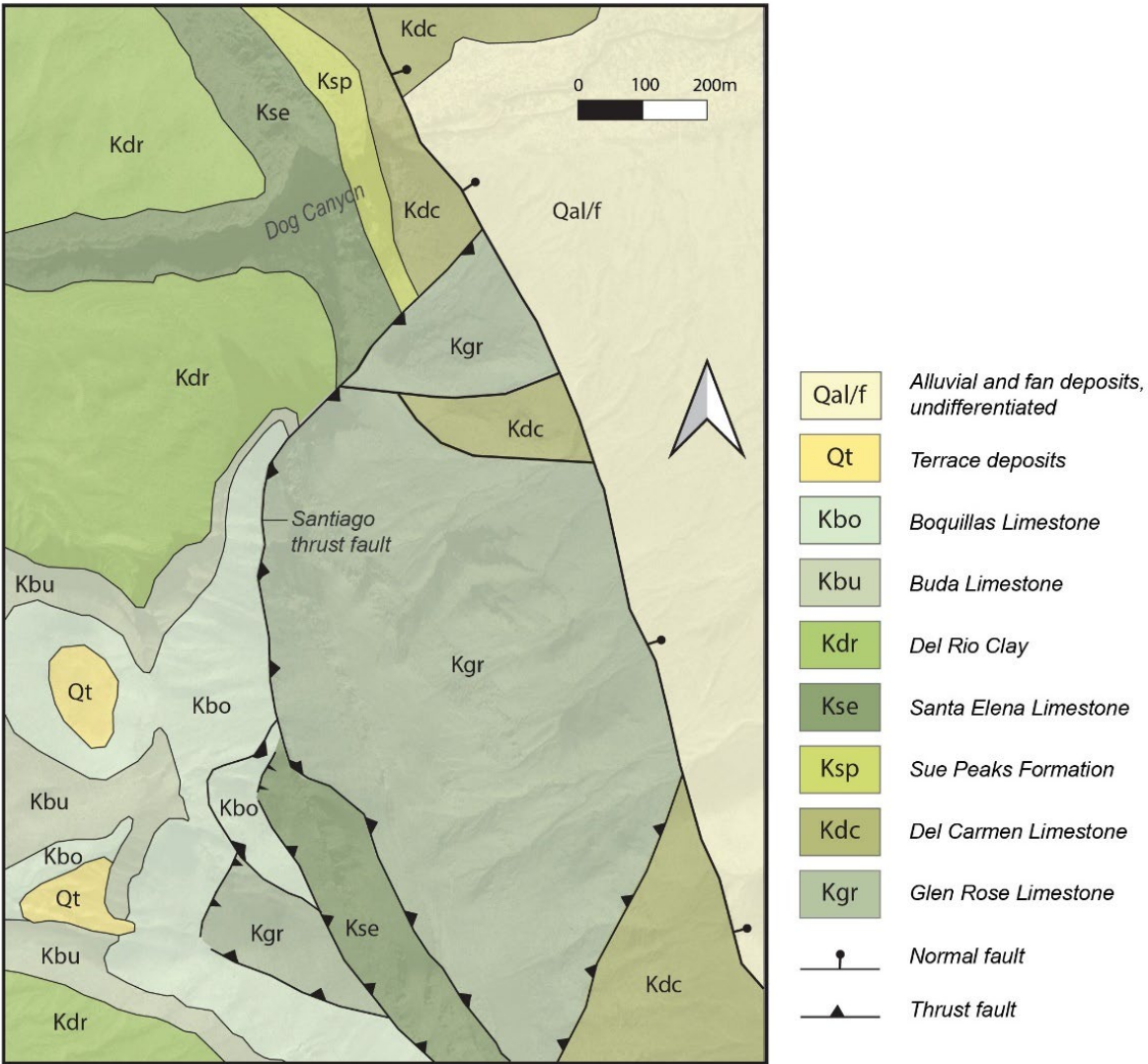


Figure 3.3. Geologic map of the Dog Canyon area. Geology from Satterfield and Dyess (2007) and Turner et al. (2011). The west-southwest-verging Santiago thrust fault expresses as a lateral ramp ~200 m south of Dog Canyon.

In the vicinity of Dog Canyon, the Santiago thrust emplaces Ordovician through lower Pennsylvanian sedimentary rock and the lower Albian Glen Rose Formation above upper Albian through Cenomanian strata in a fault-propagation fold system including overturned hanging-wall anticlines and footwall synclines (Figure 3.3) (e.g., Satterfield and Dyess, 2007; Turner et al., 2011). Dog Canyon itself is walled by near-vertical overturned beds of the Del Carmen, Sue Peaks, and Santa Elena formations in the upper limb of a reclined to slightly overturned footwall syncline (Figure 3.4; Table 3.1).

Here, the thrust fault's hanging wall is eroded. The trace of a southeast-dipping lateral ramp of the thrust fault is mapped 200 m south of the top of the cliff wall (Figure 3.3). Other unpublished maps interpret tear faults offsetting and separating sections of the upper plate south of Dog Canyon in addition to a lateral ramp. This complex and well-exposed remnant of Laramide architecture is rife for in-field learning by undergraduate students.



Figure 3.4. Photo looking north-northeast over Dog Canyon from the western (upright) limb of the footwall syncline within the Kdr (Del Rio Clay) as a group of Sul Ross State University Structural Geology students observe folding. Map symbols are explained in Table 3.1.

Table 3.1. Rock units exposed in the vicinity of Dog Canyon. Reported thicknesses are from Maxwell et al. (1967). Other thicknesses are (a) measured remotely at Dog Canyon in exposed upper limb of syncline; (b) measured by cross-section constructed from Moustafa (1988) at location ~10km east-southeast of Dog Canyon. Maxwell's reported Kse thickness is from Santa Elena Canyon ~70km to the SW. Maxwell's reported Ksp thickness is from Heath Creek ~30km to the SSE. Strata exposed as near-vertical overturned beds in Dog Canyon are marked with asterisk.

Map symbol	Unit name	Age	Reported thickness (m)	Other thickness (m)
Kbo	Boquillas Formation (lower member)	Cenomanian-Santonian	137	--
Kbu	Buda Limestone	Cenomanian	26	--
Kdr	Del Rio Clay	Cenomanian	37	--
Kse	Santa Elena Limestone*	Upper Albian	226	124 ^(a)
Ksp	Sue Peaks Formation*	Middle Albian	77	244 ^(b)
Kdc	Del Carmen Limestone*	Middle Albian	107	---
Ktc	Telephone Canyon Formation	Middle Albian	23	--
Kgr	Glen Rose Limestone	Lower Albian	85	--
Pzu	Undifferentiated Paleozoic sedimentary rock	Lower Pennsylvanian – Ordovician	unknown	--

3.3.4 Theoretical strain partitioning in folded rock

Structural-geology textbooks introduce variable intrafold strain orientations in the model of orthogonal flexure after Ramsay (1967). In this model outer hinges of mechanical layers extend parallel to the bounding surfaces of those mechanical layers (bedding in most cases of sedimentary rock), inner hinges contract parallel to bedding, a neutral surface of no strain separates these zones of opposing orientation, and the ellipses defining strain reorient along limbs to the next adjacent hinge (Figure 3.5). This deformation is accommodated by faulting and jointing if in the brittle regime (Figure 3.5c, 3.5d), and folding and boudinage if in the ductile regime. During orthogonal flexure, local intrafold strain axes stay orthogonal to the edges of the folding layers and total layer thickness does not change, while internal thickened zones are offset by thinned ones (Figure 3.5a, 3.5e). This model exists within flexural folding, wherein mechanical layers slip adjacent to each other. It predicts deformation for one mechanical layer (no multilayers) and since stratigraphic thickness during folding is preserved it produces Class 1B or parallel folds (Fossen, 2016). However, this model governs mechanical layers with a

high stiffness, whereas adjacent lower-stiffness layers may deform into Class 2 or 3 folds via passive folding under the same applied stress. Further, Fossen (2016) notes that hinge zones remain capable of thickening even in stiffer layers, and there exists the possibility of volume change or exit from plane strain.

Couples and others (1998) counter the orthogonal-flexure model with a hypothetical intrafold stress field in which orthogonality is only present in the immediate location of hinges (Figure 3.5f). Fossen (2016) supports this by noting that many people have defined orthogonal flexure more simply by only citing outer-arc stretching and inner-arc shortening without requiring orthogonality that is restricted to hinges, in order to accommodate more real examples (e.g., Hudleston et al, 1996; Fossen, 2016). Couples and others (1998) also postulate that new slip surfaces are developed during progressive deformation within preexisting mechanical layers, creating ever-increasing numbers of mechanical layers, each of which has outer hinge extension and inner hinge contraction and rendering determination of strain history complex.

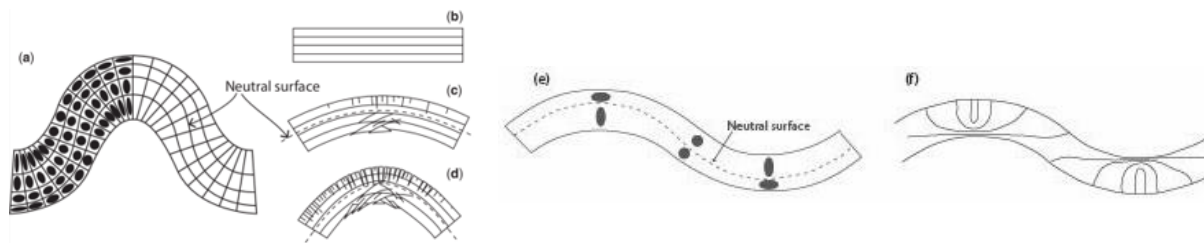


Figure 3.5a-e. Orthogonal flexure model, wherein rock in one mechanical layer is extended parallel to the layer boundary in a fold's outer hinge, and shortened parallel to the boundary in the inner hinge. C and d show brittle-regime structures accommodating that outer-hinge stretch and inner-hinge shortening. From Ramsay (1967) 3.5f. Model wherein solid lines depict orientations of σ_1 within a set of folds. After Couples et al. (1998).

3.4 Methods

3.4.1 Image capture

To begin the analysis of structures exposed in Dog Canyon, video was captured covering the approximately 200 x 65- meter southern cliff face via UAV launched from the BBNP boundary approximately 400 meters east of the canyon, per BBNP rules, in December 2019. The video was turned into an orthomosaic .tif file and a 7M-point dense point cloud in CloudCompare software. A total station and compass were brought to the canyon in April 2023 to add orientation and location data to the cloud. A GigaPan camera was hiked up the southern side of the canyon to capture images of the north wall, but these were not downloadable from GigaPan and were not used.

3.4.2 Geologic cross-section

Published and unpublished bedding orientations in the Dog Canyon area (incl. Satterfield and Dyess, 2007) were used to construct a stereographic pi diagram to determine whether the exposed fold is cylindrical at least at and near the exposed rock of the cliff. Stereonet analysis was also used to calculate the orientation of the fold axis to determine of the angle between the cliff face and a true-dip cross-section line, or a vertical plane that is orthogonal to the bedding strike. An apparent-dip cross section was constructed parallel to the exposed wall of Dog Canyon, 45 to 55 meters south and southeast of the cliff wall; the apparent-dip cross-section line is shown in Figure 3.6. The east end of the section line is 20° from the true-dip section and the west end is 15° from it. Because the cross-section line parallels the cliff face, orthomosaic imagery of the cliff face from the drone video was superimposed on the interpreted cross-section.

3.4.3 Mapping of intrafold structures

The higher-resolution orthomosaic .tif file was used as a base in Adobe Illustrator on which to map traces of bedding planes and of the following three categories of fracture surfaces:

1. Conjugate shear fractures. These are identified by their angles of approximately 60° and 120° from each other, as modeled in Figure 3.7a.
2. Mode I joints. The traces of these fractures are parallel to each other as presumably are their surfaces into the outcrop. These may occur in parallel groups (e.g., Figure 3.7a) or at terminations of faults or shear fractures as wing cracks or tension fractures (e.g., Figure 3.7b and c).

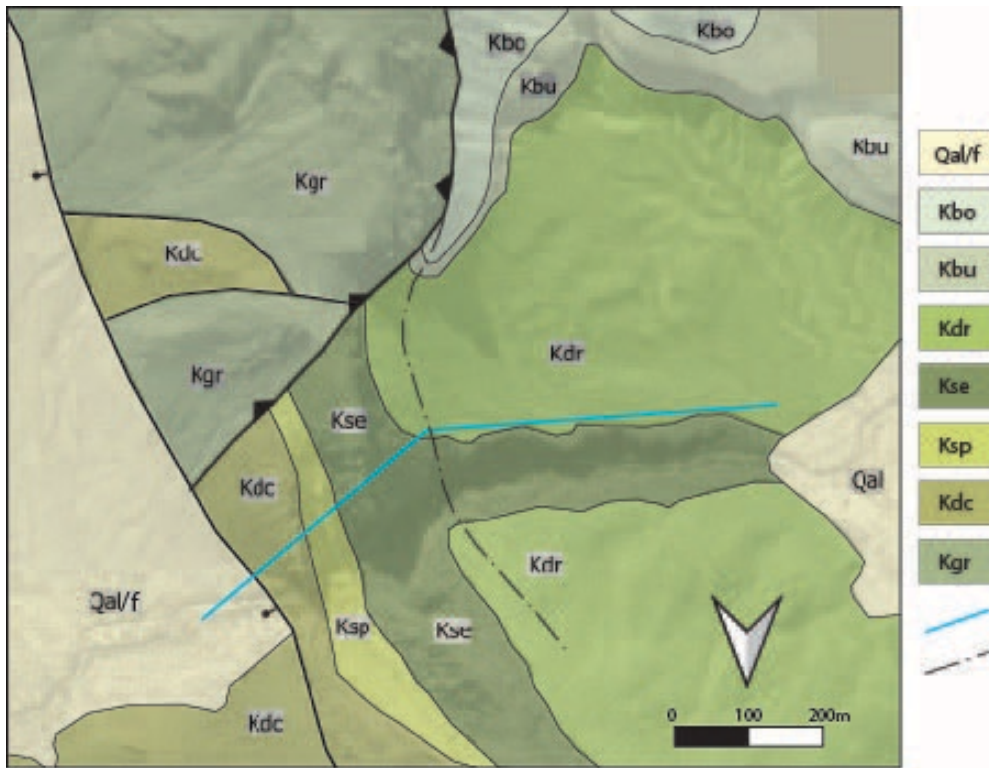


Figure 3.6. Southward-up geologic map of the Dog Canyon area showing cross section line (blue) for Figure 3.17. Section line bends to represent view of south canyon wall, and to allow orthomosaic of cliff face to be superimposed on cross section. Fold hinge trend near the cross section and across Dog Canyon was calculated with bedding orientations in Kse, Ksp, and Kdc. Fold hinge line away from Dog Canyon to south and north is taken from Satterfield and Dyess (2007).

3. Faults. Fault traces may have small enough displacement to determine the sense of slip, and may terminate in any of the structures presented as Figure 3.8.

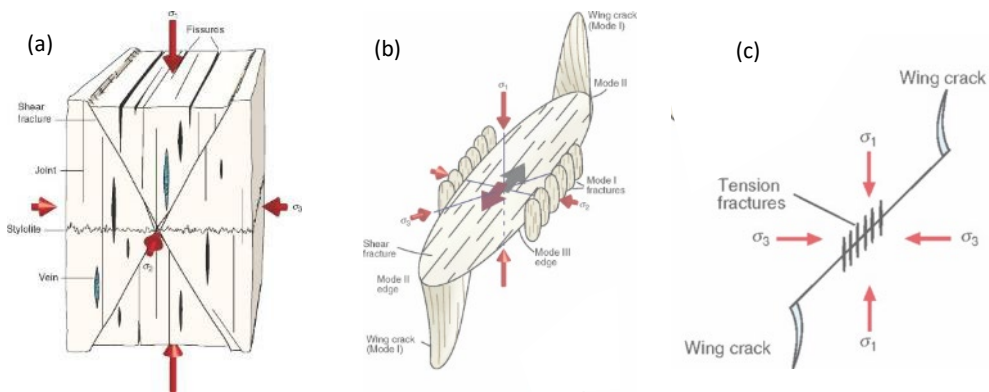


Figure 3.7. Mechanical-strain models used to map fractures and interpret strain axes. a. Block shows conjugate shear fractures, Mode I joints, and stylolites. b. Schematic oblique-view drawing of a shear fracture plane (Mode II joint) and associated Mode I joints. c. Side view of the structure in 3.7b in the S1-S3 (σ_3 - σ_1) plane. Figures from Fossen (2016).

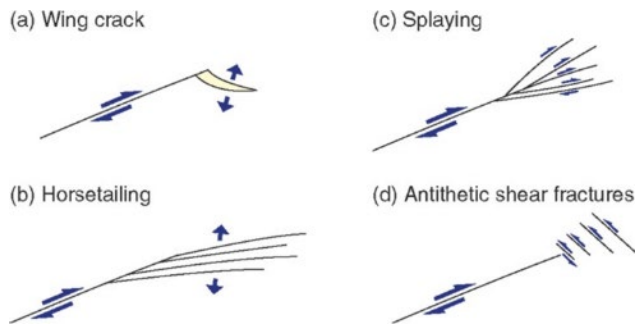


Figure 3.8. Traces of structures possible at fault terminations. Wing cracks (a) and horsetailing (b) are localized Mode I fractures and give ready indication of stretch directions (short arrows.) Splaying (c) and antithetic shear fractures (d) are additional localized small faults. Figure from Fossen (2016).

3.4.4 Interpretation of local strain ellipses

Oriented two-dimensional strain ellipses presenting S1 and S3 directions were interpreted where possible from mapped fractures on the orthomosaic image. These strain ellipse orientations are based on mechanical models relating fault and joint geometries to orientations of applied principal stress axes (summarized in Figure 3.7a), assume that stretch (S1) parallels tension (σ_3), and consider that the apparent dip on the cliff face is negligible at a 15-20° difference between true- and apparent-dip directions. Amounts of offset and therefore strain ratios were not calculable from the imagery, making these ellipses only schematic in dimension.

Where Mode I joints are mapped, S1 is interpreted to be perpendicular to those joint traces. Where conjugate shear fractures are mapped, S3 is plotted bisecting the obtuse angle between them. Where faults or isolated shear fractures are mapped, S1 is only interpreted if offset is apparent and reveals motion direction, in which case S1 is plotted 30° from that sense of motion; or if there are associated structures like termination Mode-I wing cracks or pull-apart structures that themselves reveal motion direction.

3.4.5 Direct measurements of lineated surfaces at canyon floor

Two-meter-scale, pull-apart mesostructures with lineated surfaces are partly accessible from the canyon floor and by ladder. Eight kinematic measurements of strike, dip, and rake were taken in these two structures and on another exposed fault surface, and strain axes were calculated using FaultKin (Marrett and Allmendinger, 1990; Allmendinger et al., 2012).

3.4.6 Creation of on-trail interpretive exhibit

A 42" x 24" panel was designed to be printed on and installed as an interpretive wayside exhibit along the Dog Canyon trail across the arroyo from one of the pull-apart mesostructures and in view of the most area of the cliff face as possible. This was designed in the same style as an existing wayside exhibit shared by the BBNP NPS geologist as a model (Figure 3.1).

3.5 Results

3.5.1 Fracture map

The orthomosaic photo produced from drone video and used as a base map is presented as Figure 3.9. Traced fractures are presented on the vertical map in Figure 3.10. This map reveals that multiple conjugate shear fractures are present, particularly in the upper portion of the cliff where Kse beds are overturned. Conjugate shear fractures are not everywhere present in pairs but do have at least two fractures, sometimes more, in rhombohedral clusters. They do not in all cases cross-cut each other but may only expose “half” of a crossed structure (e.g., upper left of Figure 3.11).

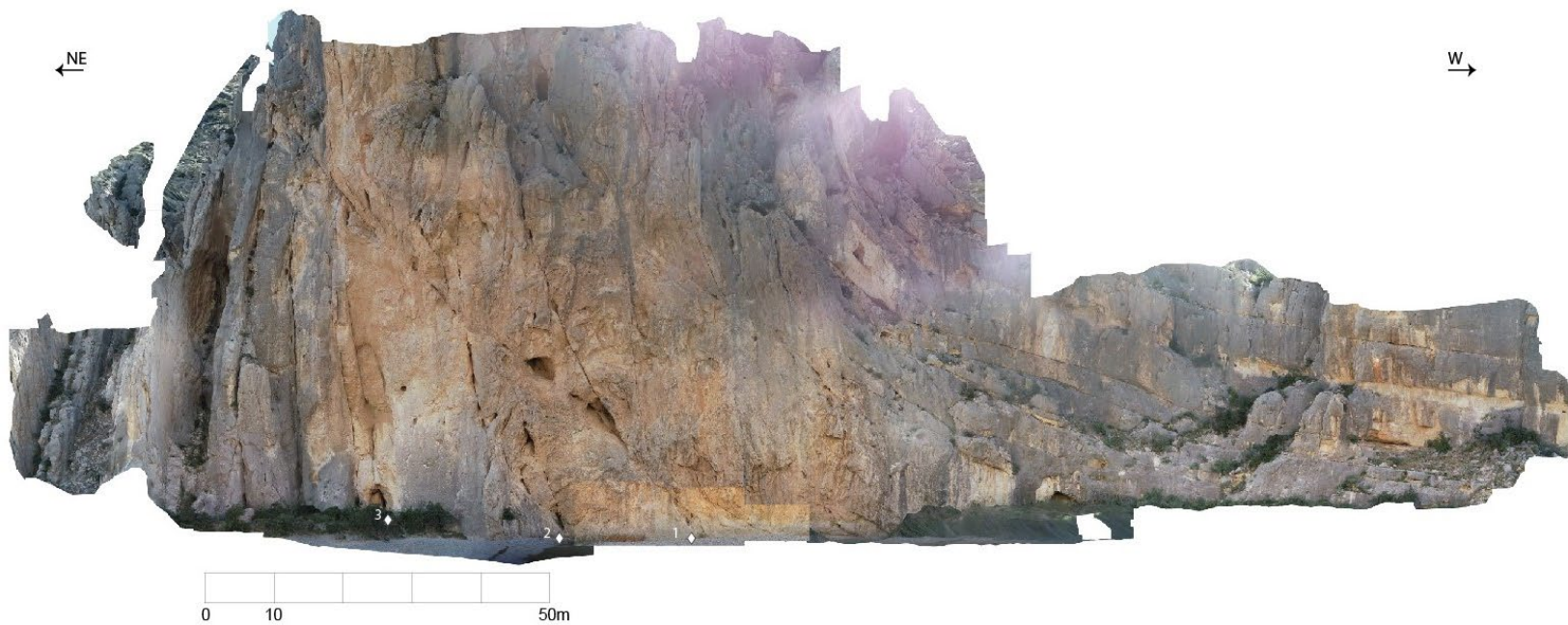


Figure 3.9. Orthomosaic of southern wall used as a base map in Dog Canyon. View is to southeast on the left, and to the south on the right, separated by a bend corresponding to the bend in the cross section. The stratigraphic base of the Albian-age Santa Elena limestone (Kse) is on the left and stratigraphic top is on the right, visibly folded in a syncline. Left view is $\sim 20^\circ$ from true dip of the fold; right view is $\sim 15^\circ$ from true dip of the fold. However, drone flight did not change view orientation during image capture. Numbered sites of field kinematic measurements are noted with white diamond.

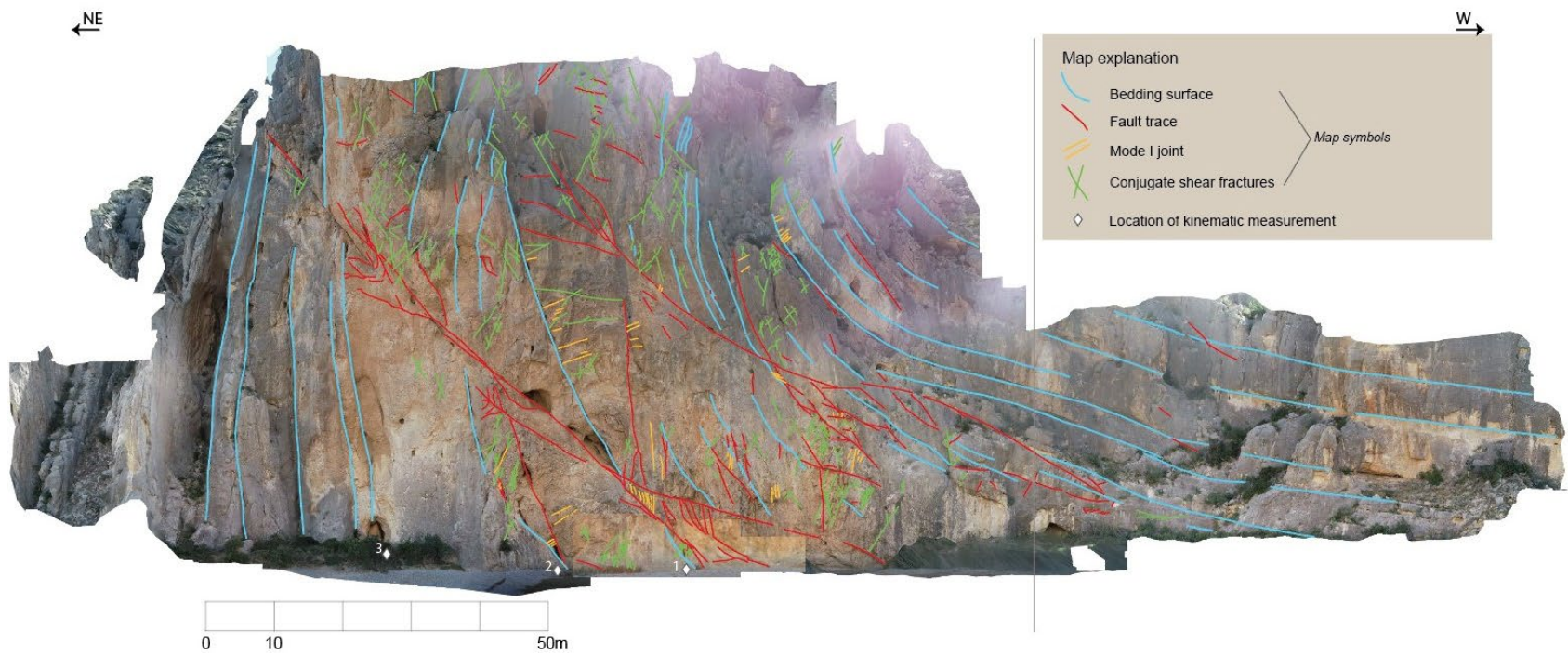


Figure 3.10: Vertical geologic map, remotely interpreted from orthomosaic, with traces of bedding, fractures, and fault surfaces mapped. See map explanation for symbology. Like a geologic map constructed on an irregular horizontal surface, some bedding surfaces' traces do not appear parallel.

Mode I joints are present either perpendicular to an adjacent bedding-plane trace, or associated with pull-apart structures. Mode I fractures that are oriented perpendicular to folded bedding surfaces of the Kse are consistent with either outer-arc stretching or inner-arc shortening (Figure 3.12). Additional Mode I fractures are present within pull-apart structures that are bounded rhombohedrally on the cliff-face view by a bedding surface and a fault (Figure 3.13).

Faults and isolated shear fractures in some cases are indistinguishable from bedding planes, particularly where one soles into the other (e.g., Figure 3.14,) because bedding is mapped by its orientation and association with other bedding. Some faults are mapped where bedding surfaces appear to be offset (e.g., Figure 3.15). Where offset is exposed, 'normal faults' reveal S1 parallel to folded bedding or 'reverse faults' reveal S1 perpendicular to folded bedding (e.g., Figure 3.15). Terminations of faults are mapped in places as splays and wing cracks (Figure 3.13, Figure 3.15), although those mapped as wing cracks may be considered Mode I fractures.



Figure 3.11. Section of cliff wall with conjugate shear fractures (green.)



Figure 3.12. Mode I fractures (yellow) perpendicular to bedding surface (blue) indicating outer-arc stretching.



Figure 3.13. Mode I fractures (yellow) "inside" three separate pull-apart structures bounded by bedding (blue) and fault (red) surfaces. Also in this location are fault terminations mapped as splays (upper left) and wing cracks (lower right,) although the latter may be instead mapped as Mode I fractures indicating sense on that fault.



Figure 3.14. Faults (red) and bedding surfaces (blue) in places are difficult to distinguish. Without outcrop access bedding is mapped by its orientation and association with other bedding.

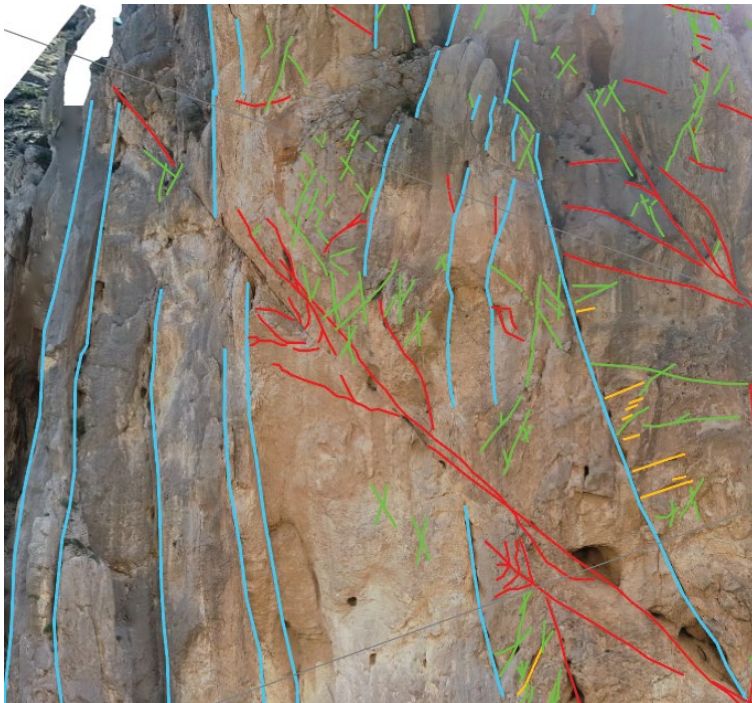


Figure 3.15. Bedding surface (blue) interpreted to be offset by fault (red) in upper left quadrant of image. Sense is normal as considered relative to the outer folded arc defined by the bedding surface. See Figure 3.5 for example.



Figure 3.16. Small fault (red) offsetting bedding surface (blue) in a reverse sense.

3.5.2 Cross-section

The cliff wall image with its interpreted intra-fold strain partitioning is presented in the context of the apparent-view cross-section parallel to the southern cliff face, looking generally south (Figure 3.17). A bend in the section line separates the northeast portion of the line on the interpretation's left, which is 20° from the true-dip cross-section line, from the west portion of the line which is 15° from the true-dip section line (Figure 3.6). These calculations are based on the calculation of the fold axis orientation from folded bedding surfaces. The calculated fold axis plunges 2.5° toward 341° (Figure 3.18). Such a negligible plunge allows for the vertical section to be considered as a down-plunge projection without modifying. Nearby geologic mapping used to construct the cross-section is taken from Satterfield and Dyess (2007) and Turner and others (2011) (Figure 3.3, Figure 3.6).

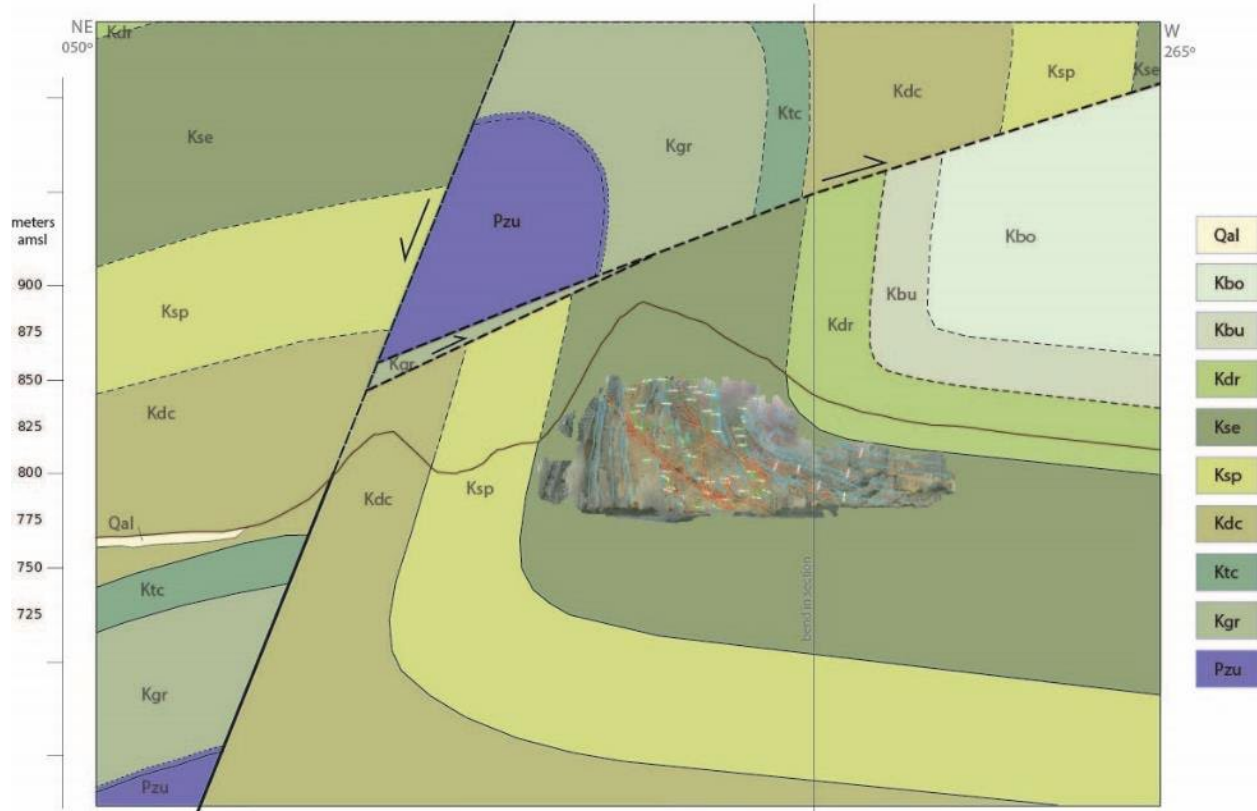


Figure 3.17. Apparent-view geologic cross-section through south wall of Dog Canyon (looking southeast and south). Section line bends to maintain view of the cliff wall from the trail in the canyon. Section line for geological interpretation is ~40m behind the visible cliff wall. Orthomosaic of cliff wall is superimposed on the cross-section to orient the viewer to its place in the local geology. The canyon floor (at the base of the image) is approximately 770m above mean sea level.

This interpretation suggests a fault-propagation fold that was formed and then cut by the Santiago thrust fault system, preserving a footwall syncline exposed in Dog Canyon. These structures have subsequently been cut by a younger extensional fault and are preserved in the footwall of a northeast-dipping normal fault. A lateral ramp of the Santiago thrust truncates an older thrust-fault branch separating Glen Rose limestone beds of a thrust-parallel orientation in the thrust's hanging wall (Figure 3.17; from Figures 3.3 and 3.6).

The fold has a moderately inclined axial surface that dips approximately 45° to the northeast. Exposed beds of both limbs allow an interlimb angle calculation of approximately 100° to 110° ,

classifying this as an open fold. The moderately sharp angle exposed in the hinge, and visible thinning of the Sue Peaks in the upper limb, require thickening of strata in the subsurface portion of the hinge, particularly in the lower-strength rock of the Sue Peaks Formation, suggesting a Class 1C fold (without the constant thickness of parallel or Class 1B folds). Alternatively, the higher-stiffness limestone layers like Santa Elena may be Class 1B or 1C and the adjacent lower-strength clay formations Class 2 or 3. No parasitic folds are visible in the drone imagery or in person at the canyon floor.

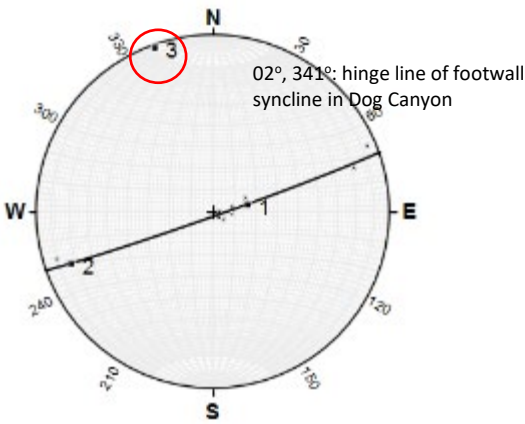


Figure 3.18. Pi-diagram calculation of the fold axis.

In Dog Canyon the Santa Elena limestone in the exposed, near-vertical upper limb is measured in GIS at 124 m thick. This apparent cross-section line is 20° from a line that would be perpendicular to the fold hinge and the bedding strike, making a true apparent thickness of 117m. Maxwell (1967) defines the Santa Elena limestone at its type locality at Santa Elena Canyon 70 km to the southwest, the site of the only complete measured section in the region. There it is 226 m (740 feet) thick and was measured “by triangulation,” with outcrop described only at its top because of inaccessibility. Elsewhere in BBNP and Black Gap, the section is either incomplete by erosion or deformed by folds or faults (Maxwell, 1967). The upright, shallowly-west-dipping strata in the west limb of the syncline comprising

the west end of Dog Canyon measure 67 meters (220 ft) at the top of a mostly buried section (Maxwell, 1967).

The nearest measured section of the Sue Peaks Formation (Ksp) is 30km to the south-southeast where it is 77m thick (Maxwell, 1967). Ksp crops out in the upper limb of this reclined footwall syncline at only approximately 50m. Moustafa's (1988) geologic map projects 244 m (800 feet) of complete Ksp thickness when projected into cross-section (Satterfield, personal communication 2023), which is thicker than anywhere measured. Maxwell (1967) records 23 to 24 meters (73.5 to 79 ft) in the Sierra del Carmen, and 80 m (265 ft) at Santa Elena Canyon. The interpretation in this study thins the upper limb to what is apparent on the satellite imagery (and was mapped in Turner et al., 2011) and thickens the Ksp to the nearest complete measured thickness of 77m in the lower fold limb.

Thinning is visible in the older Sue Peaks Formation under the thrust fault at the top of the cliff (Figure 3.6) and therefore the upper limb is drawn to the exposed thickness of approximately 50m and its lower limb is interpreted at a thickness matching the closest reported measurement at Heath Creek approximately 30 km to the south-southeast, or 77m (Table 3.1). Thinning of the Sue Peaks in the upper fold limb suggests the Santa Elena Formation may also have thinned in the upper limb of the fold, although the Sue Peaks' weaker shales are more able to flow into a Class 2 or 3 fold than the rigid and massive limestone of the Santa Elena. Surpless and others (2015) demonstrated that the Sue Peaks acted as a decollement flat portion of an east-verging blind thrust forming the Stillwell anticline due to its lower strength, supporting the observation of it thinning in the upper limb of the Dog Canyon fold.

In the absence of outcrop the northeast-dipping normal fault is assumed to dip approximately 60° to the northwest following Anderson's theory of faulting. To place the Del Carmen formation at the surface as mapped in the normal fault's hanging wall (Satterfield and Dyess, 2007), offset of 380 m is interpreted. Along strike to the south, this normal fault is mapped to juxtapose the Cenomanian-age

Boquillas Formation and Albian-age Glen Rose Formation, requiring a minimum of 380 m of stratigraphic offset, supporting the offset interpreted here.

3.5.3 Three-dimensional mapping of fracture patterns and kinematic indicators

Surfaces that are hand-measurable in the field at arroyo level expose measurable slickenlines on two pull-apart structures formed by bedding surfaces and faults with mode-I veins and fractures in between (Figure 3.19; Sites 1 and 2) and on a small fault surface obscured by trees from the imagery on the eastern end of the canyon (Site 3). The internal structures at Site 1 include both mode-I and conjugate shear fractures. Kinematic measurements are presented stereographically in Figure 3.20. Sense of motion is not indicated in lineations on the pull-apart structures but presence of the internal fractures indicates normal sense on each. At site 1 the calculated trend of the extension axis is 247° , and at site 2 it is 240° . The single fault measurement at site 3 yields 236° as the primary strain axis, either extension or contraction depending on whether sense was input as normal or reverse. All surface orientations are presented as Table 3.2.



Figure 3.19. Two pull-apart structures on Dog Canyon's south wall at the canyon floor with annotated senses of motion (arrows) and locations of measured slickenlines (red squares). Site 1 is west of Site 2. Ladder for scale in left image; right image is of similar scale.

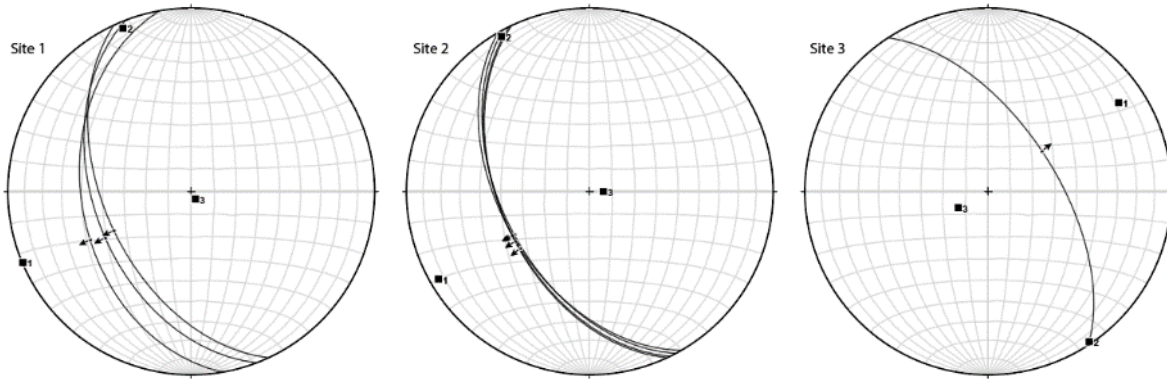


Figure 3.20. Slip surfaces with slickenlines measured at ground level in Santa Elena limestone in Dog Canyon. Sense of motion at sites 1 and 2 was assumed from associated fractures (Figure 3.19). T axes are calculated via FaultKin at 247°, 240°, and 236° respectively. These are approximately 100° from the 341° hinge line of the footwall syncline (ten degrees from orthogonal) suggesting association with syn-thrust folding.

Table 3.2. Kinematic data collected from ground-level outcrops. Trend of primary strain axis identical for S3 axis where thrust sense is used and S1 axis where normal sense is used. Lack of sense indicators on outcrops requires leaving this open. Locations 1 and 2 are inferred as normal-left slip by inclusion on pull-apart structures with Mode-I joints. Location 3 is an isolated fault surface behind the cluster of trees on the northeast.

Site number	Strike	Dip	Rake (if available)	Trend of primary strain axis
1a	170	40	78 S	247/67
1b	155	51	91 S	
1c	159	46	85 S	
2a	152	51	89 S	240/60
2b	155	50	87 S	
2c	154	50	85 S	
2d	150	50	84 S	
3	327	60	88 N	236/56

3.6 Discussion

3.6.1 Interpretation of deformation at Dog Canyon

3.6.1.1 The fold is a syncline in the footwall of a fault-propagation fold

Rocks exposed in the cliff face in Dog Canyon are part of the hinge and upper limb of a fault-propagation fold's remnant footwall syncline under the southwest-verging Santiago thrust fault. These features were exposed by canyon cutting on the north face and down-to-east normal faulting to the east. A structural cross-section restored to pre-extension deformation is presented in Figure 3.21. Theoretically, fault-propagation folds are preserved only in hanging-wall rock after the thrust fault moves through, but the propagating fault may also cut the short limb of the fold that developed in front of the propagating fault and leave a synform in the footwall, or alternatively drag the rock of the footwall into a synform while the fault cuts the fold (Fossen, 2016 figs 16.18 – 16.19; Suppe et al., 1990). Either of these occurred to form the Dog Canyon syncline. At this cross-section line no hanging-wall rock is preserved, but near-vertical, overturned Glen Rose limestone of the hanging wall does crop out 300 meters south at the ridge top to further preserve evidence of fault-propagation folding (Figure 3.6). Paleozoic strata crop out 300 m farther south.

Exposed tops and bottoms of both the Kse and Ksp in the upper limb of the footwall syncline reveal that both formations are thinner in the Dog Canyon exposure than measured elsewhere. This may indicate footwall-restricted two-dimensional volume loss (strain out of the plane of the cross-section) resulting from motion on the lateral ramp portion of the Santiago thrust. The older thrust that is cut by the Santiago thrust and which is only known by a small, shallowly-eastward-dipping outcrop of Kgr may also have contributed to volume loss before Santiago thrusting. The Ksp may also have thinned by volume loss under orthogonal vergence of the Santiago thrust strictly by virtue of its lower strength. Neither of the adjacent clay-rich formations (Ktc and Kdr) are exposed enough to test this hypothesis.

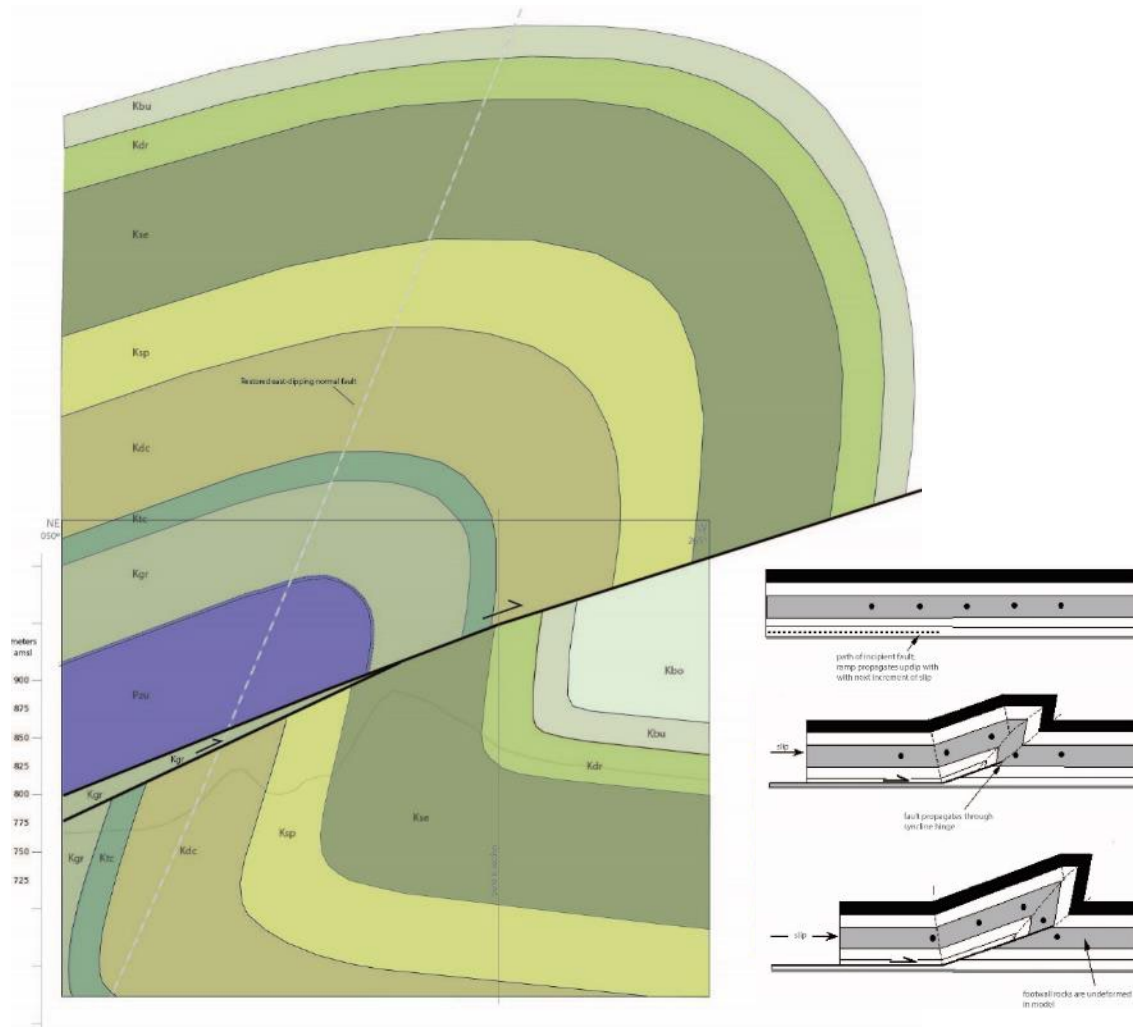


Figure 3.21. Structural cross section restored to before normal faulting shows the fault-propagation fold of the Santiago thrust. Inset: Development model of fault-propagation fold (after Davis et al., 2011). An anticline/syncline pair is formed in front of a propagating thrust tip, and progressive faulting cuts that fold. In this theoretical model footwall rock remains undeformed, but the propagating fault tip may cut higher in the forelimb of the fold and leave some upturned limb in the footwall.

3.6.1.2 Fractures in the cliff wall record multiple strain events

Strain ellipses in the S1-S3 plane, interpreted from mapped fractures, are superimposed on the cliff-wall image (Figure 3.22). While the most apparent structure in the rock of Dog Canyon is a footwall syncline, all observed strain ellipses do not fit the orthogonal flexure model. Rather, three separate strain events appear to be recorded in these mesoscale structures: (1) Orthogonal flexure during fault-propagation folding, (2) horizontal contraction during southwest movement on the Santiago thrust, and (3) horizontal extension caused either by vertical loading after horizontal contraction relaxed, or by

active lithospheric extension associated with Rio Grande rifting and accommodated by the normal fault at the northeast end of Dog Canyon (Figure 3.23).

1. Some strain ellipses are orthogonal to the mapped bedding surfaces within the fold's hinge zone, recording inner-arc shortening and outer-arc stretching. These are not bounding surfaces of the Santa Elena Formation and therefore are internal mechanical-layer boundaries formed *either* during its deposition or lithification, *or* during folding via syn-folding separation of newly formed mechanical layers (after Couples et al., 1988). Absence of a complete measured section prevents correlation by internal stratigraphic thickness. Although by this model the Santiago thrust had not yet breached this rock while it folded, thrusting was the cause and so the fold hinge trend calculated from bedding orientations can predict a vergence of the Santiago thrust of approximately 251° or west-southwest at this time.

Stretch direction calculated from accessible lineated surfaces is no more than 15° from the 251° trend of the line perpendicular to the fold hinge, suggesting association with syn-thrust folding. The strain ellipses mapped at both of these mesostructures also align with folding. If the two intra-fold pull-apart structures at ground level in Dog Canyon were formed during syn-thrust folding, then southwest to west-southwest vergence of approximately 240° on the Santiago thrust is indicated. However, slickenlines on the Santiago thrust surface itself are required to confirm that determination because internal fold deformation will only be orthogonal in a purely cylindrical fold. Whether deformation here aligns with sinistral transpressive regional deformation can only be spoken to with that information.

2. Strain at the west end of the cliff is orthogonal to bedding, but because this location is geometrically far from the fold hinge (Figure 3.17) the strain ellipses don't appear to model inner-arc shortening, and therefore fold-related deformation is unlikely. These small reverse faults are

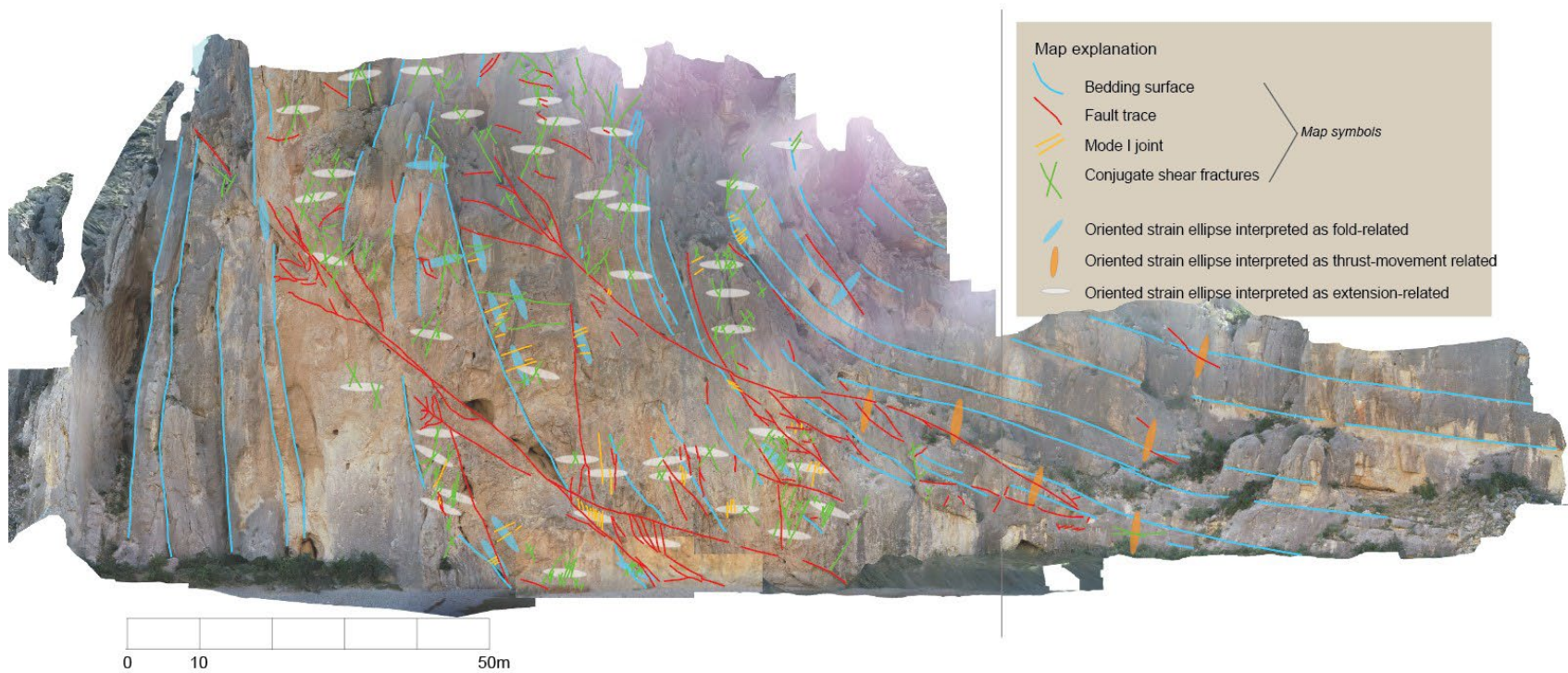


Figure 3.22. Oriented strain ellipses interpreted from fracture orientations. Ellipses are S1-S3 projection of ellipsoid but do not represent strain ratios, only orientations. Three separate strain patterns are annotated with three colors of ellipse as explained on the figure.

proposed to have formed as part of horizontal contraction during movement on the Santiago thrust, and thus these are synchronous with thrusting but would post-date fault-propagation folding.

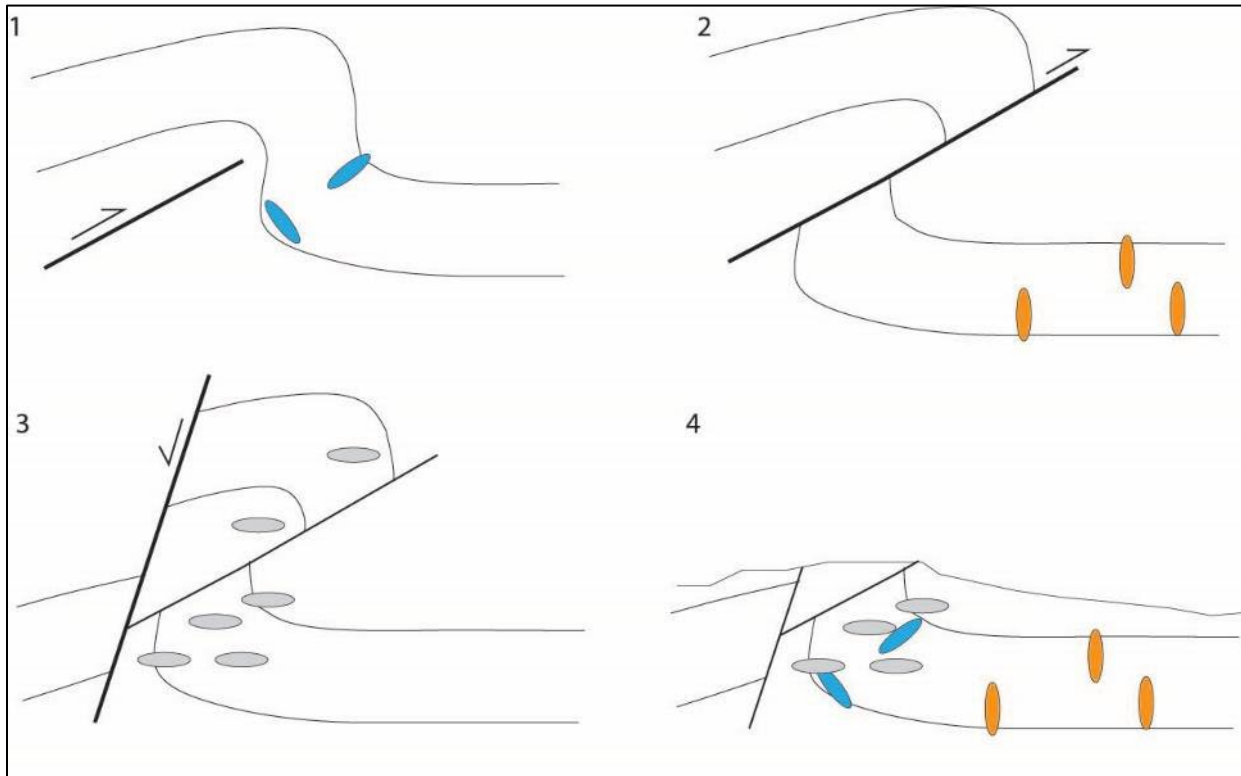


Figure 3.23. Proposed geologic history of the Dog Canyon area from earliest to most recent. 1: During NE-SW Laramide contraction at some time between 75 and 50 Ma, the fold currently preserved at Dog Canyon formed ahead of the propagating tip of the Santiago thrust fault, causing a strain pattern consistent with orthogonal flexure in the Albian Santa Elena limestone (blue strain ellipses.) 2: The Santiago thrust fault cut through the forelimb of the fault-propagation fold, preserving a syncline in the footwall and an anticline in the hanging wall. Horizontal compressional stress formed shortening/thickening structures away from (to the west of) the hinge of the syncline (orange strain ellipses.) 3: After Laramide contraction had ceased, horizontal extension occurred, forming numerous conjugate shear fractures revealing horizontal stretch and vertical contraction (grey strain ellipses.) This could have happened upon relaxation of Laramide horizontal compression, or after northeast-southwest directed Rio Grande rift extension had begun. (The latter is shown in 3). 4: Today's erosional surface of a cliff wall adjacent to a canyon exposes the upright limb of the footwall syncline, with strain indicators of each of the three previous events preserved.

3. Conjugate shear fractures throughout the east part of the outcrop reveal a generally horizontal S1 orientation that can have been caused by one or both of two different events: Either relaxation of northeast-southwest contraction enabling downward loading and thinning, or horizontal extension associated with Rio Grande rift extension via the down-to-east normal fault bounding the eastern edge of this outcrop and the edifice of the Sierra del Carmen. Apparent proximity of these shear fractures to the effective S1-S3 orientation of the cliff face indicates that they may align with the

earliest Rio Grande rift stretch direction (S1) of northeast – southwest, which would support the latter scenario. Improved point-cloud resolution that would allow surface mapping of the conjugate pairs of shear fractures would provide helpful 3D geometric data to contribute to that question, determining S2-axis orientation into the outcrop, and therefore orientation of S1. Some of these conjugate fractures may also be accessible by foot at the cliff top. In both possible cases this horizontal-stretch event occurred the most recently. The ubiquity of these structures also supports horizontal extension as the latest deformation event affecting the Dog Canyon outcrop.

Some strain is indistinguishable from events 1 or 3 and could be either. Some structures hypothetically could have been rotated but these are not apparent.

Prior sedimentological and structural data indicate that the Laramide Orogeny in Trans-Pecos Texas operated in two pulses between at least 75 and 50 Ma, and in two separate directions. While Dog Canyon records two local contractional strain events acting on the Santa Elena formation, fold-and-thrust-belt models still support fault-propagation folding and subsequent thrust-faulting of that fold as one contractional event, so these rocks do not provide further evidence to the regional two-stage hypothesis. Either Dog Canyon contracted in one stage, or evidence for both stages has not yet been found here.

The sparse kinematic data accessible for this analysis show an average thrust vergence of approximately 240°, or a range from 236° to 247°, which aligns with the documented later-Laramide east-northeast to west-southwest contraction stage.

3.6.2 Panel to submit to NPS for interpretive wayside exhibit at end of Dog Canyon trail.

This project was undertaken to conduct a geoscientific study and then to bridge geoscience and public knowledge. To that end, a model 42-inch x 24-inch image to submit to NPS to be installed as an

interpretive wayside exhibit at the end of the Dog Canyon trail in front of the exposed upper limb of the fold is presented as Figure 3.24. Only one exhibit was requested, and extra information may be presented with a QR code at the trail end and the parking area as suggested by NPS. Themes presented beyond the interpretation of this area’s deformation history outlined above are understandable tools that geoscientists use like strain ellipses, geologic time and regional tectonic events, and the relevance of geoscientific work to human society (in this case, geologists’ prediction of 3D fabrics in the subsurface and the accumulation of natural resources aligning with those fabrics). Some of the Earth Science Literacy Initiative’s “Big Ideas” are also represented (Table 3.3). As such standards percolate into the populace, these may be unknowingly recognized by park visitors and these exhibits would help to underscore a connection with local geologic history and the relevance of geoscience.

Table 3.3. Relevant "Big Ideas" and supporting concepts from the Earth Science Literacy Initiative's Earth Science Standards for US public education.

Earth Science Standards' Big Idea number	
1	Scientists use repeatable observations and testable ideas to understand and explain our planet
1.3	Earth science investigations take many forms
7	Humans depend on Earth for resources
7.4	Resources are distributed unevenly around the planet
2	Earth is 4.6 billion years old
2.1	Earth's rocks and other materials provide a record of its history

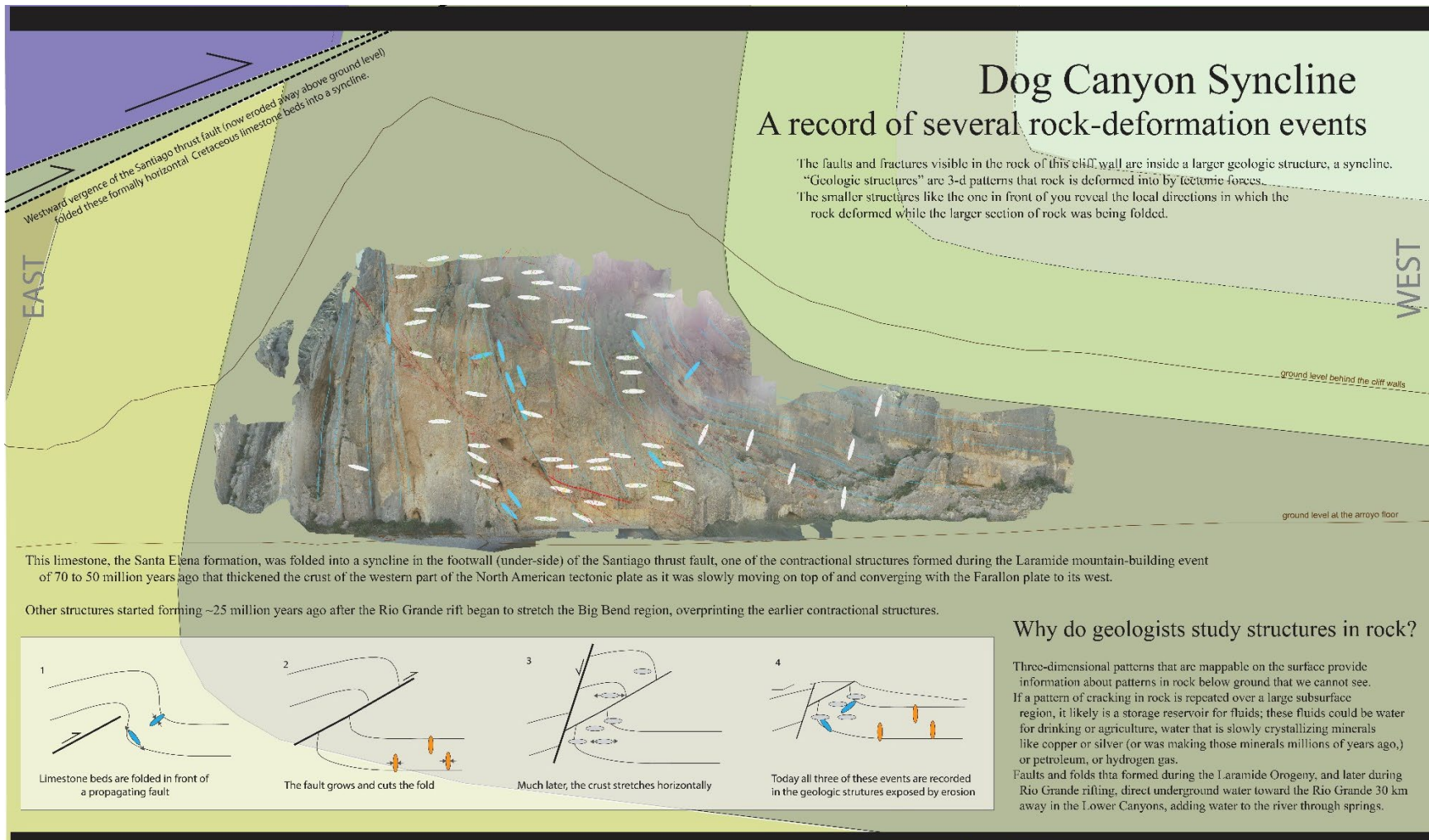


Figure 3.24 Plan for interpretive wayside exhibit at end of Dog Canyon trail.

3.7 Conclusions

Remote imagery of vertical beds and visible deformation along the Dog Canyon trail allows mapping of a vertical wall not accessible by foot. These new data and mapping reveal two separate strain events during propagation of the Santiago thrust, as well as later-Cenozoic extension. This mapping also affords an opportunity to expose recreating non-scientists to some of the methods, learnings, and utility of geoscience.

Previous work documenting Laramide transpression throughout the Big Bend area is not testable with data from the canyon, but may be with kinematic measurements at the top of the cliff along the Santiago thrust fault.

A 7-million-point cloud created with the remote imagery has both resolution and orientation that are too coarse to map visible surfaces with precision, but this cloud may be used for an in-class exercise for structural geology students.

CHAPTER 4: A CASE STUDY COMPARING UNDERGRADUATE STUDENTS'
ENGAGEMENT, KNOWLEDGE RETENTION, AND PERCEPTIONS OF RELEVANCE OF
GEOSCIENCE AFTER IN-CLASS EXERCISES USING DATA THAT IS EITHER LOCALLY OR
GLOBALLY SOURCED

4.1 Abstract

In-class exercises that expose students to real geoscientific data were developed and delivered to five sections of Physical and Historical Geology undergraduate university classes, with three sections using data that had originated locally and two sections using data that had originated more distantly, or “globally.” Students were surveyed to assess their engagement, knowledge retention, critical thinking, and perception of the relevance of geoscience after each exercise, to test how these outcomes differ between the students working on global data and those working on local data. The group exposed to local data returned higher scores and rankings after four of the five exercises indicating a lead in each of those outcomes, particularly in answering questions with a higher Bloom’s level of complexity measuring critical-thinking skill, and in their perception of the relevance of the geoscientific topic. Unavoidable variation between exercise topics in the level of contact with and manipulation of data reveals an additional conclusion that more contact, for example downloading data vs. opening a provided file, and more manipulation, i.e. graphing vs viewing completed graphs, also produces more engagement, knowledge retention, and connection to the relevance of these geoscientific topics among both student groups, albeit those working with local data more so than global.

4.2 Introduction

Undergraduate introductory geoscience courses provide many students with their very first exposure to the workings of Earth science. This differs from biology, chemistry, and physics courses, all commonly required in US high schools and therefore a part of students' background when they get to college. These introductory geoscience courses are instructors' opportunity to influence students to become geology majors (McConnell et al 2017), but they are of broader importance as they are an opportunity to reveal the relevance of geoscience to human society on Earth, and could also be the only exposure to Earth science that these students obtain in their lifetime. These classes can be seen as a means to educate a larger portion of the country's populace in geoscience literacy than the small group embarking in STEM careers, so that these young people can participate intelligently in societal decisions with an understanding of Earth science (Gosselin et al., 2019).

This case study of students in five sections of core introductory geology classes at Sul Ross State University and Angelo State University in rural west Texas quantifies relative success in the outcomes of knowledge retention, student engagement, critical-thinking skills, and perceptions of the relevance of geoscience by presenting in-class active-learning exercises that use real geoscientific data while varying the proximity of the data between groups of students: one group's in-class exercises use locally derived geologic data, including from the Big Bend region, and the other group's exercises use only distantly derived, or global data.

This study aims to learn how to best increase an appreciation for the geoscientific process and for the relevance of geoscientific work and information among undergraduate students of all majors, in part by introducing some tectonic data from the prior two projects, and also expanding into more topics for physical and historical geology classes. For hope of a prosperous society to continue within tightening ecological limitations on Earth, it is imperative that more people, especially non-scientists, are

taught to regularly and naturally think critically. For these reasons it is also imperative for these reasons that this skill is cultivated in the presence of positively impressionable classroom experiences in working on Earth-science problems that bear on human society and that impress on these students the relevance of Earth science.

4.3 Background and Previous Work

Teaching with data is a pedagogical method that has demonstrated success in STEM courses, especially in K-12 and upper-division courses (e.g., Manduca and Mogk, 2022; McConnell et al., 2017; (MacKay, n.d.). Such real-data-rich classroom exercises are also lauded anecdotally as an important part of geoscience education by experienced undergraduate teachers. Manduca and Mogk (2002) express in the final report of the National Science Digital Library Workshop that the best evidence showing that the use of real data in science classrooms improves learning comes only from anecdotal data from experienced STEM faculty observations. Their report therefore calls on the STEM community to “undertake a rigorous, documented evaluation of the impacts of data-rich experiences on student learning” in undergraduate STEM classrooms. Specifically they are asking the undergraduate teaching community to undertake experiments to determine whether using data in science teaching causes students to improve on each or any of the following: Knowledge absorption and retention, improvement of life skills like critical thinking and decision making, and/or an improvement in attitude of science and data (Manduck and Mogk, 2002). This was a broad call for more research to learn which aspects of teaching with data will support these particular learning gains.

McConnell and others (2013) refer to classroom and homework exercises that use real data as problem-based learning. Ruiz-Primo and others (2011) combined categories they called “tech” (which includes using real data) and inquiry-based problem solving (IBP) into a single category of teaching styles reviewed for their effect on student learning in undergraduate science classes, and this combined category scored the highest. Kim and others (2013) also found that when students address problems that require them to retrieve, analyze, evaluate, and synthesize data, their complex thinking skills are supported. McConnell and others (2017) assessed eleven active-learning strategies for best outcomes in geoscience instruction: They grouped both case-based learning activities and problem-based learning

activities in a single of their eleven assessed categories and found that this grouping scored highest in their assessment for student-learning efficacy. Their assessment also includes teacher utility, in which this grouping achieved a moderate score because of preparation on the part of the instructor for these classroom activities.

Manduca & Mogk define “data” for their 2002 report on teaching with data in all STEM classrooms to include any information “that supports student inquiry and participation in the scientific method, including experimental or observational data as well as simulated data derived from models.” This definition had utility in their report to ensure a broad group of scopes that they were calling on the STEM-education community to investigate. MacKay (2018) expands on that definition to add that data used in the right kind of exercise will also support students’ effective evaluation of uncertainties in and applicability of those data, as well as improving their quantitative and critical-thinking skills.

SERC (n.d.) defines two categories of data that are useable in geoscience classes. First are existing real-time or archived data from remote networks such as satellites, buoys, or seismic networks. Students have opportunity through exposure to these types of data to learn about not just physical processes but data availability and access, and then through the classroom exercise, the processes of analysis and interpretation of those data that reveal physical processes. The second of two types of data that SERC defined is that collected by the students themselves, by which they also have opportunity to learn about design of experiments, variability of data quality, and techniques of measurement. This study consistently uses SERC’s first category rather than the data collected by students. SERC introduces three frequently encountered data structures as follows, and I have added one data structure to their list.

1. Unordered data or replicates, for example those data that would be displayed in frequency plots or histograms (Figure 4.1).

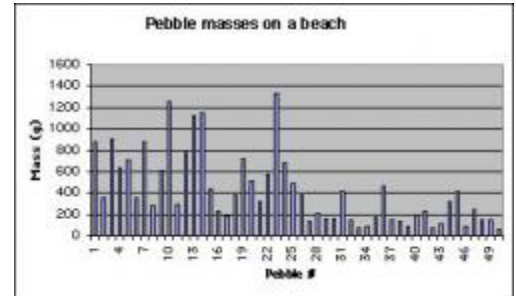


Figure 4.1. Example of unordered data. From SERC, n.d.

2. One-dimensional spatial data or bivariate data, for

example well logs, vertical profiles of ozone or

temperature through height in atmosphere. This category

could also include sediment and ice core data, but only before their depth is correlated to time,

at which stage these core data become part of the next category.

3. Data with two variables, e.g. (1) time-series data, for example atmospheric or ocean

temperatures through time, surface-water discharge amount through time, and water-table

level through time. (2) Also in this category are other two-variable relationships like earthquake

intensity vs earthquake magnitude. SERC (n.d.) asserts that trend analysis is appropriate for

introductory college courses.

4. Two- or three-dimensional spatial data, for example geometric and kinematic data from

geologic structures and from earthquakes.

Active learning is another pedagogical method that has been widely employed, well observed, and well documented at all levels and disciplines of STEM classes including introductory college geoscience courses (e.g. Kim et al. 2013; Huguet et al. 2020; McConnell et al., 2017). McConnell and others (2003) analytically demonstrated that such methods are preferred by students, they improve student retention, they promote deeper understanding of course material, and they increase logical thinking skills. McConnell and others (2017) further demonstrated that active learning techniques in classrooms reduce the “achievement gap” between different populations of students. Additionally, active learning is currently more popular among teachers in K-12 schools than in colleges and

universities, so introductory undergraduate students will relate to it, thrive, and use it (Doser, pers. comm., 2019). Among many specific and well defined active learning strategies are those that employed in this study: participatory experiences classified as “doing,” followed by opportunities to reflect on learnings from those experiences (McConnell et al., 2017 after Fink, 2005); and more specifically, in-class partner work using Excel (e.g., Leckie, n.d.).

Place-based learning has been investigated as another pedagogical tool that can increase student engagement, knowledge, and perceptions of relevance, particularly in environmental science programs wherein local environmental challenges can be analyzed (Kirkby, 2014; Gosselin et al., 2019). Some researchers have analyzed the relative impact on student learning outcomes of the origins of data used in classroom assessments specifically to communities believed to be the most inherently grounded in a sense of place. Semken and others (2017) found that while most undergraduate geoscience teaching emphasizes information on a global scale, emphasis instead on very local processes and landforms is more compelling to Native American introductory geology students. Their analysis promotes that instructors who teach exercises by “authentic experiences, ecological/sustainable living and integrating diverse meanings,” in addition to integrating other natural sciences, see results of better learning. Ward and others (2014) suggest that the local landscape is a key link in designing geoscience assessment that is both culturally and geologically meaningful to Native American communities, finding that place-based relevance should be fundamental to assessments, which typically instead ask questions about overarching models of processes with only distant or global examples if any. While place-based learning is especially appealing to native ethnic groups and cultures, it is also reasonable that it is appealing to many people from rural communities because they may have seen geologic processes in action and it may be relatable as something that can impact their lives. Further, both Davies (2006) and Kirkby (2014) prove the utility of place-based learning to non-Native, urban schools, removing the expectation of a rural background to be able to cultivate relevance.

This investigation follows the known efficacy of contact with real, archived geoscientific data; the use of active, in-class exercises that allow manipulation of and reflection on those data; and of place-based learning that draws on connections to a local place. This study tests the hypothesis that in-class use of archived or published geoscientific data that is locally instead of globally sourced will result in better comprehension and therefore retention of inherently whole-earth geoscientific process concepts, in better demonstration of critical-thinking skills, and in increased engagement with and recognition of the relevance of geoscience. These geoscientific concepts include earthquakes, rock deformation from plate tectonic processes, volcanic processes, surface-water behaviors, and global climate change.

4.4 Methods

4.4.1 Creation and delivery of demographic-data survey

At the beginning of both of the tested semesters, students who signed an Informed Consent were given a survey to assign an identifier code that they would place on each subsequent survey and to collect demographic data and information about their prior exposure to science. Because this analysis compares responses and experiences between two groups of students exposed to either “local” or “global” (non-local, or distant) geoscientific data, demographic data were collected on beginning-semester surveys to test for significant differences among the backgrounds of the student groups. In addition to race/ethnicity and GPA, students were asked to indicate their major, the size of their hometown, and their previous exposure to science. Students indicated their prior exposure to science by selecting all applicable of the following options: Very little exposure; Was into science classes in high school or as non-physical-science major; Read science news; Watch science documentaries or docuseries; discuss science topics at home; Follow science podcasts or channels (e.g. “Science Friday;” “Global Weirding;” “PBS Eons”); Physical Science major. Major, size of hometown, and previous exposure to science are presented as Figures 4.2 to 4.4. Students were also asked to numerically rank their impression of the relevance of geoscience to them or someone they know, to their community, and to human society. The student-identifier code was used to allow anonymity of students but to link their responses between each of their surveys, including their demographic information should it be needed to drill down to compare to bulk responses. Per the IRB agreement, these surveys were collected and stored until after each semester ended. A blank, beginning-of-semester survey is presented in Appendix 4.

4.4.2 Creation and delivery of exercises

Exercises were developed for this project in topics from a Physical Geology curriculum and were chosen to (1) be spaced out through the normal semester, (2) use live or archived real data available in class via internet and manageable in Excel or another data-manipulation tool where appropriate, and (3)

use data available in both a local and a “global” or distant, non-local example. The proximity of local data was dependent on the type of exercise; for example local climate data were retrieved for the student’s hometown, but the Jemez volcanic field provided local volcanic data. In attempt to provide equal value of geologic information between the two student groups (those using local and those using global data,) some “global” data were within the United States but reasonably far away. Heretofore, the students whose exercises used local data are referred to as the local-data group (LG) and those whose exercises only used distant or “global” data are referred to as the global-data group (GG). Exercises were on the topics of structural geology, earthquakes, volcanoes, streams, floods, and climate. They are summarized in Table 4.1 and each presented in Appendix 3.

These exercises were delivered to two sections of Physical Geology at Sul Ross State University (SRSU) in the Fall 2021 semester as part of the curriculum and to three sections of Historical Geology at Angelo State University (ASU) in the Spring 2023 semester, also as part of the curriculum. At SRSU, one section was given the exercises with global data sources, and one section the local data. Both of these class periods were 50 minutes. At ASU, two sections were given the exercises with local data sources, and one section was given the global data. ASU students worked on exercises in one or two 50-minute or 75-minute classes. Determination of redundancy between the stream and flood projects at SRSU, plus recognition that six exercises were too many for one semester and concerns for time at ASU, caused elimination of the streams project at ASU. Two sections at ASU (one receiving local data, one global) did not receive the volcanoes exercise because of time constraints. The exercises were developed for Physical Geology at SRSU but were delivered in a different order in ASU’s Historical Geology classes. A summary of the five in-common exercises, data types, sources, and descriptions follows and is presented as Table 4.1.

In the two geologic structures exercises, the LG worked entirely on data from the Big Bend area of Texas while the GG worked entirely on data from the Palisades and eastern Appalachian areas of New

Jersey and Pennsylvania; the unique portion of each exercise therefore totaled 100%. Both groups entered planar fault and fold-axis data into the 'Stereonet' program (Allmendinger et al., 2012; Cardozo and Allmendinger, 2013), observed those planes in the 3D view tab, viewed and considered given paleogeographic maps (Scotese, 1998) and used those and the online HHMI Interactive viewer (HHMI, n.d.) to determine relationships between structure geometries of given ages and known tectonic events. The structure exercise was delivered first at SRSU, and third at ASU.

Between the two earthquake exercises, the LG and GG worked on the same problems and data for the first two thirds of each exercise and each used unique data for the last third of the exercise. Both groups graphed an equation comparing earthquake magnitude to ground shaking and used their chart to investigate shaking data from the 2019 Ridgecrest, California earthquake. The GG then used earthquake data from Nepal, and the LG from west Texas, to make a similar analysis. The earthquake exercise was delivered second at SRSU, and fourth at ASU.

In the two volcano exercises the LG and GG worked on the same problems and data for the first two thirds of each exercise, and data in the remaining third of each exercise were unique to each group. Both groups located and downloaded earthquake data from the USGS' online earthquake viewer near Mt. St. Helens before, during, and after its 1980 eruption and graphed them in Excel. They also viewed earthquake data from the 2021 La Palma eruption which was active during the time the SRSU students worked on this exercise. La Palma data came from Spain's IGN website. By the time the ASU class worked on the volcanoes exercise, IGN's time-series La Palma data was compressed in view and could not be expanded. For the final, unique part of the exercise, the GG then found online earthquake data from the Aleutian Islands using the USGS and the Alaska Volcano Observatory, and the LG from Valles caldera using online USGS and NMGS data. The volcano exercise was delivered third at SRSU, and fifth at ASU only to the two LG sections; the ASU GG section did not use it.

Between the two climate exercises, the LG and GG student groups worked on the same problems and data for the majority of each exercise, using unique data for only approximately 20% of the exercises. Both groups analyzed a photograph of ~700-year-old tree rings and time-series temperature data surrounding the Medieval Warm Period and the Little Ice Age; and three time-series graphs of CO₂ and temperature. The GG then looked up, downloaded, and graphed temperature data from Pennsylvania, and the LG from their own hometown. The climate exercise was delivered fourth at SRSU, and first at ASU.

The LG and GG worked entirely on separate data between the two exercises on stream flooding, making the unique portion of each exercise 100%. The GG graphed given tabular stream-discharge data from two sites on Mercer Creek in Washington state for two different years to determine recurrence intervals for floods of certain discharges, and the LG from two sites on the Guadalupe River in Texas for two different years. The flood exercise was delivered last at SRSU, and second at ASU.

Table 4.1. Descriptions of in-class exercises distinguishing type and source of data, type of analysis required, and how much of exercise is unique to GG and LG students. 1: Paleotectonic maps from Scotese, 1998. 2 : HHMI Interactive Viewer (HHMI, n.d). Green shading highlights where students download data themselves. Yellow shading highlights where students graph or otherwise manipulate data themselves.

Exercise; Order given at each school	In-common part of exercise				Tested (different) parts of exercise					Percent of exercise differing
	Data type	Analysis: making, reading, or interpreting graph or other data	Data provided or downloaded by students / source	Data location		Data type	Analysis: making, reading, or interpreting graph or other data	Data provided or downloaded by students / source	Unique-data location	
Structure (created for this study); 1-SR; 4- ASU					Global	2d and 3d spatial; maps online Interactive Viewer	Entering data and visualization with Stereonet program	Data table and maps provided ¹ ; Maps online ²	Palisades, New Jersey	100
					Local				Big Bend, Texas	
Earth-quakes (modified and added to from Baer, 2007); 2-SR; 3-ASU	2-variable	Calculation and graphing in Excel	Provided in class		Global	USGS earthquake viewer, Shakemaps, reports ONLINE	Interpreting maps	Download/ USGS	2015 Nepal + other large EQ in world	33%
	3D oblique subsurface aftershock map	Interpreting 3D image	Download/ USGS	2019 Ridge- crest	Local				1995 Marathon, TX	
Volcanoes (created for this study); 3-SR; 5-ASU	Time series	Graphing in Excel	Download/ USGS	MSH 1980	Global	USGS earthquake viewer; information on AVO website	Qualitative	USGS; AVO ONLINE	Aleutian Islands	33%
	Time series	Reading and interpreting	Provided/ viewed online at IGN	La Palma 2021	Local			USGS; LANL ONLINE	Valles Caldera	
Climate (modified from Sun et al., EER 2020); 4-SR; 1-ASU	Photo of tree rings	Interpret	Provided in class		Global	Time series	Graphing in Excel	Download / Climate Toolbox website	Pennsylvania	20%
	Time series (temp)	Interpret graph								
	Time series (Temp & CO ₂)	Graphing in Excel		Local					Student's Hometown	
	Time series (Temp & CO ₂)	Interpret graph	Provided in class							
	Time series (Temp)	Interpret graph	Provided in class							
Floods (created for this study); 5-SR; 2-ASU					Global	2-variable	Graph and analyze	Table given	Mercer Creek, WA	100%
					Local				Guadalupe River, TX	

4.4.2 Design & delivery of student assessment for evaluation of effects of exercises

Short surveys measuring content knowledge and students' perception of relevance were administered before each exercise with the intention of comparing content retention and relevance rankings after the exercise. The introductory lecture on each topic had occurred by the time students answered these pre-exercise questions although class attendance was not compared between it and survey dates.

After each exercise, participating students were given longer surveys that measured knowledge retention, students' perception of relevance of the topic, student engagement, and critical-thinking skill. The difference between knowledge-retention and critical-thinking questions is here interpreted as representing low or high levels of Bloom's taxonomy of questions, respectively (Forehand, 2005). Survey questions queried students' (1) knowledge retention, by asking lower Bloom's-level content questions; (2) critical thinking, by asking higher Bloom's-level content questions; (3) engagement, by asking students to rank whether they learned something new and something relevant; and (4) perception of relevance, by both directly asking how the topic is relevant, and to ask them to provide a numerical ranking of relevance. Examples of each question type are presented as Table 4.2 and complete surveys are presented in Appendix 4.

Question type	Example question	Level in Bloom's Taxonomy
Knowledge retention: scored content	What is one way to predict volcanic eruptions?	1: Recall, or 2: Comprehension
Critical thinking: scored content	Describe the relationship between earthquake occurrence and plate tectonic activity	4: Analysis
Relevance: scored content	What is one way that the knowledge of Earth's past climate affects human society?	6: evaluation (but here tallied with 'relevance' and not critical thinking)
Engagement: student ranking	I learned something new with this exercise (1-10)	n/a
	I learned something interesting with this exercise (1-10)	n/a
Relevance: student ranking	I learned something relevant to human society with this exercise (1-10)	n/a

Table 4.2. Types and examples of questions on post-exercise surveys.

A final, end-semester survey asking the students to rank their perception of the relevance of geoscience to themselves or to someone they know, to their local community, and to human society was delivered to the SRSU classes only.

4.4.3 Evaluation of student survey data

Content and critical thinking questions on the anonymous student-coded surveys were scored by Dr. Thomas Shiller at SRSU who also teaches Physical and Historical geology, and reviewed by me after scoring. These were fact-based questions that were not opinions or self-ranked experiences of the students. Content questions were given a score of three if correct; two if partially correct, including if an incorrect idea was added to a correct one, or if the student's language was hedging; a score of one if incorrect or if the student wrote "I don't know;" and a score of zero if there was nothing written but if the student had completed answers on the rest of the survey. Answers to questions that were categorized as critical thinking were given a score of three if the response was correct and contained detail if warranted; two if partially correct or was missing detail if warranted; one if incorrect or if the student did not address the question, and also if the student only repeated words from the question; and zero as above, if the student left it blank but had completed other questions in the survey. Question types were labeled for the scorer even if they had not been for the student. An explanation of scoring is presented as Table 4.3.

Table 4.3. Rubric for scoring answers to content questions (left) and higher Bloom's level critical-thinking questions (right).

	Knowledge questions (lower Bloom's level)	Critical thinking questions (higher Bloom's level)
3 pts	Correct	Correct, on the mark, with detail
2 pts	Partial idea; additional incorrect part that detracts from correct answer; or imprecise or hedging language	On the mark, without detail, or partial
1 pt	Incorrect and "I don't know"	Incorrect, or missed the point of the question, or only repeats words from question
0 pts	No answer but answered other questions in survey	No answer but answered other questions in survey

4.4.4 Data analysis

All survey responses and scores were transcribed to an Excel spreadsheet with anonymous student identifier codes as rows, survey questions as columns, and separate exercise types as tabs. Each tab's survey data were sorted first by LG versus GG. Scored student responses to content questions were separated by survey, but maintaining the identifier codes as the first column of each tab.

First, intending to determine whether the whole semester's project did indeed provide the two data groups among students with different outcomes in knowledge retention, critical thinking, engagement and perception of relevance, the data were separated by question type and grouped across all exercises. Each student score was tallied within groups defined by the four separate question types across all exercises, and the percent of each score within each student group was displayed on a double-bar graph for all content questions, all critical thinking questions, and all relevance questions, without distinction between the five exercises. Results were first grouped this way to identify possible influence of data proximity (i.e. locally vs globally sourced) on students' responses to different types of questions.

Because only a slight difference was apparent in these data arrangements, the scored student responses were then separated by exercise and graphed in double-bar charts by percentage of the count of each score within a group comprising a question type for each student group. This arrangement of data compares the responses of LG and GG students to the different scored question types within each exercise. Also, double-bar charts of students' self-reported rankings from 1 to 10 of their engagement (whether they learned something new and something interesting) and their

perception of the relevance of the topic to human society were made to graph percentage of each rank selected, also comparing responses between each exercise for the LG and GG students.

4.5 Results

Data from “post-exercise” surveys administered at both schools (Structures, Earthquakes, Volcanoes, Climate, and Floods) were all separated into LG and GG. The responses were further ordered by question type before also being ordered by separate exercise. The initial separation of survey responses into groups that used the local or global data sets was to determine whether groups exposed to the different data types responded differently to the surveys. Pre-exercise survey results and demographic data are also presented here.

Sixty-three students in LG consented to participate but only 57 took at least one survey. Thirty-five students in GG consented to participate but only 29 took at least one survey.

4.5.1 Pre-exercise survey results comparing local-data group to global-data group

4.5.1.1 *Demographic data.*

Percentages of declared academic majors at the beginning of each study semester are presented in Figure 4.2. An equal number of GG and LG students participating in the study were declared geoscience majors at the beginning of the semester (14% and 13%; Figure 4.2). More of the LG than GG students were another kind of science or engineering major (38% LG vs. 21% GG). An equal percentage between groups were liberal arts majors (24% and 23%) while more of the GG group were majoring in professional studies like criminal justice or business (41% of GG vs. 25% of LG). That 16% more LG than GG students were declared science or engineering majors may predispose the LG students to better engage with scientific projects than the GG students.

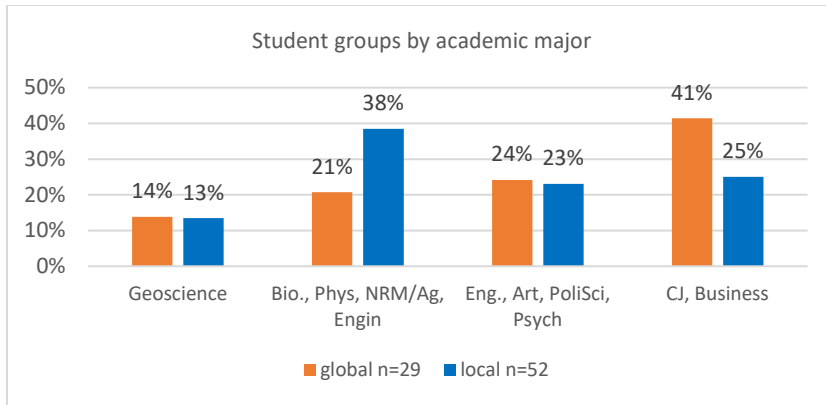


Figure 4.2. Student groups by academic major. Majors are grouped into four categories of geology, non-geology physical sciences and engineering, liberal arts including English, art, political science, and psychology; and professional studies like criminal justice and business. In this and all bar graphs comparing LG and GG data, LG data are shown as blue and GG data as orange.

The size of hometown was queried on the presumption that students from a smaller town may have more interaction with the natural world, which might bear on the weighting of post-exercise engagement, relevance, or knowledge-retention results. More of the LG students are from cities with a population greater than 80,000 (43%), while more of the GG students are from smaller communities of less than 10,000 (40%). This may predispose the GG students to increased readiness to understand the natural world in the context of these exercises.

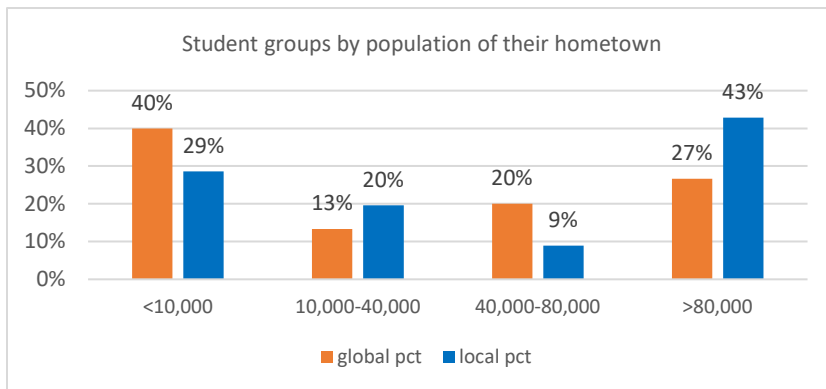


Figure 4.3. Student groups by population of their hometowns. GG n=29, LG n=52

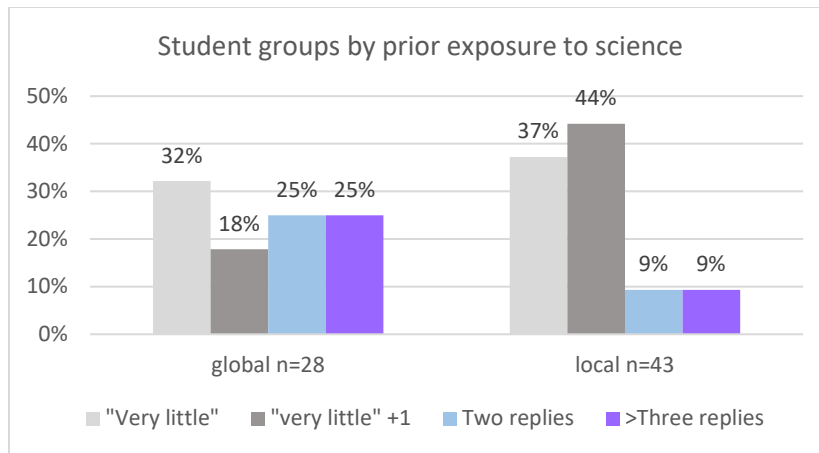


Figure 4.4. Student groups by their previous experience with science. This was a multiple-answer question to select all that apply for the student from possible answers listed in 4.4.1. Student answers were grouped by how many of the answers they selected.

GG students showed more *a priori* exposure to science, with 50% of GG vs. 18% of LG selecting two or more replies (excluding “Very little”) from the options describing previous science exposure (Figure 4.4). Similar to the size of the students’ hometowns, this may predispose the GG students to more engagement with the geoscientific methods and data in these exercises.

4.5.1.2 Pre-exercise content results

Students’ average scores of answers to each of the pre-exercise survey questions reveal no *a priori* difference in content knowledge or perception of relevance between the two groups (Figure 4.5). Among pre-exercise content questions, 22% of each group scored correctly (3 out of 3) and 51%-54% scored partially correct. Among relevance questions (example: “What is one effect of earthquakes on human society?”), GG and LG students scored similarly, at 5%-8% correct scores and 77%-81% partially correct scores. No critical-thinking-type questions were asked on the surveys preceding the exercises. Students had been exposed to introductory information on each topic in lecture before they took the pre-exercise surveys.

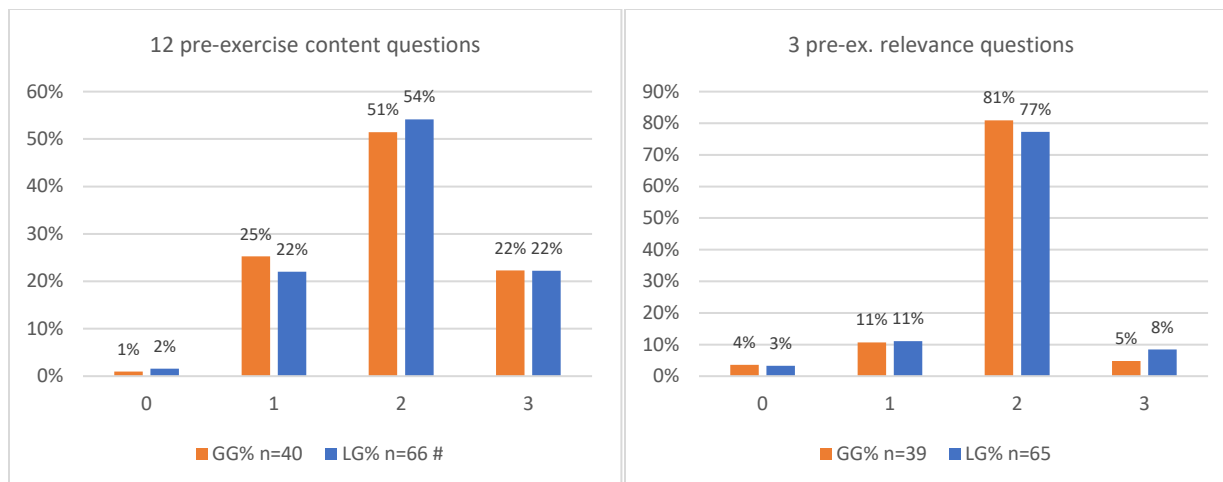


Figure 4.5. Percent of scores attained by students in the local (LG) and global (GG) data groups by type of questions, across all exercises. Table 4.4 describes the scoring rubric; a score of 3 is correct.

4.5.2 Post-exercise survey data

Most survey data were collected after each of the in-class exercises to query the students on the learning outcomes of knowledge retention, engagement, critical thinking ability, and perceptions of relevance.

4.5.2.1 Post-exercise survey questions across all exercises

Toward addressing the question of how a data source influences these learning outcomes, the scored and ranked post-exercise survey data were tallied by LG or GG and by type of question answered (knowledge-retention, etc.; Figure 4.6). On knowledge-retention questions, students in both data groups scored similarly, with 58-61% of students scoring correctly (3 points), and 13-14% of students scoring partially correct (2 points). On critical-thinking questions, 40% of GG students answered correctly compared to 32% of LG students. Scored questions from the post-exercise surveys that are categorized as “relevance” questions asked why the topic was relevant to human society and were scored on content. More students in both groups in this amalgamated total scored only partially correctly (score of 2; 61% of GG, 53% of LG).

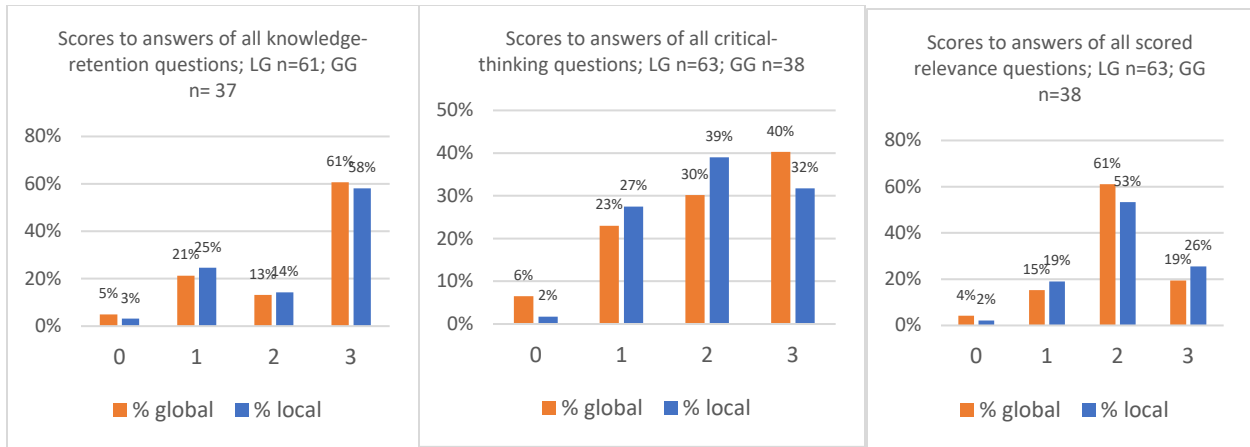


Figure 4.6. (a) Percentages of each score (0, 1, 2, and 3) for all knowledge-retention questions across all exercises. No clear difference in scores occurred between the LG and GG. (b) Percentages of each score for all critical-thinking questions across all exercises. (c) Percentages of each score for all relevance questions across all exercises.

Averages of student scores reveal no clear leading group in the correct answering of questions when accounted with all post-exercise surveys together (Table 4.4). Both groups obtained similar high scores in knowledge-retention questions; eight percent more GG students answered critical-thinking questions correctly; and seven percent more LG answered relevance questions correctly. Proximity in compared percentages of these results then led to separating the data by exercise. These are presented in the following section.

Table 4.4. Summary of percentages of correct scores between local and global groups by question type.

Question type	Correct scores (3/3)		Leading group
	Global -data group	Local-data group	
Knowledge-retention	61%	58%	Neutral (global +3%)
Critical-thinking	40%	32%	Global (+8%)
Relevance	19%	26%	Local (+7%)

4.5.3 Scored and self-ranked answers by exercise, comparing local-data group to global-data group

Survey data were analyzed by exercise to identify effects of the topics or exercise formats on different student groups. The results are reported in the same manner as the aggregated results across all exercises that were shown in the previous section.

4.5.3.1. *Geologic structures exercise*

The two geologic structures exercises (GG and LG) were 100% unique. Seventeen GG students and 44 LG students completed these questions. Among all scored content questions in the post-exercise survey, 64% of the LG responded correctly compared to 50% of the GG (Figure 4.10). The LG responded correctly most often in all three question types (knowledge-retention, critical thinking, and relevance). The most separation between the amount of those correct responses occurred in the 'relevance' content question, on which 30% more of LG responded correctly than GG. The gap in correct answers to critical-thinking questions is also significant, with 17% more of LG than GG responding correctly. In the knowledge retention questions 9% more of LG than GG responded correctly (Figure 4.7; Table 4.6).

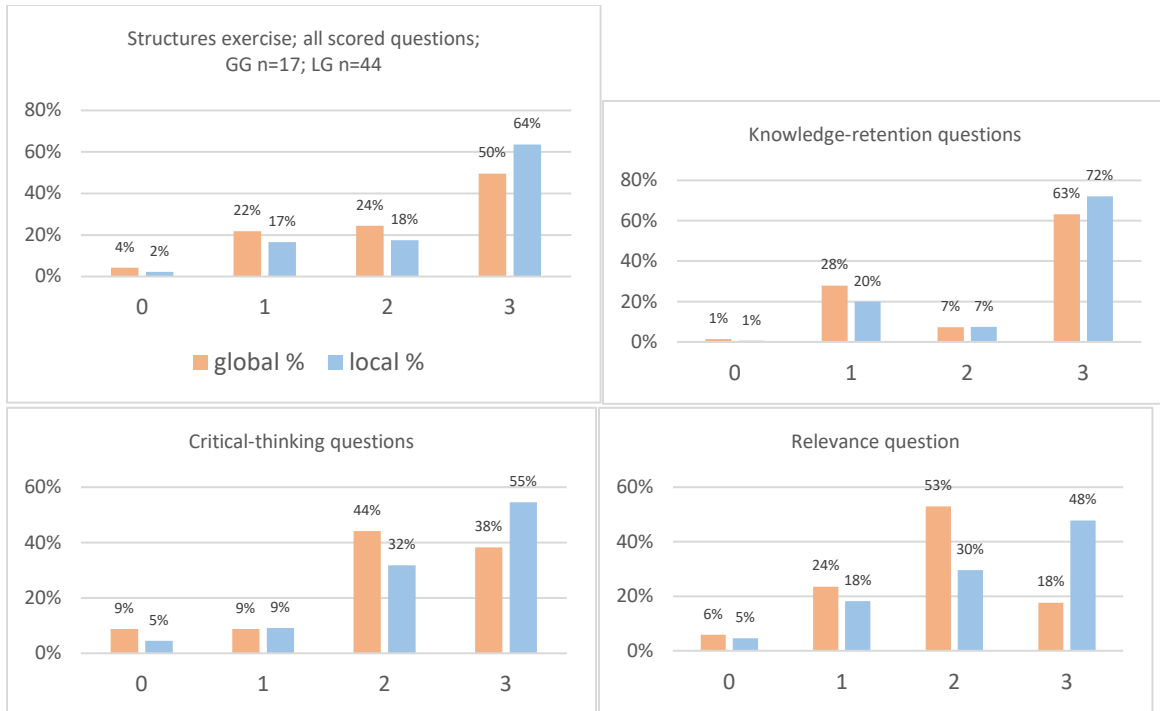


Figure 4.7. Percentages of scores of student responses to questions on the post-structure-exercise survey. Graphed are all scored questions together (upper left), and each of the three scored question types.

4.5.3.2 Earthquakes exercise

For the earthquake exercises, the LG and GG worked on the same problems and data for the first two thirds of each exercise and then used unique data for the last 33% of the exercise. Twenty-five GG students and 26 LG students completed the scored content questions on the survey. Fourteen percent more of LG than GG responded correctly to the scored relevance question. On the critical thinking question, 9% more of LG responded correctly. Among all scored content questions 67% of the LG responded correctly compared to the GG's 59% correct. Neither group led in the knowledge-retention questions as the separation was only 3% (Figure 4.8; Table 4.6).

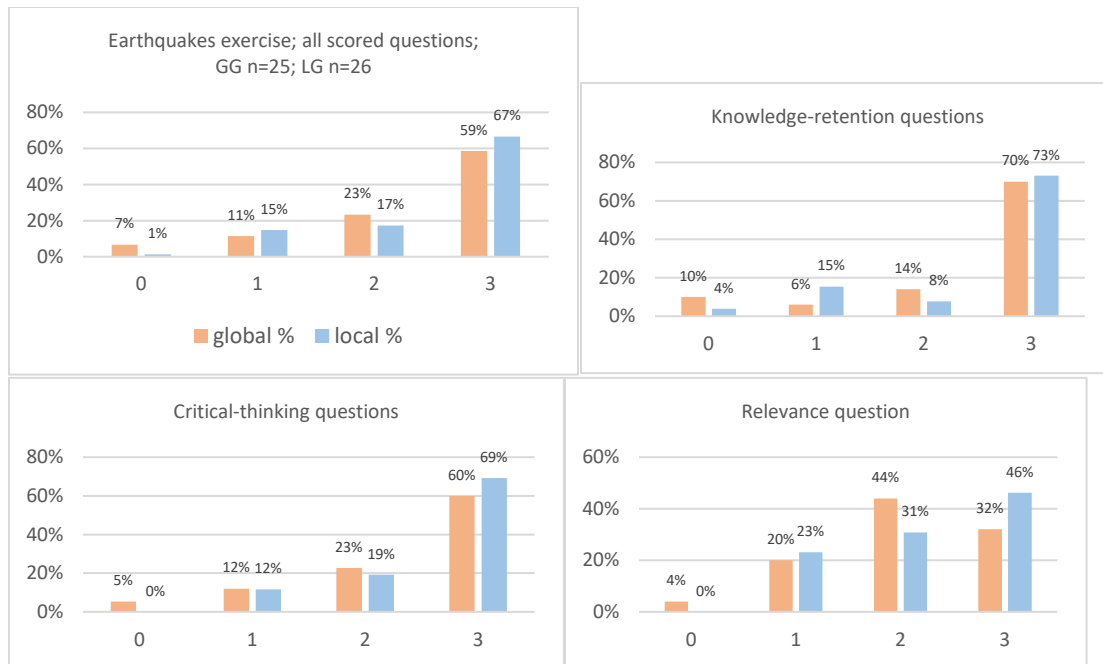


Figure 4.8. Percentages of scores of student responses to questions on the survey following the earthquake exercise. Graphed are all scored questions together (upper left), and each of the three scored question types.

4.5.3.3 Volcanoes exercise

In the two volcano exercises the LG and GG worked on the same problems and data for the first two thirds of each exercise, and data in the remaining 33% of each exercise was unique to each group. The single section at ASU using global data did not undertake this exercise due to time constraints and therefore sample numbers between local- and global-data student groups differ most significantly in this exercise. Nine students in the GG and 23 students in the LG completed the scored content questions. The resultant comparisons reveal that 60% of the LG responded correctly to all scored questions compared to the GG's 47% correct. The LG led in the relevance and knowledge-retention question types, and most of the separation between those correct responses occurred in the relevance content question, where 45% more of LG than GG responded correctly. On the knowledge-retention questions 9% more LG students responded correctly; neither group led in correct answers on critical-thinking question (Figure 4.9, Table 4.6).

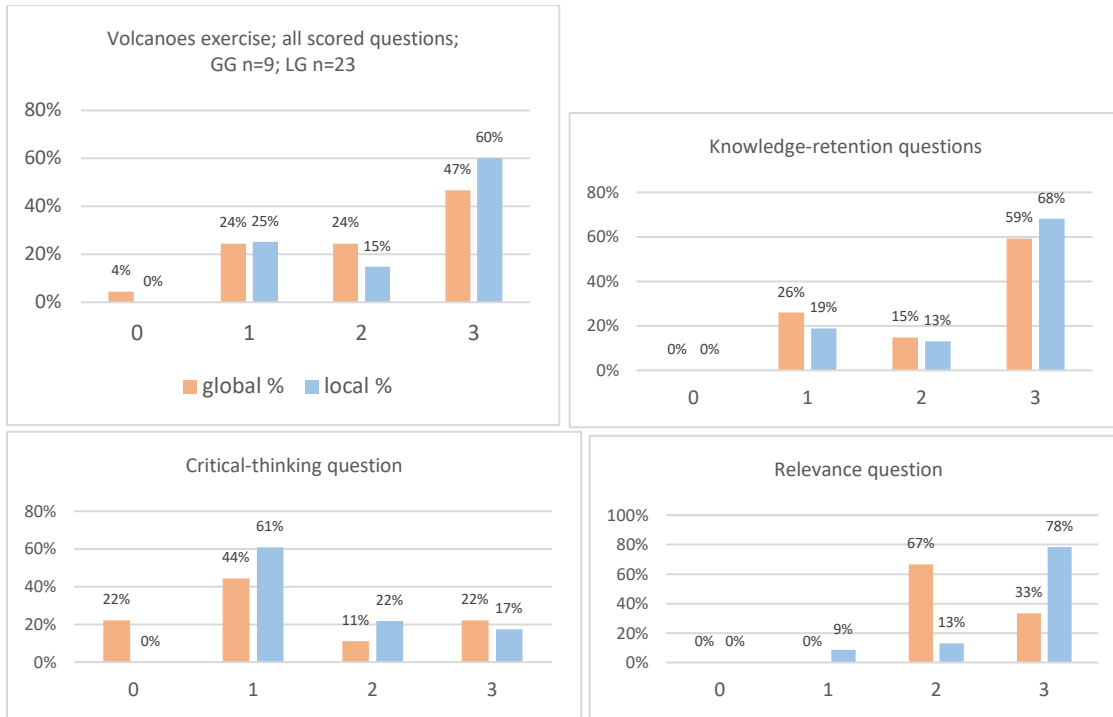


Figure 4.9. Percentages of scores of student responses to questions on the survey following the volcanoes exercise. Graphed are all scored questions together (upper left), and each of the three scored question types.

4.5.3.4 Climate

Between the two climate exercises, the LG and GG worked on the same problems and data for the majority of each exercise, using unique data for only approximately 20% of the exercises. Twenty-two GG students and 44 LG students completed these questions on the surveys. Among all scored questions, a similar percentage of GG and LG students scored correctly, at 56% and 54% respectively. The GG answered 9% more knowledge-retention questions correctly, while the LG answered 13% more critical-thinking questions correctly (Figure 4.10, Table 4.6).

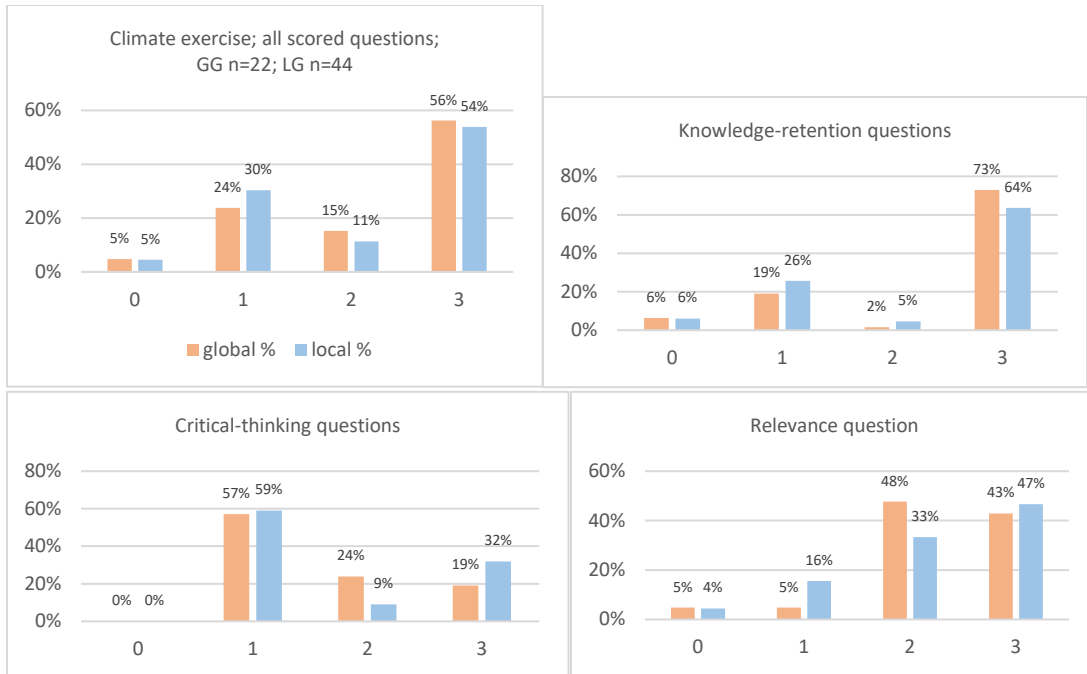


Figure 4.10. Percentages of scores of student responses to questions on the survey following the climate exercise. Graphed are all scored questions together, and each of the three scored question types..

4.5.3.5 Flooding exercise

The LG and GG worked entirely on separate data between the two exercises on stream flooding, making the unique portion of each exercise 100%. Among all scored content questions, 40% of the LG responded correctly compared to the GG's 33% correct. The LG led by 6% in knowledge-retention questions and by 12% in critical-thinking questions. There was no relevance question on this scored survey. (Figure 4.11; Table 4.6).

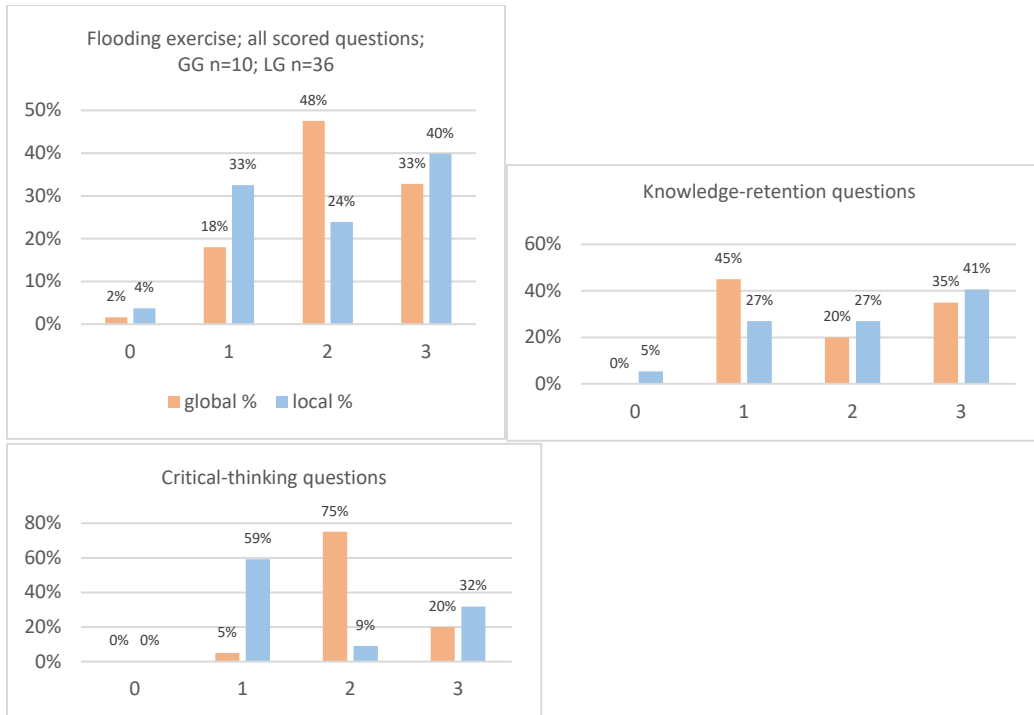


Figure 4.11 Percentages of scores of student responses to questions on the survey following the Floods exercise. Graphed are all scored questions together (upper left), and each of the two scored question types following this exercise.

The group with the highest percentage of correct scores is displayed for each exercise and by each question type as Table 4.5. In considering all question types together, LG students answered more questions correctly in four out of the five exercises. The structure exercise shows the most difference between the groups, while the climate exercise shows the least. Overall the group exposed to local data showed more perception of relevance, critical thinking, and knowledge retention than the group exposed to global data.

Table 4.5. Table showing differences in total percent of correct scored answers on five post-exercise surveys between student groups exposed to local or global data sets in the in-class exercises. Table also indicates number of students responding to each set of questions on that survey. Student groups defined by exposure to either local or global data sets in the unique portions of the exercises. Where more LG students responded correctly the cell is colored blue. Where more GG students responded correctly the cell is colored orange. 6%-10% more, light shade. 11%-20% more, medium shade. >21% more, dark shade. Defining a leading student group requires more than 5% difference from the other group. Where number of respondents is less than 10, n is colored red.

Exercise (and portion of exercise that is different between the student groups)	Scored content questions					
	Number of students responding (n)		Group with highest percentage of correct answers by question type. Correct = score of 3 out of 3.			
	GG total = 29. LG total = 57	n	All questions	Knowledge questions ("Knowledge retention")	Critical thinking questions ("Critical thinking")	Relevance question ("Perception of relevance")
Structure (100%)	Global	17	Local (+14%)	Local (+9%)	Local (+17%)	Local (+30%)
	Local	44				
Earth-quakes (33%)	Global	25	Local (+8%)	Neutral (local +3%)	Local (+9%)	Local (+14%)
	Local	26				
Volcanoes (33%)	Global	9	Local (+13%)	Local (+9%)	Neutral (global +5%)	Local (+45%)
	Local	23				
Climate (20%)	Global	22	Neutral (global +2%)	Global (+9%)	Local (+13%)	Neutral (local +4%)
	Local	42				
Floods (100%)	Global	10	Local (+7%)	Local (+16%)	Local (+12%)	n/a (no scored relevance question on this survey)
	Local	36				

4.5.3.6 Students' rankings on their engagement and perception of relevance

The final three questions on each post-exercise survey were not short-answer questions scored like those presented above, but were designed for the students to rank their impression of their engagement and their perception of the relevance of the topic to human society. Data are not included in the analysis from three of the five surveys, however, either because of low responses or an error in question delivery.

Only four GG students responded to the ranking questions after the structures exercise, compared to between 19 and 23 LG students. (This number varies by which of the three ranking questions were answered.) Only one GG student circled the ranking numbers after the volcanoes exercise compared to 16 LG students, and so these data do not contribute to the comparative analysis. (Because the volcanoes exercise was not run in the ASU GG section and was therefore only run in one section at SRSU the total number of students taking the post-volcanoes-exercise survey was nine; but only 1 completed the ranking questions.) Ranking questions from the post-climate-exercise survey are

discounted because the questions typed on this survey displayed an error of placing the “yes” close to 1 and the “no” close to 10, instead of the reverse on each of the other surveys. Even though this was the fourth exercise for SRSU students who may have recognized dissimilarity from the previous surveys, it was the first exercise for the ASU students. Therefore the self-ranking data in engagement and perception of relevance are discarded for the post-climate survey, although they are shown in graphical form in Appendix 5.

Among the ranking questions on the surveys following the earthquakes exercise, nine GG students and 12-13 LG students responded. The LG submitted the highest percentage of “10” rankings for learning something new, and also had more responses among 8, 9, and 10 rankings. The LG also entered more of the positive responses (both 10 and 8, 9, and 10 totaled) for having learned something relevant to human society. The GG submitted the most “10” responses for having learned something interesting, though more of the LG responses ranged between 8 and 10.

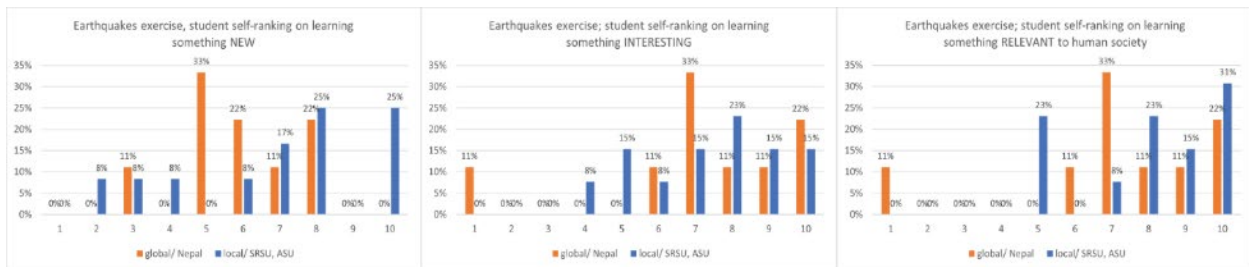


Figure 4.12. Ranked scores from questions following the earthquake exercise. 1=no; 10=yes.

Student self-ranking on engagement and relevance following the floods exercise revealed more “yes” rankings of 10 among the GG in the engagement questions (learning something “new” and something “interesting,” 63% vs 40% for a ranking of 10 in learning something new; 38% vs 32% in learning something interesting). When considering the high-ranking responses of 8, 9, and 10 together, however, the two groups’ rankings of having learned something new and interesting are equal. In

ranking their perceptions of relevance to human society, the LG's 56% versus the GG's 51% among high-ranking 8, 9, and 10 scores is not a significant lead.

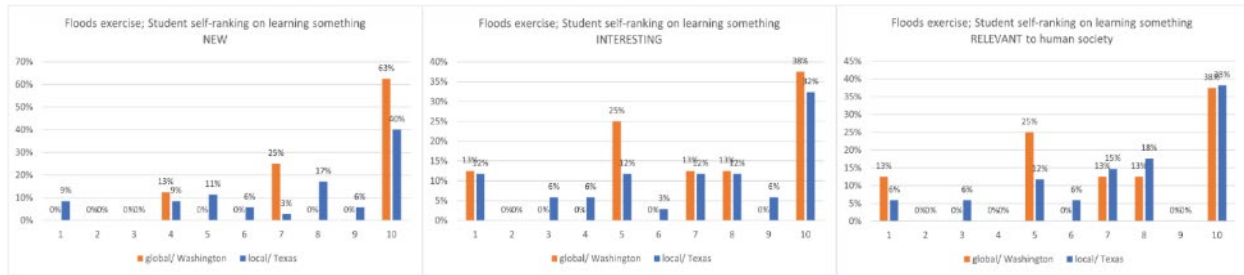


Figure 4.13. Ranked scores from questions following the floods exercise. 1=no; 10=yes.

Data from the ranking questions on surveys following the Earthquakes and Floods exercises are grouped as Table 4.6. After the earthquakes exercise, more LG students than GG students reported higher rankings of their engagement and their perceptions of the relevance of the topic to human society (28% more having learned something new, 9% more having learned something interesting, and 15% more having learned something relevant to human society).

Table 4.6. Percentage of high ranked impressions following the earthquakes and floods exercises.

Ranked impressions; "I learned something ___ during this exercise;" rank of 1 (no) to 10 (yes)											
Exercise (and portion of exercise that is different between the student groups)	Number of students responding GG total = 29, LG total = 57	n, %	"...New" (Engagement)			"...Interesting" (Engagement)			"...Relevant to human society" (Perception of relevance)		
			Rank of 10	Rank of 8,9,or10	Group with highest pct of 8,9, or 10 (by _%)	Rank of 10	Rank of 8,9,or10	Group with highest pct of 8,9,or 10 (by _%)	Rank of 10	Rank of 8,9,or10	Group with highest pct of 8,9, or 10 (by _%)
Structure (100%)	Global	4, 14%	(Results discarded; Disparate numbers of returns)								
	Local	19-23, ~40%									
Earthquakes (33%)	Global	9, 31%	0%	22%	Local (+28%)	22%	44%	Local (+9%)	22%	44%	Local (+15%)
	Local	12-13, 22%	25%	50%		15%	53%		31%	69%	
Volcanoes (33%)	Global	1, 3%	(Results discarded; Disparate numbers of returns)								
	Local	16, 28%									
Climate (20%)	Global	14, 48%	(Results discarded; Questions were delivered erroneously.)								
	Local	38, 67%									
Floods (100%)	Global	8, 28%	63%	63%	Neutral (=)	38%	51%	Neutral (=)	38%	51%	Neutral (local +5%)
	Local	34-35, 60%	40%	63%		32%	50%		38%	56%	

While many students did not answer the 1-10 rankings on the surveys after various exercises, most did respond to the associated question that followed each one asking “What was that ____ (*new, interesting, relevant*) thing?” Those text responses were grouped and presented as word clouds, although even with certain words removed in the creation of each cloud, they are not included in the data analysis because the short-answer format may preclude enough original thought to compare unique responses. In other words, many students in both data groups responded by repeating most words in the question, and yet their arrangement could still reflect import to the student. These word clouds are presented in Appendix 6.

4.5.4 Final survey results

A final, end-semester survey was given to the SRSU students only. As the SRSU classes were smaller than the ASU classes, only 9 GG students and 12 LG students completed the questions asking to rank their perception of the relevance of geoscience to themselves or someone they know, to the local community, and to human society. These data are presented in Figure 4.14 and the high rankings in Table 4.7. Within this SRSU-only group, 44% of GG students ranked an 8, 9, or 10 for “yes,” compared to 36% of LG students in response to whether geoscience has relevance to the local community. For stated perception of relevance to the student or to someone that they know, 33% of GG students gave high rankings of 8, 9, or 10, compared to 50% of LG students. Regarding their perception of relevance to human society, 51% of GG students gave a high rank of 8, 9, or 10, compared to 63% LG students.

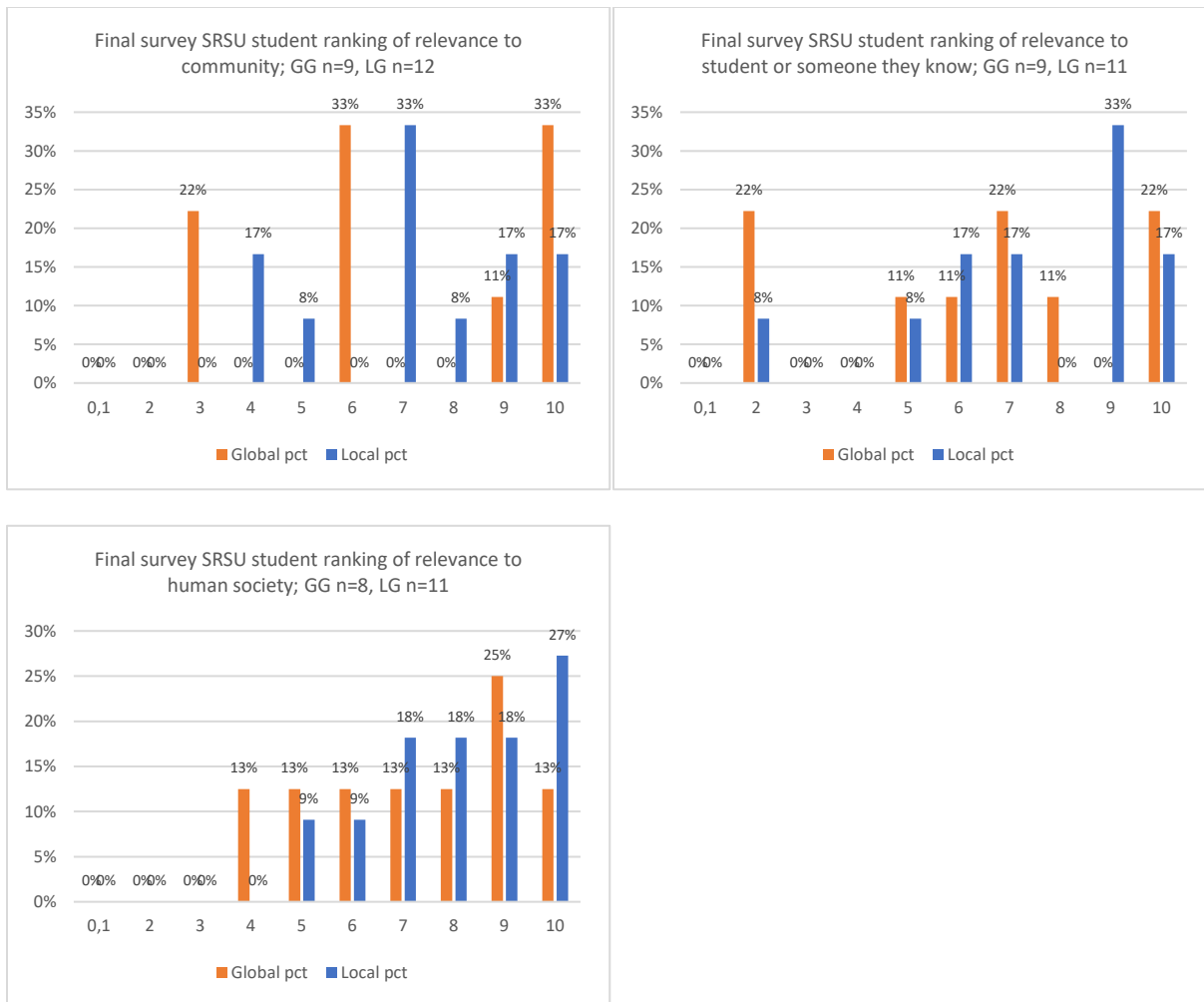


Figure 4.14. Final survey relevance-ranking results from students at SRSU.

Table 4.7. Tabulations of relevance-ranking data from final-survey questions administered to SRSU students.

No. responding	Final ranking of relevance of geoscience to local community			Final ranking of relevance of geoscience to student or someone they know			Final ranking of relevance of geoscience to human society		
	Rank of 10	Rank of 8,9,or10	Group with highest pct of 8,9, or 10 (by %)	Rank of 10	Rank of 8,9,or10	Group with highest pct of 8,9, or 10 (by %)	Rank of 10	Rank of 8,9,or10	Group with highest pct of 8,9, or 10 (by %)
GG n=10	33%	44%	Global (+12%)	22%	33%	Local (+17%)	13%	51%	Local (+12%)
LG n=13	17%	36%		17%	50%		27%	63%	

The beginning-semester surveys that collected demographic data also asked for rankings of the students' perception of relevance of geoscience to the student or to someone they know and also to the

local community, though they omitted asking to rank relevance to human society. To compare initial to final then, only the SRSU students' beginning-semester rankings are employed to compare to the same ranking questions on the final survey. Because only the smaller SRSU classes completed the final surveys the population numbers of GG (n=8 and 9 between the questions) and LG (n=12) are small. These comparisons among SRSU students are presented as Figure 4.15 and the total percent change for each student group for each question are presented as Table 4.8.

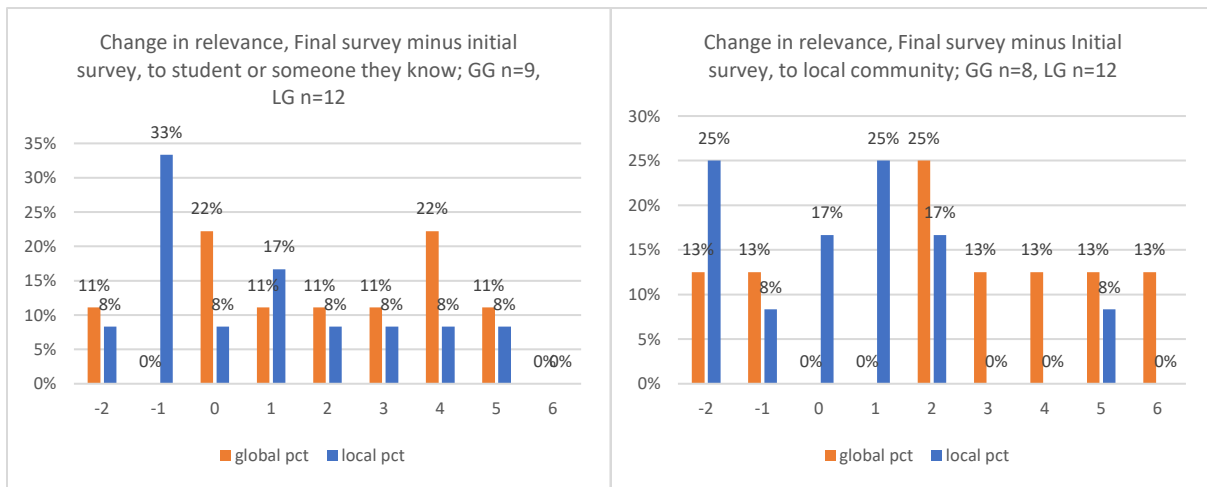


Figure 4.15. Comparisons between ranking results on end-semester and beginning-semester surveys among SRSU students.

Table 4.8. Percent change among both data groups at SRSU from the beginning to end of the semester in their perceptions of the relevance of geoscience.

	Change in perception of relevance of geoscience to student or someone they know				Change in perception of relevance of geoscience to local community			
	n	% students giving lower rank	% students giving higher rank	Group with most increased rank (by__%)	n	% students giving lower rank	% students giving higher rank	Group with most increased rank (by__%)
Global-data group (GG)	9	11	66	Global (+17%)	8	26	77	Global (+27%)
Local-data group (LG)	12	41	49		12	33	50	

Among this smaller student set, 66% of the GG students gave a higher rank than they did at the beginning of the semester; 22% no change; and 11% gave a lower rank (Figure 4.15 left). Forty nine percent of LG students gave a higher rank to the relevance of geoscience to the student or someone they know than they did at the beginning of the semester (a positive-numbered change in relevance); 8% no change; and 41% gave a lower rank. Regarding relevance of geoscience to the local community, 77% of the global-data respondents gave a higher rank to this question than they did at the beginning of the semester; and 26% gave a lower rank than they did at the beginning of the semester (Figure 4.22 right). Fifty percent of the local-data group gave a higher rank than they did at the beginning of the semester; 17% no change; and 33% gave a lower rank than they did at the beginning of the semester. While more of both student groups at SRSU gave higher ranking to their perception of the relevance of geoscience to both themselves and their local community at the end of the semester than they did at the beginning of the semester, the increase from the beginning to end of the semester was higher among the GG students (Table 4.8).

4.6 Discussion

Between two groups of university students completing in-class exercises within introductory geoscience courses using real geoscientific data, a recognizable lead is observed in knowledge retention, critical thinking, engagement, and perception of the relevance of that exercise's topic to society among the students who were exposed to local-proximity data sets in these exercises, as opposed to those students exposed to strictly distant or global data sets (Tables 4.5; 4.6). This lead is documented from surveys taken after four out of five given exercises (structures, earthquakes, volcanoes, and floods).

The outcome with the highest lead among local-data students is the measured perception of relevance. Relevance was measured both with one scored question and one student-ranked question on each of the surveys following the exercises. On questions that were scored to measure this outcome, the LG had 30% more correct answers than the GG students on the structures exercise that investigated Big Bend tectonics; 14% more on the earthquake exercise that investigated ground shaking from local earthquakes; and 45% more on the volcanoes exercise that investigated seismicity under the Jemez mountains. Among the questions asking students to rank their perception of the relevance of the topic, the LG indicated 15% more high rankings than the global-data group after the earthquake exercise. Neither group led after the flood exercise, and the data from the other exercises are unusable. Future surveys using such rankings should clarify and simplify the question delivery for students to rank their experiences as this measure could be not only illuminating but simple to compile.

Engagement was also measured by ranking questions and suffered the same issue of incomplete or discountable data returns on the surveys following three of the five exercises (Table 4.6). Nonetheless, the LG group again returned more higher rankings in reporting their engagement after completing the earthquake exercise, in having learned something new (28% more than GG) and something interesting (9% more).

The LG students also led among critical-thinking questions (between 9% and 17% more correct answers) and knowledge retention (between 9% and 16% more correct answers). Both of these outcomes were measured by scored content questions which differed by their level of complexity; critical thinking questions, for example, required connections to be made while “knowledge retention” questions on these surveys required the recall of facts.

Although questions at a higher level of Bloom’s taxonomy were included in the surveys, these in-class exercises did not deliberately cultivate critical thinking as much as they did a connection to the relevance of Earth science in the form of exposure to live data and methods used by geoscientists. The aim of building critical thinking skills within these exercises relied only on conclusions that active learning techniques like graphing real, archived data promote critical thinking (e.g., SERC, 2018; McConnell et al., 2017; Yuretich et al., 2001). Further, assessment of critical thinking in this study simply employed questions with higher Bloom’s taxonomy numbers but did not consistently employ parallel scaffolding techniques in the asking of content questions among all the post-exercise surveys. Bloom’s levels of questioning may be employed to promote critical thinking by scaffolding questions on the same topic from lower to higher complexity (e.g., Yuretich, 2020) but because these surveys were taken immediately after completing the exercises, which themselves are internally scaffolded to more complexity and end with higher Bloom’s-level questions, I was indecisive about starting the post-exercise surveys with questions of higher or lower Bloom’s level.

Because the exercises at the center of this study were designed around the availability of real data that is most fitting for the topic and which is available from both local and global sources, the type and level of analysis is different for each exercise. Responses to the different question types for each exercise are therefore compared within each student group to explore whether individual exercises influenced students’ engagement, knowledge retention, or perception of relevance (Figure 4.16). While some of the same observations illuminated in Table 4.6 are apparent here, others come forth: Both

student groups' lowest scores were lowest in knowledge-retention and critical-thinking questions following the floods exercise. Both groups scored lower on critical-thinking questions after the climate and volcanoes exercises than after the structures and earthquakes exercises. This arrangement also highlights that the GG students saw less relevance in all exercises than the LG students – an observation evident in Table 4.5.

The five exercises each have a unique combination of data sources, methods used on those data, and how much of the exercise is unique to the separate student data groups (Table 4.9). The exercise may have provided already complete graphs to analyze, as in most of the climate exercise, or a file of tabular data for the students to graph themselves as in the floods exercise, or it may have required that the students locate and download data themselves from a public geoscientific hub, as in the earthquakes exercise, and then to graph. Data for the flooding exercise were provided to the students in static tables because their range was selected ahead of time to illuminate scenarios of flood-level changes. These tabular data were graphed by students in Excel, but it may be that the lack of finding online data diminished engagement and caused the lower scores among both GG and LG students on the knowledge-retention and critical-thinking questions.

Table 4.9. Delineation of data sources and methods of manipulation of data in the five exercises, from information presented in Table 4.1. Cells are shaded green where data source or activity provides most involvement from students.

Exercise (percent unique)	Data sought online? Or provided?	Methods of analysis
Structure (100%)	provided	Manipulation in Stereonet
Earthquakes (33%)	found online	Graph and analyze in Excel
Volcanoes (33%)	found online	Some manipulation in Excel and some visualization
Climate (20%)	mostly provided	Data mostly viewed and interpreted
Floods (100%)	provided	Graph and analyze in Excel

The one exercise after which the LG students did not lead in desired outcomes was climate, whose data were mostly provided as already-complete time-series graphs that were only viewed and interpreted, rather than manipulated (Table 4.9; Table 4.5). These data for the climate exercise were

mostly provided in complete form in order to present global CO₂ and temperature data, with the just last 20% of the exercise exposing students to online climate data to graph (either for their hometown or for a location in Pennsylvania). This exercise also had low critical-thinking scores among both groups, although both groups had more correct scores in knowledge-retention questions (73% of GG and 64% of LG). The lower amount of unique local data ($\leq 20\%$ vs $\geq 33\%$ in the other exercises) may also support the conclusion that the use of local data indeed contributes to more positive targeted student outcomes. Further supporting this is that the LG students' greatest lead among all questions is in the structure exercise, whose unique portion was 100%. After that exercise the LG students answered the relevance question correctly 30% more; the critical thinking questions 17% more; and the knowledge-retention questions 9% more than the GG group. It appears that exercises with at least 33% uniqueness are required to discern a difference between student groups.

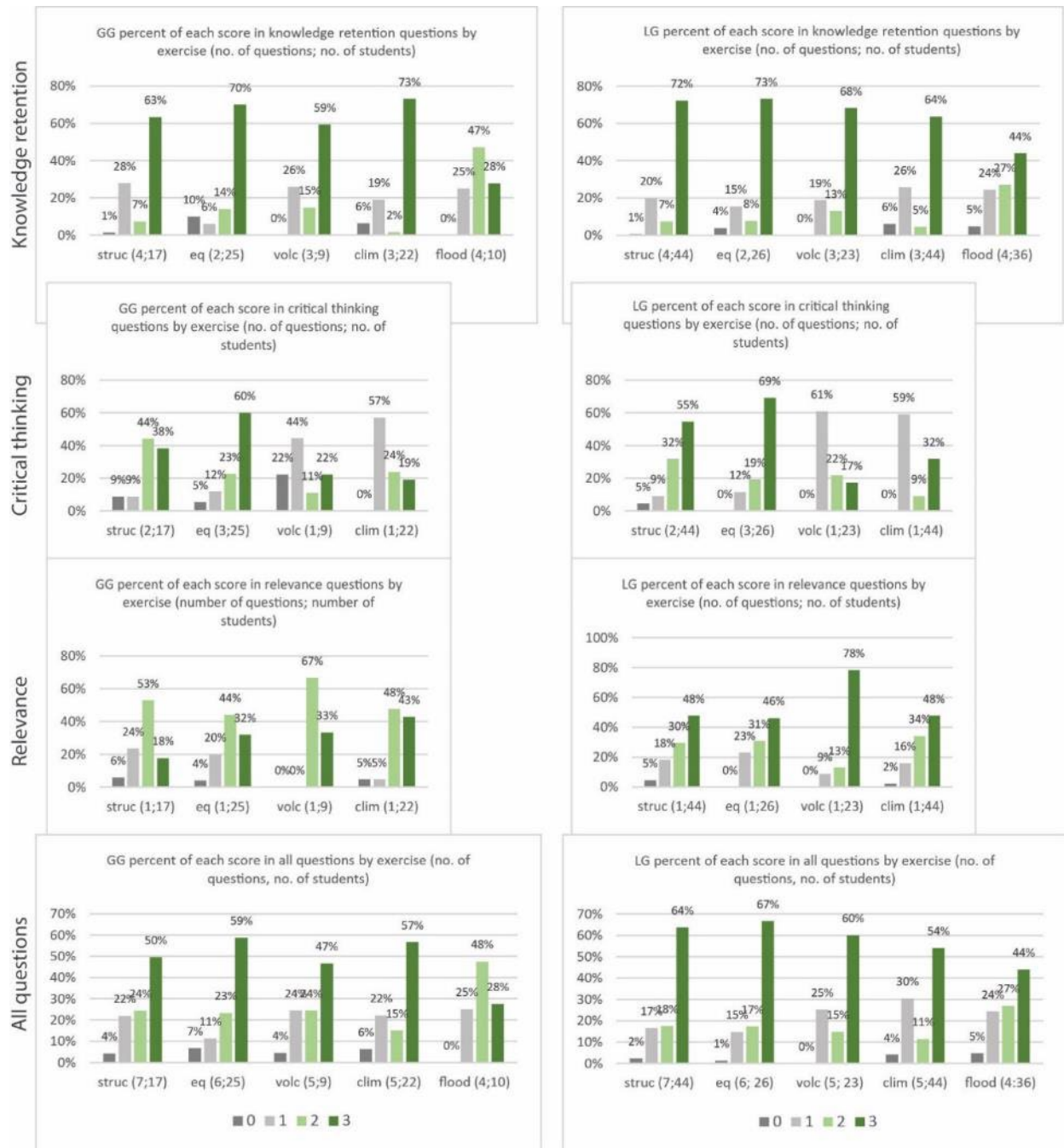


Figure 4.16. Comparison of student scores within data groups but between exercises. Global-data student scores are on the left side, LG on the right. Four horizontal rows of graphs are separated by question type (knowledge-retention, etc.). Within each graph is a cluster for each of the five exercises' survey question response scores. Percent of the students' correct scores (3/3), partially correct scores (2/3), incorrect scores (1/3), and blank answer (0) are arranged by color. For each exercise's cluster of scores, the number of questions on the survey and the number of students answering those questions are shown in parentheses following the exercise label.

Additional variables, indeterminate outcomes

Figure 4.16 reveals lower scores among both student groups on the critical thinking questions not just following the climate exercises but also the volcano exercises. Investigation of these questions reveals that (1) there is only one of this question type on the volcano and climate exercises but two and three on the structure and earthquake exercises, and (2) they are more challenging than the critical-thinking questions following the other exercises (Table 4.10). Either of these may also have influenced the measurement of critical-thinking ability. Confirming parallelism between surveys would eliminate this variable.

Table 4.10. Critical-thinking questions asked following the structures, earthquakes, volcanoes, and climate exercises.

post struct critical thinking	post struct critical thinking	EQ post: critical thinking	EQ post: critical thinking	EQ post: critical thinking	post volc: critical thinking	post climate: critical thinking
Describe one way that tectonic plate motion affects the formation of geologic structures in the crust.	How might the orientation of geologic structures influence resources that are found below the surface, such as water, minerals, or fossil fuels?	How does earthquake intensity relate to earthquake magnitude?	Describe the relationship between earthquake occurrence and plate tectonic activity	How might knowledge of ground shaking affect planning for people living in or near earthquake zones?	Given what you have learned previously about earthquakes, can you think of a way that volcano-related earthquakes are different than other earthquakes?	The recent Little Ice Age in the late 1400s to mid-1800s was <u>(similar or different)</u> [choose one] in duration and temperature to the last global ice age of 21,000 years ago. Elaborate briefly on this.

Also, the order in which the exercises were presented differed between the two schools' classes, because the opportunity to add more students to the study at ASU necessitated that they be presented in a class with a different semester schedule (Table 4.11). The complexity of a different order of exercises may have influenced student engagement and therefore the other outcomes in a manner that is undetected. Additionally, survey fatigue from the completion of twelve surveys may on its own be a variable, but would also vary between ASU and SRSU students by the differing order of exercise delivery.

Table 4.11. Order in which the five in-class exercises were presented and worked at SRSU and ASU. *A streams/watersheds exercise was presented fifth at SRSU and discarded.

	SRSU	ASU
Structures	1 st	3 rd
Earthquakes	2 nd	4 th
Volcanoes	3 rd	5 th in two LG sec; not run in GG sec
Climate	4 th	1 st
Floods	6 th *	2 nd

In terms of predisposition to understand and engage more with the exercises, demographic data from the beginning-of-semester surveys do not make it clear that either group of students had a distinct advantage over the other. Thirty-two percent more GG students than LG students had more previous exposure to science which might create an increased interest among them at the beginning, but 16% more LG students were science or engineering majors at the beginning of the semester, suggesting that *they* may start the semester with increased interest. Eleven percent more of the GG students were from a smaller town, and this may have predisposed them to have seen more geological processes in action, but of course these students did not interact with any local data that may have triggered that engagement. However, in the final survey taken by SRSU students the GG students' end-semester ranking of the relevance of geoscience to their local community was 12% higher than rankings from the LG students, which may reflect their higher numbers from a smaller town and their having made the connections themselves. On the same survey, LG students gave 17% more high rankings than GG students to their perception of the relevance of geoscience to themselves or to someone they know, and 12% more to their perception of the relevance of geoscience to human society. The data from this study suggest that these increased perceptions of relevance among LG students comes from their exposure to and manipulation of local data through the semester, but their increased proportion of science and engineering majors may contribute some part.

When grouping all exercises together but split by question type (Figure 4.6, left; Figure 4.16, top), 61% of GG students and 58% of LG students scored correctly (3/3) on knowledge-retention

questions. These high percentages among both groups suggest that regardless of the use of local or global data, engagement with real data and use of in-class partner work with Excel or other data-manipulation programs aid in increasing students' knowledge, at least temporarily. Surveying a control class section that does not participate in the exercises with most of the same questions may support this observation, although on its own it indicates success.

4.7 Conclusions

This small case study of responses from 29 students using global data and 57 students using local data supports the hypothesis implicit in the growth of teaching with place-based learning (e.g., Kirkby, 2014) and active learning (e.g., McConnell et al., 2017; Ruiz-Primo et al., 2012), that working in classes with geoscientific data that originate locally increases student interest, knowledge retention, critical thinking, and perception of relevance, particularly when students either download or graph those data themselves, or both. Because of this greater increase following exercises with more interaction with the data, in fact, instructors in regions without geologic activity like earthquakes or volcanoes could see that their students' experiences have the most data interaction even when the data are not local. Examples are retrieving and downloading data themselves and graphing them in Excel before they move to interpretation. This study contributes to the call from Manduca and Mogk (2002) to study increased uses of data in undergraduate instruction.

Some aspects of the five exercises and the surveys varied enough between exercise topics to add complexity to the interpretation of which data group led in desired outcomes. These are the order in which the exercises were delivered, the level of complexity of survey questions following each exercise, and as discussed the difference in amount of contact with original data between exercises. Additionally, background of the students might influence their level of engagement. Future analyses should maintain parallelism between surveys and as much as possible in content delivery.

REFERENCES

- Allmendinger, R.W., Cardozo, N., Fisher, D., 2012. *Structural geology algorithms: Vectors and tensors in structural geology*: Cambridge University Press.
- Ammon, W.L., 1981. Geology and plate tectonic history of the Marfa basin, Presidio County, Texas. In Marathon-Marfa region of west Texas: Society of Economic Paleontologists and Mineralogists Permian Basin Section, 81-20, p. 75-102.
- Angelier, J., 1984. Tectonic analysis of fault slip data sets. *J. Geophys. Res.* 89, 5835–5848. <https://doi.org/10.1029/JB089iB07p05835>
- Angelier, J., 1989. From orientation to magnitudes in paleostress determinations using fault slip data. *Journal of structural geology*, 11(1-2), pp.37-50.
- Armour, L.K., Langford, R.P. and Ricketts, J.W., 2018. Pliocene–Holocene deformation in the southern Rio Grande rift as inferred from topography and uplifted terraces of the Franklin Mountains, southern New Mexico and western Texas. *Geosphere*, 14(4), pp.1677-1689.
- Baer, E., 2007. Shaking Ground: Linking earthquake magnitude and intensity. © The Washington Center for Improving the Quality of Undergraduate Education.
- Berglund, H.T., Sheehan, A.F., Murray, M.H., Roy, M., Lowry, A.R., Nerem, R.S. and Blume, F., 2012. Distributed deformation across the Rio Grande rift, Great Plains, and Colorado plateau. *Geology*, 40(1), pp.23-26.
- Bird, P., 2002. Stress direction history of the western United States and Mexico since 85 Ma: STRESS DIRECTION HISTORY. *Tectonics* 21, 5-1-5–12. <https://doi.org/10.1029/2001TC001319>
- Caine, J.S., Minor, S.A., Grauch, V.J.S., Budahn, J.R., Keren, T.T., 2017. A comprehensive survey of faults, breccias, and fractures in and flanking the eastern Española Basin, Rio Grande rift, New Mexico. *Geosphere* 13, 1566–1609. <https://doi.org/10.1130/GES01348.1>
- Carciumaru, D., Ortega, R., 2008a. Geologic structure of the northern margin of the Chihuahua trough: Evidence for controlled deformation during Laramide Orogeny. *BSGM* 60, 43–69. <https://doi.org/10.18268/BSGM2008v60n1a4>
- Cardozo, N., Allmendinger, R.W., 2013. Spherical projections with OSX Stereonet: *Computers & Geosciences*, v.51, p. 193-205. Doi: 10.1016/j.cageo.2012.07.021.
- Charleston, S., 1981. A summary of the structural geology and tectonics of the state of Coahuila, Mexico. *Lower Cretaceous Stratigraphy and Structure, Northern Mexico: West Texas Geological Society, Publication*, pp.81-74.
- Chorowicz, J., 1989. Transfer and transform fault zones in continental rifts: examples in the Afro-Arabian rift system. Implications of crust breaking. *Journal of African Earth Sciences (and the Middle East)*, 8(2-4), pp.203-214.

- Cobb, R.C. and Poth, S., 1980. Superposed deformation in the Santiago and northern Del Carmen Mountains, Trans-Pecos Texas. *in*: Dickerson, P. W.; Hoffer, J. M.; Callender, J. F., eds., *Trans Pecos Region (West Texas)*, New Mexico Geological Society 31st Annual Fall Field Conference Guidebook, 308p.
- Conley, A., 2021. *Reconstructing the Transition from Laramide Contraction to Rio Grande Rift Extension* (MS thesis, The University of Texas at El Paso).
- Conley, A., Ramirez, S.E., Ricketts, J.W., Langford, R.P., Pavlis, T.L. and Heizler, M.T., 2023. Reconstructing the erosional and tectonic record of Laramide contraction to Rio Grande rift extension, southern Indio Mountains, western Texas, USA. *Geosphere*, 19(3), pp.849-877. <https://doi.org/10.1130/GES02620.1>
- Couples, G.D., Lewis, H. and Geoff Tanner, P.W., 1998. Strain partitioning during flexural-slip folding. *Geological Society, London, Special Publications*, 127(1), pp.149-165.
- Daggett, P.H., Keller, G.R., Morgan, P., Wen, C.-L., 1986. Structure of the southern Rio Grande Rift from gravity interpretation. *J. Geophys. Res.*, 91, 6157. <https://doi.org/10.1029/JB091iB06p06157>
- Dasch, E.J., Armstrong, R.L. and Clabaugh, S.E., 1969. Age of rim rock dike swarm, Trans-Pecos, Texas. *Geological Society of America Bulletin*, 80(9), pp.1819-1824. [https://doi.org/10.1130/0016-7606\(1969\)80\[1819:SORRDS\]2.0.CO;2](https://doi.org/10.1130/0016-7606(1969)80[1819:SORRDS]2.0.CO;2)
- Davies, C.P., 2006. Implementing Earth systems science curriculum: Evaluating the integration of urban environments for an urban audience. *Journal of Geoscience Education*, 54(3), pp.364-373.
- Davis, G.H., Reynolds, S.J. and Kluth, C.F., 2011. *Structural geology of rocks and regions*. John Wiley & Sons.
- DeCamp, D.W., 1985. Structural Geology of Mesa de Anguila, Big Bend National Park, Texas. *In*: Dickerson, P.W. and Muehlberger, W.R., 1985. *Structure and tectonics of Trans-Pecos Texas* (No. 85). West Texas Geological Society.
- Dickerson, P.W., 1980. Structural zones transecting the southern Rio Grande rift. *In* Dickerson, P.W., Hoffer, J.M., eds., the Trans-Pecos region: New Mexico Geological Society, 31st Field Conference Guidebook, p.63-70.
- Dickerson, P.W., 1995. *Tascotal Mesa transfer zone, Rio Grande Rift of West Texas (Presidio, Brewster counties): a structural, mechanical, and thermal characterization*. (Doctoral dissertation, The University of Texas at Austin).
- Dickerson, P.W., 2013. Tascotal Mesa transfer zone—An element of the Border Corridor transform system, Rio Grande rift of West Texas and adjacent Mexico. *In* Hudson, M., Grauch, T., eds., *New Perspectives on Rio Grande Rift Basins: From Tectonics to Groundwater*. Geological Society of America Special Paper 494, pp.475-500.
- Dickerson, P.W. and Muehlberger, W.R., 1994. Basins in the Big Bend segment of the Rio Grande rift, trans-Pecos Texas. *In* Keller, G.R., and Cather, S.M., eds., *Basins of the Rio Grande Rift: Structure,*

Stratigraphy, and Tectonic Setting: Boulder, Colorado, Geological Society of America Special Paper 291, pp.283-297.

Dickerson, P.W., 2010. Geologic map of Mariscal Mountain Quadrangle, Big Bend National Park, Texas. 1:24,000. Austin, Texas: Bureau of Economic Geology.

Doser, D.I., 1987. The 16 August 1931 Valentine, Texas, earthquake: evidence for normal faulting in west Texas. *Bulletin of the Seismological Society of America*, 77(6), pp.2005-2017.

Edelman, S.H., 1989. Limitations of the concept of stress in structural analysis. *Journal of Geological Education*, 37(2), pp.102-106.

Erdlac Jr, R.J., 1990. A Laramide-age push-up block: The structures and formation of the Terlingua-Solitario structural block, Big Bend region, Texas. *Geological Society of America Bulletin*, 102(8), pp.1065-1076.

Eyal, Y., Kaufman, A., Bar-Matthews, M., 1992. Use of ²³⁰Th/U ages of striated carnotites for dating fault displacements. *Geology*, 20, 829. [https://doi.org/10.1130/0091-7613\(1992\)020<0829:UOTUAO>2.3.CO;2](https://doi.org/10.1130/0091-7613(1992)020<0829:UOTUAO>2.3.CO;2)

Fink, L.D., 2005. Creating significant learning experiences: An integrated approach to designing college courses. *Journal of Chemical Education*, 82(6), p.819.

Forehand, M., 2005. Bloom's taxonomy: Original and revised. *Emerging perspectives on learning, teaching, and technology*, 8, pp.41-44.

Fossen, H., 2016. *Structural geology*. Cambridge University Press.

Gosselin, D., Burian, S., Lutz, T. and Maxson, J., 2016. Integrating geoscience into undergraduate education about environment, society, and sustainability using place-based learning: three examples. *Journal of Environmental Studies and Sciences*, 6, pp.531-540.

Gosselin, D.C., Egger, A.E. and Taber, J.J. eds., 2019. *Interdisciplinary teaching about Earth and the environment for a sustainable future*. Cham: Springer.

Haenggi, W.T., 2002. Tectonic history of the Chihuahua trough, Mexico and adjacent USA, Part II: Mesozoic and Cenozoic. *Boletín de la Sociedad Geológica Mexicana*, 55(1), pp.38-94.

Helesic, J.B., 2020. *Paleomagnetic Analysis of Vertical Axis Rotation Along the Tascotal Mesa Fault Zone in Far West Texas* (MS thesis, Sul Ross State University).

Henry, C.D., 1977. *Geologic setting and geochemistry of thermal water and geothermal assessment, Trans-Pecos Texas. Final report, June 1, 1976-May 31, 1977* (No. ORO-5106-1). Texas Univ., Austin (USA). Bureau of Economic Geology. <https://doi.org/10.2172/5716546>

Henry, C.D., 1998. Basement-controlled transfer zones in an area of low-magnitude extension, eastern Basin and Range province, Trans-Pecos Texas. *SPECIAL PAPERS-GEOLOGICAL SOCIETY OF AMERICA*, pp.75-88.

- Henry, C.D., Price, J.G., 1986. Early basin and range development in Trans-Pecos Texas and adjacent Chihuahua: Magmatism and orientation, timing, and style of extension. *J. Geophys. Res.* 91, 6213. <https://doi.org/10.1029/JB091iB06p06213>
- Henry, C.D., Price, J.G., James, E.W., 1991. Mid-Cenozoic stress evolution and magmatism in the Southern Cordillera, Texas and Mexico: Transition from continental arc to intraplate extension. *J. Geophys. Res.* 96, 13545–13560. <https://doi.org/10.1029/91JB00202>
- Hentz, T.F. and Henry, C.D., 1989. Evaporite-hosted native sulfur in Trans-Pecos Texas: Relations to late-phase Basin and range deformation. *Geology*, 17(5), pp.400-403.
- HHMI Biointeractive, (n.d.). HHMI Biointeractive Viewer. Retrieved September 2021, from <https://www.biointeractive.org/>
- Hudleston, P.J., Treagus, S.H. and Lan, L., 1996. Flexural flow folding: does it occur in nature?. *Geology*, 24(3), pp.203-206. Lehman, T.M., 1991. Sedimentation and tectonism in the Laramide Tornillo Basin of west Texas. *Sedimentary Geology*, 75(1-2), pp.9-28.
- Huguet, C., Pearse, J., Noè, L.F., Valencia, D.M., Ruiz, N.C., Heredia, A.J. and Avedaño, M.A.P., 2020. Improving the motivation of students in a large introductory geoscience course through active learning. *Journal of Geoscience Education*, 68(1), pp.20-32.
- Imrecke, D.B., Robinson, A.C., Murphy, M.A., 2015. Kinematic Evolution of the Eastern Chalk Draw Fault during Basin and Range Extension: Evaluating the Role Played by Preexisting Structural Fabrics in Along-Strike Displacement Patterns. *The Journal of Geology* 123(5), pp.385–403. <https://doi.org/10.1086/682935>
- James, E.W. and Henry, C.D., 1991. Compositional changes in Trans-Pecos Texas magmatism coincident with Cenozoic stress realignment. *Journal of Geophysical Research: Solid Earth*, 96(B8), pp.13561-13575.
- Keller, G.R., Morgan, P., Seager, W.R., 1990. Crustal structure, gravity anomalies and heat flow in the southern Rio Grande rift and their relationship to extensional tectonics. *Tectonophysics* 174, 21–37. [https://doi.org/10.1016/0040-1951\(90\)90382-I](https://doi.org/10.1016/0040-1951(90)90382-I)
- Kim, K., Sharma, P., Land, S.M. and Furlong, K.P., 2013. Effects of active learning on enhancing student critical thinking in an undergraduate general science course. *Innovative Higher Education*, 38, pp.223-235.
- Kirkby, K.C., 2014. Place in the City: Place-Based Learning in a Large Urban Undergraduate Geoscience Program. *Journal of Geoscience Education* 62, 177–186. <https://doi.org/10.5408/12-396.1>
- Kluth, C.F., Schaftenaar, C.H., Keller, G.R. and Cather, S.M., 1994. Depth and geometry of the northern Rio Grande rift in the San Luis Basin, south-central Colorado. *SPECIAL PAPERS-GEOLOGICAL SOCIETY OF AMERICA*, pp.27-27.

- Landman, R.L. and Flowers, R.M., 2013. (U-Th)/He thermochronologic constraints on the evolution of the northern Rio Grande Rift, Gore Range, Colorado, and implications for rift propagation models. *Geosphere*, 9(1), pp.170-187.
- Leckie, R.M., (n.d.), Engage Students with Active Learning Strategies, Teach the Earth, <https://serc.carleton.edu/NAGTWorkshops/intro/activelearning.html>, retrieved October 7, 2023.
- Lehman, T.M., 1991. Sedimentation and tectonism in the Laramide Tornillo Basin of west Texas. *Sedimentary Geology*, 75(1-2), pp.9-28.
- Liu, Y.A., Murphy, M.A., van Wijk, J., Koning, D.J., Smith, T., Andrea, R.A., 2019. Progressive opening of the northern Rio Grande rift based on fault structure and kinematics of the Tusas-Abiquiu segment in north-central New Mexico, U.S. *Tectonophysics* 753, pp.15–35. <https://doi.org/10.1016/j.tecto.2019.01.004>
- MacKay, R., 2018. Teaching With Data, *Starting Point*. Retrieved August 2020, from <https://serc.carleton.edu/introgeo/teachingwdata/index.html>.
- Maler, M.O., 1990. Dead horse graben: A west Texas accommodation zone. *Tectonics* 9, pp.1357–1368. <https://doi.org/10.1029/TC009i006p01357>
- Marrett, R. and Allmendinger, R., 1990. Kinematic analysis of fault-slip data, *Journal of Structural Geology* 12, p.973-986.
- Manduca, C. and Mogk, D.W., 2002, April. Using data in undergraduate science classrooms. In *Final report of the National Science Digital Library Workshop*.
- Martin, D.M., 2007. *The structural evolution of the McKinney Hills Laccolith, Big Bend National Park, Texas* (Doctoral dissertation).
- Maxwell, R.A., 1967. Geology of Big Bend National Park, Brewster County, Texas. *Virtual Landscapes of Texas*.
- McConnell, D.A., Chapman, L., Czajka, C.D., Jones, J.P., Ryker, K.D., Wiggen, J., 2017. Instructional Utility and Learning Efficacy of Common Active Learning Strategies. *Journal of Geoscience Education* 65, 604–625. <https://doi.org/10.5408/17-249.1>
- McConnell, D.A., Steer, D.N., Owens, K.D., 2003. Assessment and Active Learning Strategies for Introductory Geology Courses. *Journal of Geoscience Education* 51, 205–216. <https://doi.org/10.5408/1089-9995-51.2.205>
- McConnell, T.J., Parker, J.M. and Eberhardt, J., 2013. Problem-based learning as an effective strategy for science teacher professional development. *The Clearing House: A Journal of Educational Strategies, Issues and Ideas*, 86(6), pp.216-223.
- McDowell, F. W., 1979, Potassium-argon dating in the Trans-Pecos Texas volcanic field, in Walton, A. W., and Henry, C. D., eds., Cenozoic geology of the Trans-Pecos volcanic field of Texas: University of Texas at Austin Bureau of Economic Geology Guidebook 19, p. 10-18.

- Miggins, D.P., 2009. *Temporal And Geochemical Insights Related to Volcanic and Plutonic Activity within Big Bend National Park* (Doctoral dissertation, The University of Texas at El Paso).
- Minor, S.A., Hudson, M.R., Caine, J.S., Thompson, R.A., 2013. Oblique transfer of extensional strain between basins of the middle Rio Grande rift, New Mexico: Fault kinematic and paleostress constraints, *in*: Hudson, M., Grauch, T., eds., *New Perspectives on Rio Grande Rift Basins: From Tectonics to Groundwater*. Geological Society of America. [https://doi.org/10.1130/2013.2494\(14\)](https://doi.org/10.1130/2013.2494(14))
- Mottram, C.M., Kellett, D.A., Barresi, T., Zwingmann, H., Friend, M., Todd, A., Percival, J.B., 2020. Syncing fault rock clocks: Direct comparison of U-Pb carbonate and K-Ar illite fault dating methods. *Geology* 48, 1179–1183. <https://doi.org/10.1130/G47778.1>
- Morley, C.K., 2010. Stress re-orientation along zones of weak fabrics in rifts: An explanation for pure extension in 'oblique' rift segments?. *Earth and Planetary Science Letters*, 297(3-4), pp.667-673.
- Moustafa, A.R., 1988. *Structural geology of Sierra del Carmen, Trans-Pecos Texas*. Bureau of Economic Geology, University of Texas at Austin. 1:48,000.
- Mraz, J.R., Keller, G.R., 1980. Structure of the Presidio Bolson area, Texas, interpreted from gravity data (No. DOE/ET/28388-T1, 6376136). <https://doi.org/10.2172/6376136>
- Muehlberger, W.R., 1980. The Texas lineament revisited, *in* Dickerson, P.W., Hoffer, J.M., eds., *The Trans-Pecos region: New Mexico Geological Society, 31st Field Conference Guidebook*, p.113-121.
- Murray, K.D., Murray, M.H. and Sheehan, A.F., 2019. Active deformation near the Rio Grande Rift and Colorado Plateau as inferred from continuous Global Positioning System measurements. *Journal of Geophysical Research: Solid Earth*, 124(2), pp.2166-2183.
- NPS.gov, 2017. Mission, Purpose and Significance Statements for Big Bend National Park (WWW Document). Available at: <https://www.nps.gov/bibe/learn/management/mispursig.htm#:~:text=The%20park's%20mission%20is%20to,to%20foster%20understanding%20and%20appreciation> (accessed 09.10.23).
- NPS.gov. (n.d.). *MP Ch 7: Interp & Ed - Policy (U.S. National Park Service)*. [online] Available at: <https://www.nps.gov/subjects/policy/mp-7-interpretation-education.htm#:~:text=Interpretive%20programs%20are%20the%20methods> [Accessed 9 Dec. 2023].
- Nuriel, P., Rosenbaum, G., Uysal, T.I., Zhao, J., Golding, S.D., Weinberger, R., Karabacak, V., Avni, Y., 2011. Formation of fault-related calcite precipitates and their implications for dating fault activity in the East Anatolian and Dead Sea fault zones. *Geological Society, London, Special Publications* 359, 229–248. <https://doi.org/10.1144/SP359.13>
- Nuriel, P., Rosenbaum, G., Zhao, J.-X., Feng, Y., Golding, S.D., Villemant, B., Weinberger, R., 2012. U-Th dating of striated fault planes. *Geology* 40, 647–650. <https://doi.org/10.1130/G32970.1>

- Oldow, J.S. and Craig, S.D., 1992, April. Late Cenozoic displacement partitioning in the northwestern Great Basin. In *Geological Society of Nevada Walker Lane symposium: Structure, tectonics and mineralization of the Walker Lane: Reno, Geological Society of Nevada* (pp. 17-52).
- Olig, S.S., Eppes, M.C., Forman, S.L., Love, D.W., Allen, B.D., Audemard, M., Michetti, F.A. and McCalpin, J.P., 2011. Late Quaternary earthquakes on the Hubbell Spring fault system, New Mexico, USA: Evidence for noncharacteristic ruptures of intrabasinal faults in the Rio Grande rift. *Geologic Criteria for Evaluating Seismicity Revisited: Forty Years of Paleoseismic Investigations and the Natural Record of Past Earthquakes: Geological Society of America Special Paper, 479*, pp.47-77.
- Olsen, K.H., Baldridge, W.S. and Callender, J.F., 1987. Rio Grande rift: an overview. *Tectonophysics, 143*(1-3), pp.119-139.
- Page, W.R., Turner, K.J., Bohannon, R.G., Berry, M.E., Williams, V.S., Miggins, D.P., Ren, M., Anthony, E.Y., Morgan, L.A., Shanks, P.W.C. and Gray, J.E., 2008. *Geological, Geochemical, and Geophysical Studies by the US Geological Survey in Big Bend National Park, Texas* (No. 1327). US Geological Survey.
- Parker, J.T., 2022. *A Structural Analysis and Synthesis of the Chisos Pen Region in Big Bend National Park* (MS thesis, Sul Ross State University).
- Price, J.G. and Henry, C.D., 1984. Stress orientations during Oligocene volcanism in Trans-Pecos Texas: Timing the transition from Laramide compression to Basin and Range tension. *Geology, 12*(4), pp.238-241.
- Reiners, P.W., Carlson, R.W., Renne, P.R., Cooper, K.M., Granger, D.E., McLean, N.M. and Schoene, B., 2017. *Geochronology and thermochronology*. John Wiley & Sons.
- Ricketts, J., Amato, J. and Gavel, M., 2021. The origin and tectonic significance of the Basin and Range–Rio Grande rift boundary in southern New Mexico, USA. *GSA Today, 31*(10), pp.4-10.
<https://doi.org/10.1130/GSATG509A.1>
- Ricketts, J.W., Karlstrom, K.E. and Kelley, S.A., 2015. Embryonic core complexes in narrow continental rifts: The importance of low-angle normal faults in the Rio Grande rift of central New Mexico. *Geosphere, 11*(2), pp.425-444.
- Ricketts, J.W., Kelley, S.A., Karlstrom, K.E., Schmandt, B., Donahue, M.S., van Wijk, J., 2016. Synchronous opening of the Rio Grande rift along its entire length at 25–10 Ma supported by apatite (U-Th)/He and fission-track thermochronology, and evaluation of possible driving mechanisms. *Geological Society of America Bulletin, 128*, 397–424.
<https://doi.org/10.1130/B31223.1>
- Roberts, N.M.W., Walker, R.J., 2016. U-Pb geochronology of calcite-mineralized faults: Absolute timing of rift-related fault events on the northeast Atlantic margin. *Geology, 44*, 531–534.
<https://doi.org/10.1130/G37868.1>

- Rodriguez, R. and Kelsch, J.M., 2022, Strain analysis and geochronology of a shear zone and slickenlines along a section of the Boquillas fault in Big Bend National Park, Texas: Geological Society of America Abstracts with Programs, v. 54, No. 5, <https://doi.org/10.1130/abs/2022AM-383443>.
- Rodriguez-Gonzales, G., 2019. *Fault kinematics of the southern Rio Grande rift: Exploring the possibility of fault reactivation* (MS thesis, The University of Texas at El Paso).
- Rodriguez-Gonzalez, G., Ricketts, J.W., 2019. Fault kinematics of the southern Rio Grande rift: Exploring the possibility of fault reactivation: Geological Society of America Abstracts with Programs, v. 53. <https://doi.org/10.1130/abs/2019AM-340907>
- Rosendahl, B.R., 1987. Architecture of continental rifts with special reference to East Africa. *Annual Review of Earth and Planetary Sciences*, 15(1), pp.445-503.
- Roy, M., Karlstrom, K.A.R.L., Kelley, S., Pazzaglia, F.J. and Cather, S., 1999. Topographic setting of the Rio Grande Rift, New Mexico: Assessing the role of flexural “riftflank uplift” in the Sandia Mountains: New Mexico Geological Society Guidebook. In *50th Field Conference, Albuquerque Geology* (pp. 167-174).
- Ruiz-Primo, M.A., Briggs, D., Iverson, H., Talbot, R., Shepard, L.A., 2011. Impact of Undergraduate Science Course Innovations on Learning. *Science*, 331, 1269–1270. <https://doi.org/10.1126/science.1198976>
- Russell, L.R. and Snelson, S., 1994. Structural Style and Tectonic Evolution of the Albuquerque Basin Segment of the Rio Grande Rift, New Mexico, USA: Chapter 6: Part II. Examples of Other Rift Basins. pp.205-258.
- Satterfield, J.I., Ashmore, R.A., 2009. Overview of recent mountain-building events in the Big Bend Region, West Texas and northern Mexico: *Journal of Borderland Studies*, 1, 35p.
- Satterfield, J.I., and Dyess, J.E., 2007. Polyphase folds and faults in a wrench fault zone, northern Big Bend National Park. *West Texas Geological Society Bulletin*, 46, p. 8 – 19.
- Scotese, C.R., 1998. The PALEOMAP Project: paleogeographic atlas and plate tectonic software. *Oceanographic Literature Review*, 3(45), pp.606-607.
- Semken, S., 2005. Sense of Place and Place-Based Introductory Geoscience Teaching for American Indian and Alaska Native Undergraduates. *Journal of Geoscience Education*, 53, 149–157. <https://doi.org/10.5408/1089-9995-53.2.149>
- SERC, n.d. Data Structures Appropriate to Introductory Geoscience. Retrieved August 2020 from <https://serc.carleton.edu/sp/library/teachingwdata/DataStructures.html>
- Snee, J.-E.L., Zoback, M.D., 2018. State of stress in the Permian Basin, Texas and New Mexico: Implications for induced seismicity. *The Leading Edge*, 37, 127–134. <https://doi.org/10.1190/tle37020127.1>

- Southard, S. and Eckert, G., 2015. Celebrating soils across the National Park System (WWW Document). *Park Science* 32(2):54-59. https://www.nps.gov/articles/parkscience32_2_54-59_southard_eckert_3836.htm (accessed 09.10.23).
- Stein, S., Stein, C., Blavascunas, E., and Kley, J., 2015. Using Lake Superior parks to explain the Midcontinent Rift (WWW Document). *Park Science* 32(1)---. https://www.nps.gov/articles/parkscience32_1_19-29_stein_et_al_3817.htm (accessed 09.10.23).
- Stevens, J.B., Stevens, M.S., 1985. Basin and Range deformation and depositional timing, Trans-Pecos Texas, in Dickerson, P.W., and Muehlberger, W.R., eds., *Structure and tectonics of Trans-Pecos Texas*: West Texas Geological Society, 85-81, p.157-164.
- Sun, S.S. and McDonough, W.F., 1989. Chemical and isotopic systematics of oceanic basalts: implications for mantle composition and processes. *Geological Society, London, Special Publications*, 42(1), pp.313-345. <https://doi.org/10.1144/GSL.SP.1989.042.01.19>
- Sun, X., Peebles, M., Kelsch, J., Davies, R., Bigio, E., and Ashwell, P., 2020. Investigating climate-change data. Collaborative work in-conference, NAGT 2020 Earth Educators' Rendezvous.
- Suppe, J. and Medwedeff, D.A., 1990. Geometry and kinematics of fault-propagation folding. *Eclogae Geologicae Helveticae*, 83(3), pp.409-454.
- Surpless, B., Hill, N. and Beasley, C., 2015. The unusual 3D interplay of basement fault reactivation and fault-propagation-fold development: A case study of the Laramide-age Stillwell anticline, west Texas (USA). *Journal of Structural Geology*, 79, pp.42-56.
- Turner, K.J., Berry, M.E., Page, W.R., Lehman, T.M., Bohannon, R.G., Scott, R.B., Miggins, D.P., Budahn, J.R., Cooper, R.W., Drenth, B.J. and Anderson, E.D., 2011. *Geologic map of Big Bend National Park, Texas* (p. 84). US Department of the Interior, US Geological Survey.
- Udden, J.A., 1907. *A Sketch of the Geology of the Chisos Country, Brewster County, Texas*. (No. 11-16). University of Texas.
- Ward, E.M.G., Semken, S. and Libarkin, J.C., 2014. The design of place-based, culturally informed geoscience assessment. *Journal of Geoscience Education*, 62(1), pp.86-103.
- White, J.C., Benker, S.C., Ren, M., Urbanczyk, K.M. and Corrick, D.W., 2006. Petrogenesis and tectonic setting of the peralkaline Pine Canyon caldera, Trans-Pecos Texas, USA. *Lithos*, 91(1-4), pp.74-94.
- Whitmeyer, S.J. and Karlstrom, K.E., 2007. Tectonic model for the Proterozoic growth of North America. *Geosphere*, 3(4), pp.220-259.
- Yamaoke, K., Ma, L., Hishikawa, K., Usui, A., 2016. Geochemistry and U-series dating of Holocene and fossil marine hydrothermal manganese deposits from the Izu-Ogasawara arc, *Ore Geology Reviews*, doi: 10.1016/j.oregeorev.2016.07.02
- Yang, P., Wu, G., Nuriel, P., Nguyen, A.D., Chen, Y., Yang, S., Feng, Y., Ren, Z., Zhao, J., 2021. In situ LA-ICPMS U Pb dating and geochemical characterization of fault-zone calcite in the central Tarim

Basin, northwest China: Implications for fluid circulation and fault reactivation. *Chemical Geology*, 568, 120125. <https://doi.org/10.1016/j.chemgeo.2021.120125>

Yuretich, R.F., Khan, S.A., Leckie, R.M., Clement, J.J., 2001. Active-Learning Methods to Improve Student Performance and Scientific Interest in a Large Introductory Oceanography Course. *Journal of Geoscience Education*, 49, 111–119. <https://doi.org/10.5408/1089-9995-49.2.111>

Zimmerman, N.M., 2005. *Host rock fracture analysis: Applying the deformation mechanics associated with shallow igneous intrusion to the fracture bridging theory, McKinney hills laccolith, Big Bend National Park* (MS Thesis, Texas Tech University).

Zoback, 1981. Cainozoic evolution of the state of stress and style of tectonism of the Basin and Range province of the western United States. *Phil. Trans. R. Soc. Lond. A* 300, 407–434. <https://doi.org/10.1098/rsta.1981.0073>

Zoback, M.L., Zoback, M., 1980. State of stress in the conterminous United States. *J. Geophys. Res.* 85, 6113–6156. <https://doi.org/10.1029/JB085iB11p06113>

APPENDICES

Appendix 1 (Chapter 2). Collected fault-surface kinematic data

Appendix 2 (Chapter 2). Geochemical and geochronologic data

Appendix 3 (Chapter 4). In-class exercises

Appendix 4 (Chapter 4). Surveys

Appendix 5 (Chapter 4). Table showing differences in total percent of high rankings for the few

Appendix 6 (Chapter 4). Word clouds formed from students' short answers to questions of what they learned.

Appendix 1. Collected fault-surface kinematic data

This table includes T-trend calculated by FaultKin8 (Marrett and Allmendinger, 1990; Allmendinger et al., 2012)

No.	Field No.	sample number	Strike	Rake	Dip	T trend	Sense	Geologist	Year	month	Day	Qual	Longitude	Latitude	Site	Kin pop
1	210123_01		141	100	76	239	normal	JMK	21	1	23	c	102.972	29.5698	N Stairway Mtn	1
3	210123_03_4		153	-84	61	239	normal	JMK	21	1	23	b	102.972	29.5683	N Stairway Mtn	1
4	2012_0103		154	117	58	263	normal	JMK	21	1	23	b	102.972	29.5683	N Stairway Mtn	1
6	210123_03_7		157	-89	63	246	normal	JMK	21	1	23	b	102.972	29.5683	N Stairway Mtn	1
7	210123_03_8		140	-85	58	226	normal	JMK	21	1	23	b	102.972	29.5683	N Stairway Mtn	1
8	210123_03_9		140	-92	62	231	normal	JMK	21	1	23	b	102.972	29.5683	N Stairway Mtn	1
9	210123_04_10		154	-91	58	245	normal	JMK	21	1	23	c	102.9717	29.5677	N Stairway Mtn	1
10	210123_05_11		150	100	57	247	normal	JMK	21	1	23	b	102.9818	29.5634	N Stairway Mtn	1
11	2012_0107		171	101	80	270	normal	JMK	21	1	23	b	102.9819	29.5629	N Stairway Mtn	2
12	210123_07_13		340	-93	87	73	normal	JMK	21	1	23	b	102.9819	29.5629	N Stairway Mtn	1
13	210123_07_14		331	-92	85	63	normal	JMK	21	1	23	b	102.9819	29.5629	N Stairway Mtn	1
14	210123_07_15		346	104	85	89	normal	JMK	21	1	23	b	102.9819	29.5629	N Stairway Mtn	1
15	210123_09_16		327	101	83	67	normal	JMK	21	1	23	b	103.0443	29.5746	BgBrsh basin	1
16	210123_03_17		148	-70	73	222	normal	satt	21	1	23	b	102.972	29.5683	N Stairway Mtn	1
17	210123_03_18		151	-89	60	240	normal	satt	21	1	23	b	102.972	29.5683	N Stairway Mtn	1
18	210123_03_19		164	-62	76	232	normal	satt	21	1	23	b	102.9819	29.5629	N Stairway Mtn	2
19	210123_03_20		150	-55	63	216	normal	cg	21	1	23	b	102.972	29.5683	N Stairway Mtn	1
20	210123_03_21		149	-70	73	223	normal	cg	21	1	23	b	102.972	29.5683	N Stairway Mtn	1
21	210123_03_22		151	-87	60	239	normal	cg	21	1	23	b	102.972	29.5683	N Stairway Mtn	1
22	210123_03_23		151	-86	64	238	normal	cg	21	1	23	b	102.972	29.5683	N Stairway Mtn	1
23	210123_07_24		156	-95	82	250	normal	cg	21	1	23	b	102.9808	29.5627	N Stairway Mtn	2
24	210123_07_25		311	-88	68	39	normal	cg	21	1	23	b	102.9808	29.5627	N Stairway Mtn	1
25	210123_07_26		343	-78	65	64	normal	cg	21	1	23	b	102.9808	29.5627	N Stairway Mtn	1
26	210123_07_26.5		164	-62	76	232	normal	cg	21	1	23	b	102.9808	29.5627	N Stairway Mtn	2
27	Sf1	sm01a	145	109	76	250	normal	JMK	2022	4	15	b	102.972	29.5682	N Stairway Mtn	1
28	Sf2		145	112	65	251	normal	JMK	2022	4	15	b	102.972	29.5682	N Stairway Mtn	1
29	Sf3	sm03	152	-48	64	213	normal	JMK	2022	4	15	b	102.972	29.5682	N Stairway Mtn	1
30	Sf4	sm04	147	-84	60	233	normal	JMK	2022	4	15	b	102.972	29.5682	N Stairway Mtn	2
31	Sf5	sm05	165	-97	62	260	normal	JMK	2022	4	15	b	102.972	29.5682	N Stairway Mtn	1
33	210124_12_32		320	123	41	253	normal	JMK	21	1	24	d	103.0536	29.5844	BgBrsh basin	1

No.	Field No.	sample number	Strike	Rake	Dip	Trend	Sense	Geologist	Year	month	Day	Quality	Longitude	Latitude	Site	Kin pop	
34	210124_13a		172	-62	76	240	normal	JMK	21	1	24	c	103.0534	29.5839	BgBrsh basin	1	
35	210124_13b		172	-76	79	250	normal	JMK	21	1	24	c	103.0534	29.5839	BgBrsh basin	1	
36	210124_13c		172	-70	79	246	normal	JMK	21	1	24	c	103.0534	29.5839	BgBrsh basin	1	
37	210124_14		321	-57	67	27	normal	JMK	21	1	24	c	103.0532	29.5849	BgBrsh basin	2	
42	220415jk.3402b		320	-89	89	49	normal	JMK				b	102.9193	29.5391	3402map	1	
43	220415jk.3402b		318	-93	58	50	normal	JMK				b	102.9193	29.5391	3402map	1	
44	210930_1a		110	-20	89	157	sinistral	JMK	2021	9	30	c	103.1206	29.6091	grotto fault	2	
45	210930_1b		122	-	100	83	221	normal	JMK	2021	9	30	c	103.1206	29.6091	grotto fault	1
46	210930_1c		110	-	100	89	210	normal	JMK	2021	9	30	c	103.1206	29.6091	grotto fault	1
47	210930_1d		110	-	112	89	220	normal	JMK	2021	9	30	c	103.1206	29.6091	grotto fault	1
48	210930_1e		109	-	125	89	228	normal	JMK	2021	9	30	c	103.1206	29.6091	grotto fault	1
49	210930_1f		112	-	120	88	228	normal	JMK	2021	9	30	c	103.1206	29.6091	grotto fault	1
50	210926_8a		127	-6	89	172	dextral	JMK	2021	9	26	c	103.1207	29.6091	grotto fault	1	
51	210926_8b		125	-4	87	170	dextral	JMK	2021	9	26	c	103.1207	29.6091	grotto fault	1	
52	210926_8c		126	0	90	171	dextral	JMK	2021	9	26	c	103.1207	29.6091	grotto fault		
53	210926_8d		130	-5	78	355	dextral	JMK	2021	9	26	b	103.1207	29.6091	grotto fault	1	
54	210926_8e		134	-12	85	180	dextral	JMK	2021	9	26	c	103.1207	29.6091	grotto fault	2	
55	210926_8f		142	-	101	77	241	normal	JMK	2021	9	26	c	103.1207	29.6091	grotto fault	1
56	210926_8g		136	-	109	86	243	normal	JMK	2021	9	26	c	103.1207	29.6091	grotto fault	1
57	210926_8h		151	-	125	61	265	normal	JMK	2021	9	26	c	103.1207	29.6091	grotto fault	1
58	210926_8i		120	-95	82	214	normal	JMK	2021	9	26	c	103.1207	29.6091	grotto fault	1	
59	210926_ac_g01		147	-74	79	224	normal	ATC	2021	9	26	c	103.1206	29.6091	grotto fault	1	
60	210926_ac_g02		146	-76	79	224	normal	ATC	2021	9	26	c	103.1206	29.6091	grotto fault	1	
61	210926_ac_g03		145	-83	75	229	normal	ATC	2021	9	26	c	103.1206	29.6091	grotto fault	1	
62	210926_ac_g04		143	-16	81	190	dextral	ATC	2021	9	26	b	103.1206	29.6091	grotto fault	2	
63	210926_ac_g05		145	-76	86	222	normal	ATC	2021	9	26	c	103.1206	29.6091	grotto fault	1	
64	210926_ac_g06		152	-8	90	197	dextral	ATC	2021	9	26	b	103.1206	29.6091	grotto fault	2	

No.	Field No.	sample number	Strike	Rake	Dip	Trend	Sense	Geologist	Year	Month	Day	Quality	Longitude	Latitude	Site	Kin pop
65	210926_ac_g07		143	-71	81	217	normal	ATC	2021	9	26	c	103.1206	29.6091	grotto fault	1
66	210926_ac_g08		144	-79	77	225	normal	ATC	2021	9	26	c	103.1206	29.6091	grotto fault	1
67	210926_ac_g09		142	-79	77	223	normal	ATC	2021	9	26	c	103.1206	29.6091	grotto fault	1
68	210926_ac_g10		143	-77	81	222	normal	ATC	2021	9	26	c	103.1206	29.6091	grotto fault	1
69	210926_ac_g11		146	-79	77	227	normal	ATC	2021	9	26	c	103.1206	29.6091	grotto fault	1
70	210926_ac_g12		142	-80	75	224	normal	ATC	2021	9	26	c	103.1206	29.6091	grotto fault	1
71	210926_ac_g13		151	-6	86	196	dextral	ATC	2021	9	26	b	103.1206	29.6091	grotto fault	2
72	210926_ac_g14		144	-80	76	226	normal	ATC	2021	9	26	c	103.1206	29.6091	grotto fault	1
73	210926_ac_g15		143	-82	80	226	normal	ATC	2021	9	26	c	103.1206	29.6091	grotto fault	1
74	210926_ac_g16		145	-83	81	229	normal	ATC	2021	9	26	c	103.1206	29.6091	grotto fault	1
75	210926_7iia		11	-84	60	97	normal	JMK	2021	9	26	c	103.1209	29.6089	grotto fault	1
76	210926_7iib		357	-91	60	88	normal	JMK	2021	9	26	c	103.1209	29.6089	grotto fault	1
77	210926_7iib2		357	-94	60	90	normal	JMK	2021	9	26	c	103.1209	29.6089	grotto fault	1
78	210926_7iic		7	-82	59	91	normal	JMK	2021	9	26	c	103.1209	29.6089	grotto fault	1
79	210926_7iid		333	-	62	70	normal	JMK	2021	9	26	c	103.1209	29.6089	grotto fault	1
80	210926_7iie		353	-90	60	83	normal	JMK	2021	9	26	c	103.1209	29.6089	grotto fault	1
81	210926_7a		2	-89	51	91	normal	JMK	2021	9	26	c	103.1209	29.6089	grotto fault	1
82	210926_7b		324	-	58	75	normal	JMK	2021	9	26	c	103.1209	29.6089	grotto fault	1
83	210926_7c		331	-	58	73	normal	JMK	2021	9	26	c	103.1209	29.6089	grotto fault	1
84	210926_7d		354	-	63	92	normal	JMK	2021	9	26	b	103.1209	29.6089	grotto fault	1
85	210926_7e		31	-95	64	125	normal	JMK	2021	9	26	c	103.1209	29.6089	grotto fault	1
86	210926_7f		324	-	54	61	normal	JMK	2021	9	26	c	103.1209	29.6089	grotto fault	1
87	JP-228		282	-93	85	15	normal	JP	2021	5	9		103.1219	29.6098	grotto fault	2
88	JP-761		179	-	75	292	normal	JP	2021	5	9		103.1219	29.6098	grotto fault	1
89	JP-51		335	-88	52	64	normal	JP	2021	5	9		103.1219	29.6098	grotto fault	1
90	JP-51		335	-	52	74	normal	JP	2021	5	9		103.1219	29.6098	grotto fault	1
91	JP-836		92	-	88	215	normal	JP	2021	5	9		103.1219	29.6098	grotto fault	1

No.	Field No.	sample number	Strike	Rake	Dip	Trend	Sense	Geologist	Year	month	Day	Quality	Longitude	Latitude	Site	Kin pop
92	JP-836		148	-135	73	269	normal	JP	2021	5	9		103.1219	29.6098	grotto fault	1
93	JP-836		186	-128	78	304	normal	JP	2021	5	9		103.1219	29.6098	grotto fault	1
94	JP-836		131	-135	86	255	normal	JP	2021	5	9		103.1219	29.6098	grotto fault	1
97	JP-452		181	-125	71	296	normal	JP	2021	5	9		103.1219	29.6098	grotto fault	1
98	JP-116		331	-166	89	105	normal	JP	2021	5	9		103.1219	29.6098	grotto fault	2
99	JP-183		173	-113	62	280	normal	JP	2021	5	9		103.1219	29.6098	grotto fault	1
100	JP-183		173	-100	62	270	normal	JP	2021	5	9		103.1219	29.6098	grotto fault	1
101	JP-183		173	-162	62	126	normal	JP	2021	5	9		103.1219	29.6098	grotto fault	1
102	210925_ac2_1		329	-89	77	58	Normal	ATC	2021	9	25	b	103.1298	29.6052	w dagg fit	1
103	210925_ac2_3		325	-99	72	62	Normal	ATC	2021	9	25	b	103.1298	29.6052	w dagg fit	1
104	210925_ac2_4		327	-97	73	63	Normal	ATC	2021	9	25	b	103.1298	29.6052	w dagg fit	1
105	210925_ac2_5		324	-87	71	52	Normal	ATC	2021	9	25	b	103.1298	29.6052	w dagg fit	1
106	210925_ac3_1		319	-98	74	55	Normal	ATC	2021	9	25	b	103.1301	29.606	w dagg fit	1
107	210925_ac3_2		314	-97	79	50	Normal	ATC	2021	9	25	b	103.1301	29.606	w dagg fit	1
108	210925_ac3_3		317	-102	78	57	Normal	ATC	2021	9	25	b	103.1301	29.606	w dagg fit	1
109	210925_1a		338	-65	51	51	Normal	JMK	2021	9	25	b	103.1299	29.6062	w dagg fit	1
110	210925_3a		349	-85	89	74	Normal	JMK	2021	9	25	a	103.1301	29.606	w dagg fit	2
111	210925_3b		0	-95	74	94	Normal	JMK	2021	9	25	c	103.1301	29.606	w dagg fit	1
112	210925_3c		348	-94	76	81	Normal	JMK	2021	9	25	c	103.1301	29.606	w dagg fit	1
113	210925_4a		163	-70	59	239	Normal	JMK	2021	9	25	a	103.1299	29.6055	w dagg fit	1
114	210925_5a		96	-124	58	209	Normal	JMK	2021	9	25	c	103.1296	29.6041	w dagg fit	1
115	210925_5b		107	-124	52	220	Normal	JMK	2021	9	25	c	103.1296	29.6041	w dagg fit	1
116	210925_6a		321	-91	87	52	normal	JMK	2021	9	25	c	103.1229	29.6014	w dagg fit	2
117	210925_6b		334	-90	87	64	normal	JMK	2021	9	25	c	103.1229	29.6014	w dagg fit	2
118	210925_6c		321	-100	88	61	normal	JMK	2021	9	25	c	103.1229	29.6014	w dagg fit	2
119	210925_6d		359	-80	88	79	normal	JMK	2021	9	25	c	103.1229	29.6014	w dagg fit	2
129	sf2	oor.02	325	-61	88	30	normal	JMK	2022	7	8	b	103.0946	29.4042	Mck hills	1

No.	Field No.	sample number	Strike	Rake	Dip	Trend	Sense	Geologist	Year	month	Day	Quality	Longitude	Latitude	Site	Kin pop
130	sf3	oor.03	315	-113	67	62	normal	JMK	2022	7	8	b	103.0946	29.4042	McK hills	1
132	sf5	oor.f5	300	-93	74	32	normal	JMK	2022	7	8	b	103.0945	29.4042	McK hills	1
139	sf13		69	-64	77	139	normal	JMK	2022	7	9	b	103.1016	29.3998	McK hills	2
140	sf14		71	-60	84	136	normal	JMK	2022	7	9	b	103.1016	29.3998	McK hills	2
150	sf21	oor.?	318	-124	71	73	normal	JMK	2022	7	9	a	103.0543	29.3674	McK hills	1
177	sf28		324	-109	83	70			2022	7	10	a	102.9157	29.2017	bqf main	
178	sf29	bqf.29	312	-106	79	55			2022	7	10	a	102.9157	29.2017	bqf main	
211	211121_1a_1		158	-75	83	235	normal	JMK	2021	11	21	c	103.2045	29.4089	Grapevine Hills	2
212	211121_1a_2		141	-55	78	204	normal	JMK	2021	11	21	c	103.2045	29.4089	Grapevine Hills	2
213	211121_1b_1		338	-135	88	103	none	JMK	2021	11	21	d	103.2045	29.4089	Grapevine Hills	
214	211121_1b_2		344	-138	89	110	none	JMK	2021	11	21	d	103.2045	29.4089	Grapevine Hills	
215	211121_1b_3		341	-133	89	105	none	JMK	2021	11	21	d	103.2045	29.4089	Grapevine Hills	
216	211121_1b_4		344	-143	88	112	none	JMK	2021	11	21	d	103.2045	29.4089	Grapevine Hills	
217	211121_2a_1		158	-19	89	205	none	JMK	2021	11	21	d	103.2041	29.4089	Grapevine Hills	
218	211121_2a_2		158	-22	89	205	none	JMK	2021	11	21	d	103.2041	29.4089	Grapevine Hills	
219	211121_3_1		245	-136	76	7	normal	JMK	2021	11	21	a	103.2018	29.4095	Grapevine Hills	2
220	211121_3_2		246	-114	80	356	normal	JMK	2021	11	21	a	103.2018	29.4095	Grapevine Hills	3
221	211121_3_3		246	-159	80	18	normal	JMK	2021	11	21	c	103.2018	29.4095	Grapevine Hills	2
222	211121_4a		124	-93	85	217	normal	JMK	2021	11	21	c	103.2016	29.4094	Grapevine Hills	2
223	211121_4b		122	-92	75	214	normal	JMK	2021	11	21	c	103.2016	29.4094	Grapevine Hills	2
224	211121_5a		184	-38	65	240	normal	JMK	2021	11	21	C	103.2024	29.4112	Grapevine Hills N	2
225	211121_5c		153	-111	48	258	normal	JMK	2021	11	21	b	103.2024	29.4112	Grapevine Hills N	2
266	Sf1i		50	-64	45	302	normal	JMK	2202	4	14	a	103.4611	29.1581	horseshoe cyn	1
267	Sf1ii		60	-61	43	310	normal	JMK	2202	4	14	a	103.4611	29.1581	horseshoe cyn	1
268	Sf2		66	-49	48	308	normal	JMK	2202	4	14	a	103.4611	29.1581	horseshoe cyn	1
269	Sf3i	hc01a	235	-30	54	107	normal	JMK	2202	4	14	b	103.4611	29.1581	horseshoe cyn	1
270	Sf3ii		63	-29	55	294	normal	JMK	2202	4	14	b	103.4611	29.1581	horseshoe cyn	1
271	Sf4		94	-90	64	184	normal	JMK	2202	4	14	b	103.4611	29.1581	horseshoe cyn	2
272	Sf5		115	-13	81	161	normal	JMK	2202	4	14	b	103.4611	29.1581	horseshoe cyn	3

No.	Field No.	sample number	Strike	Rake	Dip	Trend	Sense	Geologist	Year	month	Day	Qual	Longitude	Latitude	Site	Kin pop
273	Sf6	hc02a	105	-30	63	337	normal	JMK	220	4	14	b	103.461	29.158	horseshoe cyn	1
274	Sf7		106	-97	63	201	normal	JMK	220	4	14	c	103.461	29.158	horseshoe cyn	2
275	Sf8		112	-100	63	209	normal	JMK	220	4	14	c	103.461	29.158	horseshoe cyn	2
276	Sf8ii		113	-27	65	344	normal	JMK	220	4	14	c	103.461	29.158	horseshoe cyn	1
277	Sf9		115	-8	71	340	normal	JMK	220	4	14	c	103.460	29.158	horseshoe cyn	3
278	Sf10		224	-92	84	316	normal	JMK	220	4	14	b	103.460	29.158	horseshoe cyn	1
279	Sf11i		310	-150	85	80	normal	JMK	220	4	14	a	103.486	29.150	tuff cyn	1
280	Sf11ii		307	-149	90	78	normal	JMK	220	4	14	a	103.486	29.150	tuff cyn	0
281	Sf11iii		311	-149	75	79	normal	JMK	220	4	14	a	103.486	29.150	tuff cyn	1
282	Sf11iv		318	-151	81	87	normal	JMK	220	4	14	a	103.486	29.150	tuff cyn	1
283	Sf12i		304	-86	81	31	normal	JMK	220	4	14	b	103.486	29.150	tuff cyn	2
284	Sf12ii		332	-80	87	53	normal	JMK	220	4	14	b	103.486	29.150	tuff cyn	2
285	Sf13i		232	-22	75	281	normal	JMK	220	4	14	b	103.485	29.150	tuff cyn	1
286	Sf13ii	tc03a	165	-89	79	254	normal	JMK	220	4	14	a	103.485	29.150	tuff cyn	1
304	221110.pgh.1 a		103	-170	87	237	sinistral	jk	202	11	10	c	103.303	29.392	Paint Gap Hills	1
305	221110.pgh.1 a		279	-17	85	326	sinistral	jk	202	11	10	a-b	103.303	29.392	Paint Gap Hills	1
306	221110.pgh.1 a		277	-17	84	324	sinistral	jk	202	11	10	a-b	103.303	29.392	Paint Gap Hills	1
307	221110.pgh.1 a		278	-9	79	144		jk	202	11	10		103.303	29.392	Paint Gap Hills	
308	221110.pgh.1 a		51	-140	79	176	dextral	jk	202	11	10	b-c	103.303	29.392	Paint Gap Hills	1
309	221110.pgh.1 d		262	-22	89	309		jk	202	11	10		103.303	29.392	Paint Gap Hills	
310	22.11.10.2		100	-167	87	234	sinistral	jk	202	11	10	b-c	103.301	29.391	Paint Gap Hills	misfit
311	22.11.10.2		94	-176	85	49	sinistral	jk	202	11	10	b-c	103.301	29.391	Paint Gap Hills	1
312	22.11.10.2		88	-170	85	222	sinistral	jk	202	11	10	b-c	103.301	29.391	Paint Gap Hills	misfit
313	22.11.10.3		285	-157	87	57		jk	202	11	10		103.299	29.391	Paint Gap Hills	
314	22.11.10.3		284	-154	90	56		jk	202	11	10		103.299	29.391	Paint Gap Hills	
315	22.11.10.3		111	-22	86	159		jk	202	11	10		103.299	29.391	Paint Gap Hills	
316	22.11.10.6		106	-5	90	151	sinistral	jk	202	11	10	b	103.306	29.401	Paint Gap Hills	1
317	22.11.10.6		131	-8	90	176	sinistral	jk	202	11	10	c	103.306	29.401	Paint Gap Hills	1

No.	Field No.	sample number	Strike	Rake	Dip	Trend	Sense	Geology	Year	month	Day	Quality	Longitude	Latitude	Site	Kin pop
318	22.11.10.7		77	-149	78	205		jk	2022	11	10		103.3041	29.4002	Paint Gap Hills	
319	22.11.10.7		73	-169	74	27		jk	2022	11	10		103.3041	29.4002	Paint Gap Hills	
320	22.11.10.7		266	-6	88	311		jk	2022	11	10		103.3041	29.4002	Paint Gap Hills	
321	22.11.10.7		284	-2	85	149		jk	2022	11	10		103.3041	29.4002	Paint Gap Hills	
322	22.11.10.7		284	-13	85	330		jk	2022	11	10		103.3041	29.4002	Paint Gap Hills	
323	22.11.10.8		80	-159	84	212		jk	2022	11	10		103.3034	29.4	Paint Gap Hills	
324	22.11.10.8		79	-161	84	212		jk	2022	11	10		103.3034	29.4	Paint Gap Hills	
325	22.11.10.9		126	-153	89	257		jk	2022	11	10		103.3023	29.399	Paint Gap Hills	
326	22.11.10.9		147	-161	89	280		jk	2022	11	10		103.3023	29.399	Paint Gap Hills	
327	22.11.10.9		142	-162	90	276		jk	2022	11	10		103.3023	29.399	Paint Gap Hills	
328	22.11.10.10		90	-178	81	45		jk	2022	11	10		103.3018	29.3984	Paint Gap Hills	
329	22.11.10.10		91	-1	82	316		jk	2022	11	10		103.3018	29.3984	Paint Gap Hills	
330	22.11.11.01		162	-92	62	253	normal	jk	2022	11	11		103.2018	29.3996	Grapevine Hills	2
331	22.11.11.01		162	-175	62	119		jk	2022	11	11		103.2018	29.3996	Grapevine Hills	
332	22.11.11.02		176	-154	78	306		jk	2022	11	11		103.2018	29.3996	Grapevine Hills	
333	22.11.11.03		127	-85	73	213	normal	jk	2022	11	11		103.2012	29.3991	Grapevine Hills	2
141	sf15		55	-64	77	125	normal	JMK	2022	7	9	b	103.1016	29.3998	McK hills	2
142	sf16		68	-61	88	133	normal	JMK	2022	7	9	b	103.1016	29.3998	McK hills	2
143	sf17		320	-155	81	91	normal	JMK	2022	7	9	b	103.0968	29.4041	McK hills	1
128	sf1		325	-100	89	65	normal	JMK	2022	7	8	b	103.0946	29.4042	McK hills	1
131	sf4		173	-88	90	261	normal	JMK	2022	7	8	c	103.0946	29.4042	McK hills	2
133	sf7		320	-138	88	86	normal	JMK	2022	7	9	B	103.1007	29.3978	McK hills	1
134	sf8		305	-150	74	73	normal	JMK	2022	7	9	D	103.1007	29.3978	McK hills	1
135	sf9		169	-44	77	227	normal	JMK	2022	7	9	c	103.1011	29.3978	McK hills	1
136	sf10		139	-55	69	204	normal	JMK	2022	7	9	c	103.1011	29.3978	McK hills	2
137	sf11		122	-38	89	174	normal	JMK	2022	7	9	c	103.1014	29.398	McK hills	2
138	sf12		111	-30	84	161	normal	JMK	2022	7	9	c	103.1014	29.398	McK hills	2

No.	Field No.	sample number	Strike	Rake	Dip	Trend	Sense	Geologist	Year	month	Day	Quality	Longitude	Latitude	Site	Kin pop
144	sf17ii		320	-165	81	93	normal	JMK	2022	7	9	b	103.0968	29.4041	McK hills	1
145	sf17iii		320	-165	81	93	normal	JMK	2022	7	9	b	103.0968	29.4041	McK hills	1
146	sf17iv		320	-149	81	89	normal	JMK	2022	7	9	b	103.0968	29.4041	McK hills	1
147	sf18		314	-89	77	43	normal	JMK	2022	7	9	a	103.0543	29.3674	McK hills	1
148	sf19		313	-83	73	37	normal	JMK	2022	7	9	a	103.0543	29.3674	McK hills	1
149	sf20		315	-91	75	46	normal	JMK	2022	7	9	a	103.0543	29.3674	McK hills	1
151	sf22		317	-102	70	56	normal	JMK	2022	7	9	a	103.0543	29.3674	McK hills	1
152	sf23		317	-121	71	70	normal	JMK	2022	7	9	a	103.0543	29.3674	McK hills	1
153	sf23ii		317	-126	71	73	normal	JMK	2022	7	9	a	103.0543	29.3674	McK hills	1
154	sf24		320	-127	70	76	normal	JMK	2022	7	9	a	103.0543	29.3674	McK hills	1
155	sf24ii		320	-119	70	71	normal	JMK	2022	7	9	a	103.0543	29.3674	McK hills	1
124	211112_2b		148	-80	76	230	normal	JMK	2021	11	12	c	103.0911	29.4531	javelina draw	2
120	211112_1a		320	-116	38	248	normal	JMK	2021	11	12	C	103.0909	29.4551	javelina draw	1
121	211112_1b		336	-115	39	264	normal	JMK	2021	11	12	C	103.0909	29.4551	javelina draw	1
122	211112_1c		327	-109	42	250	normal	JMK	2021	11	12	C	103.0909	29.4551	javelina draw	1
123	211112_2a		113	-30	78	164	reverse	JMK	2021	11	12	c	103.0911	29.4531	javelina draw	2
125	211112_2c		145	-85	79	231	normal	JMK	2021	11	12	c	103.0911	29.4531	javelina draw	2
126	211112_2d_C RB		162	-54	82	224	normal	CRB	2021	11	12	c	103.0911	29.4531	javelina draw	2
127	211112_2e_C RB		164	-72	74	240	normal	CRB	2021	11	12	c	103.0911	29.4531	javelina draw	1
176	sf27	bqf.27	320	-116	87	73			2022	7	10	a	102.9157	29.2017	bqf main	1
162	jk_bf1		350	-168	87	124	dextral	JMK	2022	4	3	a	102.9135	29.2044	bqf splay	2
193	sf43		139	-176	77	94			2022	7	10	a	102.9157	29.2017	bqf main	2
194	sf43ii		138	-176	84	93			2022	7	10	a	102.9157	29.2017	bqf main	2
198	sf43vi		140	-175	86	275			2022	7	10	a	102.9157	29.2017	bqf main	2
196	sf43iv		137	-173	89	272			2022	7	10	a	102.9157	29.2017	bqf main	2
192	sf42		139	-172	90	274			2022	7	10	a	102.9157	29.2017	bqf main	2
188	sf38		144	-169	73	98			2022	7	10	a	102.9157	29.2017	bqf main	2
190	sf40		141	-164	76	274			2022	7	10	a	102.9157	29.2017	bqf main	2
195	sf43iii		140	-175	83	95			2022	7	10	a	102.9157	29.2017	bqf main	3
197	sf43v		139	-173	80	94			2022	7	10	a	102.9157	29.2017	bqf main	3

No.	Field No.	sample number	Strike	Rake	Dip	Trend	Sense	Geology	Year	month	Day	Quality	Longitude	Latitude	Site	Kin pop
170		bqtr.07	137	-171	65	92	normal	RR	2022	4	8	b	102.9153	29.2022	bqf main	3
173	sf7		140	-162	71	92	normal		2022	4	8	b	102.9153	29.2022	bqf main	3
159	jk_bf1		345	-115	89	98	normal	JMK	2022	4	3	a	102.9135	29.2044	bqf splay	3
171	0408jk.bqtr.03	bqtr.03 (also has 03x assoc)	17	-110	88	125	normal	RR	2022	4	8	b	102.9127	29.2049	bqf splay	3
170		bq6	131	-102	78	231	normal	RR	2022	4	8	b	102.9153	29.2022	bqf main	1
202	220403jk_rgv05		170	-100	80	269	normal	JMK	2022	4	3	b	102.9524	29.1786	rgv	1
203	220403jk_rgv06		168	-94	77	261	normal	JMK	2022	4	3	b	102.9523	29.1779	rgv	1
169	jk_bf2		154	-90	59	244	normal	JMK	2022	4	3	a	102.9135	29.2044	bqf splay	1
170	bqtr.b		160	-90	55	250	normal	JMK	2022	4	3	a	102.9135	29.2044	bqf splay	1
199	220403jk_rgv05		175	-90	64	265	normal	JMK	2022	4	3	b	102.9524	29.1786	rgv	1
201	220403jk_rgv05		175	-90	73	265	normal	JMK	2022	4	3	b	102.9524	29.1786	rgv	1
204	220403jk_rgv06b		185	-90	81	275	normal	JMK	2022	4	3	b	102.9521	29.1776	rgv	1
167	jk_bf2		153	-89	61	242	normal	JMK	2022	4	3	a	102.9135	29.2044	bqf splay	1
157	jk_bf1		6	-85	84	91	normal	JMK	2022	4	3	a	102.9135	29.2044	bqf splay	3
166	jk_bf2		154	-85	55	240	normal	JMK	2022	4	3	a	102.9135	29.2044	bqf splay	1
158	jk_bf1		359	-82	85	82	normal	JMK	2022	4	3	a	102.9135	29.2044	bqf splay	3
200	220403jk_rgv05		176	-82	66	260	normal	JMK	2022	4	3	b	102.9524	29.1786	rgv	1
172	sf5		183	-80	79	265	normal	JMK	2022	4	8	b	102.9153	29.2022	bqf main	1
170		bqtr.04	170	-80	59	253	normal	JMK	2022	4	8	b	102.9127	29.2049	bqf splay	1
164	jk_bf1		0	-80	86	81	normal	JMK	2022	4	3	a	102.9135	29.2044	bqf splay	3
171	sf5		181	-78	81	261	normal	JMK	2022	4	8	b	102.9153	29.2022	bqf main	1
156	jk_bf1		2	-78	89	80	normal	JMK				a	102.9135	29.2044	bqf splay	3
168	jk_bf2		160	-76	57	240	normal	JMK	2022	4	3	a	102.9135	29.2044	bqf splay	1
170		bqtr.05	182	-70	81	255	normal	JMK	2022	4	8	b	102.9127	29.2049	bqf splay	1
160	jk_bf1		155	-64	90	221	normal	JMK	2022	4	3	a	102.9135	29.2044	bqf splay	1
163	jk_bf1		168	-28	80	218	dextral	JMK	2022	4	3	a	102.9135	29.2044	bqf splay	1
161	jk_bf1		173	-19	89	220	dextral	JMK	2022	4	3	a	102.9135	29.2044	bqf splay	1

No.	Field No.	sample number	Strike	Rake	Dip	Trend	Sense	Geologist	Year	month	Day	Quality	Longitude	Latitude	Site	Kin pop
165	jk_bf1		0	-12	86	46	dextral	JMK	2022	4	3	a	102.9135	29.2044	bqf splay	2
183	sf33	bqf.33	318	-16	79	5			2022	7	10	a	102.9157	29.2017	bqf main	2
186	sf36		319	-12	88	5			2022	7	10	a	102.9157	29.2017	bqf main	2
189	sf39	bqf.39	317	-11	74	183			2022	7	10	a	102.9157	29.2017	bqf main	2
174	sf 25		323	-11	86	9			2022	7	9	a	102.9157	29.2017	bqf main	2
184	sf34		319	-11	87	5			2022	7	10	a	102.9157	29.2017	bqf main	2
185	sf35		318	-10	86	4			2022	7	10	a	102.9157	29.2017	bqf main	2
187	sf37		323	-10	80	189			2022	7	10	a	102.9157	29.2017	bqf main	2
180	sf31i		137	108	81	242			2022	7	10	a	102.9157	29.2017	bqf main	
181	sf31ii		137	105	81	240			2022	7	10	a	102.9157	29.2017	bqf main	
175	sf26		138	-75	77	216			2022	7	9	a	102.9157	29.2017	bqf main	
182	sf32		139	-73	76	215			2022	7	10	a	102.9157	29.2017	bqf main	
191	sf41		142	-71	70	218			2022	7	10	a	102.9157	29.2017	bqf main	
179	sf30		282	100	85	21			2022	7	10	a	102.9157	29.2017	bqf main	
334	22.11.11.03		125	0	90	170		jk	2022	11	11		103.2012	29.3991	Grapevine Hills	
335	22.11.11.03		132	161	82	264		jk	2022	11	11		103.2012	29.3991	Grapevine Hills	
336	22.11.11.03		140	143	82	267		jk	2022	11	11		103.2012	29.3991	Grapevine Hills	
337	22.11.11.03		140	151	82	270		jk	2022	11	11		103.2012	29.3991	Grapevine Hills	
338	22.11.11.03		140	138	82	264		jk	2022	11	11		103.2012	29.3991	Grapevine Hills	
339	22.11.11.04		128	165	82	261		jk	2022	11	11		103.3264	29.3844	Grapevine Hills	
340	22.11.11.04		125	167	85	259		jk	2022	11	11		103.3264	29.3844	Grapevine Hills	
341	22.11.11.04		130	-80	85	211	normal	jk	2022	11	11		103.3264	29.3844	Grapevine Hills	2
342	22.11.11.05		318	-30	90	7	sinistral	jk	2022	11	11	a	103.3264	29.3844	Paint Gap Hills	1
343	22.11.11.05		315	-25	89	3	sinistral	jk	2022	11	11	a	103.3264	29.3844	Paint Gap Hills	1
344	22.11.11.05		143	170	90	278	normal	jk	2022	11	11	a	103.3264	29.3844	Paint Gap Hills	misfit
345	22.11.11.05	pgh.01	323	-19	89	10	sinistral	jk	2022	11	11	a	103.3264	29.3844	Paint Gap Hills	1
346	22.11.11.05	pgh.01	327	-13	87	13	sinistral	jk	2022	11	11	a	103.3264	29.3844	Paint Gap Hills	1
347	22.11.11.05	pgh.01	323	-20	87	10	sinistral	jk	2022	11	11	a	103.3264	29.3844	Paint Gap Hills	1
348	22.11.11.05		322	-15	88	8	sinistral	jk	2022	11	11	a	103.3264	29.3844	Paint Gap Hills	1
349	22.11.11.05		323	-14	88	9	sinistral	jk	2022	11	11	a	103.3264	29.3844	Paint Gap Hills	1
350	22.11.11.06		241	118	84	354	sinistral-normal	jk	2022	11	11	a	103.3278	29.3844	Paint Gap Hills	3
351	22.11.11.06		231	-93	80	324	normal	jk	2022	11	11	a	103.3278	29.3844	Paint Gap Hills	2
352	22.11.11.06		186	-12	88	232	dextral	jk	2022	11	11	a	103.3278	29.3844	Paint Gap Hills	1
353	22.11.11.06		6	176	90	141	dextral	jk	2022	11	11	a	103.3278	29.3844	Paint Gap Hills	1
354	22.11.11.06		186	-7	90	231	dextral	jk	2022	11	11	a	103.3278	29.3844	Paint Gap Hills	1

No.	Field No.	sample number	Strike	Rake	Dip	Trend	Sense	Geologist	Year	month	Day	Quadrant	Longitude	Latitude	Site	Kin pop
355	22.11.11.06		186	-1	90	231	dextral	jk	2022	11	11	a	103.3278	29.3844	Paint Gap Hills	1
356	22.11.11.06		184	-10	86	230	dextral	jk	2022	11	11	a	103.3278	29.3844	Paint Gap Hills	1
357	22.11.12.02		210	-47	86	267		jk	2022	11	12		103.2019	29.4089	Grapevine Hills	
358	22.11.12.02		210	-19	86	257	normal	jk	2022	11	12		103.2019	29.4089	Grapevine Hills	2
359	22.11.12.02		210	-53	86	270	normal	jk	2022	11	12		103.2019	29.4089	Grapevine Hills	2
360	22.11.12.02		209	-23	76	258		jk	2022	11	12		103.2019	29.4089	Grapevine Hills	
361	22.11.12.02		200	-68	89	270	normal	jk	2022	11	12		103.2019	29.4089	Grapevine Hills	2
362	22.11.12.02		207	-175	85	162	normal	jk	2022	11	12	a	103.2019	29.4089	Grapevine Hills	1
363	22.11.12.02		207	-87	85	294	normal	jk	2022	11	12	a	103.2019	29.4089	Grapevine Hills	2
364	22.11.12.02		314	-113	81	63	normal	jk	2022	11	12	a	103.2019	29.4089	Grapevine Hills	3
365	22.11.12.02		324	-155	86	95	normal	jk	2022	11	12	a	103.2019	29.4089	Grapevine Hills	3
366	22.11.12.02		324	-152	86	95	normal	jk	2022	11	12	a	103.2019	29.4089	Grapevine Hills	3
367	22.11.12.02		309	-126	80	67	normal	jk	2022	11	12	a	103.2019	29.4089	Grapevine Hills	3
368	22.11.12.02		309	-134	80	71	normal	jk	2022	11	12	a	103.2019	29.4089	Grapevine Hills	3
369	LJ1	LJ1	109	3	87		dextral	jk	2023	1	9	a	103.8149	29.2745		
370	LJ2	LJ2	109	-176	85		dextral	jk	2023	1	9	a	103.8149	29.2745		
371	LJ3	LJ3	109	-172	81		dextral	jk	2023	1	9	a	103.8149	29.2745		
372	LJ4	LJ4	111	-178	85		dextral	jk	2023	1	9	a	103.8149	29.2745		
gr02	GR02	GR02	321	-8	88	6		JMK/TN					103.1206	29.6091	grotto fault	
gr04	GR04	GR04	144	-78	84	223	normal	JMK/TN					103.1206	29.6091	grotto fault	1

Appendix 2. Geochronologic and geochemical data

Sample Name	Note	Total U (ug/g)	U Err (ug/g)	Total Pb (ug/g)	Pb Err (ug/g)	208Pb/204Pb	Err (2SE)	207Pb/204Pb	Err (2SE)	206Pb/204Pb	Err (2SE)	208Pb/206Pb	Err (2SE)	207Pb/206Pb	Err (2SE)
GR 02	sub a	0.180	0.001	0.469	0.003	38.431	0.004	15.624	0.001	18.634	0.003	2.0623	0.0001	0.8385	0.0001
	sub b	0.083	0.001	0.307	0.002	38.560	0.004	15.624	0.001	18.815	0.003	2.0494	0.0001	0.8305	0.0001
	sub c	0.105	0.001	0.255	0.001	38.587	0.004	15.633	0.001	18.821	0.003	2.0500	0.0001	0.8305	0.0001
GR 04	sub a	0.155	0.001	0.475	0.003	38.762	0.004	15.659	0.001	19.095	0.003	2.0298	0.0001	0.8200	0.0001
	sub b	0.234	0.001	0.447	0.002	38.822	0.004	15.659	0.001	19.153	0.003	2.0269	0.0001	0.8176	0.0001
	sub c	0.172	0.001	0.396	0.002	38.852	0.004	15.668	0.001	19.167	0.003	2.0270	0.0001	0.8175	0.0001
GR 02 AX	sub a	0.054	0.001	0.112	0.001	38.779	0.004	15.660	0.001	18.800	0.003	2.0626	0.0001	0.8331	0.0001
	sub b	0.118	0.001	0.215	0.001	38.587	0.004	15.626	0.001	18.920	0.003	2.0395	0.0001	0.8259	0.0001
	sub c	0.092	0.001	0.155	0.001	38.053	0.004	15.606	0.001	18.194	0.003	2.0915	0.0001	0.8578	0.0001
GR 04 AX	sub a	0.276	0.001	0.633	0.004	38.907	0.004	15.656	0.001	19.128	0.003	2.0339	0.0001	0.8184	0.0001
	sub b	0.446	0.002	1.137	0.006	38.803	0.004	15.659	0.001	19.099	0.003	2.0316	0.0001	0.8199	0.0001
	sub c	0.430	0.002	1.180	0.007	38.823	0.004	15.663	0.001	19.116	0.003	2.0308	0.0001	0.8193	0.0001
BCR-2	USGS std materials	1.704		10.92		38.745		15.621		18.757		2.066		0.833	
		1.700		10.93		38.746		15.622		18.759		2.065		0.833	
		1.698		10.99											
	Ave	1.701	0.005	10.95	0.06	38.746	0.001	15.621	0.001	18.758	0.003	2.0655	0.0001	0.8328	0.0001
	Reference values	1.700	0.020	11.000	0.100	38.724	0.041	15.625	0.004	18.753	0.020				

Sample Name	Note	Total U (ug/g)	U Err (ug/g)	Total Pb (ug/g)	Pb Err (ug/g)	208Pb/204Pb	Err (2SE)	207Pb/204Pb	Err (2SE)	206Pb/204Pb	Err (2SE)	208Pb/206Pb	Err (2SE)	207Pb/206Pb	Err (2SE)
GR 02	sub a	0.180	0.001	0.469	0.003	38.431	0.004	15.624	0.001	18.634	0.003	2.0623	0.0001	0.8385	0.0001
	sub b	0.083	0.001	0.307	0.002	38.560	0.004	15.624	0.001	18.815	0.003	2.0494	0.0001	0.8305	0.0001
	sub c	0.105	0.001	0.255	0.001	38.587	0.004	15.633	0.001	18.821	0.003	2.0500	0.0001	0.8305	0.0001
GR 04	sub a	0.155	0.001	0.475	0.003	38.762	0.004	15.659	0.001	19.095	0.003	2.0298	0.0001	0.8200	0.0001
	sub b	0.234	0.001	0.447	0.002	38.822	0.004	15.659	0.001	19.153	0.003	2.0269	0.0001	0.8176	0.0001
	sub c	0.172	0.001	0.396	0.002	38.852	0.004	15.668	0.001	19.167	0.003	2.0270	0.0001	0.8175	0.0001
GR 02 AX	sub a	0.054	0.001	0.112	0.001	38.779	0.004	15.660	0.001	18.800	0.003	2.0626	0.0001	0.8331	0.0001
	sub b	0.118	0.001	0.215	0.001	38.587	0.004	15.626	0.001	18.920	0.003	2.0395	0.0001	0.8259	0.0001
	sub c	0.092	0.001	0.155	0.001	38.053	0.004	15.606	0.001	18.194	0.003	2.0915	0.0001	0.8578	0.0001
GR 04 AX	sub a	0.276	0.001	0.633	0.004	38.907	0.004	15.656	0.001	19.128	0.003	2.0339	0.0001	0.8184	0.0001
	sub b	0.446	0.002	1.137	0.006	38.803	0.004	15.659	0.001	19.099	0.003	2.0316	0.0001	0.8199	0.0001
	sub c	0.430	0.002	1.180	0.007	38.823	0.004	15.663	0.001	19.116	0.003	2.0308	0.0001	0.8193	0.0001
BCR-2	USGS std materials	1.704		10.92		38.745		15.621		18.757		2.066		0.833	
		1.700		10.93		38.746		15.622		18.759		2.065		0.833	
		1.698		10.99											
	Ave	1.701	0.005	10.95	0.06	38.746	0.001	15.621	0.001	18.758	0.003	2.0655	0.0001	0.8328	0.0001
	Reference values	1.700	0.020	11.000	0.100	38.724	0.041	15.625	0.004	18.753	0.020				

Sample Name	Note	Total U (ug/g)	U Err (ug/g)	Total Pb (ug/g)	Pb Err (ug/g)	208Pb/204Pb	Err (2SE)	207Pb/204Pb	Err (2SE)	206Pb/204Pb	Err (2SE)	208Pb/206Pb	Err (2SE)	207Pb/206Pb	Err (2SE)
SM 01a	sub a	3.156	0.001	1.576	0.009	38.754	0.002	15.694	0.001	19.829	0.001	1.9544	0.0001	0.7915	0.0001
	sub b	1.677	0.001	3.006	0.017	38.769	0.002	15.689	0.001	19.539	0.001	1.9842	0.0001	0.8029	0.0001
	sub c	1.847	0.001	4.935	0.028	38.782	0.002	15.687	0.001	19.465	0.001	1.9923	0.0001	0.8059	0.0001
SM 03	sub a	2.008	0.001	0.828	0.005	38.691	0.002	15.733	0.001	20.872	0.001	1.8537	0.0001	0.7538	0.0001
	sub b	1.913	0.001	0.771	0.004	38.731	0.002	15.761	0.001	21.029	0.001	1.8418	0.0001	0.7495	0.0001
	sub c	1.987	0.001	0.949	0.005	38.701	0.002	15.748	0.001	21.241	0.001	1.8220	0.0001	0.7414	0.0001
SM 04	sub a	2.552	0.001	1.122	0.006	38.860	0.002	15.779	0.001	21.593	0.001	1.7997	0.0001	0.7308	0.0001
	sub b	2.445	0.001	0.637	0.004	38.754	0.002	15.790	0.001	21.919	0.001	1.7681	0.0001	0.7204	0.0001
	sub c	2.364	0.001	2.585	0.014	38.814	0.002	15.702	0.001	19.951	0.001	1.9454	0.0001	0.7870	0.0001
BqTR	sub a	1.520	0.001	9.017	0.050	38.882	0.002	15.683	0.001	19.613	0.001	1.9824	0.0001	0.7996	0.0001
	sub b	0.678	0.001	2.186	0.012	38.917	0.002	15.690	0.001	19.643	0.001	1.9812	0.0001	0.7987	0.0001
	sub c	0.767	0.001	2.678	0.015	38.898	0.002	15.686	0.001	19.630	0.001	1.9816	0.0001	0.7991	0.0001
BqTR 07	sub a	2.014	0.001	6.967	0.039	38.975	0.002	15.735	0.001	20.419	0.001	1.9088	0.0001	0.7706	0.0001
	sub b	2.018	0.001	6.027	0.034	38.935	0.002	15.726	0.001	20.327	0.001	1.9154	0.0001	0.7737	0.0001
	sub c	2.103	0.001	13.466	0.075	38.950	0.002	15.723	0.001	20.092	0.001	1.9386	0.0001	0.7826	0.0001

Name	X=238U/206Pb	Err (2SE)	Y=207Pb/206Pb	Err (2SE)	U-Pb isochron ages (Ma)	+/-Err (Ma)	MSWD
GR02	1.317	0.007	0.8385	0.0001	GR02	no age	
	0.928	0.005	0.8304	0.0001			
	1.411	0.007	0.8306	0.0001			
GR04	1.105	0.006	0.8200	0.0001	GR04	30.7	1.9
	1.772	0.009	0.8176	0.0001			300
	1.471	0.007	0.8175	0.0001			
GR02AX	1.642	0.008	0.8330	0.0001	GR02AX	no age	
	1.867	0.009	0.8259	0.0001			
	2.076	0.010	0.8578	0.0001			
GR04AX	1.483	0.007	0.8185	0.0001	GR04AX	35	10
	1.333	0.007	0.8199	0.0001			40
	1.238	0.006	0.8194	0.0001			
All 6 GR04 set					33.6	1.8	170

Name	X=238U/206Pb	Err (2SE)	Y=207Pb/206Pb	Err (2SE)	U-Pb isochron ages (Ma)	+/-Err (Ma)	MSWD	U-Pb isochron ages (Ma)	+/-Err (Ma)		
GR02	1.317	0.007	0.8385	0.0001	GR02	no age		GR02	20.4		
	0.928	0.005	0.8304	0.0001					60		
	1.411	0.007	0.8306	0.0001							
GR04	1.105	0.006	0.8200	0.0001	GR04	29.92	1.94/234.16	350	GR04	30.67	3.14
	1.772	0.009	0.8176	0.0001							
	1.471	0.007	0.8175	0.0001							
GR02AX	1.642	0.008	0.8330	0.0001	GR02AX	no age		GR02AX	130	260	
	1.867	0.009	0.8259	0.0001							
	2.076	0.010	0.8578	0.0001							
GR04AX	1.483	0.007	0.8185	0.0001	GR04AX	35	10/790.6	180	GR04AX	34.6	2.18
	1.333	0.007	0.8199	0.0001							
	1.238	0.006	0.8194	0.0001							
All 6 GR04 set					34.73	1.8/32	170	All 6 GR04 set	32.88	2.27	
					Maximum Likelihood model			Total least square model			
					Maximum Likelihood model			Total least square model			

Name	X=238U/206Pb	Err (2SE)	Y=207Pb/206Pb	Err (2SE)		U-Pb isochron ages (Ma)	+/-Err (Ma)	MSWD		U-Pb isochron ages (Ma)	+/-Err (Ma)
SM 01a	6.616	0.033	0.7915	0.0001	SM 01a	21.94	0.24/31.09	390	SM 01a	21.76	1.15
	1.864	0.009	0.8029	0.0001							
	1.254	0.006	0.8059	0.0001							
SM 03	7.717	0.039	0.7538	0.0001	SM 03	no age			SM 03	12.2	28.6
	7.861	0.039	0.7495	0.0001							
	6.579	0.033	0.7414	0.0001							
SM 04	7.083	0.035	0.7308	0.0001	SM 04	75.91	0.41/282.16	11000	SM 04	63.3	21
	11.804	0.059	0.7204	0.0001							
	3.011	0.015	0.7870	0.0001							
BqTR	0.562	0.003	0.7996	0.0001	BqTR	14.85	2.4/59.09	14	BqTR	13.7	0.88
	1.034	0.005	0.7987	0.0001							
	0.955	0.005	0.7991	0.0001							
BqTR 07	0.938	0.005	0.7706	0.0001	BqTR 07	168.22	4.84/935.85	890	BqTR 07	156.5	61.8
	1.089	0.005	0.7737	0.0001							
	0.513	0.003	0.7826	0.0001							

Appendix 3. In-class exercises

SRSU 1 / ASU 3: The implications of geologic structures – Page 171

SRSU 2 / ASU 4: Earthquake ground shaking – Page 183

SRSU 3 / ASU 5: Volcanic hazards and warnings – Page 192

SRSU 4 / ASU 1: Investigating climate-change data – Page 200

SRSU 5: Streams and drainage basins – Page 213

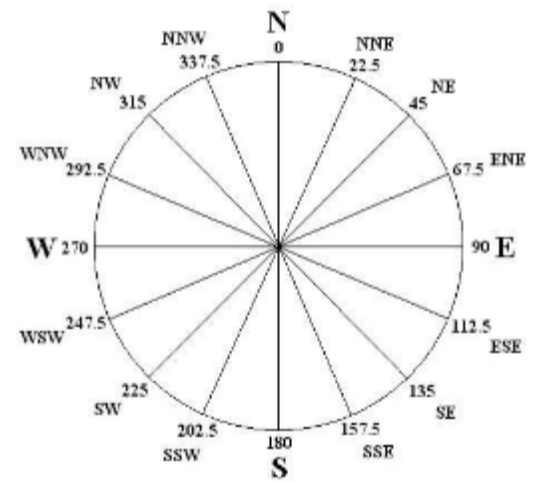
SRSU 6: ASU 2: Flood plain exercise – Page 218

Exercise 1: The Implications of Geologic Structures

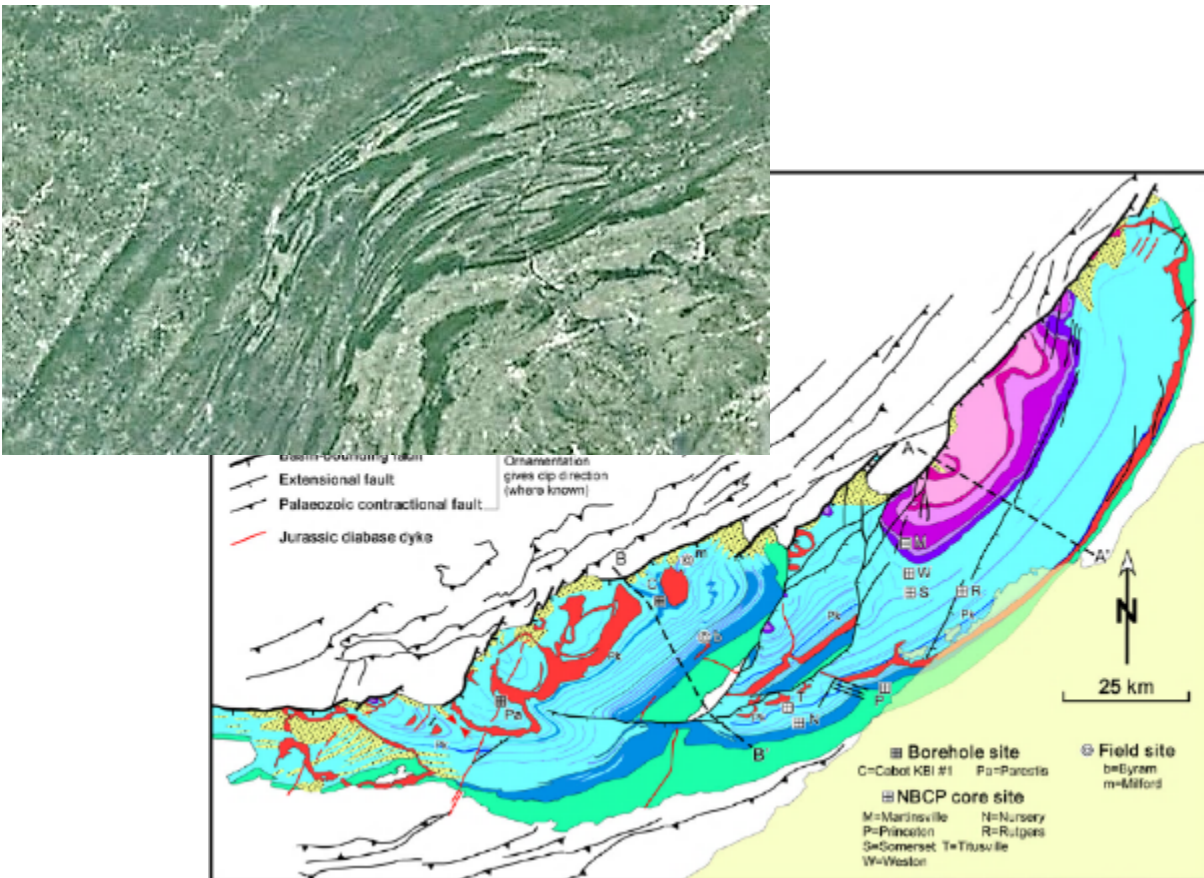
Objective: We will analyze the age and orientation of geologic structures (faults and folds) as shown in the geologic map of the eastern-US area to hypothesize a tectonic history of this region.

Facts to recall in this exercise:

- Rocks of the lithosphere experience stress in directions that relate to tectonic plate motions. Direction of stress dictates the orientation of geologic structures. (Refer to your class notes to recall the stress implications of reverse faults, normal faults, and folds.)
- “Strike” of a planar surface is the compass bearing of the horizontal line inside that plane. “Dip” of a planar surface is the inclination (degrees down from horizontal, i.e. how much it’s tipped down from “level”) of that same plane.
- Compass bearings on the 0 – 360-degree scale look like this→



I. Field Data: Entry and visualization of structures into ‘Stereonet’ program



1geologic map and satellite photo of the northern Appalachia mtns and Newark basin, Pennsylvania, New York, and New Jersey



- a. Enter the following structure-orientation data into the program 'Stereonet.' Start a new data set (of planar data) for each name below, and enter each strike/dip combo as a new datum in the appropriate dataset. (See that the appropriate dataset is selected in the top right window.) There will be three datasets, and each one has three datums.

<u>Dataset Name</u>	<u>Strike</u>	<u>Dip</u>
200 Ma normal faults	045	65
“ “	055	58
“ “	060	55
350 Ma thrust faults	045	30
“ “	051	33
350 Ma fold axes	055	75
“ “	232	82
“ “	238	78

- b. Look at each data set one by one in the '3D View' tab in Stereonet so that you can visualize the real-world orientations. (Each data set contains 2 or 3 pieces of data, or datums). IMPORTANT: to look at each of the three data sets separately, you need to "turn off" the other two data sets in the upper right window.

II. Cross Sections: Interpretations of the subsurface from our surface data

- a. Draw the approximate average of each of the three data sets' structures' orientations in SIDE VIEW in the boxes below. Include all of the following on your cross sections:

- i. Compass directions of the left and right sides of your view (use the directions on the 3D view in Stereonet, plus the compass rose figure on the previous page, to determine this).
- ii. If your structure is a fault, label the hanging wall and the footwall, and draw up or down arrows along the fault to show which block went up or down. You know this from the label of the structures in the data set; the field geologist already made the determination of the type of fault.
- iii. If your structure is a fold axis, sketch in hypothetical folded bedding, keeping the fold axis at the center of the fold's hinge zone. You could draw two fold axes so that you could draw two folds: an anticline and a syncline adjacent to each other that share a limb.

200 Ma normal faults

350 Ma reverse (thrust) faults

350 Ma folds

b. Questions:

- i. At 200 Ma, did hanging walls of faults go up or down?
- ii. What kind of stress caused this motion?
- iii. In what direction was that stress applied to these rocks?
- iv. At 350 Ma, did hanging walls of faults go up or down?
- v. What kind of stress caused this motion?
- vi. In what direction was that stress applied to these rocks?
- vii. At 350 Ma, what kind of stress was applied to these rocks to make these folds?
- viii. In what direction was that stress applied to these rocks?

III. Interpretation of stress directions during the ages these structures were created

- a. Fill in the table below, FROM OLDEST TO YOUNGEST, with one dataset for each row since all structures in each data set are the same type and age. Write your determination of the TYPE of stress (e.g. compressional or tensile, and also the DIRECTION that stress was applied to make those structures. Leave the right two columns blank for now.

Age of structures	Type of structures	Type of stress	Direction of stress		

b. Questions

- i. What can you say about the change in stress through time at this location? (This means going from your earlier/oldest time to your later/youngest time.)

- ii. What does a change in stress through time have to be revealing? Why?

IV. Paleotectonic Information: Compare our data to what is already known about orogenic (mountain-building) events in Earth's history

- a. Go to the online HHMI biointeractive viewer, AND open the 'scotese maps' pdf file. These paleogeographic maps were constructed from decades of geological research, including some of the techniques we have already discussed this semester.
 - i. Within the online HHMI viewer, You can use the "age" slider on the left side of your screen to go to the time periods of your structures. You can manipulate the view of the Earth by clicking and dragging your mouse, so that you are focused on your field area. You'll quickly note that this viewer does not show the lines of plate boundaries OR the ocean plates, so the only plate-tectonic information visible are continental collisions.
 - ii. In the Scotese map set, you'll note that plate boundaries are shown. SUBDUCTION ZONE BOUNDARIES ARE BLUE, AND COLLISION BOUNDARIES ARE PURPLE.
 - iii. Take some time to investigate each dataset's time period, and possibly the bit of time BEFORE your structures' ages to see the motion of the plates.

b. Questions

- i. What was the plate motion applying stress to our field area at 350 Ma, and how do you know?

- ii. What was the plate motion applying stress to our field area at 200 Ma, and how do you know? (Hint: look at the Scotese map, and see what was happening on the western edge of North America... there's a blue line...)

- c. Now look at the list of orogenic events that is on the board at the front of the room.

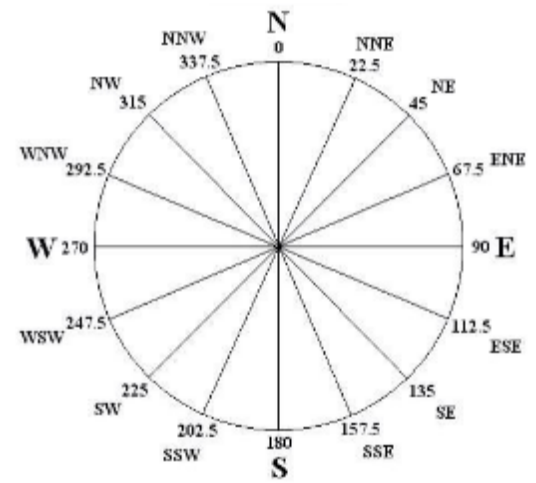
- d. Fill in the right two columns of the previous table, adding the headings (1) “Plate Boundary Type” and (2) “Orogenic Event.”
- i. Answer the questions on the following page. You will turn that page in SEPARATELY without your name, but with your three-digit code. Please do these questions after you have completed the rest of the exercise.

Exercise 1: The Implications of Geologic Structures

Objective: We will analyze the age and orientation of geologic structures (faults and folds) as shown in the geologic map of the Big Bend area to hypothesize a tectonic history of this region.

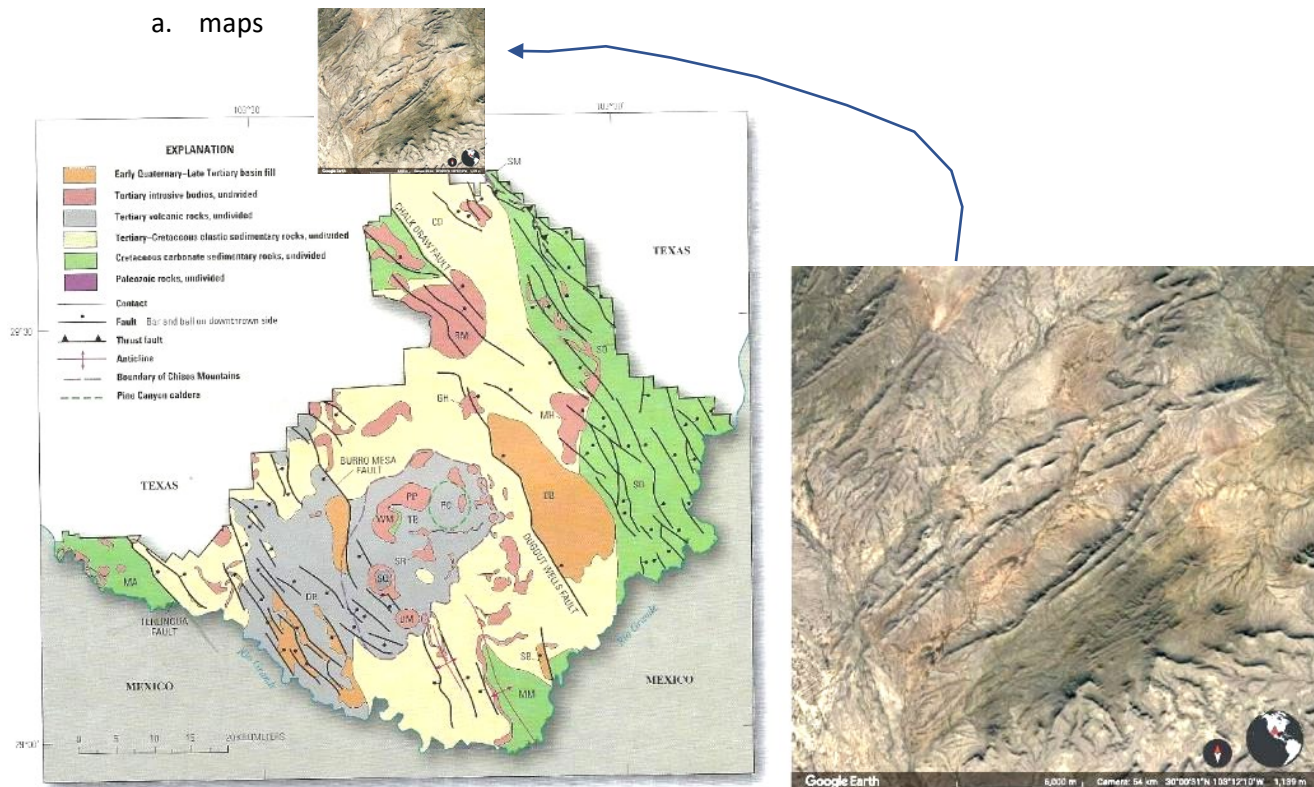
Facts to recall in this exercise:

- Rocks of the lithosphere experience stress in directions that relate to tectonic plate motions. Direction of stress dictates the orientation of geologic structures. (Refer to your class notes to recall the stress implications of reverse faults, normal faults, and folds.)
- “Strike” of a planar surface is the compass bearing of the horizontal line inside that plane. “Dip” of a planar surface is the inclination (degrees down from horizontal, i.e. how much it’s tipped down from “level”) of that same plane.
- Compass bearings on the 0 – 360-degree scale look like this →

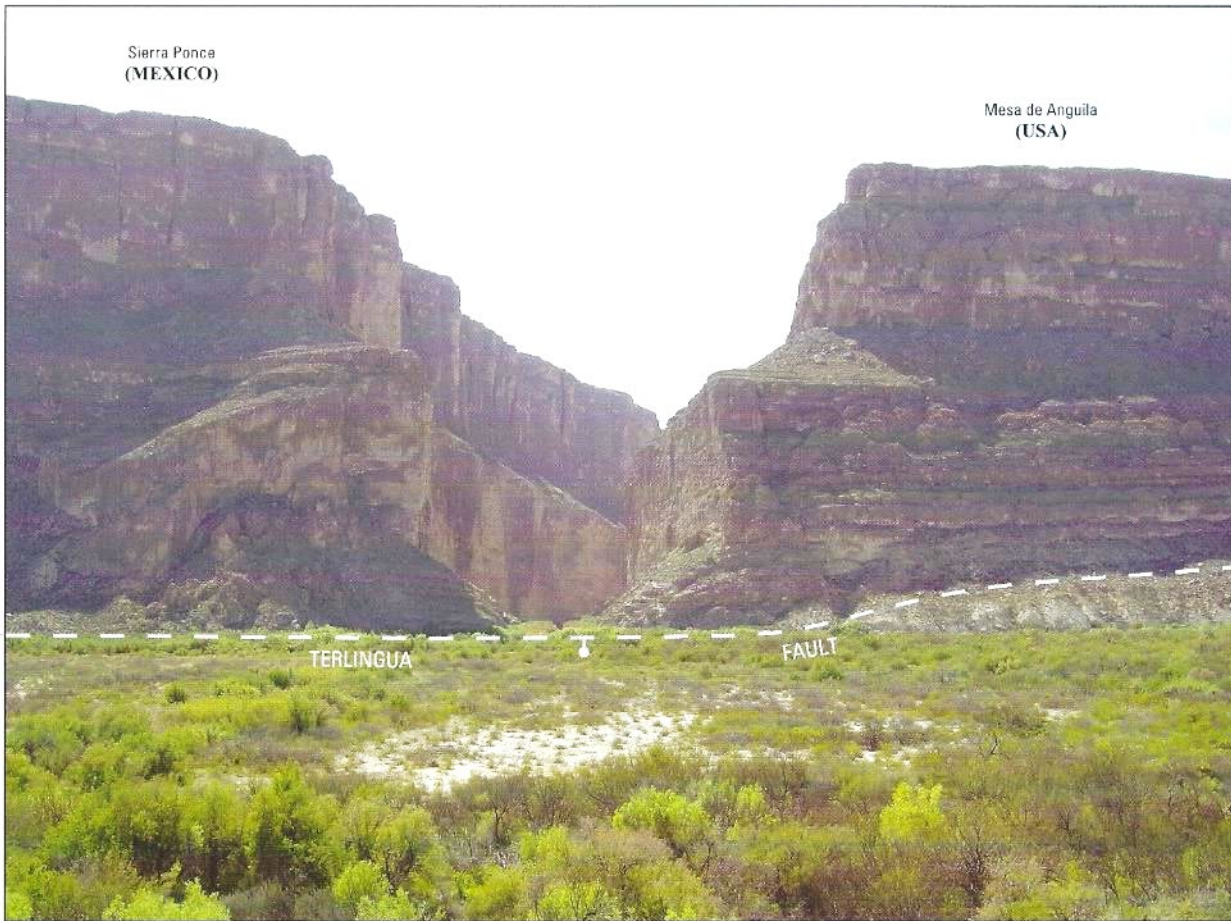


V. Field Data: Entry and visualization of geologic structures into ‘Stereonet’ program

a. maps



2Simplified geologic map of Big Bend National Park, plus inset of satellite photo north of the Park



Southwest view of Santa Elena Canyon showing the approximate trace of the Terlingua fault (thick dashed line; bar and ball on downthrown side), which forms the steep escarpment on the northeast side of Mesa de Anguila (Texas) and Sierra Ponce (Mexico). At the mouth of the canyon on the U.S. side, the fault juxtaposes Lower Cretaceous strata (Glen Rose Limestone) in the foot wall, against Upper Cretaceous strata (Aguja Formation) in the hanging wall. (Photograph by Daniel P. Miggins)

- b. Enter the following structure-orientation data into the program 'Stereonet.' Start a new data set (of planar data) for each name below, and enter each strike/dip combo as a new datum in the appropriate dataset. (See that the appropriate dataset is selected in the top right window.) There will be three datasets, and each one has three datums.

Dataset Name	Strike	Dip
20 Ma normal faults	159	65
“ “	330	58
“ “	338	55
100 Ma thrust faults	315	30
“ “	320	33
300 Ma fold axes	059	75
“ “	068	82
“ “	064	78

- c. Look at each data set one by one in the '3D View' tab in Stereonet so that you can visualize the real-world orientations. (Each data set contains 2 or 3 pieces of data, or datums). IMPORTANT: to look at

each of the three data sets separately, you need to “turn off” the other two data sets in the upper right window.

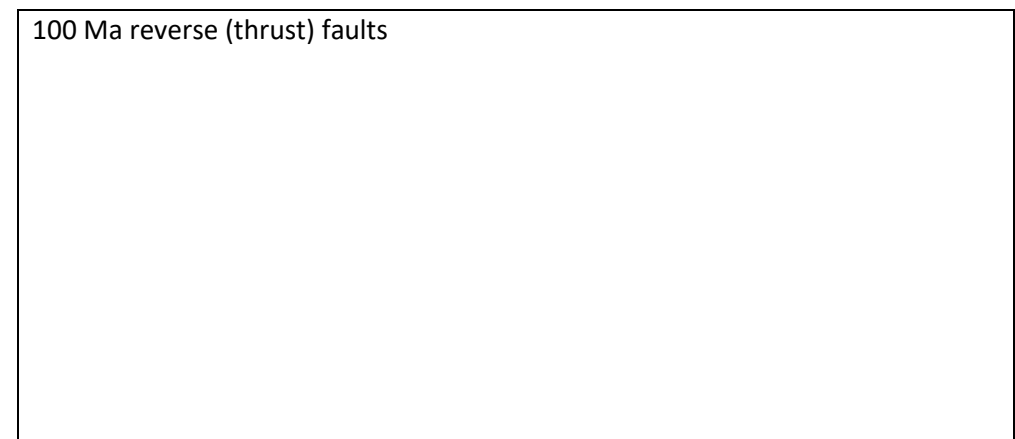
VI. Cross Sections: Interpretations of the subsurface from our surface data

- a. Draw the approximate average of each of the three data sets’ structures’ orientations in SIDE VIEW in the boxes below. Include all of the following on your cross sections:
 - i. Compass directions of the left and right sides of your view (use the directions on the 3D view in Stereonet, plus the compass rose figure on the previous page, to determine this.
 - ii. If your structure is a fault, label the hanging wall and the footwall, and draw up or down arrows along the fault to show which block went up or down. You know this from the label of the structures in the data set; the field geologist already made the determination of the type of fault.
 - iii. If your structure is a fold axis, sketch in hypothetical folded bedding, keeping the fold axis at the center of the fold’s hinge zone. You could draw two fold axes so that you could draw two folds: an anticline and a syncline adjacent to each other that share a limb.

20 Ma normal faults



100 Ma reverse (thrust) faults



300 Ma folds

b. Questions:

- i. At 20 Ma, did hanging walls of faults go up or down?
- ii. What kind of stress caused this motion?
- iii. In what direction was that stress applied to these rocks?
- iv. At 100 Ma, did hanging walls of faults go up or down?
- v. What kind of stress caused this motion?
- vi. In what direction was that stress applied to these rocks?
- vii. At 300 Ma, what kind of stress was applied to these rocks to make these folds?
- viii. In what direction was that stress applied to these rocks?

VII. Interpretation of stress directions during the ages these structures were created

- a. Fill in the table below, FROM OLDEST TO YOUNGEST, with one dataset for each row since all structures in each data set are the same type and age. Write your determination of the TYPE of stress (e.g. compressional or tensile, and also the DIRECTION that stress was applied to make those structures. Leave the right two columns blank for now.

Age of structures	Type of structures	Type of stress	Direction of stress		

b. Questions

- i. What can you say about the change in stress through time at this location? (This means going from your earlier/oldest time to your later/youngest time.)

- ii. What does a change in stress through time have to be revealing?

VIII. Paleotectonic Information: Compare our data to what is already known about orogenic (mountain-building) events in Earth's history

- a. Go to the online HHMI biointeractive viewer, AND open the 'scotese maps' pdf file. These paleogeographic maps were constructed from decades of geological research, including some of the techniques we have already discussed this semester.
 - i. Within the online HHMI viewer, You can use the "age" slider on the left side of your screen to go to the time periods of your structures. You can manipulate the view of the Earth by clicking and dragging your mouse, so that you are focused on your field area. You'll quickly note that this viewer does not show the lines of plate boundaries OR the ocean plates, so the only plate-tectonic information visible are continental collisions.
 - ii. In the Scotese map set, you'll note that plate boundaries are shown. SUBDUCTION ZONE BOUNDARIES ARE BLUE, AND COLLISION BOUNDARIES ARE PURPLE.
 - iii. Take some time to investigate each dataset's time period, and possibly the bit of time BEFORE your structures' ages to see the motion of the plates.

b. Questions

- i. What was the plate motion applying stress to our field area at 300 Ma, and how do you know?

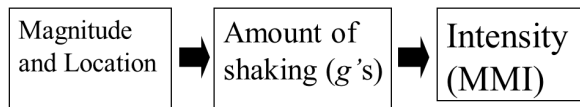
- ii. What was the plate motion applying stress to our field area at 100 Ma, and how do you know? (Hint: look at the Scotese map, and see what was happening on the western edge of North America... there's a blue line...)

- c. Now look at the list of orogenic events that is on the board at the front of the room.

- d. Fill in the right two columns of the previous table, adding the headings (1) "Plate Boundary Type" and (2) "Orogenic Event."
 - i. Answer the questions on the following page. You will turn that page in SEPARATELY without your name, but with your three-digit code. Please do these questions after you have completed the rest of the exercise.

Exercise 2: Earthquake ground shaking

Earthquake magnitude (the amount of stored stress released by an earthquake) is commonly used to represent the size of an earthquake. However, most people want to understand how much damage earthquakes do. These two concepts-- magnitude and damage-- are linked by shaking. Earthquake magnitude is measured by Moment Magnitude (M). Shaking is measured in units of acceleration (in units of g). Shaking relates to damage or intensity by the modified Mercalli intensity (MMI) scale.



We are exploring how the magnitude of an earthquake impacts the amount of shaking one feels and the extent of damage. It may seem obvious that “larger and closer” means more damage, but there is a mathematical relationship (a “function”) that can predict this, which is useful for human planning.

We use magnitude to calculate (“model”) acceleration, using one equation (function).

$$a = 1300 * (e^{0.67M}) * (D+25)^{-1.6} \quad \text{So, } a = f(M, D) \text{ or “} a \text{ is a function of } M \text{ and } D\text{”}$$

a = acceleration

M = Magnitude

D = distance (km)

Part I: comparing magnitude to intensity

➔ Start with “Sheet 1” in the Excel file “EQ exercise.xls”

A table has been created for a few values of magnitude and a few distances. A formula calculates acceleration, but still has to be converted to the “acceleration in g 's” scale commonly used. We'll do this just for a bit of practice with Excel.

Convert acceleration (column C) to “ g 's” by: a (in g 's) = $a/980$ cm/sec. (see steps below)

- Add a column D labeled “accel (g 's)” in its top row
- Type this formula into the first row: $=C2 / 980$ (no spaces; and instead of typing C2), click the box C2.
- Click the column header to select the whole column (the new one) and right click to select “Format Cells...”. Choose the “Number” category in the first tab, and select 2 decimal places if it's not already selected. Click OK.
- Now copy all the cells from D2 downward, by selecting that cell, clicking its bottom right corner, and pulling down (while still holding the click) to fill the cells to the 11th row.

- ❖ Questions: Considering what's said about how the different ground-shaking accelerations are felt, describe the damage from a M7 earthquake 2 km away from the epicenter. Describe the damage from the same size earthquake 20 km away from the epicenter.

Keep the scales on the next two pages handy for your reference.

Scale of Modified Mercalli Intensity with Description of shaking

MMI Value	Shaking Severity	Full Description
I		Not felt. Marginal and long period effects of large earthquakes.
II		Felt by persons at rest, on upper floors, or favorably placed.
III		Felt indoors. Hanging objects swing. Vibration like passing of light trucks. Duration estimated. May not be recognized as an earthquake.
IV		Hanging objects swing. Vibration like passing of heavy trucks; or sensation of a jolt like a heavy ball striking the walls. Standing motor cars rock. Windows, dishes, doors rattle. Glasses clink. Crockery clashes. In the upper range of IV, wooden walls and frame creak.
V	Light	Felt outdoors; direction estimated. Sleepers wakened. Liquids disturbed, some spilled. Small unstable objects displaced or upset. Doors swing, close, open. Shutters, pictures move. Pendulum clocks stop, start, change rate.
VI	Moderate	Felt by all. Many frightened and run outdoors. Persons walk unsteadily. Windows, dishes, glassware broken. Knickknacks, books, etc., off shelves. Pictures off walls. Furniture moved or overturned. Weak plaster and masonry D cracked. Small bells ring (church, school). Trees, bushes shaken (visibly, or heard to rustle).
VII	Strong	Difficult to stand. Noticed by drivers of motor cars. Hanging objects quiver. Furniture broken. Damage to masonry D, including cracks. Weak chimneys broken at roof line. Fall of plaster, loose bricks, stones, tiles, cornices (also unbraced parapets and architectural ornaments). Some cracks in masonry C. Waves on ponds; water turbid with mud. Small slides and caving in along sand or gravel banks. Large bells ring. Concrete irrigation ditches damaged.
VIII	Very Strong	Steering of motor cars affected. Damage to masonry C; partial collapse. Some damage to masonry B; none to masonry A. Fall of stucco and some masonry walls. Twisting, fall of chimneys, factory stacks, monuments, towers, elevated tanks. Frame houses moved on foundations if not bolted down; loose panel walls thrown out. Decayed piling broken off. Branches broken from trees. Changes in flow or temperature of springs and wells. Cracks in wet ground and on steep slopes.

IX	Violent	General panic. Masonry D destroyed; masonry C heavily damaged, sometimes with complete collapse; masonry B seriously damaged. (General damage to foundations.) Frame structures, if not bolted, shifted off foundations. Frames racked. Serious damage to reservoirs. Underground pipes broken. Conspicuous cracks in ground. In alluvial areas sand and mud ejected, earthquake fountains, sand craters.
X	Very Violent	Most masonry and frame structures destroyed with their foundations. Some well-built wooden structures and bridges destroyed. Serious damage to dams, dikes, embankments. Large landslides. Water thrown on banks of canals, rivers, lakes, etc. Sand and mud shifted horizontally on beaches and flat land. Rails bent slightly.
XI		Rails bent greatly. Underground pipelines completely out of service.
XII		Damage nearly total. Large rock masses displaced. Lines of sight and level distorted. Objects thrown into the air.

Modified Mercalli Intensity	Acceleration (g)
I	.0017-.0005
II	.0017-.005
III	0.005-0.014
IV	0.014-0.039
V	0.039-.0.092
VI	0.092-0.18
VII	0.18-0.34
VIII	0.34-0.65
IX	0.65-1.24
X+	Above 1.24

Mercalli intensity is represented by Roman Numerals in order to differentiate them from Magnitudes and to show that they are only integers.

Note: $a = 0.005g$ = barely felt

And $a = 0.05g$ = unpleasant shaking

And $a = 0.5g$ most buildings damaged

➔ Our next task in Excel will be on Sheet 2. We will use the calculated acceleration (a) values to make a scatter plot, a very common format used to express data in charts.

This is a table of D vs acceleration for different M's. Answer the following questions.

❖ What is the top row of numbers (from 3 to 9) referring to?

❖ What is the left column of numbers (from 2 to 1000) referring to?

Click on cell B4, so that the formula in that cell shows up in the “formula bar” at the top of the window. If you’re not familiar with making Excel do math for you, this looks foreign. What you’re seeing is the equation from Page 1, which basically says that acceleration *is a function of* M and D. (A “function” is an equation, or a description of how variables consistently (mathematically) relate to each other.) Note that there is a “\$B\$1” in there, which is another way of reading the cell B1, which is a value for magnitude. And there is an “A4” in there, which is the cell A4, which is a value for distance. So the cell B4 that you clicked on is calculating acceleration (in g’s) for the value of magnitude in the B2 cell and the value of distance in the A4 cell.

Given the above, answer this:

- ❖ What is the calculated value of ground acceleration (in g’s) in cell F4?

- ❖ What is the earthquake magnitude for that acceleration?

- ❖ What is the distance from the epicenter for that acceleration?

Now you see how acceleration is a function of magnitude and distance. A function is an equation that describes how variables relate to each other.

- ❖ Now make a scatter plot of acceleration vs distance for each M... so on one chart you make, there will be a curve for each M, with axes a and D
 1. Select all of the data cells AND the distance cells (so select from A4 to I12.)
 2. Click the ‘Insert’ tab at the top of the window.
 3. Over in the ‘Charts’ area midway to the right, select a scatter plot that has “scatter with smooth lines and markers”
 4. Your chart is displayed. Now you need to make some modifications so it is legible.
 - a. Right click anywhere in the chart to “Select Data”, and then click “Switch Row/Column”
 - b. Click the numbers of the Y axis, right click, and then “Format Axis”
 - Change your axis bounds from 0 to 1.2 (minimum and maximum)
 - c. Click the numbers of the X axis, right click, and then “Format Axis”
 - Change your axis bounds from 1 to 1000 (minimum and maximum)
 - Select a logarithmic scale
 - In the “Chart Design” tab at the top of the whole window, select “Add Chart Element” on the far left, and select “gridlines →”, “Primary Minor Vertical” to add logarithmic gridlines to the plot area.
 - d. Add axis titles. In the “Add Chart Element” menu at the top left, select “Add Axis Titles”, and add both “Primary Vertical” and “Primary Horizontal” one at a time. After they show up in your chart, rename them by typing to replace them. The vertical axis is “Acceleration (g’s)”. The horizontal axis is “Distance from Epicenter (km)”.

- e. Rename the “Series” stuff to what it is: accelerations for different magnitudes
 - Right click in the plot area to “Select Data” again
 - Click the first line “Series 1” just to select it, then change its name to “M3”
 - Click the second line “Series 2” to select it, then change its name to “M4”
 - Repeat to change each series name to its EQ magnitude number
- f. Change the chart title (by selecting it) to “Acceleration vs. Distance”

You will submit this chart separately on Blackboard when it is finished, for a small amount of extra credit. For the remainder of class, we will use a completed one to visualize how magnitude relates to intensity. (This is like a cooking show.)

- ❖ Question: For Magnitude 6 earthquakes, how far from the EQ will the shaking be unpleasant? (>0.05g)
- ❖ For Magnitude 6 earthquakes, how far from the EQ is there high potential to damage buildings? (>0.5g)
- ❖ On the printed graph on the next page, lightly color the horizontal bands of acceleration in g’s that show the Mercalli intensity scale. You will use the small table in an earlier page that relates MMI to acceleration in g’s. You’ll use this standard-color scale to view “shakemaps” of earthquakes catalogued by the US Geological Survey (USGS) in the next section.

Red: IX Orange: VIII Yellow: VI Green: V Blue: IV Purple: III

Part II: Investigating shaking from real earthquake data

Look at the USGS web site “Latest Earthquakes.” We’ll first look at a large southern California earthquake from 2019. Go to the website linked on your Blackboard page, or search “earthquakes USGS” and find “Latest Earthquakes.”

Change the search parameters with the “settings” icon in the top right and the button at the bottom of that list.

- Click 4.5+
 - Change the beginning year of your search to 2015
 - Draw a rectangle on the map that includes southern California
 - When your results come up, sort them by “largest first”
 - Find the Ridgecrest M7.1 earthquake from July 2019 at the top of the list
-
- ❖ Look at the “Interactive Map” that shows the shaking intensity. How far away could this EQ have been felt according to the shakemap?

 - ❖ Q: what is highest intensity, read from the colors of the map and your own scale?

 - ❖ Q: what is the highest intensity in given Roman numerals next to the shakemap? What acceleration does that correspond to?

 - ❖ Look at “Did You Feel It”. How far away was it felt according to people submitting “felt reports”?

 - ❖ Describe how these two data sets compare to each other.

Scroll down to “For More Information” to the 5th item: “Animation of Ridgecrest EQ sequence through July 6”. This shows the main shock plus all aftershocks related to the Ridgecrest earthquake. Earthquakes occur along faults.

- ❖ Can you see more than one planar fault surface? How many do you see?

- ❖ Speculate on what caused this earthquake and its aftershocks.

- ❖ Go back to the USGS search page for “Latest Earthquakes”, and change the search parameters to the following by clicking the “settings” icon.
M4.5+, date 2000-today, geographic region custom: draw rectangle on map: zoom in to the Himalayas.

Sort the earthquakes by “largest first,” find the M7.8. earthquake from 2015 in Nepal, and answer these questions.

- How intense was the shaking at the epicenter? (use ‘shakemap’ and/or ‘interactive map’)

- How intense was the shaking in the city of Kathmandu?

- How far away was the shaking felt, acc to the calculated shakemap?

- Did anyone submit a “Did you Feel It” Report? How does that mapped data compare to the calculated shake map?

- Would you submit a “Felt Report” if you experience an earthquake, after seeing some of these data?

- Speculate on the cause of this earthquake.

Search the “Latest Earthquakes” USGS page

- Zoom out to see world. Plate boundaries are lines on the map
- Click on a few of these EQs to get more info in the box in the lower left of screen. Click on the link in that info box for more information on it. The most info will be on the larger earthquakes. The info box also tells you if a shake map has been calculated. Find a large (>M6 earthquake that has had a shakemap calculated.

- ❖ Describe the fundamentals of one of these earthquakes: List its date, magnitude, location, whether it is near a plate boundary or not; also the intensity range on the shakemap and how far out it was felt.

- ❖ Do the contours of intensity on the shakemap have a round bullseye pattern, or are they a different shape?

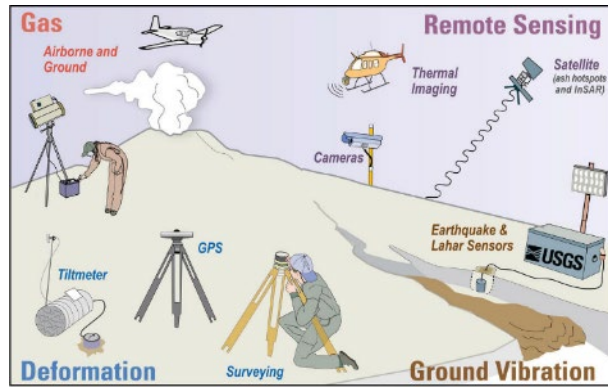
- ❖ What else besides distance from epicenter, and earthquake magnitude, could influence ground shaking?

- ❖ Go back to the USGS search page for “Latest Earthquakes”, and change the search parameters to the following by clicking the “settings” icon.
M2.5+, date 1992-2000, geographic region custom: draw rectangle on map: zoom in to Texas, Big Bend area, draw a rectangle south of I-10
Find the M5.7 EQ 1995 near Marathon and answer these questions.
 - How intense was the shaking at the epicenter? (use ‘shakemap’ and/or ‘interactive map’)
 - How intense was the shaking on the Sul Ross campus?
 - How far away was the shaking felt, acc to the calculated shakemap?
 - Did anyone submit a “Felt Report?” Speculate on why.
 - Would you submit a “Felt Report” if you experience an earthquake, after seeing some of these data?

Search the “Latest Earthquakes” USGS page

- Zoom out to see world. Plate boundaries are lines on the map
- Click on a few of these EQs to get more info in the box in the lower left of screen. Click on the link in that info box for more information on it. The most info will be on the larger earthquakes. The info box also tells you if a shake map has been calculated. Find a large (>M6 earthquake that has had a shakemap calculated.
- ❖ Describe the fundamentals of one of these earthquakes: List its date, magnitude, location, whether it is near a plate boundary or not; also the intensity range on the shakemap and how far out it was felt.
- ❖ Do the contours of intensity on the shakemap have a round bullseye pattern, or are they a different shape?
- ❖ What else besides distance from epicenter, and earthquake magnitude, could influence ground shaking?

In this exercise we will look at a few different volcanic eruptions around the world, and investigate what kinds of data geologists use to predict eruptions.



Part I: Mount St. Helen eruption of May 18, 1980

Search the USGS “Latest Earthquakes” website for the following:

- mag 1.5 and greater,
- 1979 may – 1980 Oct;
- draw a rectangle around Mount St Helen in southern Washington state

When the earthquakes are listed in the left side of the screen, scroll to the bottom of the earthquake list and click “Download.” Choose the csv file. This data will open in another browser tab, so you need to download it from the browser and then open it in Excel.

In Excel, right click and cut column E (mag), then insert that column to the right of column A (time) (To do this, right click column B [latitude,] select Insert Cut Cells in the right-click menu.)

We now need to remove the time from the date/time column A, so that we only have date in that. Do the following:

- Select all of column A
- Go to the “Data” tab, select “Text to Columns” button in the ribbon along the top.
- Select “Fixed width” so that you can separate data in that column by width. (“Next”)
- Now click in the “Data preview” window to make a vertical line separating the date numbers on the left (YYYY-MM-DD) from the time numbers (THH:MM:SS.SSSZ). (“Next”)
- Now format your date column.. it’ll be selected when you get to this window, but if not make sure the left side with the dates is blackened in color. Select the “Date” button in the upper list and select the format “YMD” in the dropdown menu next to the Date button. We don’t need the times of the earthquakes for our purposes so select the right side in the data preview window and select “Do not import column(skip)” so it goes in the trash. (“Finish”)

Make a chart. (Select columns A and B, which are your date and magnitude. Select the “Insert” tab at the top of the window. Go to the “Charts” part of the ribbon at the top, and find the top left drop down menu for “Column or Bar Charts”. Pick the first chart type within the 2-d column menu. The chart is made; have a look at it.

Q: What is this chart displaying, i.e. what are your axes?

Q: What are the data in this chart revealing? (i.e., what is the pattern of earthquakes over the time period specified?)

Make some changes to the date axis:

- In the Format Axis menu for your X-axis (select and right click the axis to open 'Format Axis' menu,) go down to "Number" and change the "Type" to the shortest possible format for reading a date, e.g. "3/14."
- Now let's change our min and max to zoom in even more on the beginning of the earthquake swarm in the MSH magma chamber: Change the bounds to something like 3/15/1980 minimum, and 6/21/1980 maximum. See if your chart shows more detail. Expand it to horizontally fill your screen.

Q: When do you think the geologists monitoring Mount St. Helen noticed that something was different?

Q: Consider the date of the eruption of Mount St. Helen. What is particular in our data before, on, and after that date?

Part II : Active La Palma volcanic eruption : began Sept 19, 2021

Q : Where is this volcano? (Search: "where is la palma volcano" and zoom out of the map that is shown.

Q: What do you know about the plate tectonic setting here? Is it near a plate boundary?

The Canary Islands are a chain formed by a mantle plume. The westernmost island, La Palma, is currently over the mantle plume.

Google "sky news la palma video" and watch any one of the videos that come up in that search.

Q: What kind of volcano is this? (mafic or felsic?)

Q: How do you know? (hint: is this lava flow viscous or non-viscous?)

The USGS only displays *global* earthquakes (outside the US) above a magnitude 4.5 or so, because other countries operate their own seismic networks and because our seismometers don't pick up distant small earthquakes. To look at smaller earthquakes (such as those caused by magma moving under volcanoes), if not in the US and its territories we use other countries' agency sites. We'll go to Spain's Instituto Geografico Nacional (IGN) to look at their data on the La Palma volcano eruption. <https://www.ign.es/web/ign/portal/vlc-serie-palma>

Unless you understand Spanish, let your browser translate it into English for you.

Select the “Seismicity” item but open it in a new tab. The top chart shown on the Seismicity page is similar to the one you just made. The volcano on La Palma began to erupt on September 19 of 2021. (*NOTE: In European and African countries the convention for writing dates is day/month/year, NOT month/day/year as is done in the US. So September 19 is shown as 19/09, not 09/19.*) The bottom-left chart in the “Histograms” section at the bottom of this page shows earthquakes since September 09, 2021. Click on this chart to make it larger. The period of interest is still very compressed, starting at 9th of September, 2021 on the left, and 2nd of April 2023 on the right.

Q: When did the earthquake activity under La Palma end? Look back at your Google search for Sky News reports about the ending of the eruption... Does that match with the Sky News report of when eruption ended?

Q: Does the pattern of earthquakes match the Mount St Helens 1980 earthquake pattern?

Q: Describe what is different and what is the same about the occurrence of earthquakes relative to eruptions. (Look at your graph, remembering when the MSH 1980 eruption occurred.)

Look at the leftmost map and cross sections showing earthquakes since 11th of September of 2021 (“Desde el dia 11/09/21”). They are shown in map view AND in two cross section views... think of this like a paper you could cut out and fold on two lines making a 3-d box view. Earthquakes are colored by DATE; the date legend on the bottom right shows those dates from 11-09 (11th of September) through 16-10 (16th of October.) Click on this to make it larger in a separate tab.

Q: Describe the spatial occurrence of the La Palma earthquakes through time. For example, “The first earthquakes were (shallow or deep, west or east); the eruption began on __; the locations of the next earthquakes after the eruption began were __; eruption has continued as earthquake activity at a (shallow or deep) level has continued.”

Return to the main La Palma eruption page (from which you opened the “Seismicity” tab.) Scroll down on this main page. The “2d Viewer” shows where the lava flowed from its vent westward toward the ocean. Look at this in relationship to the mapped epicenters of earthquakes.

Q: Where is the vent relative to the earthquake locations?

Q: Considering this information and your previous-question's description of the earthquakes, tell a geologic story of how this eruption happened.

Part III : The Aleutian Islands in Alaska

Go to the Alaska Volcano Observatory (AVO) at <https://www.avo.alaska.edu/activity/index.php#-162.268:50.516:4>

. Select the tab “Current Volcanic Activity” on the top of the page.

Notice that the bathymetry of the ocean floor is shown on the map, in addition to continental topography.

Q: What does the darker-blue arc-shaped feature south of Alaska’s volcanic chain indicate?

Q: What is the plate tectonic setting here?

Q: Approximately how many volcanoes are at an alert level of activity? AND, what do you think that might mean?

Click on the “Alaska Communities” layer in the map legend on the right side of the screen.

Q: Approximately how many people live around Great Sitkin volcano?

Click on the Great Sitkin volcano to read its summary.

Q: What kind of volcano is it? How does this relate to the plate tectonic setting? Describe what you know about both.

Click “Current Activity” in that little box to go to its Watch page. Click through the Daily Updates on the right side under “Great Sitkin Updates.”

Q: What do the daily updates have in common?

The AVO does not have a seismic database. We will go to the USGS earthquake finder to look at this seismicity. Make a note of where this volcano is along the Aleutian Islands (keep the tab open) and go back to the USGS “Latest Earthquakes” page. Start a new search:

- Magnitudes above M1.2
- In the last year (change the dates in the time search)

- Draw a rectangle around the Great Sitkin volcano and nearby area. Include the trench and a few Aleutian islands on either side of Great Sitkin.

In the layers pulldown icon in the right side of your map, choose "Street" instead of "Grayscale," so that you can see more geography. Have a look at where Great Sitkin is on the AVO website's map, and try to find it on the USGS map based on coastline shapes.

Q: Are there earthquakes shown on the USGS map at the Great Sitkin volcano?

Q: Briefly summarize the nearest earthquakes' dates and depths. What do the different depths indicate?

Q: What is the most concerning volcanic hazard from this volcano?

Take your time to complete the survey question on the next page.

Part III : Valles Caldera in New Mexico

Go to <https://www.usgs.gov/volcanoes/valles-caldera>, read the short paragraph at the top of its page.

If the rocks from the last eruption at <1Ma are tuffs and other voluminous ash deposits,

Q: What type of volcano (explosive/nonexplosive) is Valles?

Click “Monitoring Map” on the left to get to the Monitoring site. Zoom out of the map a bit so you can see the shape of this active (~1 Ma) volcano. Note what’s shown in the legend.

Q: Of the four seismometers on and around Valles Caldera, who are the operators of them? Look up the acronyms online to write them out if you don’t know what they mean.

Q: Were there any earthquakes in the last 4 weeks? If so, give the EQ details here (magnitude, depth)

Since this is a monitoring site, it is only showing earthquakes over the last 4 weeks, and none older. Go back (on a separate tab) to the USGS Latest Earthquakes page. Start a new search (settings button on the right) to find any earthquakes under Valles Caldera in the last 30 years:

- Magnitude above 1.2
- custom date & time to include 30 years
- draw a rectangle around a very large area around Valles Caldera in northern New Mexico. It is west of Santa Fe and north of Albuquerque. Include the Nacimiento Mountains and Santa Fe in your box.

When your search is complete, order the earthquakes by most recent first. Also, in the “layers”-icon menu on the right of your screen, choose ‘Street’ so you can see more of the geography. Scroll through the earthquake list and look at the dates.

Q: Are there recent earthquakes near the volcano?

Q: What do you surmise about them?

Q: If you were a volcanologist working for LANL or USGS, what more information would you request if you were considering there might be a volcanic hazard?

LANL is the national laboratory where the atomic bomb was developed. There is radioactive material stored there.

Q: What are ALL of the hazards of a future eruption here?

Take your time to complete the survey questions on the next page.

GEOL 1303/1103: Investigating climate-change data

This exercise was created as a collaboration at the NAGT 2020 Earth Educators' Rendezvous. Authors: Xin Sun, Mark Peebles, Jesse Kelsch, Rondi Davies, Erica Bigio, Paul Ashwell

Part 1. Tree rings record climate information

Examine Figure 1, a photograph of a cross section of a cut tree, which shows the tree's growth rings. The centermost rings of the tree were made when it was very young, and they get younger (forward in time) outward, as the tree grew. Every year has a light and a dark ring.

Notice the line that points to the growth ring that formed 550 years before the tree was cut. (550 years before the age of the outermost ring.)



Douglas-fir tree from Leavitt, S. & Bannister, B. (2009).

Figure 1. Cross-section of

Question 1. Where are the youngest and oldest growth rings located?

Youngest:

Oldest:

Question 2. How do the rings in the outer part of the tree appear different from the ones in the center?

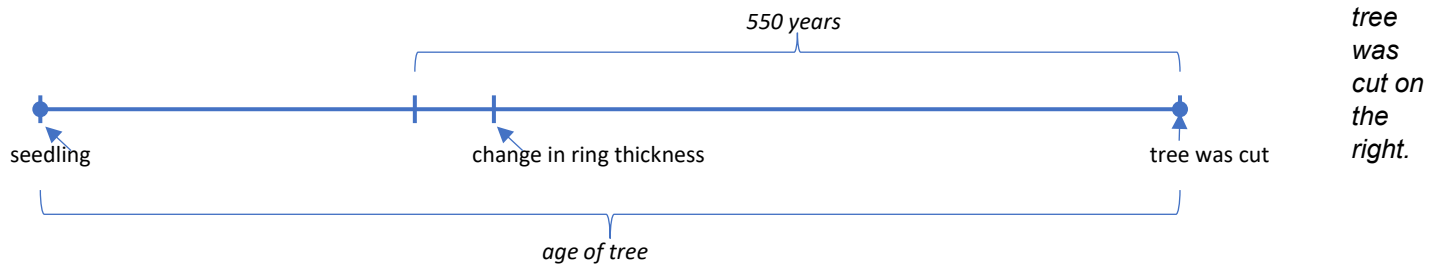
Outer rings:

Inner rings:

Mark the spot on Figure 1 where the change in tree rings thickness occurs.

Question 3. From the 550 year ring, count the number of rings to the *center* of the tree and record your findings. Then count the number of rings from 550 to the change in ring thickness and record this number. Assuming each ring represents one year of growth, how old is the tree?

Hint: use the numberline below to visualize these calculations, with the beginning of the tree's life on the left, and the year the tree was cut on the right.



550 to center = _____, 550 to change = _____,

Age of tree = _____

Question 4. Assume that the tree was cut down in the year 2000. What year did the tree rings begin to look different from the wider ones in the center? *Hint: add "2000" to the right end of your number line.*

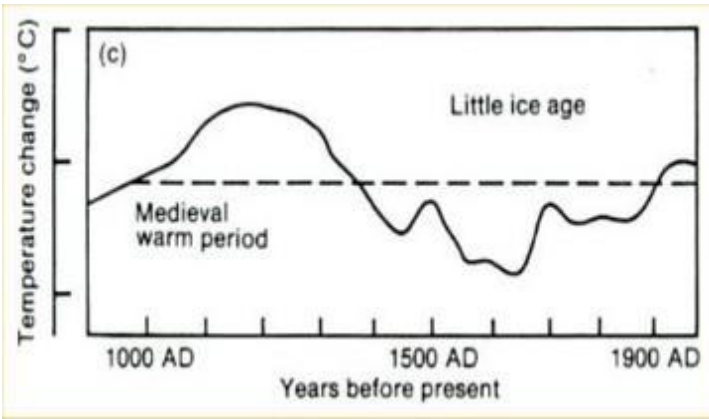


Figure 2. Temperature data from the northern hemisphere for the last 1000 years relative to an average temperature (dashed line) (IPCC 1990 report). Each tic mark on the vertical axis is one degree C.

Question 5. Look at the graph in Figure 2 showing temperature data from the northern hemisphere for the last 1000 years. Compare the date that you calculated for when the tree ring pattern changed, to the graph. What was happening to the climate during that time?

Question 6. From these observations, what would you suggest is the relationship between the tree ring thickness and climate?

Question 7. Look at the graph in Figure 2. How much did temperature change over the 400 years between AD 1600 and 2000? Note from the figure caption that each tic mark on the temperature scale is one degree C.

Part 2 - Plotted Temperature and Carbon Dioxide data

In this module you will be considering a graph of recent average global temperatures and atmospheric carbon dioxide measurements from 1999 to 2019.

Step 1. Look carefully at the chart in the Excel file you were given. It displays TWO variables on the y-axis and time on the x-axis, so it shows the changes in both temperature and atmospheric carbon dioxide over time (in this case, over a 20-year period.)

Part 2 Questions

Looking at your plot of time versus temperature and carbon dioxide (Referred to as Fig. 3), answer the following questions.

Question 1. Between 1999 and 2019, how much does the average global temperature change, and in what direction (increase or decrease?) (Quantify your answer using degrees centigrade, and does it increase or decrease)

Question 2. Between 1999 and 2019, how much do atmospheric carbon dioxide values change, and in what direction (increase or decrease?) (Quantify your answer using parts per million or ppm, and increase or decrease)

Question 3. Based on your graph, what is the relationship between temperature and carbon dioxide? (e.g., "When CO₂ increases, temperature _____" or "When temperature increases, CO₂ _____.")

Part 3 – Interpreting temperature and carbon dioxide data measured from the EPICA Ice Cores in Antarctica

Step 1. Observe the past 800,000 years of temperature and carbon dioxide data extracted from the EPICA ice core, Antarctica as presented in Figure 4, and answer the following questions.

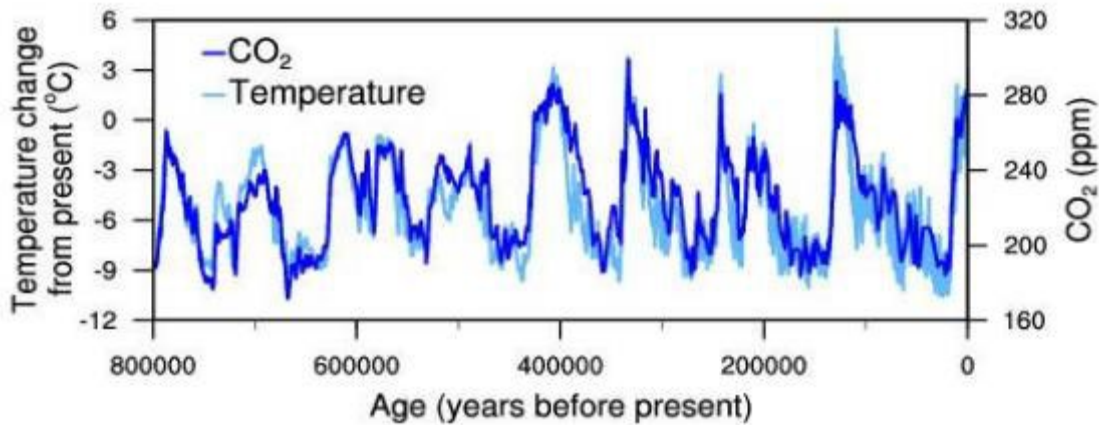


Figure 4. Temperature change (light blue) and carbon dioxide change (dark blue) measured from the EPICA Dome C ice core in Antarctica (Jouzel et al. 2007; Lüthi et al. 2008).

Question 1. What is the relationship between temperature and atmospheric CO₂ as shown in the ice core data in Figure 4?

Question 2. How does the relationship between carbon dioxide and temperature in the ice core data (Fig. 4) compare to the relationship between carbon dioxide and temperature in the graph from Part 2 (Fig. 3)? Explain. (*This is not asking about trends; it's asking if the two variables track together on both graphs.*)

Question 3. **a)** What is the greatest temperature range (= the difference between the highest and lowest value) in the 800,000 years shown in the ice core data?(Fig 4) **b)** What is the greatest temperature range between the Little Ice Age and the Medieval Warm Period shown in the graph from Part 1 (Fig. 2)? **c)** How do these temperature ranges compare?

a)

b)

c)

Question 4. What is the approximate time difference between two neighboring temperature peaks in figure 4? (representing one cycle of warm climate (interglacial) and cool climate (glacial)).

Question 5. From the ice core data, approximately how many interglacial (warmer) periods occurred during the past 800,000 years, and how many glacial periods (also known as Ice Ages)?

Question 5b. a) Does the temperature representative of the Little Ice Age (fig 2) compare to the temperature representative of the global ice ages (glacial periods) recorded in the ice core CO₂/temperature data? (***Important to determine this: Each graph shows difference from a recent global Temp average***) **b)** Explain.

a)

b)

Question 6. a) Draw on the graph: label “ice ages” and “interglacials” at the lows and highs of temperature values. **b)** How does the duration of the Little Ice Age between the years 1400 and 1800 (Fig. 2) compare to the duration of the past global ice age, or the time between the two most recent interglacial or warm periods (Fig. 4). **c)** Given your answer to b), is the Little Ice Age similar to the cyclical global glacial periods? (*Hint 1: the horizontal time scale is different for the two figures. Look at them both. Hint 2: Given the scale difference, is it possible to pick out the Little Ice Age on Figure 4?*)

b)

c)

Question 7. What are the lowest carbon dioxide values measured during cooling or glacial periods? What are the highest carbon dioxide values measured during warming or interglacial periods?

CO₂ during glacials: _____, CO₂ during interglacials: _____.

Question 7. a) What is the atmospheric carbon dioxide value in 2019 (refer to the graph in Excel)?

CO₂ in 2019: _____

Step 2: Observe the same carbon dioxide data in the following graph that compiles multiple ice core data and atmospheric measurements since 1950, and answer the following questions.

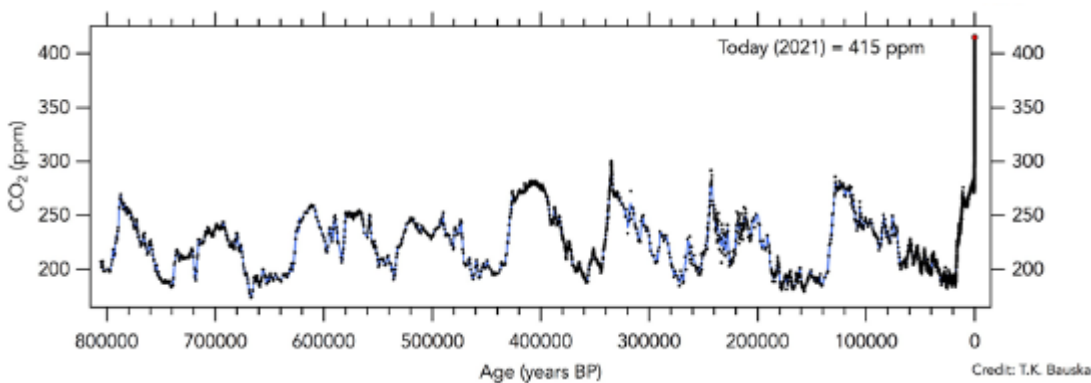


Figure 5. Atmospheric carbon dioxide concentrations changing through time. Compiled from Law Dome, Siple, Vostok, and EPICA ice cores and Keeling data measured at Mauna Loa.

Question 8. Figure 5 shows compiled CO₂ data (only CO₂) from multiple ice cores and from atmospheric measurements, such that its time range is from 800,000 years ago through today. Given what you learned through the previous questions, how would you expect temperature to plot over this same time period?

Question 9. Now that you see the data plotted in Figure 5, revisit the CO₂ values in Questions 6 and 7 and compare them with the visually displayed compiled data. **a)** Is today's CO₂ level the same as CO₂ during past interglacial periods? **b)** Given what you have learned about temperature and CO₂ correlation, what can you say about how today's global average temperature compares to past temperature during interglacial periods?

a)

b)

Step 3. Figure 6 shows the change in average global temperature and CO₂ since 1880. On Figure 6, write the temperature in degrees C on the temperature axis, next to the °F values. Use an online calculator to find those values.

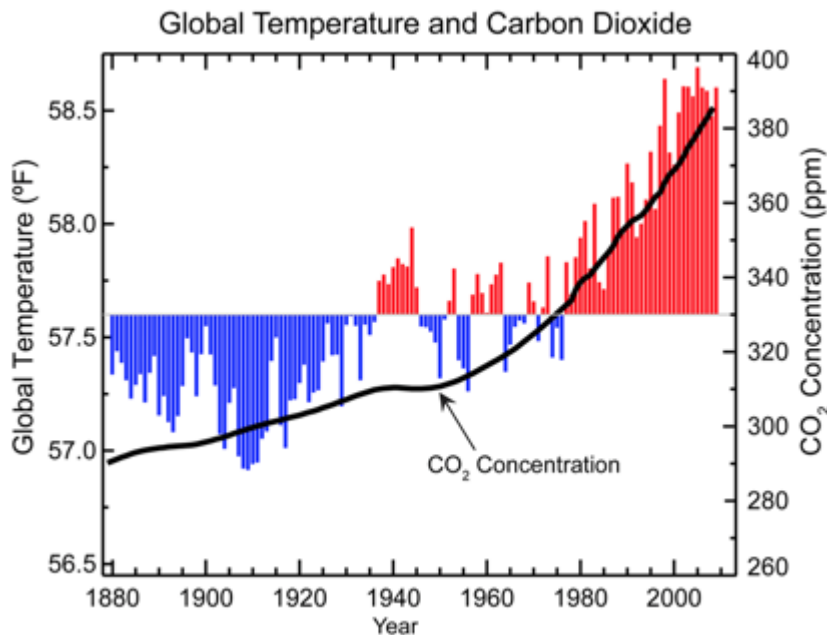


Figure 6. Global annual average temperature (as measured over both land and oceans). Red bars indicate temperatures above and blue bars indicate temperatures below the average temperature for the period 1901-2000. The black line shows atmospheric carbon dioxide (CO₂) concentration in parts per million (ppm). Source: NOAA/NCDC

Question 10. a) What is the approximate rate of change of temperature in the past 140 years? (To calculate the rate of change: Numerator = total temperature difference in degrees; Denominator = total time difference in

years) **b)** What is the approximate rate of change of atmospheric carbon dioxide concentration in the past 140 years? (Use the same mathematical process as above, but with CO₂ values)

a)

b)

Question 10. Is this current rate of change faster or slower than onsets of interglacials in the past? How did you determine your answer?

Question 11. How does this more complete picture of CO₂ data modify your understanding of the relationship of paleoclimate to modern climate, if at all?

Part 4: Global changes versus local changes

So far in this lab we have looked at global average temperature trends. However, local temperature variations may appear very different to this global trend.

Use the the toolbox presented here:

<https://climatetoolbox.org/>

- **Choose Tools → Data Download. (Do not use the graphic tool that pops up.)**
- From “Set Location” in Data Download, set a map location in Pittsburgh, Pennsylvania.
- Use ‘Historical climate (monthly) – Terra Climate
- In the Data Return box, choose to return only a single month (December) and see that your data set is from December 1958 to December 2021.
- Within the Change Variables area: Choose degrees C (not F)
- Choose to export only 2 columns (default is 4). Column 1 is time, Column 2 is tmax (maximum temperature, in degrees C)
- Download the csv file
- Open it in Excel.

In Excel:

- remove the header rows (select rows 1-8, right click, delete)
- remove the “month” column (select column B, right click, delete)
- LOOK at your temperature data and do some quality control... If there are any outliers (obviously incorrect measurements, like over 200 degrees for example), delete those whole ROWS. [select the number to the left of the data, right click, delete row.]
- Select both the A and B columns (only have to click on A and B to select all the way down)
- Insert → Chart... choose a scatter plot (bottom center of selections) and choose “Scatter with straight lines and markers”
- Your chart showing December maximum temperatures from 1958 to present in your chosen location is shown

Make a best-fit trend line:

- Select the data line in the chart, right click, select ‘Add Trendline’ and from the menu on the right, select “linear.”

Modify the temperature axis so you can read the data better

- Right-click the left (vertical) axis numbers; select ‘Format Axis’
- In the menu that opens on the right, change the Minimum bounds to a round number of degrees just below your data (select below your data so as to not cut any of it off). Hit ‘enter’ on your keyboard once you’ve typed that in for the axis bounds to change.
- In the same menu, change the Major Units to 1.0 so that you can better read temperatures on the graph.

Answer the following questions:

Question 1. What are the highest and lowest maximum temperatures recorded in this time period Pittsburgh, Pennsylvania (in the data, not the best-fit line,) and in what years did these occur?

Question 2. Does the Best Fit line show a change in temperature?

Question 3. If it does, what is the approximate rate of change? (remember: numerator = difference in temperature; denominator = difference in years, or number of years). (Also: remember your data show temperature in degrees Celsius. What is that change in Fahrenheit?)

Question 4. How does this value compare to the data you have previously plotted or observed?

Question 5. How has the mean temperature in this area changed when compared to the mean global temperature? Why do you think this is? (Remember that the temperature data in Fig. 6 is presented in °F but you added °C to the y-axis.)

Part 4: Global changes versus local changes

So far in this lab we have looked at global average temperature trends. However, local temperature variations may appear very different to this global trend.

Use the the toolbox presented here:

<https://climatetoolbox.org/>

- **Choose Tools → Data Download. (Do not use the graphic tool that pops up.)**
- From “Set Location” in Data Download, set a map location in your hometown.
- Use ‘Historical climate (monthly) – Terra Climate
- In the Data Return box, choose to return only a single month (December) and see that your data set is from December 1958 to December 2021.
- Within the Change Variables area: Choose degrees C (not F)
- Choose to export only 2 columns (default is 4). Column 1 is time, Column 2 is tmax (maximum temperature, in degrees C)
- Download the csv file
- Open it in Excel.

In Excel:

- remove the header rows (select rows 1-8, right click, delete)
- remove the “month” column (select column B, right click, delete)
- LOOK at your temperature data and do some quality control... If there are any outliers (obviously incorrect measurements, like over 200 degrees for example), delete those whole ROWS. [select the number to the left of the data, right click, delete row.]
- Select both the A and B columns (only have to click on A and B to select all the way down)
- Insert → Chart... choose a scatter plot (bottom center of selections) and choose “Scatter with straight lines and markers”
- Your chart showing December maximum temperatures from 1958 to present in your home town is shown

Make a best-fit trend line:

- Select the data line in the chart, right click, select ‘Add Trendline’ and from the menu on the right, select “linear.”

Modify the temperature axis so you can read the data better

- Right-click the left (vertical) axis numbers; select ‘Format Axis’
- In the menu that opens on the right, change the Minimum bounds to a round number of degrees just below your data (select below your data so as to not cut any of it off). Hit ‘enter’ on your keyboard once you’ve typed that in for the axis bounds to change.
- In the same menu, change the Major Units to 1.0 so that you can better read temperatures on the graph.

Answer the following questions:

Question 1. What are the highest and lowest maximum temperatures recorded in this time period in your hometown (in the data, not the best-fit line,) and in what years did these occur?

Question 2. Does the Best Fit line show a change in temperature?

Question 3. If it does, what is the approximate rate of change? (remember: numerator = difference in temperature; denominator = difference in years, or number of years). (Also: remember your data show temperature in degrees Celsius. What is that change in Fahrenheit?)

Question 4. How does this value compare to the data you have previously plotted or observed?

Question 5. How has the mean temperature in this area changed when compared to the mean global temperature? Why do you think this is? (Remember that the temperature data in Fig. 6 is presented in °F but you added °C to the y-axis.)

GEOL 1303 – Kelsch - Streams and Drainage Basins

Name _____

Tools you will use for this exercise:

- usgs water data MAP: <https://maps.waterdata.usgs.gov/mapper/index.html>
- past climate data: <https://www.weather.gov/wrh/climate>
- Google Maps (turn on the “terrain” background)
- Google Earth Pro with imported (given on Blackboard) kml files
- Microsoft Excel

Part I: Locating your river and river data

You are given a river to study for this exercise. What is its name?

Find it on Google Maps. What state is it in? _____

Is it an alluvial or bedrock stream (where the search landed you)? _____

View the watershed map and US rivers layers in Google Earth.

What watershed is your river in? _____

Is this watershed a tributary to another watershed, and which one? _____

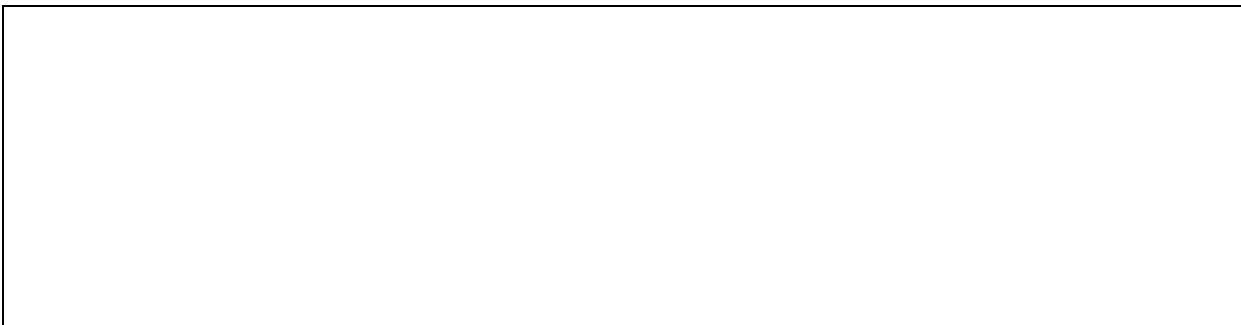
Find your river on the USGS water data site.

How many USGS streamflow gauges are in the vicinity of where your search landed you? _____

Pick one gauge station and write down its number here. _____

For that station, go to the “Water Year Summary” . What is the drainage area? _____

What does this mean? Draw a schematic map of this section of your river, the streamflow gauge, and the drainage basin including labeling the drainage area.



Look at the peak streamflow and find a medium-high year. Write it down. _____ Then go back to the previous page and choose Daily Data. Select bounding dates (from and to) to include a 3 year period that includes the medium-high year you just found. Choose the ‘graph’ bullet to look at it on this site.

This is called a hydrograph. What are the axes? _____

Given that those are the axes, what is this graph showing?

Describe the streamflow history over the 3-year period you chose. Are there any patterns from year to year? What part of the years sees highest and lowest discharge? Are there differences between years?

Identify a 2-month period when there was a change from low flow to high flow, within this 3-year graph you are displaying. Now search for that shorter time frame—this means change the From and To dates to just include that 2-month period.

Describe how flow changed over this 2-month period, e.g. “from __ cfs to __ cfs on ___ dates...”

Now choose a single month that contains a change in stream flow. Write that month down here. (It must be a calendar month to look up the climate data in the next section)

Part II: Comparing precipitation data to stream flow

Open the climate-data website and generally locate your river and watershed on the map. Observe the weather station region maps and compare them to your watershed. Do they have the same name? The same outline? Are they similar?

You want to find precipitation data that is relevant to your stream. Discuss with your group which stations are in your watershed. Compare the maps (watershed and weather stations) to find the best stations to look up. Have 2 people in the group (with Excel OR ANY OTHER spreadsheet program) look at different stations in the watershed, and 1 person document what they find. (You'll share all information among your group but this will make it go faster for now.)

What weather stations are you using? _____

For EACH of the two weather stations you are looking up:

Choose Daily Data for a month, for THE month that you chose. You are given a table. COPY and PASTE the 'date' and 'precip' columns for that month into a blank Excel (or other spreadsheet program) worksheet. You'll have to add a line at the top of your data to type in the headers "Date" and "Precip" because that text doesn't copy over.

Select those two columns in Excel and Insert a chart (2-d column; first option).

Go back to the USGS website. Change the output format of your hydrograph from "graph" to "csv tab separated." This will give you tabular data (data in a table) that you can copy into Excel. MAKE SURE THAT YOUR DATES ARE THE SAME FOR EACH LINE IN YOUR SPREADSHEET. To do this, copy both date and discharge columns from the USGS into your spreadsheet. Look to see that the same dates are on the same line. If they are not, CUT all the cells of the USGS data (what you just copied) at once, and paste them into the correct lines.

You'll now add the streamflow data into your chart. Do this FROM your chart... Click inside it, right click to open the 'select data' menu, then from that window, add another y-axis set of data. (You have done this before with CO2 and temperature data by date... what you now want are precipitation and streamflow data by date.)

Look at your completed charts. (you have two people doing this; there are two)

Do the streamflow and precipitation data correlate? _____ In both charts? _____

Discuss among your group and write some of the reasons that they would or would not correlate. What other contributors besides rain over this reach of the stream could cause streamflow to increase or decrease?

Part III. Repeat part II downstream.

Follow your river downstream past at least a few confluences. Find another USGS gauge station (on this same channel farther downstream.)

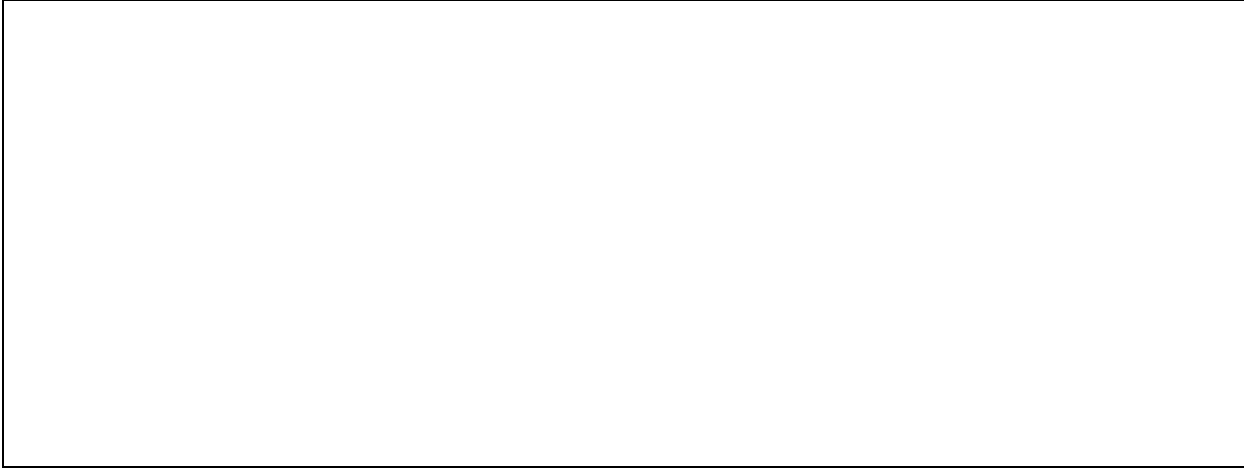
What station number is this? _____

Does the river's name change downstream? If so, to what? _____

For this station number you'll need to repeat finding the drainage area above it (this was in Part I) and also look at the streamflow data (just online this time) for the SAME month you plotted in Part II.

What is the drainage area for this stream gauge? _____

Draw a schematic map of this river, gauge, and drainage area in the space below, similar to what you did in Part I for the gauge on the same river upstream from here. What is different?

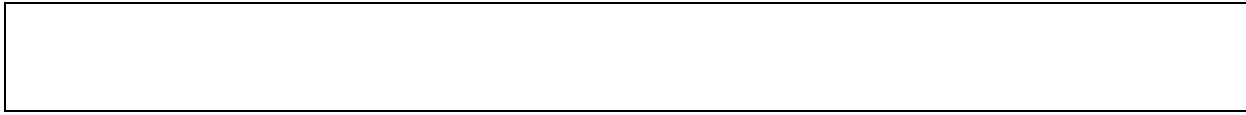


How much larger is the drainage area at this stream gauge station than it is at the upstream station? (This is a subtraction equation)

In Daily Data for a month, select the same month that you made a hydrograph for upstream, and choose “graph” to look at it on the website. Do you see high and low flows on the same dates that you do upstream? Are they the same or different actual values in cfs?

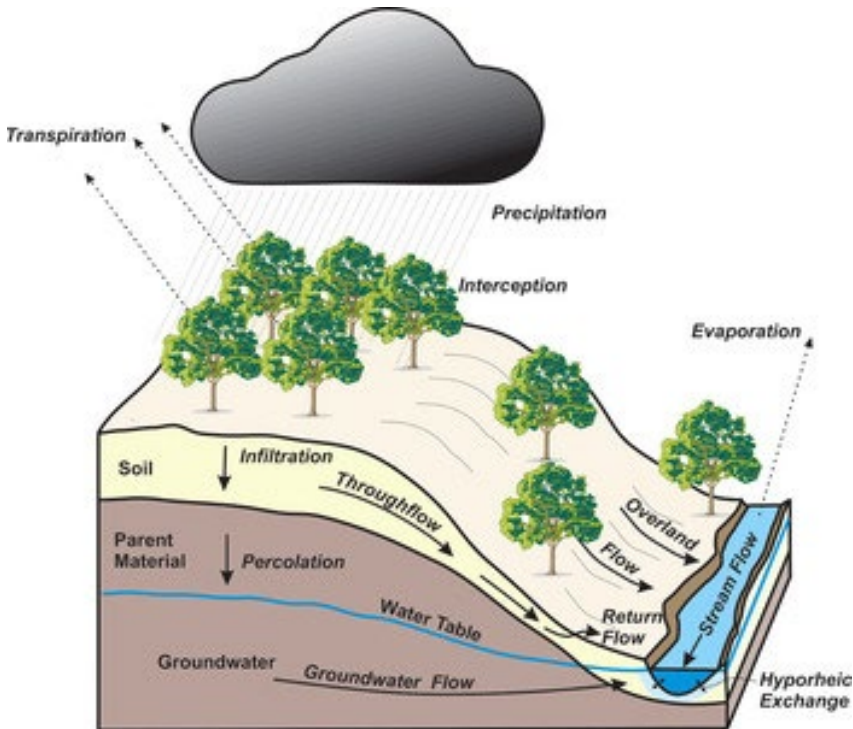
Discuss with your group any similarities or differences in the two hydrographs (one you have saved on both spreadsheets; one is on the USGS site you just searched for). List those similarities and differences and also write the reasons for them here.





Take a screenshot of this hydrograph and save it in a folder where you can find it later. Also save the Excel graphs; for those without Excel, group members will take a screenshot of their Excel graphs and email them to the rest of the group. (Each team member will have images of THREE graphs: two Excel graphs (same stream data but different climate station precip data); and the screenshot of the online hydrograph from downstream.) In the next class period (Monday,) the groups will project their graphs briefly at the front of the room and show the class where their stream is, what time period they looked at, and how flow changed downstream.

GEOL 1303 – Flood plain exercise



You will be emailed a data sheet with Peak Streamflow discharge data from the USGS site we used in the last exercises.

Notice that you have been given four data sets showing annual peak stream flow (discharge) for a range of years. The first two data sets are for the same river before and after urbanization. The second two data sets are for a farther-downstream river, also for a long-ago time and a recent time, but before and after an upstream dam installation. (The second two are for a different location than the first two, but downstream in the same watershed.) Each data set spans 11 years of record along its river. Use your assigned data set to estimate the likely discharge for a 100-year flood for each 11-year period. You should follow this procedure:

1. For each data set, rank the peak flood discharge in order of magnitude, starting with 1 for the largest and ending with 11 for the smallest. Write these results in the "Rank" column of the table.
2. Use the formula $(R.I. = (n+1)/m)$ to determine the recurrence interval of each of the 11 floods in each of the two data sets. (n is the number of entries in your data set, in this case 11. m is the value of the rank you gave that streamflow value.) The results should be recorded in the "Recurrence Interval" column of the table.

3. Plot your data with "Peak Flood Discharge" on the vertical (y) axis and "Recurrence Interval" on the horizontal (x) axis. You may do this on your own using Excel or Grapher or Sheets if you are comfortable with that, or you may do this with the enclosed graph paper. If you are using paper, use the following instructions:

- a. Examine the graph paper provided in this activity. The Recurrence Interval is plotted along the horizontal axis. The graph begins at 1.01 years and increases to the right. The left set of numbers 1-10 on the horizontal (x) axis should remain as printed. Modify the right set of numbers by adding a zero, so they read 10 – 100. These are years of recurrence of a flood, so for example the "100" on the right edge of your graph paper is the "100-year flood" occurrence.

You will use TWO sheets of this graph paper with the same modification to the horizontal axis. You will use one sheet for each of your two streams.

- b. For each stream, so on two separate sheets of graph paper (one for each stream,) you will be plotting the peak flood discharge for both sets of data on the vertical axis of the graph. To do this you need to select an appropriate vertical scale for your discharge data by examining the value of the highest and lowest discharges found in your two data sets. For instance, if the low discharge is 500 ft³/s and the high discharge is 4000 ft³/s, then your range of discharge is 3,500 ft³/s. Choose a vertical scale so that the numbers you plot from your data fill about one-half of the length of the vertical axis, from the bottom. Label the vertical axis by writing the appropriate numbers for your discharge along the left edge of the graph paper.
 - c. For your assigned stream, plot the discharge and recurrence interval for each of the 11 floods from Data Set 1. Using a ruler, draw a best-fit straight line through the data points. (If you do not know how to draw a best-fit line, ask your instructor.) The line should be extended all the way to the right side edge of the graph.
 - d. Now plot the discharge and recurrence interval for each of the 11 floods from Data Set 2 on the same graph paper. Using a ruler, draw a best-fit straight line for these data. The line should be extended all the way to the right side edge of the graph.
4. If you are using Excel or other graphing software, make a best-fit line for each of your four river data sets. Extend this best-fit line to the "100" value of the x axis.
5. Answer the questions on the following pages.

Worksheet

1. Based on your data, what is the predicted discharge for a 100-year flood? To find this information, you must read the value from your graph where it intersects the 100 yr recurrence interval line. Include the units (cubic feet per second)

Data Sets	River name	Over what years are the data from?	Predicted discharge for a 100-year flood
Data Set 1			
Data Set 2			
Data Set 3			
Data Set 4			

2. How do your predictions for the first river (data set 1 and 2) compare to each other, between the early years and the later years? Describe it in words.

3. Suggest possible human activities in the watershed that could have caused the differences in predicted floods that result from the two sets of data for this river (data sets 1 and 2).

8. What information do you need to know if you are about to buy a house that is located adjacent to, but just outside the 100-year floodplain?

It is possible to calculate the probability (or chance) that the annual maximum flood will equal or exceed a given discharge within any single year. This is called the annual probability of exceedence, P , and it is the reciprocal of T (the recurrence interval). Written as a formula:

Use the formula to calculate the following:

9. What is the probability in any given year that the stream discharge will exceed the discharge of the 100-year flood recurrence interval?

10. What is the probability in any given year that the stream discharge will exceed the discharge of the 10-year flood recurrence interval?

Mercer Creek (Ellensburg) – Data Set 1				Mercer Creek (Ellensburg)– Data Set 2			
Year	Peak Flood Discharge	Rank (1 = greatest)	Recurrence interval	Year	Peak Flood Discharge	Rank (1 = greatest)	Recurrence Interval
1957	180			1979	518		
1958	238			1980	414		
1959	220			1981	670		
1960	210			1982	612		
1961	192			1983	404		
1962	168			1984	353		
1963	150			1985	832		
1964	224			1986	504		
1965	193			1987	331		
1966	187			1988	228		
1967	254			1989	664		
Green River (Seattle) – Data Set 3				Green River (Seattle) – Data Set 4			
Year	Peak Flood Discharge	Rank (1 = greatest)	Recurrence interval	Year	Peak Flood Discharge	Rank(1 = greatest)	Recurrence Interval
1941	9310			1976	4490		
1942	10900			1977	9920		
1943	12900			1978	6450		
1944	13600			1979	8730		
1945	12800			1980	5200		
1946	22000			1981	9300		
1947	9990			1982	10800		
1948	6420			1983	9140		
1949	9810			1984	10900		
1950	11800			1985	7030		
1951	18400			1986	11800		
Guadalupe Riv (Comfort) – Data Set 1				Guadalupe Riv (Comfort) – Data Set 2			
Year	Peak Flood Discharge	Rank (1 = greatest)	Recurrence interval	Year	Peak Flood Discharge	Rank (1 = greatest)	Recurrence Interval

1940	7520			1992	54700		
1941	15400			1993	1880		
1942	7010			1994	18900		
1943	3870			1995	3110		
1944	74200			1996	1740		
1945	15000			1997	73700		
1946	6400			1998	20000		
1947	14400			1999	2580		
1948	1390			2000	4175		
1949	12100			2001	59400		
1950	2630			2002	128000		
Guadalupe River (Sattler) – Data Set 3				Guadalupe River (Sattler) – Data Set 4			
Year	Peak Flood Discharge	Rank (1 = greatest)	Recurrence interval	Year	Peak Flood Discharge	Rank(1 = greatest)	Recurrence Interval
1960	15500			2011	224		
1961	20800			2012	237		
1962	2200			2013	446		
1963	1450			2014	2470		
1964	1520			2015	6110		
1965	1010			2016	7100		
1966	5756			2017	1130		
1967	5476			2018	1496		
1968	1240			2019	3130		
1969	6106			2020	1690		
1970	1170			2021	296		

GEOL 1303 – Kelsch - Streams and Drainage Basins

Name _____

Tools you will use for this exercise:

- **usgs water data MAP:** <https://maps.waterdata.usgs.gov/mapper/index.html>
- **past climate data:** <https://www.weather.gov/wrh/climate>
- **Google Maps (turn on the “terrain” background)**
- **Google Earth Pro with imported (given on Blackboard) kml files**
- **Microsoft Excel**

Part I: Locating your river and river data

You are given a river to study for this exercise. What is its name?

Find it on Google Maps. What state is it in? _____

Is it an alluvial or bedrock stream (where the search landed you)? _____

View the watershed map and US rivers layers in Google Earth.

What watershed is your river in? _____

Is this watershed a tributary to another watershed, and which one? _____

Find your river on the USGS water data site.

How many USGS streamflow gauges are in the vicinity of where your search landed you? _____

Pick one gauge station and write down its number here. _____

For that station, go to the “Water Year Summary” . What is the drainage area? _____

What does this mean? Draw a schematic map of this section of your river, the streamflow gauge, and the drainage basin including labeling the drainage area.

Look at the peak streamflow and find a medium-high year. Write it down. _____ Then go back to the previous page and choose Daily Data. Select bounding dates (from and to) to include a 3 year period that includes the medium-high year you just found. Choose the ‘graph’ bullet to look at it on this site.

This is called a hydrograph. What are the axes? _____

Given that those are the axes, what is this graph showing?

Describe the streamflow history over the 3-year period you chose. Are there any patterns from year to year? What part of the years sees highest and lowest discharge? Are there differences between years?

Identify a 2-month period when there was a change from low flow to high flow, within this 3-year graph you are displaying. Now search for that shorter time frame—this means change the From and To dates to just include that 2-month period.

Describe how flow changed over this 2-month period, e.g. “from __ cfs to __ cfs on ___ dates...”

Now choose a single month that contains a change in stream flow. Write that month down here. (It must be a calendar month to look up the climate data in the next section)

Part II: Comparing precipitation data to stream flow

Open the climate-data website and generally locate your river and watershed on the map. Observe the weather station region maps and compare them to your watershed. Do they have the same name? The same outline? Are they similar?

You want to find precipitation data that is relevant to your stream. Discuss with your group which stations are in your watershed. Compare the maps (watershed and weather stations) to find the best stations to look up. Have 2 people in the group (with Excel OR ANY OTHER spreadsheet program) look at different stations in the watershed, and 1 person document what they find. (You'll share all information among your group but this will make it go faster for now.)

What weather stations are you using? _____

For EACH of the two weather stations you are looking up:

Choose Daily Data for a month, for THE month that you chose. You are given a table. COPY and PASTE the 'date' and 'precip' columns for that month into a blank Excel (or other spreadsheet program) worksheet. You'll have to add a line at the top of your data to type in the headers "Date" and "Precip" because that text doesn't copy over.

Select those two columns in Excel and Insert a chart (2-d column; first option).

Go back to the USGS website. Change the output format of your hydrograph from "graph" to "csv tab separated." This will give you tabular data (data in a table) that you can copy into Excel. MAKE SURE THAT YOUR DATES ARE THE SAME FOR EACH LINE IN YOUR SPREADSHEET. To do this, copy both date and discharge columns from the USGS into your spreadsheet. Look to see that the same dates are on the same line. If they are not, CUT all the cells of the USGS data (what you just copied) at once, and paste them into the correct lines.

You'll now add the streamflow data into your chart. Do this FROM your chart... Click inside it, right click to open the 'select data' menu, then from that window, add another y-axis set of data. (You have done this before with CO2 and temperature data by date... what you now want are precipitation and streamflow data by date.)

Look at your completed charts. (you have two people doing this; there are two)

Do the streamflow and precipitation data correlate? _____ In both charts? _____

Discuss among your group and write some of the reasons that they would or would not correlate. What other contributors besides rain over this reach of the stream could cause streamflow to increase or decrease?

Part III. Repeat part II downstream.

Follow your river downstream past at least a few confluences. Find another USGS gauge station (on this same channel farther downstream.)

What station number is this? _____

Does the river's name change downstream? If so, to what? _____

For this station number you'll need to repeat finding the drainage area above it (this was in Part I) and also look at the streamflow data (just online this time) for the SAME month you plotted in Part II.

What is the drainage area for this stream gauge? _____

Draw a schematic map of this river, gauge, and drainage area in the space below, similar to what you did in Part I for the gauge on the same river upstream from here. What is different?

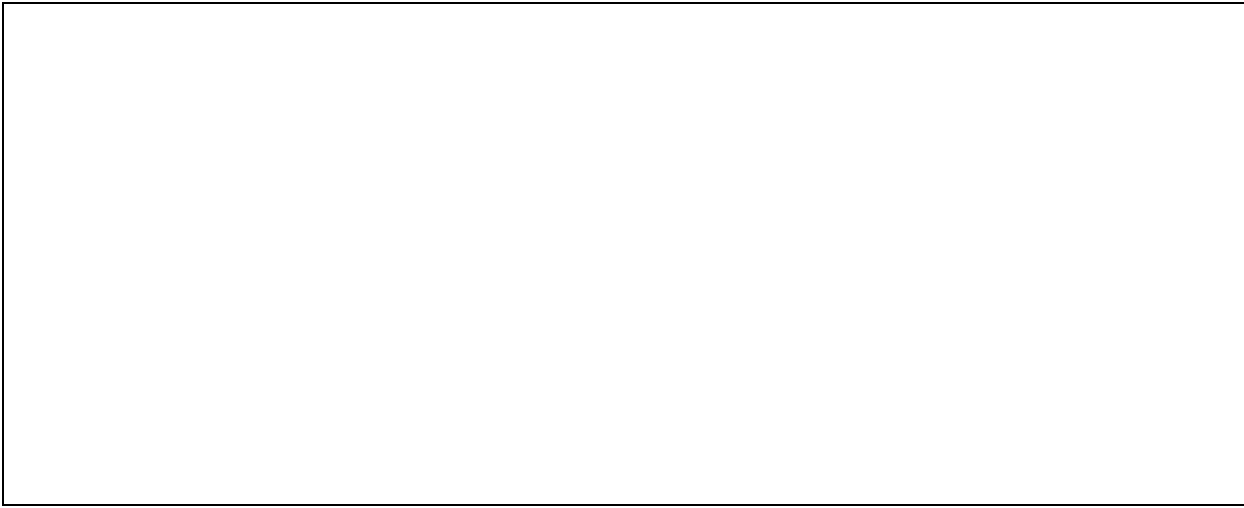


How much larger is the drainage area at this stream gauge station than it is at the upstream station? (This is a subtraction equation)

In Daily Data for a month, select the same month that you made a hydrograph for upstream, and choose "graph" to look at it on the website. Do you see high and low flows on the same dates that you do upstream? Are they the same or different actual values in cfs?

Discuss with your group any similarities or differences in the two hydrographs (one you have saved on both spreadsheets; one is on the USGS site you just searched for). List those similarities and differences and also write the reasons for them here.





Take a screenshot of this hydrograph and save it in a folder where you can find it later. Also save the Excel graphs; for those without Excel, group members will take a screenshot of their Excel graphs and email them to the rest of the group. (Each team member will have images of THREE graphs: two Excel graphs (same stream data but different climate station precip data); and the screenshot of the online hydrograph from downstream.) In the next class period (Monday,) the groups will project their graphs briefly at the front of the room and show the class where their stream is, what time period they looked at, and how flow changed downstream.

Appendix 4. Survey questions

Survey questionnaire 1:

your 4 digit code: _____

A research project in geoscience education as one portion of doctoral dissertation work
Ms. Jesse M Kelsch, MS, Principal Investigator
Instructor of Geology, Sul Ross State University
PhD Candidate in Geological Sciences, University of Texas at El Paso

1. What is your current major?

2. What is your *approximate* GPA?

3. What year of college are you enrolled in?

4. How far from the ASU campus is your hometown?
 - a. 0 to 1 hour drive
 - b. 1 to 3 hour drive
 - c. 3 to 5 hour drive
 - d. 5 to 7 hour drive
 - e. >7 hour drive

5. What is the approximate population of your hometown?
 - a. <10,000 people
 - b. 10,000-40,000 people
 - c. 40,000 – 80,000 people
 - d. >80,000 people

6. What is your race and/or ethnicity?

7. What has been your exposure to physical science (geology, chemistry, biology, physics, OR astronomy) before this class? (select all that apply; continued on next page)

- a. Very little exposure
- b. Read science news
- c. Discuss science topics at home
- d. Follow science podcasts or channels (e.g. "Science Friday;" "Global Weirding;" "PBS Eons")
- e. Watch science documentaries or docuseries
- f. Was into science classes in high school or as non-physical-science major
- g. Physical Science major
- h. Social Science major

8. Rank your impression of the relevance of geoscience/geology to human society (scaled answer; 1-10)

(low) 1 2 3 4 5 6 7 8 9 10 *(high)*

9. Rank your impression of the relevance of geoscience/geology to the local community (scaled answer; 1-10)

(low) 1 2 3 4 5 6 7 8 9 10 *(high)*

10. Does geoscience have relevance to you or to someone you know? (scaled answer; 1-10)

(no) 1 2 3 4 5 6 7 8 9 10 *(yes)*

11. If there is relevance for any of the above three questions, please describe that relevance.

12. How are tectonic plate motions related to faults?

13. What is a fault?

14. What is one way that faults are relevant to human society?

1. How are tectonic plate motions related to faults?
2. What is a fault?
3. What is one way that faults are relevant to human society?

Critical thinking

1. Describe one way that tectonic plate motion affects the formation of geologic structures in the crust.

2. Two tectonic plates converge from the north and south toward each other.
 - a. What are the types of geologic structures that are formed?

 - b. In what direction are those structures *oriented*?

3. How might the orientation of geologic structures influence resources that are found below the surface, such as water, minerals, or fossil fuels?

Content retention

4. Where a fault's hanging wall has moved DOWN relative to the foot wall, this is a _____ fault.
5. Folds form under _____ stress, where two tectonic plates are _____ (what type of plate boundary)

Engagement

6. I learned something new today. (yes) 10 9 8 7 6 5 4 3 2 1 (no)
 - a. What was that new thing?

7. I learned something interesting today. (yes) 10 9 8 7 6 5 4 3 2 1 (no)
 - a. What was that interesting thing?

8. I learned something relevant to human society today . (yes) 10 9 8 7 6 5 4 3 2 1 (no)
 - a. What was that relevant thing?

9. What is one way that the knowledge of Earth's geologic structures affects human society?

Survey questionnaire 3 (pre-Earthquakes exercise):

9/27/21

1. What is an earthquake?
2. What type of scale is used to measure earthquakes?
3. How do earthquakes relate to fault motion?
4. What is one effect of earthquakes on human society?

Critical thinking

1. Describe the relationship between earthquake occurrence and plate tectonic activity
2. How does earthquake intensity (ground shaking) relate to earthquake magnitude (the amount of stress released in an EQ?)
3. How might knowledge of ground shaking affect planning for people living in or near earthquake zones?

Content retention

4. What is a mathematical “function?”
5. On what geological structures do earthquakes occur?
6. Real earthquake data can be found at what organization’s website?

Engagement

7. I learned something new today (1-10)
 - a. What was that new thing?
8. I learned something interesting today (1-10)
 - a. What was that interesting thing?

Relevance

9. I learned something relevant to human society today (1-10)
 - a. What was that relevant thing?
10. What is one way that the knowledge of volcanic activity affects human society?

Post-volcanoes-exercise survey

Your 3-digit code: _____

1. What is one way to predict volcanic eruptions?

2. What is the primary hazard of felsic volcanoes?

3. What is the primary hazard of mafic volcanoes?

4. Why do you think that small EQs outside of the US are not shown on the USGS website? There could be more than one answer.

5. Given what you have learned previously about earthquakes, can you think of a way that volcano-related earthquakes are different than other earthquakes?

6. What is one way that the knowledge of volcanic activity affects human society?

7. I learned something new with this exercise (1-10)
 - a. What was that new thing?

8. I learned something interesting with this exercise (1-10)
 - a. What was that interesting thing?

9. I learned something relevant to human society with this exercise (1-10)
 - a. What was that relevant thing?

Pre-climate-exercise survey

your 3 digit code: _____

1. What is one natural (not involving humans) influence on Earth's climate? (This is asking what is one natural factor that can modify Earth's surface's climate.)
2. What is one *human* influence on Earth's climate?
3. Why is the study of Earth's climate important?

Post-climate-exercise survey

your 4 digit code: _____

1. Describe the relationship between atmospheric carbon dioxide and global temperature during Earth's climate history. (e.g. when one is high or low, the other is...)
2. What is the difference between modern CO2 levels and those during the cyclical, warm interglacial periods of the last 800,000 years?
3. What is one type of *proxy* temperature data?
4. The recent Little Ice Age in the late 1400s to mid-1800s was _____ (similar or different) [choose one] in duration and temperature to the last global ice age of 21,000 years ago. Elaborate briefly on this.

5. I learned something *new* today. (Select a number between strong yes and strong no)

(yes) (no)

1 2 3 4 5 6 7 8 9 10

What was that new thing?

6. I learned something *interesting* today. (Select a number between strong yes and strong no)

(yes) (no)

1 2 3 4 5 6 7 8 9 10

What was that interesting thing?

7. I learned something *relevant to human society* today. (Select a number between strong yes and strong no)

(yes) (no)

1 2 3 4 5 6 7 8 9 10

What was that relevant thing?

8. What is one way that the knowledge of Earth's past climate affects human society?

1. What is one way that human activity impacts river processes?
2. What does the "100-year flood" refer to?
3. What is the difference between overland flow and return flow?
4. Which parts of the hydrologic cycle are important in planning for flooding?

5. I learned something I did not know from this exercise. yes/10 9 8 7 6 5 4 3 2 1/no
a. what was that thing?

6. I learned something relevant to human society from this exercise. yes/10 9 8 7 6 5 4 3 2 1/no
a. what was that thing?

7. I learned something interesting from this exercise. yes/10 9 8 7 6 5 4 3 2 1/no
a. what was that thing?

Final survey

Streams and floods

(critical thinking) Explain how precipitation affects streamflow (streamflow = discharge in a river), and also whether it ALWAYS affects streamflow.

(critical thinking) What is one reason it is important to have streamflow gauges (monitors) in river channels?

(content) What is a watershed? (also called a drainage basin)

(content) Does discharge increase or decrease down-river from a confluence of two tributaries, and why?

(relevance) What is one impact of rivers on human society?

(relevance) Rank your impression of the relevance of knowledge of streams and flooding to your community.

highly relevant 10 9 8 7 6 5 4 3 2 1 *not relevant*

(relevance) Rank your impression of the relevance of knowledge of streams and flooding to other parts of the world.

highly relevant 10 9 8 7 6 5 4 3 2 1 *not relevant*

Ciimate

(critical thinking) Draw in this space a rough sketch of Earth's global average temperature as it has changed over the last 800,000 years as revealed through ice cores. This is a graph you have seen and used several times this semester. Y-axis is temperature; X-axis is time, with today at the right end of the graph, and 800,000 years ago at the left end. Higher temperature is the top of the Y-axis; lower temperature is the bottom of the Y-axis.

(critical thinking) What is the connection between (1) Earth's global average temperature and (2) the amount of greenhouse-gas molecules like CO₂ in the atmosphere?

(content) What is one example of "proxy" temperature data? (Proxy means that we don't have direct measurements from a thermometer, but it is data that nonetheless reveals temperature.)

(content) What is the difference between today's modern CO₂ levels and those during the cyclical interglacial periods of the last 800,000 years?

(relevance) What is one impact of climate on human society?

(relevance) Rank your impression of the relevance of knowledge of climate processes to your community. *highly relevant* 10
9 8 7 6 5 4 3 2 1 *not relevant*

(relevance) Rank your impression of the relevance of knowledge of climate processes to other parts of the world.

highly relevant 10 9 8 7 6 5 4 3 2 1 *not relevant*

Volcanism

(critical thinking) What do earthquakes underneath a volcano signify is happening inside that volcano?

(critical thinking) Given what you have learned previously about earthquakes, can you think of a way that volcano-related earthquakes are different than other earthquakes?

(content) What is the primary hazard of felsic volcanoes?

(content) What is the primary hazard of mafic volcanoes?

(relevance) What is one way that the knowledge of volcanic activity affects human society?

(relevance) Rank your impression of the relevance of knowledge of volcanic processes to your community.

highly relevant 10 9 8 7 6 5 4 3 2 1 *not relevant*

(relevance) Rank your impression of the relevance of knowledge of volcanic processes to other parts of the world.

highly relevant 10 9 8 7 6 5 4 3 2 1 *not relevant*

Earthquakes

(critical thinking) Describe the relationship between earthquake occurrence and plate tectonic activity.

(critical thinking) How does earthquake intensity (ground shaking) relate to earthquake magnitude (the amount of stress released in an earthquake)?

(critical thinking) How might knowledge of ground shaking affect planning for people living in or near earthquake zones?

(content) On what geological structures do earthquakes occur?

(content) Real earthquake data and shake maps for those earthquakes can be found at what government organization's website?

(relevance) What is one way that earthquakes affect human society?

(relevance) Rank your impression of the relevance of knowledge of earthquake processes to your community.

highly relevant 10 9 8 7 6 5 4 3 2 1 *not relevant*

(relevance) Rank your impression of the relevance of knowledge of earthquake processes to other parts of the world.

highly relevant 10 9 8 7 6 5 4 3 2 1 *not relevant*

Geologic structures and plate tectonics

(critical thinking) Two tectonic plates converge from the north and south toward each other. What are the types of geologic structures that are formed in the rock of the crust?

(critical thinking) How might the orientation of geologic structures influence *resources* that are found below the surface, such as water, minerals, or fossil fuels?

(content) Where a fault's hanging wall has moved DOWN relative to its foot wall, it is this type of fault:
_____ (either name the fault or say what kind of stress caused it.)

(content) Folds form under _____ stress, where two tectonic plates are _____.

(relevance) What is one way that the knowledge of the geologic structures below the surface impacts human society?

(relevance) Rank your impression of the relevance of the knowledge of geologic structures to your community.

highly relevant 10 9 8 7 6 5 4 3 2 1 *not relevant*

(relevance) Rank your impression of the relevance of knowledge of geologic structures to other parts of the world.

highly relevant 10 9 8 7 6 5 4 3 2 1 *not relevant*

Rank your impression of the relevance of geoscience to human society

highly relevant 10 9 8 7 6 5 4 3 2 1 *not relevant*

Rank your impression of the relevance of geoscience to the local community

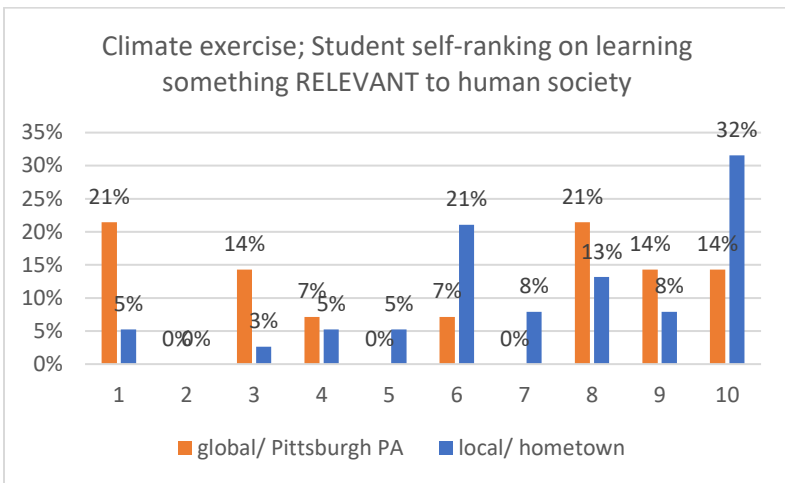
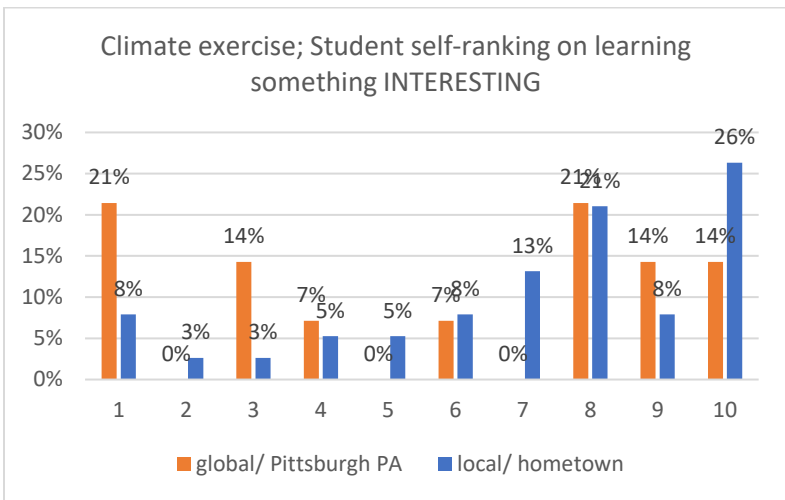
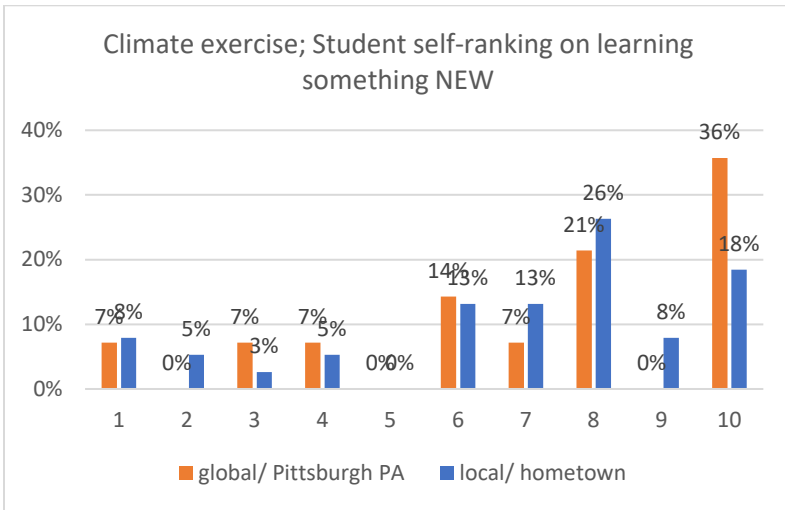
highly relevant 10 9 8 7 6 5 4 3 2 1 *not relevant*

Does geoscience have relevance to you or to someone you know?

yes 10 9 8 7 6 5 4 3 2 1 *no*

Appendix 5. Post-climate-exercise ranking data

These 1-10 ranking questions were delivered with “1” and “10” ordered incorrectly.



Appendix 6: Word clouds

Students' short answers to the questions following each numeric ranking request were grouped into word clouds to make a visual comparison of the most common words (WordArt.com, 2023.) One cloud was constructed for each group of student answers (LG and GG) within each exercise, and by what the student learned that was new, interesting, and relevant to human society. Words were removed that pertained directly to the exercise topic. (for example, "fault," "earthquake," etc.).

VITA

I received my bachelor's degree from the University of Arizona in 1996 with a sound intrigue into solving puzzles of plate tectonics. I stayed an extra year at UofA after graduation to complete a project with Dr. Peter Coney in his creation of a basement map of North America. For my MS thesis from the University of New Mexico in 2000 I again used stratigraphy and structural geology to contribute to the understanding of the onset of part of the northern Rio Grande rift. At ExxonMobil from 2000 to 2003 I continued to solve puzzles of stratigraphy and structural geology to find oil and gas deposits in the subsurface below Alaska's north slope and the Gulf of Mexico, but I returned to New Mexico to help locate accessible ground water for municipal and state clients as a hydrogeologist. I left this work in 2007 to move to Alpine, Texas to sort out family matters, and soon was teaching undergraduate geology classes at Alpine's Sul Ross State University as a lecturer. While college instruction was where I was meant to land, the remoteness of Alpine and Sul Ross did not afford my continued education until 2019, when I returned to graduate school at UTEP while maintaining my teaching schedule at Sul Ross.

Had I continued in tectonics research in 2000 I would not have studied geoscience education in addition to structural geology, but after eight years of teaching physical geology to non-majors as a core science class, and more years of attention to society's increasing push against the physical limitations of the Earth system and simultaneous cultural demoting of Earth science, I readily took advantage of the UTEP Geoscience faculty's detailed attention to effective geoscience education and included this field as part of my Ph.D. research. I will continue to investigate the multi-dimensional puzzles of structural geology and plate tectonics, but I will also continue to research how to improve the understanding and appreciation of any aspects of the Earth system among non-geoscientists.

I may be reached at jkelsch@sulross.edu.

ProQuest Number: 30818018

INFORMATION TO ALL USERS

The quality and completeness of this reproduction is dependent on the quality and completeness of the copy made available to ProQuest.



Distributed by ProQuest LLC (2023).

Copyright of the Dissertation is held by the Author unless otherwise noted.

This work may be used in accordance with the terms of the Creative Commons license or other rights statement, as indicated in the copyright statement or in the metadata associated with this work. Unless otherwise specified in the copyright statement or the metadata, all rights are reserved by the copyright holder.

This work is protected against unauthorized copying under Title 17, United States Code and other applicable copyright laws.

Microform Edition where available © ProQuest LLC. No reproduction or digitization of the Microform Edition is authorized without permission of ProQuest LLC.

ProQuest LLC
789 East Eisenhower Parkway
P.O. Box 1346
Ann Arbor, MI 48106 - 1346 USA